

Bioactive trace metals and their isotopes as paleoproductivity proxies: An assessment using GEOTRACES-era data

T.J. Horner^{1,2,*}, S.H. Little^{3,*}, T.M. Conway^{4,*}, J.R. Farmer^{5,6,*}, J.E. Hertzberg^{7,†}, D.J. Janssen⁸, A.J.M. Lough^{9,‡}, J. McKay¹⁰, A. Tessin¹¹, S.J.G. Galer⁶, S.L. Jaccard^{8,§}, F. Lacan¹², A. Paytan¹³, K. Wuttig^{14,||}, and GEOTRACES–PAGES Biological Productivity Working Group Members¹⁵.

¹NIRVANA Labs, ²Department of Marine Chemistry & Geochemistry, Woods Hole Oceanographic Institution, Woods Hole, MA, USA; ³Department of Earth Sciences, University College London, London, GBR; ⁴College of Marine Science, University of South Florida, FL, USA; ⁵Department of Geosciences, Princeton University, Princeton, NJ, USA; ⁶Max-Planck Institute for Chemistry, Mainz, DEU; ⁷Department of Ocean, Earth & Atmospheric Sciences, Old Dominion University, Norfolk, VA, USA; ⁸Institute of Geological Sciences and Oeschger Center for Climate Change Research, University of Bern, Bern, CHE; ⁹University of Southampton, National Oceanography Centre, Southampton, GBR; ¹⁰College of Earth, Ocean, and Atmospheric Sciences, Oregon State University, Corvallis, OR, USA; ¹¹Department of Geology, Kent State University, Kent, OH, USA; ¹²LEGOS, University of Toulouse, CNRS, CNES, IRD, UPS, Toulouse, FRA; ¹³Institute of Marine Sciences, University of California Santa Cruz, Santa Cruz, CA, USA; ¹⁴Antarctic Climate and Ecosystems Cooperative Research Centre, University of Tasmania, Hobart, AUS; ¹⁵A full list of working group members and their affiliations appears at the end of the manuscript.

*To whom correspondence should be addressed: T.J.H. (Tristan.Horner@whoi.edu), S.H.L. (susan.little@ucl.ac.uk), T.M.C. (tmconway@usf.edu), or J.R.F. (jesse.farmer@princeton.edu).

†Now at: International Ocean Discovery Program, Texas A&M University, College Station, TX, USA; ‡Now at: School of Geography, University of Leeds, Leeds, GBR; §Now at: Institute of Earth Sciences, Université de Lausanne, Lausanne, CHE; ||Now at: Federal Maritime and Hydrographic Agency (BSH), Hamburg, DEU.

Key Points

- Distributions, drivers, and depositional archives described for iron, zinc, copper, cadmium, molybdenum, barium, nickel, chromium, & silver
- Cadmium, barium, nickel, and chromium isotopes offer the most promise as paleoproductivity tracers, but key uncertainties remain
- Future priorities include quantification of ‘missing’ flux terms, constraining circulation influences, and identifying sedimentary archives

Keywords: biological pump; marine chemistry; biogeochemical cycles; micronutrients; phytoplankton; paleoceanography

Abstract

1
2 Phytoplankton productivity and export sequester climatically significant quantities of atmospheric carbon
3 dioxide as particulate organic carbon through a suite of processes termed the biological pump. How the
4 biological pump operated in the past is therefore important for understanding past atmospheric carbon
5 dioxide concentrations and Earth's climate history. However, reconstructing the history of the biological
6 pump requires proxies. Due to their intimate association with biological processes, several bioactive trace
7 metals and their isotopes are potential proxies for past phytoplankton productivity, including: iron, zinc,
8 copper, cadmium, molybdenum, barium, nickel, chromium, and silver. Here we review the oceanic
9 distributions, driving processes, and depositional archives for these nine metals and their isotopes based on
10 GEOTRACES-era datasets. We offer an assessment of the overall maturity of each isotope system to serve
11 as a proxy for diagnosing aspects of past ocean productivity and identify priorities for future research. This
12 assessment reveals that cadmium, barium, nickel, and chromium isotopes offer the most promise as tracers
13 of paleoproductivity, whereas iron, zinc, copper, and molybdenum do not. Too little is known about silver
14 to make a confident determination. Intriguingly, the elements that are least sensitive to productivity may be
15 used to trace other aspects of ocean chemistry, such as nutrient sources, particle scavenging, organic
16 complexation, and ocean redox state. These complementary sensitivities suggest new opportunities for
17 combining perspectives from multiple proxies that will ultimately enable painting a more complete picture
18 of marine paleoproductivity, biogeochemical cycles, and Earth's climate history.

19 1. Introduction

20 The ocean plays host to three carbon ‘pumps’ that redistribute climatically significant quantities of carbon
21 dioxide (CO₂) from the atmosphere to the ocean interior and seafloor (Volk & Hoffert, 1985). These ocean
22 carbon pumps—biological, carbonate, and solubility—influence Earth’s climate over timescales ranging
23 from decades to millions of years (e.g., Volk & Hoffert, 1985; Sigman et al., 2010; Khatiwala et al., 2019).
24 The biological pump refers specifically to the production of particulate organic carbon (POC) within the
25 sunlit surface ocean (euphotic zone) and export of POC to the intermediate and deep ocean, where POC is
26 largely (but not wholly) regenerated. The biological pump is of particular interest as it connects the cycles
27 of C to those of dissolved O₂, nutrients, and marine biology, and today accounts for as much as 70 % of the
28 carbon concentration gradient between the euphotic zone and the deep ocean (Sarmiento & Gruber, 2006).

29 The biological pump acts to redistribute CO₂ from the atmospheric/surface ocean carbon reservoir to the
30 deep ocean and sediment carbon reservoirs via two steps. First, phytoplankton, photoautotrophic microbes,
31 use sunlight (represented here by $h\nu$) to transform ambient DIC (dissolved inorganic carbon) into POC
32 (particulate organic carbon), represented here by CO₂ and a simple sugar (CH₂O), respectively, by the
33 simplified reaction:



35 The second step requires that some fraction of the newly formed POC sinks into the ocean interior through
36 a combination of biological and physical aggregation processes (e.g., Alldredge & Silver 1988), where
37 ultimately some POC may be buried in marine sediments. The resulting surface ocean DIC deficit promotes
38 dissolution of atmospheric CO₂ into seawater to maintain air–sea CO₂ equilibrium, driving an overall
39 reduction in the partial pressure of atmospheric CO₂ ($p\text{CO}_2$). Note that this definition of the biological pump
40 neglects dissolved organic carbon export, which is comparatively understudied, though may account for as
41 much as one-third of C export (e.g., Carlson et al., 2010; Giering et al., 2014). Importantly, Reaction [1]
42 requires sunlight and can only occur in the euphotic zone of the ocean. In contrast, aerobic heterotrophic
43 respiration can occur wherever POC and O₂ are present:



45 (There are also a number of O₂-independent respiration pathways that are reviewed in detail elsewhere;
46 e.g., Froelich et al., 1979.)

47

48 While the representation of all POC as a simple sugar (CH₂O) is instructive for illustrating an important
49 biotic transformation in the ocean, it is also simplistic; microbial biomass consists of dozens of bioactive

50 elements that serve many essential functions (e.g., da Silva & Williams, 1991). The elemental stoichiometry
51 of POC can thus be expanded to include a number of major and micronutrient elements, as illustrated by
52 the extended Redfield ratio reported by Ho et al. (2003):

53 $C_{124,000}N_{16,000}P_{1,000}S_{1,300}K_{1,700}Mg_{560}Ca_{500}Sr_{5.0}Fe_{7.5}Zn_{0.8}Cu_{0.38}Co_{0.19}Cd_{0.21}Mo_{0.03}$ [3]

54 With this extended stoichiometry in mind, it is clear that Reactions [1] and [2]—the production and
55 regeneration of organic matter, respectively—will not only generate gradients in the dissolved
56 concentration of DIC and O₂, but also for many other bioactive elements associated with POC cycling.
57 These gradients will be steepest for those elements possessing shorter residence times and where biological
58 uptake and regeneration are the most important processes driving their vertical distributions. Likewise, such
59 gradients may be almost absent for elements that possess long residence times or are primarily cycled by
60 processes other than productivity.

61

62 For those bioactive metals where biological processes are important, the implication of Reactions [1] and
63 [2] is that many of the elements listed in [3] may, in turn, be used as proxies of POC cycling and, potentially,
64 paleoproductivity. Indeed, aspects of past ocean productivity that impact carbon and nutrient cycling are
65 routinely reconstructed using the stable isotope compositions of carbon and macronutrient elements (N and
66 Si; see Farmer et al., *this issue*). It thus follows that the abundance and isotopic compositions of bioactive
67 trace metals cycled along with POC could also provide valuable information on past ocean productivity.
68 However, in order to use systems of trace elements and their isotopes as proxies for productivity, it is
69 necessary to develop a comprehensive understanding of the marine behavior of these elements, including:
70 mapping their distribution in the ocean; elucidating the drivers of the distribution; characterizing sources,
71 sinks, and transformations associated with biological, physical and chemical (notably redox) reactions; and,
72 recognizing if (and how) a given element is incorporated and preserved in marine sediments.

73

87 The wealth of new TEI (trace element and isotope) data from the GEOTRACES program (e.g., Fig. 1) now
88 permits an assessment of whether certain bioactive TEI metals are promising proxies for past ocean
89 productivity. This contribution represents such an assessment. Our study synthesizes what is known about
90 the processes governing the cycling of nine bioactive metal in seawater, explores the level of development
91 and readiness of each isotope system to inform on aspects of past ocean productivity, and identifies areas
92 where further research is most needed to improve our understanding of the geochemistry of trace metals in
93 the past and present ocean. We base our assessment on publicly available results from the international
94 GEOTRACES programme (e.g., Mawji et al. 2015; Schlitzer et al., 2018). Our study is not intended to be
95 a thorough review of all available techniques used to reconstruct paleoproductivity. Instead, we focus on
96 bioactive metal isotope systems that are either recognized as micronutrients (such as those in Eq. [3]) or
97 exhibit nutrient-like dissolved profiles in seawater, regardless of their nutritional status to phytoplankton
98 (e.g., Ba, Cr, Ag). This will not be the last word on the topic; our understanding of many of these metal
99 isotope systems has rapidly evolved in recent years, and will continue to evolve as new data are generated.

100

101

102 **2. Key concepts**

103 In this section we introduce several key concepts to which we refer throughout the review. First, we provide
104 definitions for reporting bioactive metal concentrations and isotope variations, and for the concept of
105 paleoproductivity (Sec. 2.1.). Second, we describe an idealized framework for reconstructing
106 paleoproductivity based on the coupled cycling of bioactive trace metals and their isotopes (Sec. 2.2.).
107 Finally, we introduce a number of additional trace metal cycling processes that are important considerations
108 in the application of bioactive trace metal isotope systems to reconstruct paleoproductivity (Sec. 2.3.). The
109 review of each metal system follows.

110 The review sections are structured such that each bioactive metal isotope system is described similarly and
111 systematically. The order in which metals are reviewed follows the extended Redfield ratio—Fe (Sec. 3.),
112 Zn (Sec. 4.), Cu (Sec. 5.), Cd (Sec. 6.), and Mo (Sec. 7.)—before describing the nonessential elements Ba
113 (Sec. 8.), Ni (Sec. 9.), Cr (Sec. 10.) and Ag (Sec. 11.) in order of decreasing dissolved concentration in
114 seawater. The review of each metal isotope system is organized around four questions:

- 115 1. What is the modern marine distribution of this trace metal isotope system?
- 116 2. Which biological, chemical, and physical processes are most important for maintaining this
117 distribution?
- 118 3. In what form is this trace metal isotope system incorporated into sediments?
- 119 4. What are the priorities for improving the utility of this trace metal isotope system to track
120 paleoproductivity?

121 This structure results in some repetition of the main distributions, drivers, and sedimentary archives
122 between individual isotope systems. This redundancy is deliberate: each section can be read independently
123 without reference to the other bioactive trace metals. We close our review by assessing the ‘maturity’ of
124 each system based on a comparison to more established productivity proxies, offer suggestions for future
125 studies, and discuss prospects for paleoproductivity reconstructions using bioactive trace metal isotope
126 systems.

127

128 **2.1. Definitions**

129 *2.1.1. Data reporting conventions*

130 The isotope literature abounds with isotope notations (e.g., ϵ , δ), reference materials (e.g., IRMM, JMC,
131 NIST), and isotope ratio pairs (e.g., $^{57}\text{Fe}/^{54}\text{Fe}$ versus $^{56}\text{Fe}/^{54}\text{Fe}$; $^{137}\text{Ba}/^{134}\text{Ba}$ versus $^{138}\text{Ba}/^{134}\text{Ba}$). There are

132 merits to each of these choices and we do not intend to review these here. However, we believe that the
133 sheer number of ways in which trace metal isotope data have been reported can be confusing to scientists
134 in other disciplines and this ultimately diminishes the reach and utility of isotope-based research. To avoid
135 furthering this confusion, we have adopted a number of conventions that apply throughout this review,
136 regardless of how literature data were originally reported. First, we use a single isotope notation throughout
137 (δ^i ; i.e., the delta notation). Second, we express all data relative to the most widely accepted standard for
138 each isotope system. For many isotope systems, the most widely accepted standard may have since been
139 exhausted (e.g., JMC-Lyon for Zn). In those cases, there are usually cross-calibrated secondary materials
140 that can be used to report new isotope data in terms of ‘legacy’ materials (e.g., AA-ETH for Zn, Archer et
141 al., 2017). Third, we report trace metal isotope data using the same isotope ratio pairs and reference
142 materials as used in the GEOTRACES data products (e.g., Mawji et al., 2015; Schlitzer et al., 2018). We
143 note that isotope data are a unitless ratio quantity (Coplen, 2011), though are commonly reported with
144 ‘units’ of ‰ (i.e., parts per one thousand):

$$145 \quad \delta^i \text{Me} = R_{\text{sample}} / R_{\text{standard}} - 1 \quad [4]$$

146 where $\delta^i \text{Me}$ and R are listed for each element in Table 1. For clarity, all isotopic data reviewed here have
147 been calculated using notation in Eq. 4, and renormalized to the standards listed in Table 1, regardless of
148 how the data originators reported their results.

149 We denote the concentrations of different species using square brackets (i.e., []). Unless specifically stated,
150 all concentrations refer to dissolved species; for example, [Fe] denotes dissolved Fe concentrations, and
151 [Me] denotes the concentration of a metal (‘Me’) in a general case. Salient features of each trace metal
152 isotope system are summarized in Table 1.

153

154

155

156 **Table 1 | Summary of oceanic dissolved concentrations, isotope notation, standards, and isotopic**
 157 **compositions, and mean ocean residence times for trace metals discussed in this review.** Superscripts denote
 158 references listed in the Data Sources section.

159

Element	Dissolved concentration range (nmol kg ⁻¹)	$\delta^i\text{Me}$ and R	Standard used for $\delta^i\text{Me}$	Mean Upper Continental Crust $\delta^i\text{Me}$ (‰)	Mean deep ocean $\delta^i\text{Me}$ (‰)	Range of deep ocean $\delta^i\text{Me}$ (‰)	Residence time estimates (kyr)
Fe	0.01–100 ^a	$\delta^{56}\text{Fe}$, $^{56}\text{Fe}/^{54}\text{Fe}$	IRMM-014 ^e	+0.1 ^m	Variable ^t	-2.4 to +1.5 ^t	0.004–0.6 ^{aa}
Zn	0.01–10 ^a	$\delta^{66}\text{Zn}$, $^{66}\text{Zn}/^{64}\text{Zn}$	JMC-Lyon ^f	+0.3 ^f	≈+0.5 ^u	-0.2 to +0.6 ^u	1–11 ^{aa}
Cu	0.5–4 ^a	$\delta^{65}\text{Cu}$, $^{65}\text{Cu}/^{63}\text{Cu}$	NIST SRM 976 ^f	+0.1 ^f	≈+0.7 ^v	+0.6 to +0.8 ^v	2–5 ^{aa}
Cd	0.00003–1.2 ^a	$\delta^{114}\text{Cd}$, $^{114}\text{Cd}/^{110}\text{Cd}$	NIST SRM 3108 ^g	0.0 ⁿ	≈+0.3 ^w	+0.2 to +0.4 ^w	22–105 ^{aa}
Mo	100 ^b	$\delta^{98}\text{Mo}$, $^{98}\text{Mo}/^{95}\text{Mo}$	NIST SRM 3134 + 0.25‰ ^h	≤0.4 ^o	≈+2.3 ^x	Homogeneous ^x	440 ^{ab}
Ba	35–160 ^a	$\delta^{138}\text{Ba}$, $^{138}\text{Ba}/^{134}\text{Ba}$	NIST SRM 3104a ⁱ	0.0 ^p	≈+0.3 ^y	+0.2 to +0.4 ^y	8 ^{ac}
Ni	1.5–11 ^a	$\delta^{60}\text{Ni}$, $^{60}\text{Ni}/^{58}\text{Ni}$	NIST SRM 986 ^j	+0.1 ^q	≈+1.3 ^z	+1.2 to +1.5 ^z	10–30 ^{ad}
Cr	1–7 ^c	$\delta^{53}\text{Cr}$, $^{53}\text{Cr}/^{52}\text{Cr}$	NIST SRM 979 ^k	-0.12 ^f	≈+0.8 ^c	0.6–1.2 ^c	6 ^{ac}
Ag	0.0002–0.1 ^d	$\delta^{109}\text{Ag}$, $^{109}\text{Ag}/^{107}\text{Ag}$	NIST SRM 978a ^l	0.0 ^s	Unknown	Unknown	0.4 ^{af}

160

161 **2.1.2. Paleoproductivity**

162 We define paleoproductivity as the productivity of an ecosystem that contributes to the sequestration of
 163 atmospheric CO₂ as POC in the ocean interior and on the seafloor. Our definition of paleoproductivity is

164 therefore analogous to that of NEP (net ecosystem productivity), which is defined as gross primary
165 production minus autotrophic and heterotrophic respiration and where gross primary production is the total
166 autotrophic production of POC (or O₂; Eq. 1; Sigman & Hain, 2012). If considering only the euphotic zone,
167 NEP is equivalent to export production, which is an important component of the biological carbon pump
168 (Boyd et al., 2019); indeed, changes in export production have been implicated as a major driver of
169 variations in glacial–interglacial *p*CO₂ and hence climate (e.g., Broecker, 1982; Boyle, 1988a; Berger et al.,
170 1989; Paytan, 2009). Many of these changes in past export production were inferred on the basis of
171 variations in the cycling of major nutrients and their isotopes (e.g., N, Si; Farmer et al., *this volume*). The
172 net consumption of nutrients can be interpreted in terms of export production by assuming a fixed
173 proportionality between the major nutrients and C. This proportionality therefore allows the connection of
174 major nutrient cycles to the sequestration of atmospheric CO₂ via biological productivity. In the next
175 section, we outline how such a framework can be similarly applied to interpret the distributions of bioactive
176 metals and their isotopes in terms of export productivity.

177

178 **2.2. From nutrients to productivity**

179 The cycling of nutrients is intimately connected with productivity; along with sunlight, nutrients are the
180 fuel that powers the biological pump. In turn, the biological pump renders systematic changes in the
181 concentration and isotopic composition of nutrients throughout the oceans. Assuming that these changes
182 follow certain known rules, we can use bioactive metals and their isotopes as tracers of biological
183 productivity in Earth’s past. In this section we describe how nutrient uptake can generate isotope variations
184 in seawater and develop a framework for linking nutrients with productivity that applies to several of the
185 isotope systems reviewed here.

186

187 *2.2.1. The isotope reactor model*

188 Here we use an example whereby an hypothetical micronutrient metal (‘Me’) is supplied to, and consumed
189 within, an isotope reactor (Fig. 2). Though a simple, non-dimensional representation of myriad
190 oceanographic processes, isotope reactor models have found utility in describing the marine behaviors of
191 macro- (e.g., N; Sigman et al., 1999; Si, Reynolds et al., 2006) and micronutrients (e.g., Ba, Horner et al.,
192 2015; Cd, Abouchami et al., 2011; Cr, Scheiderich et al., 2015; Ni, Yang et al., 2020). Reactor models
193 assume that a Me is only consumed within the reactor, and that consumption is modeled as a single reaction
194 with a fixed isotope separation factor, Δ_{P-R} , defined as:

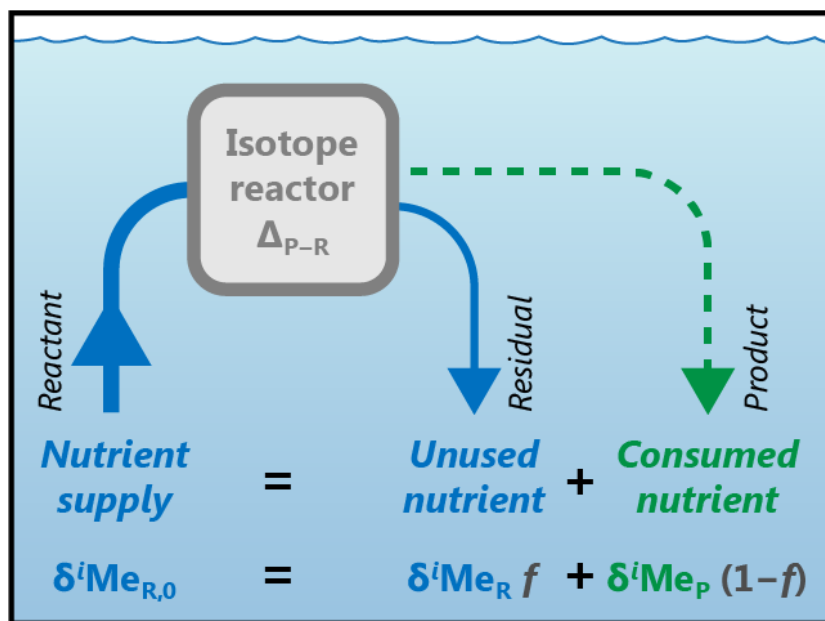
195 $\Delta_{P-R} \equiv \delta^i Me_P - \delta^i Me_R$ [5]

196 where $\delta^i Me_P$ and $\delta^i Me_R$ are the stable isotope compositions of the product (phytoplankton) and reactant
 197 (dissolved nutrient), respectively (see Eq. 4).

198 Following reaction, there may be a fraction of the initial micronutrient Me that remains unused, which we
 199 term f :
 200

201 $f = \text{Unused nutrient} / \text{Nutrient supplied}$ [6]

202 where the nutrient terms represent quantities and f is unitless. (It follows that the fraction of nutrient
 203 consumed by phytoplankton equals $1 - f$.) In systems where most nutrients are consumed, f will be close
 204 to zero. However, when productivity is limited by some other resource, such as another nutrient (e.g., Fe,
 205 Co) or light, systems will exhibit f that can approach the theoretical maximum of one.
 206
 207
 208
 209

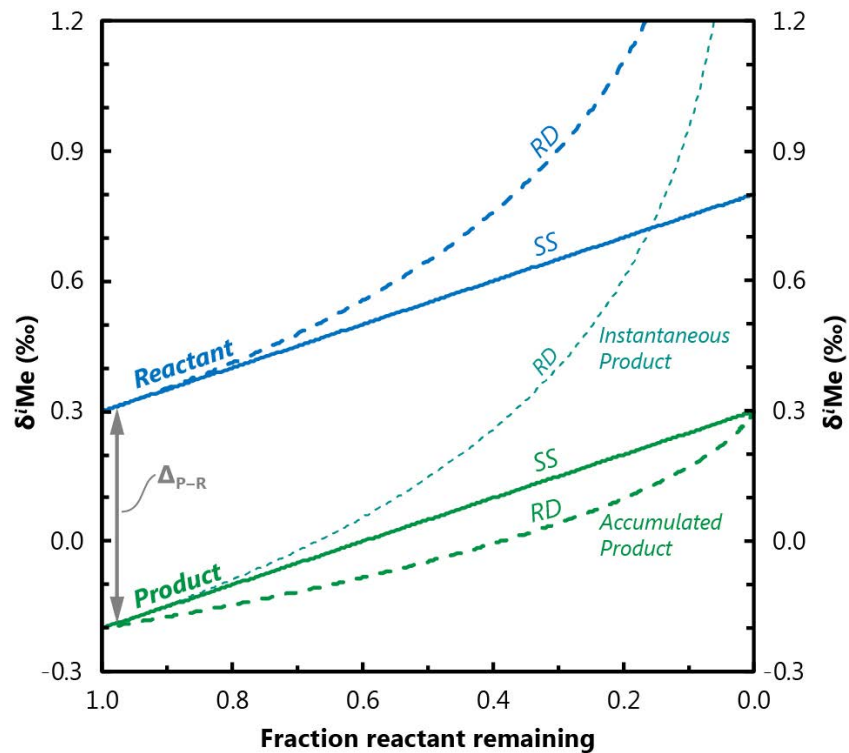


210
 211 **Figure 2 | Overview of a single-process reactor with an isotope separation factor Δ_{P-R} .** The reactor is assumed
 212 to follow the principles of isotope mass balance, in that the isotope composition of the residual unused nutrient ($\delta^i Me_R$)
 213 and consumed nutrient ($\delta^i Me_P$) sum to the isotope composition of metal initially supplied to the reactor ($\delta^i Me_{R,0}$)
 214

215
 216 The isotope composition of the residual nutrients and product phytoplankton will evolve over the course of
 217 a reaction. The precise nature of their evolution depends on three factors: the progress of the reaction,

218 quantified in terms of the fraction of the initial reactant remaining (i.e., f); the magnitude and sign of Δ_{P-R} ;
 219 and, whether the system is ‘open’ or ‘closed.’ If the system remains open during the course of reaction,
 220 with the addition of new reactants balanced by the removal of product plankton and residual reactant, the
 221 system will follow Steady State behavior (SS). Alternatively, if the system is closed before and during the
 222 reaction, the system will follow Rayleigh Distillation (RD). We illustrate the effect of open- versus closed-
 223 system behavior using an example in which a reactant metal, possessing an initial isotope composition,
 224 $\delta^i\text{Me}_{R,0}$, of +0.3 ‰ is reacted to form a product assuming $\Delta_{P-R} = -0.5 \text{ ‰}$ (Fig. 3).

225
 226



227

228 **Figure 3 | Isotopic evolution of a hypothetical metal (Me) in a reactor as a function of initial reactant remaining.**
 229 The metal is supplied to a reactor with an initial composition, $\delta^i\text{Me}_{R,0}$, of +0.3 ‰, where it is reacted with an isotope
 230 separation factor, Δ_{P-R} , of -0.5 ‰. The evolution of the reactants and products are shown for open-system behavior at
 231 SS (Steady State, solid lines; Eqs. 7, 8) and closed-system RD (Rayleigh Distillation, dashed lines) for both the
 232 Instantaneous (Eq. 10) and Accumulated Products (Eq. 11). This example illustrates that the isotope evolution of the
 233 residual reactant is strongly dependent on whether the system is open or closed during the course of the reaction.

234

235

236 If Me supply and removal from the system are continuous, the system is considered open and will follow
 237 the lines marked SS (Fig. 3). The SS scenario applies if the residual reactant Me is exported along with Me
 238 consumed by plankton, and that the sum of these removal terms are exactly balanced by Me resupply to the

239 reactor. To define SS behavior, we draw on the simplifying approximations described by Johnson et al.
 240 (2004), whereby the the isotope composition of the SS product follows:

$$241 \delta^i \text{Me}_P \approx \delta^i \text{Me}_{R,0} + f \Delta_{P-R} \quad [7]$$

242
 243 Because of this simplification, the isotope composition of the SS reactants, $\delta^i \text{Me}_R$, at a given value of f is
 244 simply:
 245

$$246 \delta^i \text{Me}_R \approx \delta^i \text{Me}_P - \Delta_{P-R} \quad [8]$$

247
 248 and thus the reactant isotope composition will not exceed $\delta^i \text{Me}_{R,0} - \Delta_{P-R}$.
 249

250
 251 If the reactor is closed before and during reaction, the system will follow the lines marked RD (Fig. 3). We
 252 define RD using the simplifying approximations of Mariotti et al. (1981). These approximations are
 253 unlikely to introduce significant systematic errors for the metals discussed here since they exhibit modest
 254 isotope variations (see Hayes, 2004). Unlike SS, the RD residual reactant isotope composition can evolve
 255 to extremely fractionated isotope compositions under as $f \rightarrow 0$:

$$256 \delta^i \text{Me}_R \approx \Delta_{P-R} \ln f + \delta^i \text{Me}_{R,0} \quad [9]$$

257
 258 The RD product formed at any point in the reaction is always offset from the reactant by -0.5% . This is
 259 termed the instantaneous product, $\delta^i \text{Me}_{IP}$ (Fig. 3), defined as:
 260

$$261 \delta^i \text{Me}_{IP} \approx \delta^i \text{Me}_R + \Delta_{P-R} \quad [10]$$

262
 263 The RD Accumulated Product, $\delta^i \text{Me}_{AP}$, represents the integration of the instantaneous products formed up
 264 until that point in the reaction, given by:
 265

$$266 \delta^i \text{Me}_{AP} \approx \frac{\Delta_{P-R} f \ln f}{f-1} + \delta^i \text{Me}_{R,0} \quad [11]$$

267
 268 Regardless of whether the system follows SS or RD behavior, the first product formed will exhibit $\delta^i \text{Me}_P$
 269 offset from $\delta^i \text{Me}_{R,0}$ by Δ_{P-R} (double-ended arrow in Fig. 3). Likewise, at $f = 0$, $\delta^i \text{Me}_P = \delta^i \text{Me}_{R,0}$.
 270

271

272

273 *2.2.2. From reactors to relative nutrient utilization*

274 The isotope reactor models may be used to interpret metal isotope variations in the geological record in
 275 terms of Me supply and demand in the surface ocean. This is possible if one considers the reaction progress
 276 term in the reactors as being analogous to the fraction of initially supplied nutrient left unconsumed by
 277 phytoplankton (i.e., f). A major benefit of this approach is that it does not require that the initial
 278 concentration of metal ($[Me_{R,0}]$) supplied to the reactor be known, only its initial isotope composition,
 279 $\delta^i Me_{R,0}$. However, the models do require assuming that the isotope separation factor during Me removal
 280 from seawater, Δ_{P-R} , has remained constant over time and that $\delta^i Me_{R,0}$ does not vary. If these assumptions
 281 are justified, the reactor framework enables estimation of f from the Me isotope composition of either the
 282 residual reactants (seawater) or products (exported Me). For example, if a sedimentary archive were to
 283 accurately capture $\delta^i Me_R$, the isotope composition of a metal following reaction, f can be calculated
 284 assuming RD using:

285

$$286 \quad \ln f \approx (\delta^i Me_R - \delta^i Me_{R,0}) / \Delta_{P-R} \quad [12]$$

287

288 or, if the reaction follows SS, using:

289

$$290 \quad f \approx (\delta^i Me_R + \Delta_{P-R} - \delta^i Me_{R,0}) / \Delta_{P-R} \quad [13]$$

291

292 Likewise, f can be estimated from the isotope composition of exported products, $\delta^i Me_P$, assuming SS
 293 behavior using:

294

$$295 \quad f \approx (\delta^i Me_P - \delta^i Me_{R,0}) / \Delta_{P-R} \quad [14]$$

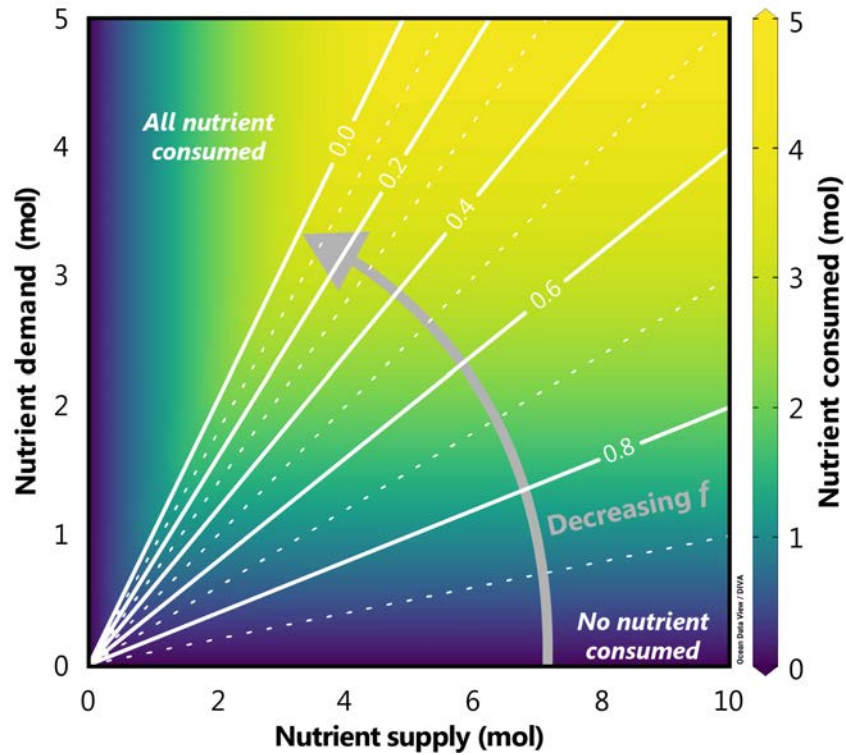
296

297 (There is no equivalent approximation for computing f from $\delta^i Me_P$ assuming Rayleigh Distillation.)

298

299 Equations 12–14 illustrate how metal isotope compositions can be used to calculate f . However, f is a
 300 measure of the relative utilization of nutrients in a system, and does not confer direct information about the
 301 size and thus total productivity of that system. This point is illustrated in the example shown in Fig. 4,
 302 where we plot the demand for a nutrient by phytoplankton in a reactor against the initial quantity of nutrient
 303 supplied to the reactor (i.e., both axes represent quantities), with contours representing various f . These
 304 lines illustrate that a wide range of possible nutrient consumptions—and thus net ecosystem production—

305 are possible for any value of f . Put another way, if all that was known about a system was f , it would be
306 difficult to determine the productivity of that system.
307



308
309 **Figure 4 | Relationships between nutrient demand, supply, and consumption.** The y- and x-axes represent
310 combinations of nutrient demand and supply, respectively. The total nutrient consumed by phytoplankton for each
311 combination is illustrated by the shading; productive systems exist in the upper-right portion of the figure, where nutrient
312 supply and demand are high, and unproductive systems are found close to the figure axes, where supply and demand
313 are mismatched. Between these two extremes are moderately productive systems. The fraction of nutrients unused in
314 these systems, f , is shown by the contour lines. This figure illustrates that f cannot be used in isolation to estimate
315 productivity.

316
317 Interpreting f in terms of ocean productivity requires an independent constraint on the nutrient supply,
318 unused nutrient, or consumed nutrient (Fig. 4). A common and powerful approach is to use the flux of
319 bioactive metals to sediments as an indicator of past nutrient consumption (e.g., Eagle et al., 2003;
320 Brumsack, 2006; Tribovillard et al., 2006). By assuming a fixed Me:C stoichiometry, bioactive metal fluxes
321 can then be interpreted in terms of C export productivity. The isotope composition of Me is then used as an
322 indicator of the balance between supply and demand for Me in that system (i.e., f), which is sensitive to
323 factors such as ocean circulation and ecosystem structure (e.g., François et al., 1997). These approaches are
324 especially powerful when the constraints on export and f are derived from the same Me system—barite
325 mass accumulation rates and $\delta^{138}\text{Ba}$ (e.g., Bridgestock et al., 2019), [Cd] and $\delta^{114}\text{Cd}$ (e.g., Georgiev et al.,

326 2015), [Zn] and $\delta^{66}\text{Zn}$ (e.g., Kunzmann et al., 2013)—since this minimizes potential confounding influences
327 from other metal cycling processes, discussed next.

328

329 **2.3. Other trace metal cycling processes**

330

331 The framework outlined in Sec. 2.2. represents an idealized situation that implicitly assumes that
332 phytoplankton productivity dominates the marine cycling of a trace metal. As we show in subsequent
333 sections, many other processes cycle the bioactive trace metals and their isotopes in the marine realm;
334 indeed, depending on the metal and the type of process, other factors—not directly related to productivity—
335 may even dominate the cycling of that metal. Below we introduce a number of these processes, which we
336 group into three broad categories: biological, chemical, and physical. While these three categories of
337 cycling processes may appear as insurmountable obstacles to the reliable application of a metal isotope
338 system to reconstruct paleoproductivity, there are two reasons to be optimistic. First, that so many cycling
339 processes are now recognized highlights how far our understanding of trace metal geochemistry has evolved
340 in recent years. Second, the multiple sensitivities of these metal systems to various ocean processes means
341 that bioactive metals and their isotopes may be applied in concert to constrain multiple aspects of past ocean
342 chemistry. Multi-proxy approaches are a familiar feature of the paleoredox landscape and are likely to
343 become increasingly common for constraining paleoproductivity (e.g., Cd and Zn, John et al., 2017, Sweere
344 et al., 2020; Cd and Cr, Frei et al., 2021).

345

346 *2.3.1. Biological*

347 Biological processes exclusive of productivity can play an important role in marine trace metal behavior.
348 The example described above assumes that organisms exhibit inflexible Me:C stoichiometries, whereas in
349 reality many marine microbes appear to have wide tolerances for the intracellular proportions of certain
350 trace elements compared to those of C, N, and P. The physiological mechanisms enabling these wide
351 tolerances, and the feedback interactions that drive them, are beyond the scope of this review, and are
352 discussed in detail elsewhere (e.g., Sunda, 2012; Morel et al., 2020). From a proxy perspective, this
353 flexibility may cause uncertainty in paleoproductivity estimates; the more variable the Me:C stoichiometry
354 of organisms within an ecosystem, the more uncertain the paleoproductivity estimate derived from that Me.
355 (The corollary being that the more rigid the stoichiometry, the more robust the paleoproductivity estimate.)
356 An extreme example concerns nonessential elements (e.g., Ag), or metals that are only essential for certain
357 groups of organisms within an ecosystem (e.g., Mo for nitrogen fixers). Productivity estimates derived from

358 the export of these nonessential elements are potentially most susceptible to decoupling from productivity
359 cycles as their export is not intrinsically tied to the overall functioning of an ecosystem.

360

361 Similarly, the reactor models assume that nutrient uptake is well described by a single and fixed isotope
362 separation factor, Δ_{P-R} . A number of studies showed that this assumption is violated for Zn; different
363 phytoplankton (e.g., Köbberich & Vance, 2017; 2019) and—depending on environmental conditions—even
364 a single organism (e.g., John et al., 2007; Köbberich & Vance, 2017) can exhibit a range of Δ_{P-R} . Whether
365 such behavior is also seen for other metal isotope systems is unknown, but could be important given that
366 calculation of f is dependent on Δ_{P-R} (Eqs. 12–14).

367

368 Biological processes can potentially exert an additional control on bioactive metal isotope distributions
369 through remineralization—the regeneration of POC to inorganic nutrients. In the case of a scarce nutrient,
370 such as Fe, individual organisms (e.g., Saito et al., 2011) and even entire ecosystems (e.g., Rafter et al.,
371 2017) may have evolved mechanisms to retain certain nutrients. Likewise, macro- and micronutrients may
372 be regenerated by heterotrophic organisms at different rates (e.g., Twining et al., 2014; Ohnemus et al.,
373 2019), which could affect the Me:C stoichiometry of exported POC and thus the accuracy of Me-derived C
374 export fluxes. Even less is known about the role of heterotrophs in fractionating POC-associated metal
375 isotope compositions, which could be significant for some metals (e.g., Cd, Janssen et al., 2019).

376

377 Lastly, many of the metals reviewed here form complexes with organic ligands. Indeed, for some metals,
378 such as Fe and Cu, almost the entire oceanic inventory is bound to organic ligands. The effect of ligands on
379 trace metal cycling is an area of active research, and is potentially important from the perspective of
380 modulating isotope fractionation during uptake by plankton and into secondary Me sinks. Where known,
381 these effects are discussed in the relevant sections.

382

383 *2.3.2. Chemical*

384 There are several chemical transformations that can modulate marine trace metal distributions without
385 affecting C, such as scavenging and precipitation–dissolution reactions. Scavenging, meaning adsorption
386 and desorption, can alter Me:C relationships by redistributing metals, but not C. Originally developed in
387 the context of dissolved and particulate thorium isotopes (Bacon & Anderson, 1982), reversible scavenging
388 is now suggested to play a role in the vertical cycling of other metals, including Cu (e.g., Little et al., 2013),
389 Fe (e.g., Abadie et al., 2017), and Zn (e.g., Weber et al., 2018). Reversible scavenging is a continuous
390 process that occurs between particle surfaces and dissolved species. While this process can occur at any
391 depth, scavenging intensity is positively correlated with the quantity of particles, and so is most important

392 in the upper water column. Likewise, while dissolved metals may be scavenged by any class of particle
393 (e.g., opal, lithogenics), certain particle types may preferentially scavenge certain elements (e.g., Lerner et
394 al., 2018). Scavenging can even affect trace metals cycled predominantly by organic matter; secondary
395 phases may scavenge metals during remineralization, which can affect trace metal distributions in the upper
396 water column (e.g., Zn, John & Conway, 2014; Co, Hawco et al., 2018; Fe, Tagliabue et al., 2019).

397
398 Precipitation and dissolution of minerals is also a consideration for certain trace metals discussed here.
399 However, the relative importance of mineral cycling depends on the metal and the redox environment. For
400 example, Ba is primarily cycled by the mineral barite, rather than POC, and the thermodynamics of
401 precipitation vary throughout the ocean (e.g., Rushdi et al., 2000). Changes in the ambient redox
402 environment, such as in an oxygen minimum zone (OMZ), may even enhance dissolved–particulate
403 transformations for certain trace metals. Some metals, such as Fe, may have large sources in OMZs
404 associated with the reductive dissolution of particulate Fe–Mn oxides. Other metals may experience
405 enhanced removal via precipitation into sulfide minerals (e.g., Zn, Cu, Cd, Mo, Ni, Ag; Helz et al., 1996;
406 McKay & Pedersen, 2008; Kramer et al., 2011; Janssen et al., 2014; Vance et al., 2016; Bianchi et al., 2018;
407 Guinoiseau et al., 2019). The net effect of these non POC-associated transformations is that processes other
408 than POC cycling may redistribute trace metals, but not C, within the ocean interior. If significant, these
409 processes could drive the ocean to a different Me:C stoichiometry and/or dissolved metal isotope
410 composition that could impact calculations of export and f , respectively, when using the nutrient utilization
411 framework described in Sec. 1.3.

412 413 *2.3.3. Physical*

414 The physical circulation of the ocean exerts a major control on many oceanic TEI distributions and we
415 describe this influence on our 9 trace metals in detail in later sections. In addition to circulation, there are
416 also scale dependencies that can affect trace metal based productivity estimates at both small and large
417 scales, as well as other, non-productivity metal sinks. At the local to regional scale, Me point sources may
418 be significant if they mask any POC-related Me drawdown. Though perhaps less significant for C, point
419 sources—rivers, dust, desorption from particles, sediments, and hydrothermalism—may be significant
420 terms in local and regional trace metal budgets if the magnitude is comparable to the dissolved supply from
421 ocean circulation. Examples include dust-derived Cu to surface planktonic communities (e.g., Paytan et al.,
422 2009) and hydrothermal-derived Fe to the deep ocean (e.g., Resing et al., 2015). Consideration of these
423 external sources is particularly important when productivity estimates are derived close to such point sources
424 and for metals with residence times that are less than or similar to the mixing time of the ocean (~1 kyr).

425

426 At larger scales, the location of a site and the assumption of steady state can influence the calculation of f .
427 The importance of location is illustrated using the examples in Fig. 4. Close to an upwelling source of metal,
428 such as in the modern Southern Ocean, f is, by definition, close to one and decreases downstream into the
429 low latitudes. Given this dependence, it follows that a change in ocean circulation geometry could influence
430 the spatial pattern of f without any net changes in productivity. This is particularly important to consider
431 from a paleoceanographic perspective, since records are typically generated from fixed locations (i.e.,
432 sediment cores), making it challenging to determine if variations in f originated from overlying changes in
433 ocean circulation or productivity. One solution to this challenge is to obtain an independent constraint on
434 ocean circulation, such as from another isotope system or using a model. Alternatively, the spatial pattern
435 of f could be discerned from multi-site reconstructions of Me distributions.

436

437 On a global scale, the assumption of steady state can affect how productivity is estimated from Me reactor
438 models. The input and output fluxes of a metal through the ocean should balance, regardless of productivity.
439 Likewise, the flux-weighted metal isotope composition of inputs and outputs should also balance. Thus, at
440 large scales, the isotopic composition of a sedimented Me should reflect the average input $\delta^i\text{Me}$, regardless
441 of mean ocean f . Such a situation is possible because the flux terms interact. As an example, we return to
442 the metal in Fig. 3. We will assume that this metal follows SS behavior and that biological productivity is
443 the only sink of this metal from seawater. If the mean marine input of this metal possessed $\delta^i\text{Me} = -0.1 \text{ ‰}$,
444 the system would only be in steady state if, on a global basis, $f = 0.8$. However, if mean global f were to
445 decrease to 0.2 (i.e., a smaller fraction of this nutrient Me is left unused), mean global $\delta^i\text{Me}_P$ would increase
446 from -0.1 to $+0.2 \text{ ‰}$, which no longer matches the input $\delta^i\text{Me}$ of -0.1 ‰ . Such an imbalance cannot be
447 sustained indefinitely, since the ocean would be losing more ‘heavy’ Me than is being added. As such, the
448 ocean would gradually compensate by a lowering of $\delta^i\text{Me}_{R,0}$ to 0.0 ‰ . In turn, mean ocean $\delta^i\text{Me}_P$ would
449 return to values $\approx -0.1 \text{ ‰}$, even if f remained at 0.2. This example illustrates how ocean-scale processes
450 can influence the relationship between trace metals and productivity, even if productivity is the main sink
451 of a metal from a system.

452

453 Lastly, the relationship between Me and productivity— $\delta^i\text{Me}_{R,0}$, and potentially, $[\text{Me}_{R,0}]$ —can also be
454 influenced by non-productivity Me sinks. Indeed, non-productivity sink terms are of considerable
455 significance for many of the trace metals reviewed here. The significance of these terms may offer another,
456 indirect means to constrain paleoproductivity: if non-productivity Me sinks possess different Δ_{P-R} and/or
457 Me:C to productivity-related sinks, mean deep ocean $\delta^i\text{Me}$ and/or $[\text{Me}]$ will be sensitive to the relative
458 balance of Me burial between the various sink terms, analogous to the canonical C cycle mass balance (e.g.,
459 Berner et al., 2000). For example, if assuming fixed Me inputs over time and that whole-ocean productivity

460 abruptly decreased, the relative significance of non-productivity Me sinks would increase to compensate
461 for the decrease in productivity. This compensation could drive deep ocean $\delta^3\text{S}$ and/or [Me] to new values
462 that are sensitive to the balance between productivity and Me burial by other sinks. This multi-sink
463 framework similarly underpins the use of many TEI-based redox proxies (e.g., Tl, Owens et al., 2017; U,
464 Montoya-Pino et al., 2010), though this approach is relatively underexplored in the context of reconstructing
465 paleoproductivity.

466

467

468 3. Iron

469 Iron plays a key role within phytoplankton as an electron carrier for photosynthesis and respiration
470 processes, as well as within enzymes necessary for photosynthesis and nitrogen fixation (Morel & Price,
471 2003). However, in oxygenated seawater, Fe(II) is rapidly oxidized to Fe(III), which is highly insoluble
472 (Liu & Millero, 2002). Intense biological demand coupled to low solubility results in generally sub-
473 nanomolar [Fe] throughout the oceans, approaching the low picomolar range in some surface regions far
474 from Fe sources, such as the vast Southern Ocean and North Pacific (e.g., Fig. 5; Chever et al., 2010;
475 Klunder et al., 2011; Schlitzer et al., 2018). Consequently, biological production in about 30 % of the
476 modern surface ocean is thought to be limited primarily by Fe (Moore et al., 2013), principally in upwelling
477 regions where deep water is depleted in Fe relative to the macronutrients nitrate (NO_3^-) and phosphate
478 (PO_4^{3-} ; e.g., Moore, 2016; Boyd et al., 2017). In these regions, termed ‘High Nutrient Low Chlorophyll’
479 (HNLC), Fe supply can limit primary productivity (e.g., Martin & Fitzwater, 1988) and potentially the
480 exchange of carbon between the ocean and atmosphere. Furthermore, a changing supply of Fe from sources
481 such as atmospheric dust, hydrothermal venting, or sedimentary release to the surface oceans through
482 geological time can exert a significant control on both the distribution of primary productivity in the oceans
483 and, through this, the global carbon cycle. Changes in supply of dust to the Fe-limited Southern Oceans has
484 been shown to correlate with climate variability on millennial time scales and has also been invoked to
485 explain the dramatic sawtooth glacial–interglacial shifts in atmospheric carbon dioxide (Martin, 1990;
486 Sigman & Boyle, 2000; Martínez-García et al., 2011; 2014).

487 The strong link between Fe supply and primary productivity suggests that ratios of Fe to other elements
488 and/or Fe isotope ratios ($\delta^{56}\text{Fe}$) might be useful proxies for paleoproductivity. However, in the vast majority
489 of settings, $\delta^{56}\text{Fe}$ and Fe flux records do not reflect paleoproductivity; the influence of the major Fe sources
490 and their redox-driven cycling exert far stronger controls over marine Fe geochemistry compared to
491 biological productivity. Thus, a simple reactor framework, as outlined in Sec. 2.2.1, cannot be applied to
492 $\delta^{56}\text{Fe}$. However, we note that there are a number of promising archives of paleo Fe isotope chemistry,
493 particularly for the deep ocean, and we anticipate that these records will prove most valuable as context for

494 interpreting other proxy records, or for generating novel hypotheses regarding the connections between Fe
495 sources, biological productivity, and global climate.

496

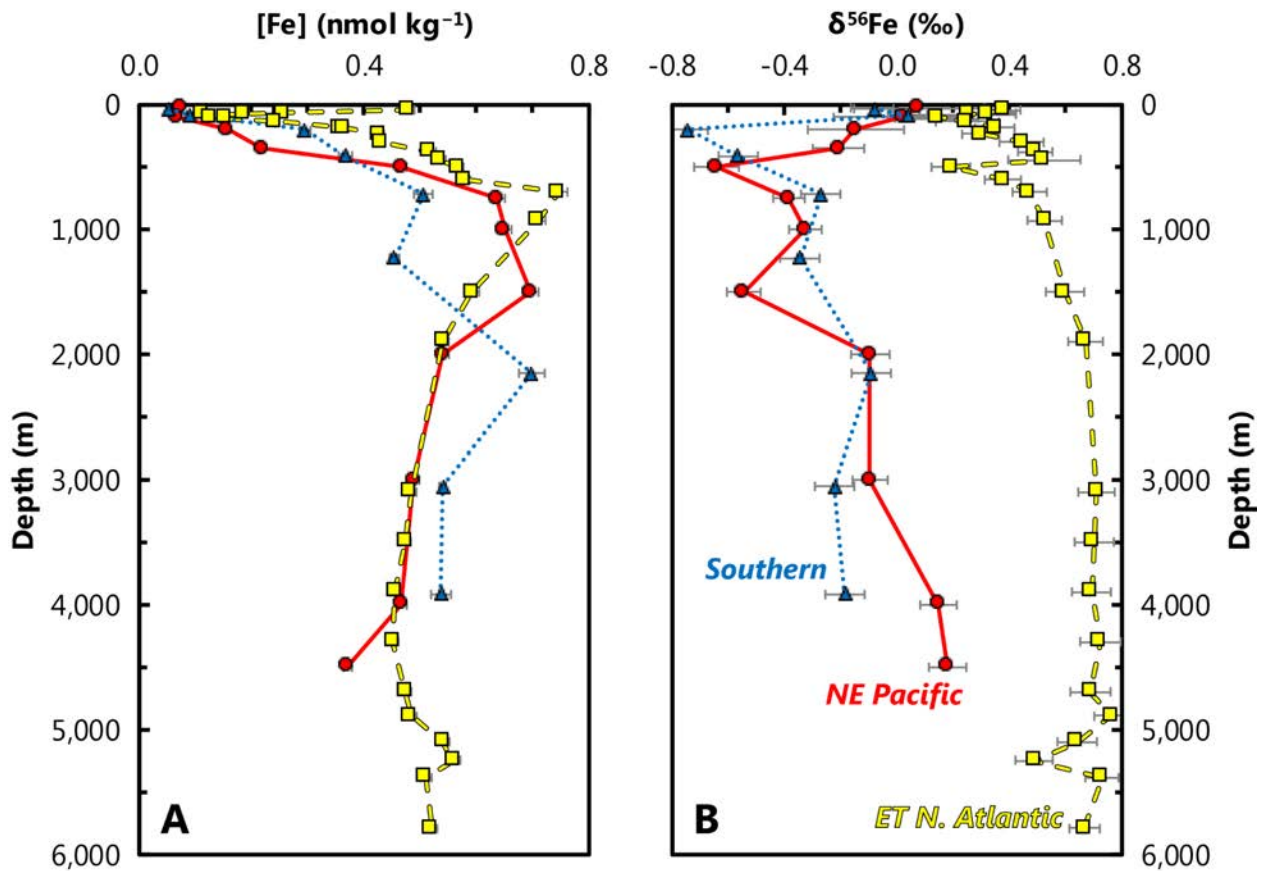
497 **3.1. Marine distribution**

498 The distribution of dissolved Fe in seawater is driven by a mixture of competing processes, including:
499 biological uptake and regeneration; distinct sources of Fe at shallow, intermediate, and deep depths;
500 adsorption–desorption processes onto organic and lithogenic particles; dissolution and precipitation
501 processes; and, complexation to organic ligands (Fig. 6; e.g., Boyd & Ellwood, 2010; Labatut et al. 2014;
502 Tagliabue et al., 2017). As a result, [Fe] displays what has historically been termed as a hybrid-type depth
503 profile in the open ocean, which exhibits a number of similarities between different ocean basins (Fig. 5).
504 Surface Fe is drawn down in surface waters by biological uptake, and [Fe] can even be as low as 0.01 nmol
505 kg⁻¹ in Fe limited regions (Schlitzer et al., 2018). However, some areas of the oceans, such as the ‘dusty’
506 North Atlantic, surface [Fe] can be driven as high as 2 nmol kg⁻¹ as a result of dust deposition events
507 (Sedwick et al., 2005). Below the surface mixed layers, regeneration of biogenic material, reversible particle
508 scavenging, and complexation by organic ligands all act to keep the background deep ocean [Fe] at around
509 0.4–0.6 nmol kg⁻¹ (e.g., Lauderdale et al., 2020). Against this background, it has been known for decades
510 that [Fe] in deeper waters are elevated near point sources such as sedimentary margins (Johnson et al.,
511 1999). Recently, however, a range of studies including those conducted as part of the GEOTRACES
512 program, have illuminated this picture, showing that deep sources of Fe—such as sedimentary and
513 hydrothermal release—are widespread, may have distinct traceable $\delta^{56}\text{Fe}$ source signatures, and that this
514 Fe can be transported over large distances through the ocean interior (e.g., Radic et al. 2011; Saito et al.,
515 2013; Conway and John, 2014; Resing et al., 2015; Nishioka et al., 2020). Despite exhibiting well-defined
516 deep maxima close to point sources, [Fe] distributions at shallow and intermediate depths are much more
517 variable and models have struggled to reproduce these variations (e.g., Tagliabue et al., 2016). The extent
518 to which deeply sourced Fe is supplied to surface seawater is thus equivocal (e.g., Tagliabue et al., 2010;
519 Roshan et al., 2020).

520

521 The origin of [Fe] variability in the shallow and intermediate ocean is thought to reflect local differences in
522 the competition between uptake, regeneration, sources, and scavenging. The same processes influence
523 $\delta^{56}\text{Fe}$; however, unlike variations in [Fe], $\delta^{56}\text{Fe}$ exhibits dramatic variability between—and even within—
524 ocean basins (Fig. 5; Schlitzer et al., 2018). Such water column variability in $\delta^{56}\text{Fe}$, from isotope
525 compositions as light as -4‰ (Charette et al., 2020), to as heavy as $+2\text{‰}$ (Ellwood et al., 2020), is thought

526 to be driven by Fe source signatures and therefore also oceanic circulation, and a combination of biological
 527 uptake, Fe complexation to organic ligands in surface waters, and non-reductive release of dissolved Fe
 528 from particles (notably lithogenic particles) during desorption and/or ligand-promoted dissolution (e.g.,
 529 Conway and John, 2014; Abadie et al. 2017; Ellwood et al., 2020; Fig. 6). These processes can render
 530 remarkably different $\delta^{56}\text{Fe}$ profiles, even when profiles of $[\text{Fe}]$ are similar, such as in the examples from
 531 the Northeast Pacific, Eastern Tropical North Atlantic, and the Weddell Sea of the Southern Ocean (Fig.
 532 5). In the North Pacific and North Atlantic examples, the deep distribution of $\delta^{56}\text{Fe}$ is considered to be most
 533 strongly influenced by the dominant regional Fe source—dust in the Atlantic and Fe released from
 534 continental margins in the Pacific (Conway and John, 2014; Conway and John, 2015b). In the Weddell Sea,
 535 the deep $\delta^{56}\text{Fe}$ distribution has been attributed to regeneration of biogenic light Fe at depth (Abadie et al.,
 536 2017), or, more recently, to addition of light Fe from regional sedimentary release (Sieber et al., 2021).
 537 Thus, $\delta^{56}\text{Fe}$ may provide insight to the contribution of Fe sources at the basin scale (e.g., Conway & John,
 538 2014a), as well as for Fe cycling processes such as uptake and regeneration.
 539



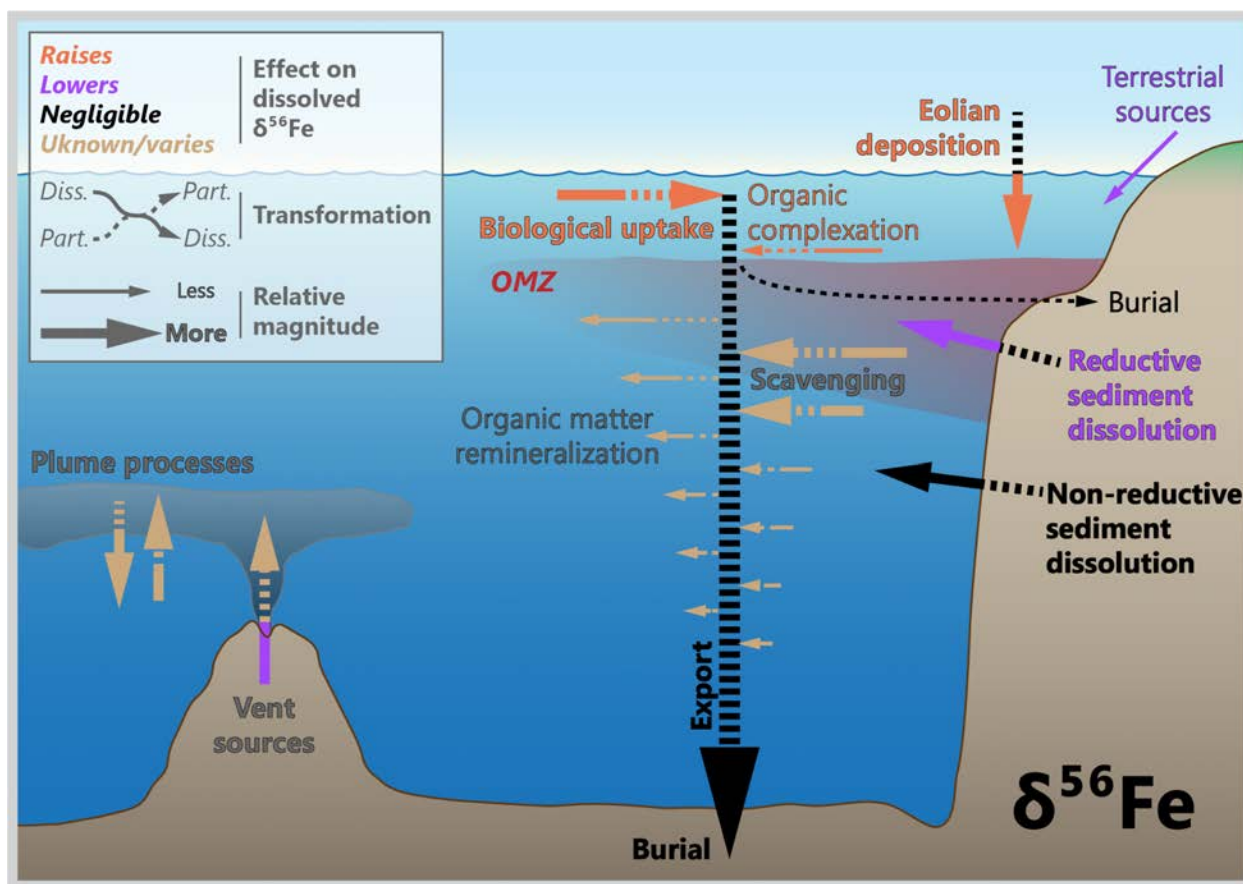
541 **Figure 5 | Representative profiles of dissolved Fe concentrations ($[\text{Fe}]$; A) and Fe isotopic compositions ($\delta^{56}\text{Fe}$;**
 542 **B).** Data from the Eastern Tropical North Atlantic (squares, dashed line; Conway & John, 2014a), Northeast Pacific
 543 (circles, solid line; Conway & John, 2015a), and Southern Oceans (triangles, dotted line; Abadie et al., 2017). Station

544 locations as per Fig. 1. This comparison illustrates that despite possessing similar dissolved concentration profiles, the
545 isotopic behavior of Fe is markedly different between basins.
546

547
548 Despite synthesis of numerous studies of both small- (e.g., Martin et al., 1990; Coale, 1991; Coale et al.,
549 2003) and large-scale iron fertilization events (e.g., de Baar et al., 2005; Boyd et al., 2007; Boyd & Ellwood,
550 2010; Urban et al., 2020), there are still uncertainties in how changing Fe supply to the surface ocean may
551 affect phytoplankton growth in Fe-limited regions, and/or nitrogen fixers under NO_3^- limitation, leading to
552 gaps in our understanding of linking Fe cycling directly to climate change (Misumi et al., 2014). One major
553 challenge is assessing what portion of the dissolved Fe pool is available for uptake by different microbes,
554 termed 'bioavailable' Fe. Such uncertainties on Fe supply, speciation, and bioavailability in the surface
555 ocean are compounded by limitations in our ability to constrain the supply of dissolved Fe in upwelled deep
556 waters. For example, while the ratio of C to macronutrients such N and P in the deep ocean is well known
557 and the residence time and distribution can be accurately reproduced using apparent oxygen utilization
558 (AOU), this is not the case for Fe. Only around 10–15 % of cellular Fe ($\text{Fe:C} = 18\text{--}33 \mu\text{mol:mol}$) appears
559 to be regenerated in the deep ocean ($\text{Fe:C} = 4\text{--}6 \mu\text{mol:mol}$; Twining & Baines, 2013), leading to a weaker
560 correlation between $[\text{Fe}]$ and AOU, even in regions away from Fe sources (Rijkenberg et al., 2014) and
561 upwelling deep waters that are depleted in dissolved Fe relative to macronutrients. Since incubation
562 experiments show that Fe associated with sinking organic matter from the subsurface is effectively
563 regenerated (Velasquez et al., 2016), much of the released Fe must be rapidly scavenged (Tagliabue et al.,
564 2019). Despite this scavenging, vertical transport is still thought to be the major source of dissolved Fe for
565 phytoplankton in most Fe-limited regions, indicating that additional research into the interplay between Fe
566 supply (sources, stabilization, and transport) and demand (biological uptake, scavenging) are required.

567

568



569

570 **Figure 6 | Processes driving Fe isotope variations in modern seawater.** The oceans' internal cycle of Fe is perhaps
 571 the most complex of the trace metals discussed here, exhibiting several significant sources, sinks, and transformations
 572 not directly associated with biological productivity.

573

574 3.2. Driving processes

575 3.2.1. Biological

576 Initial studies of processes that fractionate Fe isotopes were optimistic that $\delta^{56}\text{Fe}$ would make for a powerful
 577 proxy of physiological 'biosignatures' (Beard et al., 1999), especially once measurement of $\delta^{56}\text{Fe}$ was
 578 extended to seawater by Lacan et al. (2008). However, much of this early optimism faded once it was found
 579 that other factors were also important in setting dissolved $\delta^{56}\text{Fe}$, such as external Fe sources (e.g., Radic et
 580 al., 2011; John et al., 2012; Sec. 2.2.3.). Moreover, organisms exhibit significant variability in Fe:C ratios
 581 (e.g., Twining & Baines, 2013), suggesting that Fe cycling may be partially decoupled from ecosystem
 582 productivity. Despite the more nuanced picture, there is a growing body of evidence suggesting that
 583 phytoplankton probably preferentially incorporate light Fe isotopes from seawater and, in some
 584 circumstances, can render detectable changes in dissolved $\delta^{56}\text{Fe}$ (Fig. 6). For example, studies from isolated
 585 eddies, the Mertz Polynya, and the open Southern Ocean showed that surface $\delta^{56}\text{Fe}$ at picomolar [Fe] are

586 isotopically heavy ($>+1\%$), which has been attributed to the combination of surface uptake, regeneration,
587 and organic complexation (Ellwood et al., 2015; 2020; Sieber et al., 2021). Estimates for the magnitude of
588 fractionation due to biological uptake, Δ_{P-R} , range between -0.1 (Radic et al., 2011) and -1.0% (Ellwood
589 et al., 2020; Sieber et al., 2021). The magnitude and direction of any Fe isotope fractionation during uptake
590 may depend on the phytoplankton species, uptake mechanism, and Fe species consumed. Thus, additional
591 research is required on all three fronts.

592 Below the surface mixed layer, dissolved $\delta^{56}\text{Fe}$ compositions appear to be primarily a reflection of the
593 isotope signature of Fe sources, rather than reflecting a dominant influence from the biological processes
594 of remineralization (Fig. 6; e.g., Abadie et al., 2017; Conway & John, 2014a; John et al., 2018a; Labatut et
595 al., 2014; Sieber et al., 2021). Accordingly, there remains the possibility for $\delta^{56}\text{Fe}$ of surface seawater to be
596 linked to productivity in some oceanographic settings, though the relative role of other Fe-cycling processes
597 and the degree to which they erase any diagnostic productivity signatures requires further investigation.

598

599 3.2.2. Chemical

600 The chemical behavior of Fe in seawater is complex and has the potential to decouple Fe cycling from
601 macronutrients and thus productivity. Unlike the macronutrients, which are present as aqueous ions in
602 solution, Fe is scarcely soluble in seawater, and much of what constitutes ‘dissolved’ Fe—operationally
603 defined as that which can pass through a 0.2 or $0.4 \mu\text{m}$ filter—is in actuality a ‘soup’ containing organic
604 complexes, nanoparticles, colloids, and a small fraction of truly ionic Fe. The controls governing, and the
605 extent to which exchange occurs between these forms of dissolved Fe, are areas of focused interest (e.g.,
606 Fitzsimmons & Boyle, 2014; Fitzsimmons et al., 2015). Additionally, dissolved Fe is subject to strong
607 removal via scavenging, which lowers the Fe:macronutrient ratio of waters returned to the surface via
608 upwelling (Moore, 2016). Chemical processes can also exert a significant influence over the isotopic
609 composition of Fe in seawater, such as through redox transformations, exchange reactions (e.g.,
610 complexation, particle interactions), and by authigenic precipitation, discussed below.

611 Redox transformations drive large Fe isotope effects (e.g., Johnson et al., 2002; Skulan et al., 2002; Welch
612 et al., 2003; Anbar et al., 2005). Indeed, much of the Fe isotope variation in Earth’s ancient, more-reducing
613 past likely derives from fractionations associated with redox transformations (see e.g., Rouxel et al., 2005;
614 Johnson et al., 2008 and references therein). While the role of redox relative to other processes is somewhat
615 diminished in today’s largely oxygenated ocean, it remains an important mediator of Fe isotope source
616 compositions, particularly within the ocean interior. This is neatly illustrated using the example of sediment

617 dissolution, which can occur with or without a change in the redox state of Fe (Fig. 6). Bulk marine
618 sediments typically possess a composition similar to the crustal composition of +0.1 ‰ (Beard et al., 2003;
619 Poitrasson, 2006). However, dissolved Fe(II) derived from bacterially mediated reductive dissolution in
620 sediments has been characterized by $\delta^{56}\text{Fe}$ between -1 and -3 ‰ (Berquist & Boyle, 2006; Severmann et
621 al., 2006; 2010; Homoky et al., 2009; 2013; Klar et al., 2017a; Henkel et al., 2018), whereas Fe derived
622 from non-reductive dissolution processes is thought to be considerably heavier, between +0.1 to +0.3‰,
623 and also likely to be present in the colloidal phase (Homoky et al., 2009; 2013; 2021; Radic et al., 2011).
624 Further modification of reductive endmember compositions is possible upon contact with oxidizing
625 seawater, potentially masking true source signatures. Oceanic water column dissolved $\delta^{56}\text{Fe}$ compositions
626 attributed to either non-reductive (+0.1 to +0.4 ‰) or reductive (-0.3 to -4 ‰) release of Fe from sediments
627 have now been observed globally (Radic et al., 2011; John et al., 2012; Staubwasser et al., 2013; Conway
628 & John, 2014a; Labutut et al., 2014; Conway & John 2015a; Chever et al., 2015; Fitzsimmons et al., 2016;
629 Klar et al., 2017a; Abadie et al., 2017; Klar et al., 2018; Rolison et al., 2018; John et al., 2018a; Charette et
630 al., 2020).

631 Exchange reactions can also fractionate primary Fe isotope compositions. For example, natural lithogenic
632 dust is thought to possess a relatively narrow range of Fe isotope compositions (i.e., $\delta^{56}\text{Fe} \approx +0.1 \pm 0.2$ ‰;
633 Waeles et al., 2007; Mead et al., 2013; Conway et al., 2019; Chen et al., 2020), reflecting the overall
634 homogeneity of the upper continental crust. However, dissolved Fe in seawater attributed to dissolving dust
635 particles is isotopically heavy, around +0.7 ‰ (Fig. 6; Conway & John, 2014a). This fractionation is thought
636 to reflect dissolution in concert with, and complexation by, strong organic ligands (Fishwick et al., 2014),
637 which have been experimentally shown to preferentially bind heavy Fe isotopes (Dideriksen et al., 2008;
638 Morgan et al., 2010). Fractionation effects may also arise during exchange of Fe between dissolved and
639 particulate forms, though the magnitude of the effect depends on whether the exchange is primarily physical
640 (negligible fractionation; e.g., Fitzsimmons et al., 2017) or chemical (from $\approx +0.3$ up to +1‰; Labutut et
641 al., 2014; Fitzsimmons et al., 2015).

642 Lastly, authigenic precipitation can control the isotopic composition of Fe released by large point sources,
643 such as hydrothermal vents and margin sediments (Fig. 6). Iron in hydrothermal vent fluids possesses
644 endmember compositions ranging from -0.7 to +0.1‰ (Sharma et al., 2001; Beard et al., 2003; Severmann
645 et al., 2004; Rouxel et al., 2008; Bennett et al., 2009; Rouxel et al., 2016; Nasemann et al., 2018; Rouxel et
646 al., 2018). However, precipitation of Fe into authigenic minerals can render significant changes in dissolved
647 $\delta^{56}\text{Fe}$ (e.g., Severmann et al., 2004; Bennett et al., 2009). The direction of fractionation depends on—and
648 may thus be diagnostic of—the specific transformations occurring (e.g., Horner et al., 2015b; Lough et al.,
649 2017): Fe sulfides and oxides preferentially incorporate isotopically light and heavy Fe, respectively (e.g.,

650 Skulan et al. 2002; Rouxel et al., 2008). Mineral precipitation can drive $\delta^{56}\text{Fe}$ of residual Fe stabilized in
651 seawater to values ranging between -2.4 to $+1.5$ ‰, depending on the authigenic mineral produced
652 (Conway & John, 2014a; Ellwood et al., 2015; Fitzsimmons et al., 2016; 2017; Klar et al., 2017b; Lough
653 et al., 2017; Rouxel et al., 2018). Analogous processes appear to operate along continental margins,
654 whereby ‘light’ Fe, mobilized by reductive dissolution, encounters oxidizing seawater and forms
655 precipitates that are heavier than the source Fe (though overall still considerably lighter than background
656 seawater; e.g., Marsay et al., 2018; Fig. 6).

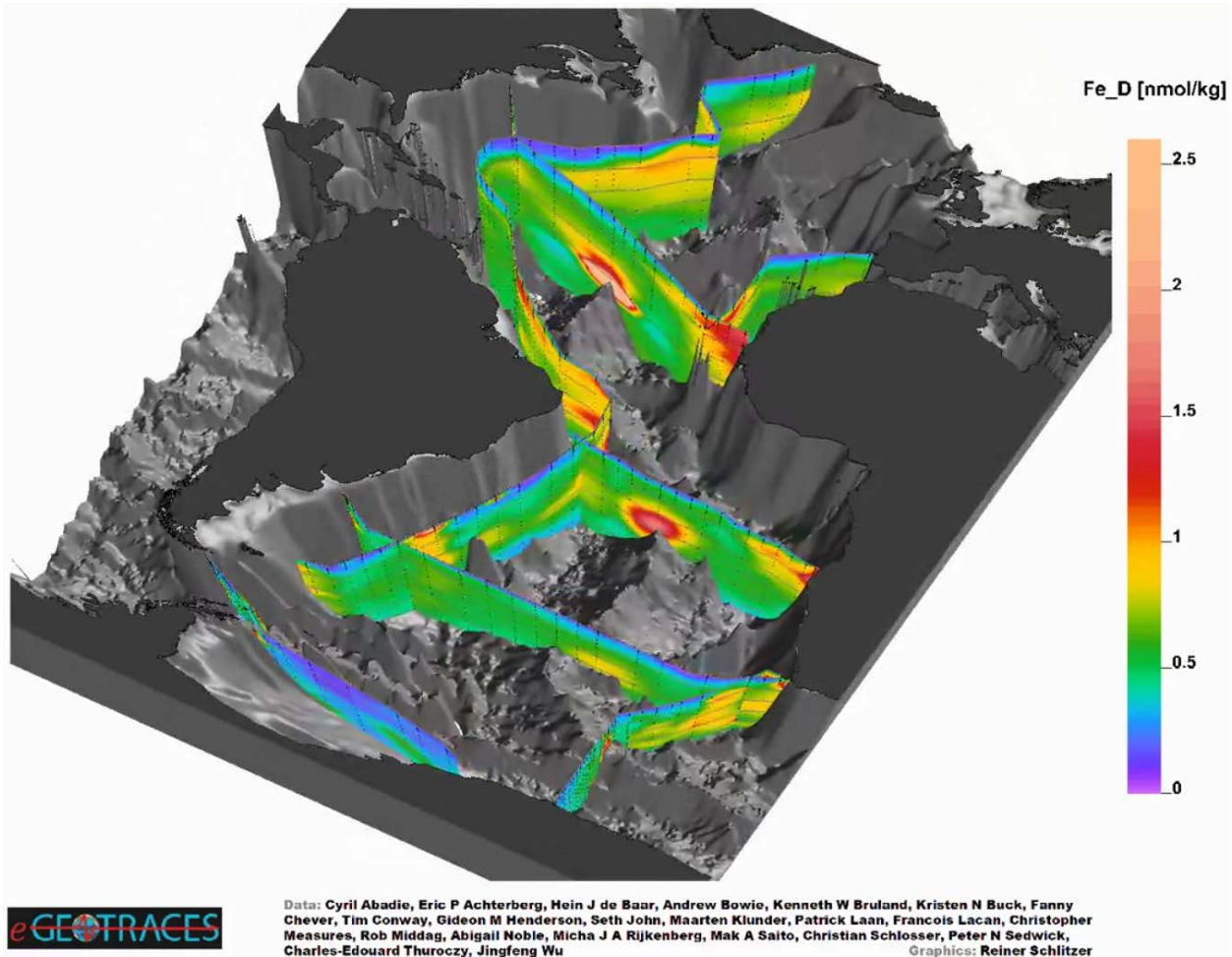
657 Additionally, the importance of local point sources on dissolved $\delta^{56}\text{Fe}$ continue to emerge, including from
658 anthropogenic aerosol dust (e.g., Mead et al., 2013; Kurisu et al., 2016a,b; Conway et al., 2019; Pinedo-
659 González et al., 2020), glaciers and meltwater (e.g., Zhang et al., 2015; Stevenson et al., 2017), and rivers
660 (e.g., Fantle & DePaolo, 2004; Bergquist & Boyle, 2006; Ingri et al., 2006; Escoube et al., 2009; Ilina et
661 al., 2013; Akerman et al., 2014; Chen et al., 2014; Poitrasson et al., 2014; Escoube et al., 2015; Mullholland
662 et al., 2015). These local point sources can vary dramatically over short spatial and temporal scales and
663 with *in situ* chemical conditions. The net effect of the dominance of Fe sources on dissolved $\delta^{56}\text{Fe}$ in
664 seawater means that any signal from biological uptake in the Fe-depleted mixed layer, even if could be
665 recorded in an archive, may be easily overprinted by even a small addition of new Fe from either above or
666 below.

667

668 3.2.3. Physical

669 The residence time of Fe in seawater is substantially less than the mixing time of the global ocean (Table
670 1). Local and regional Fe sources can thus drive large differences in [Fe] and dissolved $\delta^{56}\text{Fe}$ between ocean
671 basins (Fig. 5). Local source signatures—[Fe], $\delta^{56}\text{Fe}$, and perhaps Fe speciation—can be transported and
672 retained over the scale of individual ocean basins (Fig. 7; Conway & John, 2014a; Abadie et al., 2017).

673 This is arguably one of the marquee findings of the GEOTRACES program, and underpins the utility of
674 sedimentary $\delta^{56}\text{Fe}$ to reconstruct past marine Fe sources, discussed next.



676 **Figure 7 | Three-dimensional scene depicting dissolved Fe concentrations in the Atlantic Ocean** (Schlitzer,
677 2017). This perspective illustrates the density of GEOTRACES data in the region as well as the influence of multiple
678 Fe 'hot spots', such as mid-ocean ridges and continental margins. Data are available in the GEOTRACES Intermediate
679 Data Product 2017 (Schlitzer et al., 2018); names of data originators appear in the figure. Three-dimensional scenes
680 for other TEIs are available from <https://eGEOTRACES.org/>.

681

682

683 3.3. Marine archives

684 3.3.1. Surface ocean

685 A requirement of the application of any paleoproxy is the availability of suitable sedimentary archives.
686 These archives must have both a high fidelity for the signal of interest and be robust to post-depositional
687 alteration. Archives most relevant to reconstructing paleoproductivity should capture surface ocean $\delta^{56}\text{Fe}$;

688 however, there are few—if any—reliable archives. The lack of surface water archives reflects two related
689 challenges. First, most archives for surface seawater are derived from biominerals, such as foraminifera,
690 diatoms, sponges, and corals. These archives possess vanishingly low Fe content compared to Ca or Si,
691 such that Fe isotopic analysis of these substrates has proven difficult. Second, following burial, many
692 biominerals will act as substrates for authigenic mineral formation. These authigenic minerals, such as clays
693 (e.g., Badaut & Risacher, 1983) and Fe–Mn oxides (e.g., Boyle, 1981), possess Fe contents far in excess of
694 those in the underlying biomineral, necessitating significant physical and chemical cleaning (e.g., Cheng et
695 al., 2000).

696 Despite these obstacles, there are three positive signs that reconstructing past surface seawater $\delta^{56}\text{Fe}$ is
697 possible. First, biogenic opal may contain Fe at concentrations in the $\mu\text{g g}^{-1}$ range (Ellwood & Hunter, 2000;
698 Lal et al., 2006; Shemesh et al., 1988; Sun et al., 2016), which is tractable for $\delta^{56}\text{Fe}$ analysis. Second, the
699 Fe content of diatoms is correlated with ambient [Fe] (Twining & Baines, 2013). Lastly, the positive
700 relationship between the Fe content of diatoms and corresponding seawater appears to hold through sinking
701 and sedimentation (Pichevin et al., 2014), indicating that diatoms are a potential window into past surface
702 ocean Fe chemistry. Whether these relationships also extend to $\delta^{56}\text{Fe}$ remains to be seen, and will require
703 additional coretop calibrations, incubation experiments, and detailed assessment of the efficacy of chemical
704 cleaning.

705

706 3.3.2. *Deep ocean*

707 There are several studies examining Fe sources and fluxes in the meso- and bathypelagic ocean using
708 sedimentary archives. Given the considerable spatial variability in modern $\delta^{56}\text{Fe}$, it is likely that
709 sedimentary reconstructions will reflect, at most, a regional view of the past Fe cycle. This means that
710 multiple, contemporaneous records will be required to diagnose whole-ocean changes in Fe cycling, but
711 that individual records will still have utility in offering basin-scale perspectives. To constrain Fe sources,
712 researchers have examined the Fe isotope composition of Fe-rich sediments, including red clays (Dunlea et
713 al., 2021), polymetallic nodules (Marcus et al., 2015), and Fe–Mn crusts (Zhu et al., 2000; Levasseur et al.,
714 2004; Chu et al., 2006; Horner et al., 2015b; Liu et al., 2020). Ferromanganese crusts are currently the best
715 studied for Fe isotopes (Fig. 8); Fe–Mn crusts are slowly accumulating deposits ($\sim\text{mm Myr}^{-1}$) that record
716 ambient seawater $\delta^{56}\text{Fe}$ with a spatially invariant offset of $-0.77\pm 0.06\text{‰}$ (Levasseur et al., 2004; Horner et
717 al., 2015b). The constancy of the offset between crusts and seawater implies that the Fe isotope composition
718 of individual Fe–Mn crust layers can be interpreted in terms of past dissolved $\delta^{56}\text{Fe}$, and thus past Fe
719 sources. Iron is effectively immobile in Fe–Mn crusts, with a calculated effective diffusivity $<10^{-12}\text{ cm}^2$

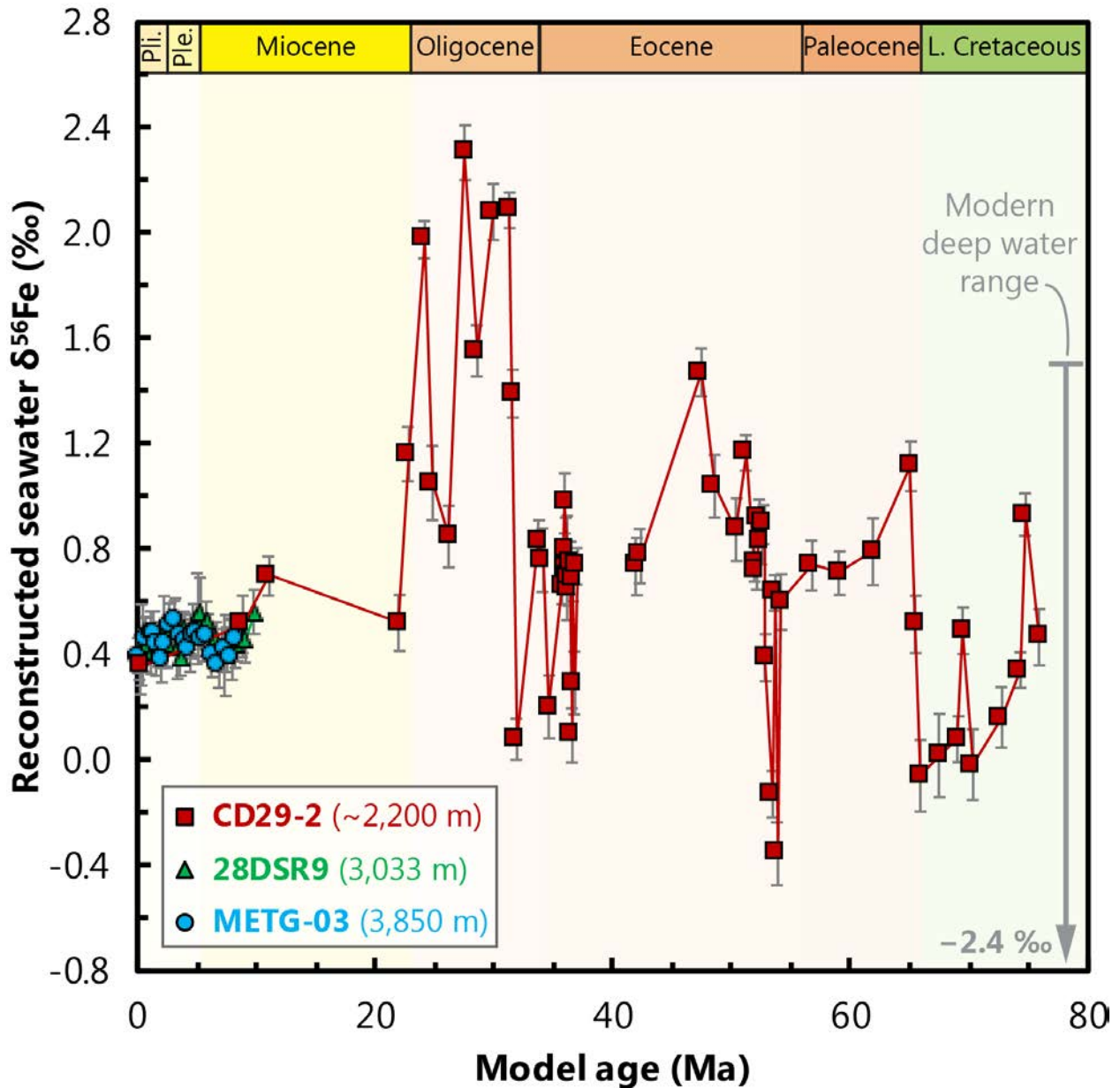
720 yr⁻¹ (Henderson & Burton, 1999), implying that post-depositional diffusion of Fe is unlikely to reset
721 primary $\delta^{56}\text{Fe}$ (Horner et al., 2015b; Marcus et al., 2015). Curiously, however, the Fe isotopic variability of
722 Fe–Mn deposits recovered from the central Pacific—particularly layers formed before ~20 Ma—exceed
723 the range of modern deep ocean $\delta^{56}\text{Fe}$ (though only in the positive direction; Fig. 8). The reasons for
724 elevated $\delta^{56}\text{Fe}$ in the past are debated. Horner et al. (2015b) report that heavy $\delta^{56}\text{Fe}$ could arise through
725 widespread secondary modification of large Fe sources through authigenic reactions, such as sulfide
726 precipitation. In contrast, Johnson et al. (2020) contend that the elevated $\delta^{56}\text{Fe}$ reflects extensive biological
727 modification of dissolved Fe, driven by large-scale Fe fertilization. Regardless, the variation in these
728 records points to a dynamic and enigmatic Fe cycle in Earth’s past, and indicates that Fe–Mn crusts have a
729 largely untapped potential to reconstruct spatiotemporal variations in this cycle.

730 Other approaches are also showing promise to study Fe fluxes to the deep ocean through time. For example,
731 researchers have constrained the rate of sedimentary accumulation of hydrothermally derived Fe and Cu
732 using constant flux proxies such as extraterrestrial helium-3 (e.g., Middleton et al., 2016) or thorium-230
733 (Costa et al., 2017). These studies report that hydrothermal activity may be coherent with sea level changes
734 on Quaternary glacial–interglacial cycles, suggesting a potentially remarkable set of connections between
735 the solid Earth, ocean chemistry, and global climate (e.g., Cullen & Coogan, 2017). Reconstruction of

736 hydrothermal metal fluxes over million-year timescales may also be possible using the geochemistry of
737 pelagic clays (e.g., Dunlea et al., 2015), though such approaches are still in their infancy.

738

739



740

741 **Figure 8 | Ferromanganese crust records of central Pacific $\delta^{56}\text{Fe}$ since the Late Cretaceous.** Records from CD29-
742 2, 28DSR9, and METG-03 from Horner et al. (2015b), Chu et al. (2006) and Liu et al. (2020), respectively. The record
743 from CD29-2 was interpreted by Horner et al. (2015b) as evidencing the importance of deep (non-eolian) Fe sources
744 to central Pacific Fe budgets throughout much of the Cenozoic and Late Cretaceous. In contrast, the $\delta^{56}\text{Fe}$ recorded
745 by three central Pacific Fe–Mn crusts have been similar since the late Miocene, consistent with a regional Fe source
746 derived largely from non-reductive sediment dissolution and/or eolian deposition.

747

748 **3.4. Prospects**

749 While the marine Fe cycle is complex, Fe isotopes are proving to be a valuable tool for untangling the many
750 processes that are involved. Detailed study of the Fe cycle reveals that it is driven by a multitude of
751 biological, physical and chemical processes, amongst which productivity is but one small part. In our view,
752 this means that there is no clear path to using $\delta^{56}\text{Fe}$ as a paleoproductivity tracer. However, this does not
753 preclude $\delta^{56}\text{Fe}$ from emerging as a powerful tracer for studying the dynamics of the Fe cycle in the modern
754 and paleo oceans. Such a tracer would be especially powerful given the proximal connection between Fe
755 supply and the biological productivity of the ocean.

756 Exploiting $\delta^{56}\text{Fe}$ will require resolving and refining several ambiguities. First, there is a clear need to better
757 constrain the Fe isotope fractionation factor associated with biological uptake (in variable conditions and
758 from different species) and to diagnose locations where dissolved $\delta^{56}\text{Fe}$ is most affected by productivity.
759 Second, the fractionation factors for remineralization and scavenging are essentially unknown, though field
760 data suggests that the net result of these effects is relatively small (e.g., Radic et al., 2011; Labutut et al.,
761 2104). Constraining these fractionation factors will be particularly important for developing novel archives
762 of the paleo Fe cycle, such as pelagic clays (e.g., Dunlea et al., 2021). Third, any sedimentary reconstruction
763 of past Fe isotope chemistry will need to consider the high degree of spatial variability in modern $\delta^{56}\text{Fe}$.
764 This will necessitate spatially distributed core sampling, similar to the approach used to constrain basin-
765 scale patterns of dust deposition over glacial–interglacial timescales (e.g., Costa et al., 2016; Winckler et
766 al., 2016). Addressing these priorities will provide valuable constraints on the extent to which the Fe cycle
767 has influenced primary productivity over recent geological history, and provide key insights into the
768 potential sensitivity of Earth’s climate to perturbations in marine trace element cycles.

769

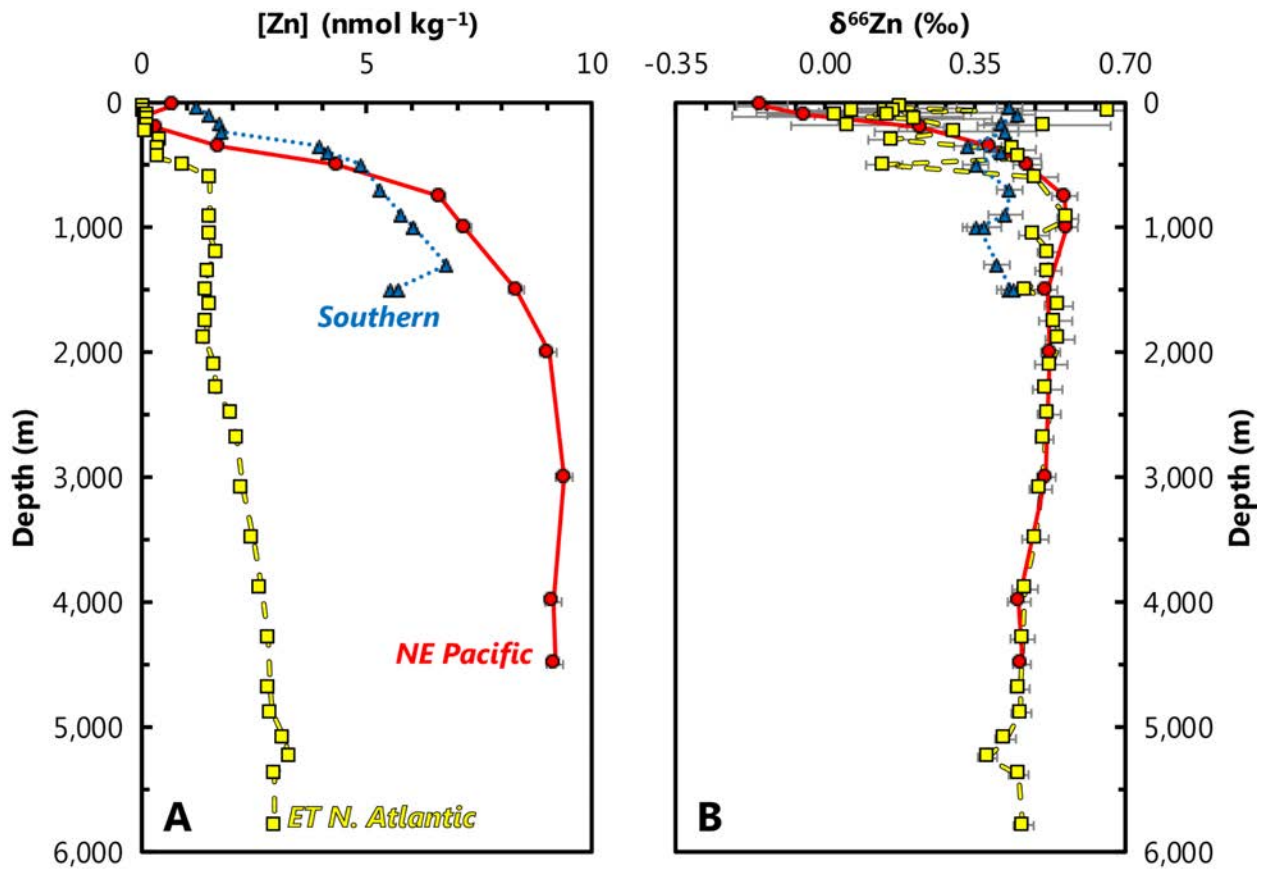
770 **4. Zinc**

771 After Fe, Zn is the second most abundant transition metal in marine phytoplankton (e.g., Twining & Baines,
772 2013) and is involved in many cellular processes ranging from RNA synthesis to nutrient acquisition (e.g.,
773 Maret, 2001). Consistent with its importance to organisms, [Zn] exhibits a nutrient-type distribution in the
774 ocean most similar to that of [Si] (e.g., Bruland et al., 1978). Additionally, there are some sedimentary
775 archives that faithfully capture variations in ambient [Zn], particularly for the deep ocean (e.g., Marchitto
776 et al., 2000). In contrast, there remains considerable debate surrounding the influence of biological
777 productivity on dissolved $\delta^{66}\text{Zn}$ compared to other processes such as scavenging, ligand binding, non-
778 productivity sinks, and anthropogenic contamination. This complexity prevents the simple modelling of Zn
779 uptake via a simple reactor framework (as outlined in Sec. 2.2.1.), and at present, it seems unlikely that
780 there is a direct link between $\delta^{66}\text{Zn}$ and paleoproductivity. That said, there are a number of promising
781 sedimentary archives of past seawater $\delta^{66}\text{Zn}$ that may inform on the myriad other processes that cycle Zn
782 in seawater.

783

784 **4.1. Marine distribution**

785 Typical surface ocean [Zn] are 0.01 to 0.5 nmol kg⁻¹, compared to deep water [Zn] of ~2.5 nmol kg⁻¹ in the
786 north Atlantic and ~10 nmol kg⁻¹ in the north Pacific (Fig. 9). The [Zn] distribution in the ocean closely
787 follows that of the macronutrient Si (Bruland, 1980), at least partially due to the similar behaviour of both
788 elements in the Southern Ocean (Vance et al., 2017; de Souza et al., 2018; Weber et al., 2018; Roshan et
789 al., 2018; Middag et al., 2019). The largest decouplings of [Zn] from [Si] are observed in regions remote
790 from Southern Ocean influence, such as the North Pacific (Janssen & Cullen, 2015; Vance et al., 2019) or
791 North Atlantic (Conway and John, 2014b).



792

793

794

795

796

797

798

799

800

801

802

803

804

805

806

807

808

809

Figure 9 | Representative profiles of dissolved Zn concentrations ([Zn]; A) and Zn isotopic compositions ($\delta^{66}\text{Zn}$; B). Data from the Eastern Tropical North Atlantic (squares, dashed line; Conway & John, 2014b), Northeast Pacific (circles, solid line; Conway & John, 2015a) and Southern Oceans (triangles, dotted line; Wang et al., 2019a). Station locations as per Fig. 1. This comparison illustrates that despite possessing distinct dissolved concentration profiles, the isotopic behavior of Zn is similar between basins.

Given the apparent importance of biological uptake to [Zn] distributions, it was initially expected that Zn isotope ratios would be similarly sensitive to biological processes. Indeed, culture studies consistently showed that phytoplankton assimilated isotopically light Zn from their environment (e.g., John et al., 2007; Köbberich and Vance, 2017; Samanta et al., 2018). It was therefore expected that dissolved profiles of $\delta^{66}\text{Zn}$ would exhibit similar features to those of the macronutrients (e.g., $\delta^{13}\text{C}$, $\delta^{15}\text{N}$, $\delta^{30}\text{Si}$; Farmer et al., *this issue*) and certain micronutrient metals (e.g., $\delta^{114}\text{Cd}$, $\delta^{138}\text{Ba}$; Secs. 6., 8.), whereby Zn-depleted surface waters would exhibit isotopically heavy compositions relative to deeper waters. In contrast, the first Zn isotope profile for seawater, obtained by Bermin et al. (2006) in the northeast Pacific, showed that surface and deep waters exhibited Zn isotope equivalence, with a slight decrease in $\delta^{66}\text{Zn}$ just below the euphotic zone. Recent methodological improvements (e.g., Conway et al., 2013; Takano et al., 2017) have permitted investigation of this surprising pattern in detail for a number of ocean basins.

810

811

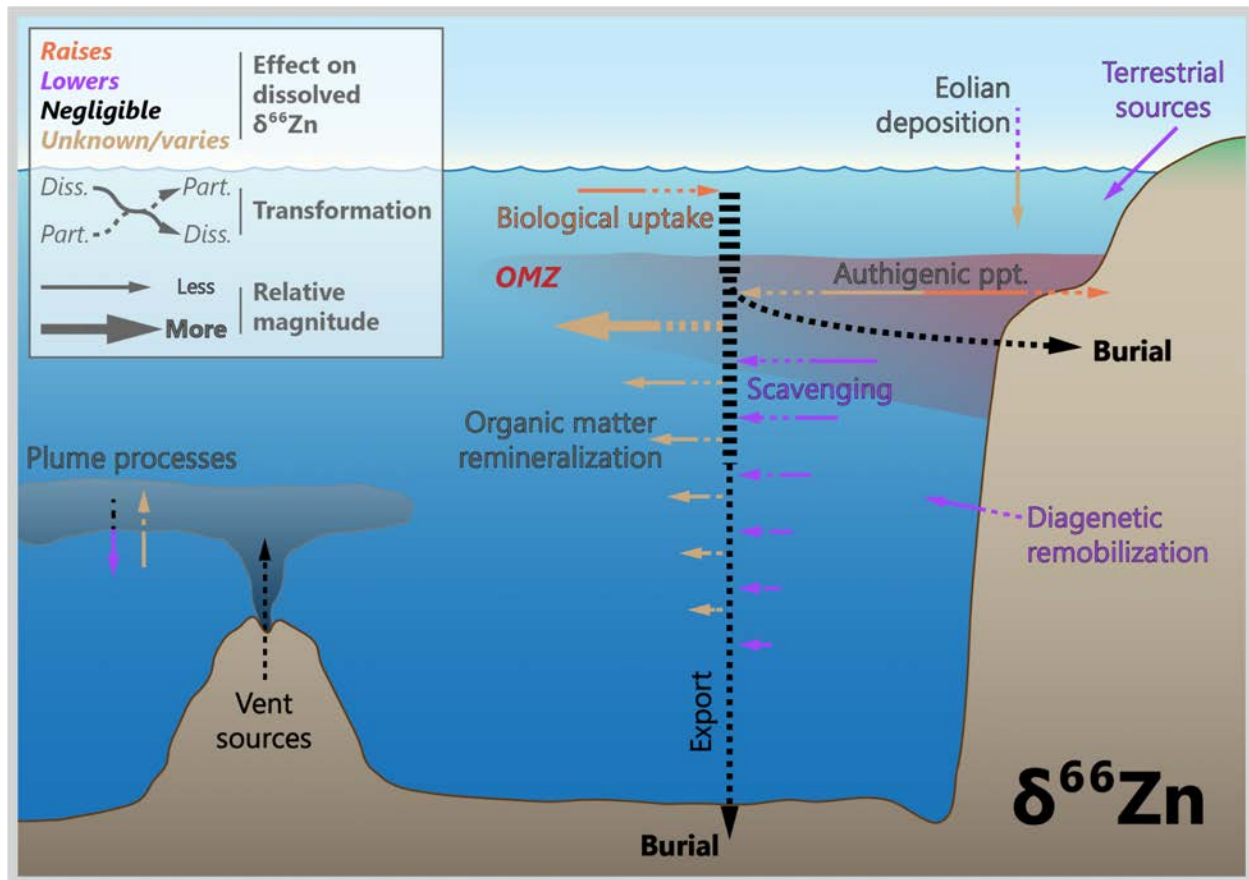
812 A consistent picture of the distribution of $\delta^{66}\text{Zn}$ in the ocean has since emerged. The deep ocean is almost
813 homogeneous, with a $\delta^{66}\text{Zn}$ of about +0.45 ‰ (Fig. 9; Conway & John, 2014b; Zhao et al., 2014; Conway
814 & John, 2015a; Samanta et al., 2017; Takano et al., 2017; John et al., 2018b; Wang et al., 2019a; Vance et
815 al., 2019; Sieber et al., 2020; Liao et al., 2020; Lemaitre et al., 2020). The deep ocean is thus slightly
816 isotopically heavier than the upper continental crust (UCC), which possesses $\delta^{66}\text{Zn} = +0.3$ ‰ (Moynier et
817 al., 2017). We note that Zn isotope data are reported relative to JMC-Lyon, though since this standard is
818 now exhausted, most data are measured relative to AA-ETH or IRMM-3702 and reported relative to JMC-
819 Lyon by means of a fixed offset of ≈ 0.3 ‰ (see Moeller et al., 2006; Archer et al., 2017).

820 Though most of the deep ocean is characterized by $\delta^{66}\text{Zn} = +0.45$ ‰, there are some deviations to values
821 as light as -0.2 ‰ close to Zn point sources, such as margin sediments or hydrothermal vents (Conway and
822 John; 2014b; Lemaitre et al., 2020). In the surface, while heavy $\delta^{66}\text{Zn}$ isotope compositions have been
823 observed, this pattern is not seen everywhere; the upper water column for Zn is often isotopically lighter
824 compared with deeper samples or, in the Southern Ocean and North Pacific, only very slightly fractionated
825 towards heavier values (Conway & John, 2014b; 2015a; Zhao et al., 2014; Samanta et al., 2017; Takano et
826 al., 2017; Wang et al., 2019a; Sieber et al., 2020; Vance et al., 2019; Liao et al., 2020; Lemaitre et al.,
827 2020). Thus, despite the nutrient-like distribution of Zn, the lack of consistent covariation between [Zn]
828 and dissolved $\delta^{66}\text{Zn}$ precludes the use of the isotope reactor framework outlined in Sec. 2.2. Possible reasons
829 for the lack of ‘heavy’ surface $\delta^{66}\text{Zn}$ are discussed in the next section, and include: preferential scavenging
830 of isotopically heavy Zn on particle surfaces (e.g., John & Conway, 2014; Weber et al., 2018) and pervasive
831 isotopically light sources of Zn to the surface ocean, possibly from shallow remineralization of organic
832 material (Samanta et al., 2017; Vance et al., 2019) or from anthropogenic aerosols (Liao et al., 2020;
833 Lemaitre et al., 2020). Given these complexities, we believe it will be extremely challenging to use Zn
834 isotopes as a paleoproductivity proxy.

835

836

837



838

839 **Figure 10 | Processes driving Zn isotope variations in modern seawater.** Though biological processes are capable
 840 of influencing dissolved $\delta^{66}\text{Zn}$, they do not appear to be the dominant driver of Zn isotope variations in the marine realm.

841

842 4.2. Driving processes

843 4.2.1. Biological

844 Zinc is a metal center in two key enzymes: carbonic anhydrase, necessary for carbon fixation, and alkaline
 845 phosphatase, necessary for dissolved organic phosphorus uptake by marine organisms (Morel et al., 1994;
 846 Shaked et al., 2006; reviewed by Sinoir et al., 2012). Zinc also has an array of other physiological roles in
 847 marine organisms, as exemplified by the observation that Zn contents of phytoplankton cells are of similar
 848 magnitude to the micronutrient Fe (Twining & Baines, 2013).

849 Zinc can be growth-limiting for phytoplankton grown in culture (Anderson et al., 1978; Brand et al., 1983;
 850 Morel et al., 1994), but Zn colimitation (with Fe, Co) has only rarely been observed in the open ocean (e.g.,
 851 Coale, 1991; Coale et al., 2003; Franck et al., 2003; Ellwood, 2004; Lohan et al., 2005; Chappell et al.,
 852 2016). This difference between culture and field may reflect the ability of some phytoplankton to substitute

853 Cd or Co for Zn in some enzyme systems when ambient [Zn] is low (e.g., Morel et al., 1994; Lee & Morel,
854 1995; Yee & Morel, 1996; Kellogg et al., 2020). Nevertheless, Zn availability has been shown to influence
855 species composition and phytoplankton growth, including rates of calcification and alkaline phosphatase
856 activity (Sunda & Huntsman, 1995; Crawford et al., 2003; Schulz et al., 2004; Shaked et al., 2006; Mahaffey
857 et al., 2014). In culture, phytoplankton biomass is typically enriched in the light isotopes of Zn (John et al.,
858 2007; Köbberich and Vance, 2017; 2019; Samanta et al., 2018). Rather than reflecting a kinetic isotope
859 effect expressed during uptake, it has been suggested that Zn speciation in the media controls cellular $\delta^{66}\text{Zn}$;
860 specifically, strong organic ligands present in the growth media, such as ethylenediaminetetraacetic acid,
861 preferentially complex heavy Zn isotopes, rendering the bioavailable Zn pool isotopically light (Fig. 10;
862 John et al., 2007; Köbberich and Vance, 2017; 2019). An analogous process has also been suggested to
863 occur between bioavailable Zn and that bound by natural organic ligands in the surface ocean, though this
864 remains to be proven.

865

866 4.2.2. *Chemical*

867 Like most bioessential metals, Zn bioavailability is dictated by its chemical speciation (e.g., Anderson et
868 al., 1978), which is dominated in the ocean by complexation to strong ($K' \sim 10^9 - 10^{11}$) organic ligands
869 (Bruland, 1989; Donat & Bruland, 1990; Ellwood & Van Den Berg, 2000; Jakuba et al., 2012; Kim et al.,
870 2015). Inorganic Zn is considered to make up <5% of the total Zn pool in most ocean regions, with the
871 exception of the Southern Ocean, where strong upwelling of nutrient-rich deep waters leads to [Zn] in
872 excess of complexing ligands (Baars & Croot, 2011). Note that while strongly complexed Zn is unlikely to
873 be bioavailable, the presence of ‘weak’ ligands (or more labile ligands) can enhance Zn uptake (Aristilde
874 & Xu, 2012). As noted above, the role of the diversity of organic (and inorganic) Zn-binding ligands in
875 determining dissolved and particulate $\delta^{66}\text{Zn}$ values remains to be fully evaluated.

876 A role for scavenging in the marine cycling of [Zn] and Zn isotopes has been widely cited but remains
877 under debate (Fig. 10; e.g., John & Conway, 2014; Weber et al., 2018; Roshan et al., 2018; Liao et al.,
878 2020). It is argued that scavenging can explain both the widespread observation of isotopically light Zn in
879 the upper ocean, via preferential removal of heavy Zn isotopes on particles (and release at depth), and also
880 explain the elevated concentration of Zn in the deep Pacific compared to that supplied in southern-sourced
881 deep waters (Fig. 9; Weber et al., 2018; Roshan et al., 2018). Indeed, Weber et al. (2018) propose that the
882 light Zn isotope compositions exhibited by phytoplankton are a result of scavenging removing isotopically
883 heavy Zn from surface seawater, leaving the residual bioavailable Zn pool isotopically light.

884 Basin-scale elevated [Zn] in the deep Pacific has also been attributed to additional Zn inputs, particularly
885 from hydrothermalism (Roshan et al., 2018), which possesses $\delta^{66}\text{Zn} < +0.45 \text{ ‰}$ (John et al., 2018b).
886 Likewise, local- and regional-scale deviations towards lighter $\delta^{66}\text{Zn}$ in the deep Atlantic and Pacific are
887 attributed to sedimentary (Conway & John, 2014b; John et al., 2017; Liao et al., 2020; Lemaitre et al., 2020)
888 and hydrothermal inputs (Conway & John, 2014b; John et al., 2018b; Lemaitre et al., 2020). Anthropogenic
889 aerosol deposition is thought to supply significant Zn to regions of the surface ocean (e.g., Liao & Ho,
890 2018), with possible direct and indirect (via scavenging) regional impacts on upper ocean $\delta^{66}\text{Zn}$ values
891 (Liao et al., 2020; Lemaitre et al., 2020).

892 Lastly, Janssen & Cullen (2015) suggest that decoupling of [Zn] and [Si] in the northeast Pacific reflects
893 the formation of Zn sulfides within the North Pacific OMZ, directly equivalent to proposed Cd sulfide
894 precipitation; this hypothesis is discussed in more detail in Sec. 5.2.3. To date, however, there remains scant
895 evidence for water column Zn-sulfide precipitation in OMZs (e.g., Conway & John, 2014b; John et al.,
896 2018b; Vance et al., 2019), with the patterns described by Janssen & Cullen alternatively attributed to
897 shallower remineralisation of Zn (from organic ‘soft parts’) relative to Si (from opal; Vance et al., 2019).
898 That said, Zn-sulfide precipitation is undoubtedly important in euxinic basins such as the Black Sea and
899 Cariaco Basin (Vance et al., 2016; Isson et al., 2018), and has been postulated to occur within the porewaters
900 of oxygen deficient, organic-rich sediments (Sec. 4.3.4.; Little et al., 2016).

901

902 4.2.3. *Physical*

903 In common with many of the trace metal isotope systems discussed here, the physical ocean circulation
904 exerts a first order control on the distribution of [Zn] and dissolved $\delta^{66}\text{Zn}$ compositions (Vance et al., 2017;
905 de Souza et al., 2018; Weber et al., 2018; Sieber et al., 2020). Subantarctic water masses have distinctive
906 and low [Zn]:[PO_4^{3-}] and [Si]:[PO_4^{3-}] ratios, due to the elevated uptake of Zn and Si by diatoms in the
907 surface Southern Ocean (Sarmiento et al., 2004; Vance et al., 2017). Remineralization of these Zn- and Si-
908 rich diatoms at depth imprints a correspondingly high [Zn]:[PO_4^{3-}] and high [Si]:[PO_4^{3-}] fingerprint on
909 Antarctic bottom waters. This coupling of [Zn] and [Si] in the Southern Ocean forms the basis of the global
910 [Zn]:[Si] correlation via the advection of southern sourced water masses towards the low latitudes, where
911 they fill much of the ocean interior (de Souza et al., 2012; Holzer et al., 2014). The homogeneity of deep
912 ocean dissolved Zn isotope compositions reflects the limited degree of Zn isotope fractionation on uptake
913 by Southern Ocean diatoms (Zhao et al., 2014; Wang et al., 2019a), which results in intermediate and deep
914 southern-sourced water masses with limited or no Zn isotope contrast (Sieber et al., 2020). Although
915 exceptions exist (see Section 4.2.2.), generally, the oceanic [Zn]:[Si] correlation persists despite shallower

916 remineralization of Zn relative to Si (Twining et al., 2014), and is especially clear in the South Atlantic,
917 underlining that the mixing of water masses acts as the dominant control on [Zn] (Vance et al., 2017; de
918 Souza et al., 2018; Middag et al., 2019). While Weber et al. (2018) concur with these other studies about
919 the dominant importance of ocean circulation on setting [Zn] and [Zn]:[Si] distributions, they also argue
920 that reversible scavenging is needed to fully explain the observed global patterns. Further, any Zn addition
921 from hydrothermal vents or sediments will also be superimposed on the circulation pattern, adding further
922 complexity to the [Zn]:[Si] relationship (Sec. 4.2.2.).

923

924 **4.3. Sedimentary archives**

925 *4.3.1. Ferromanganese sediments*

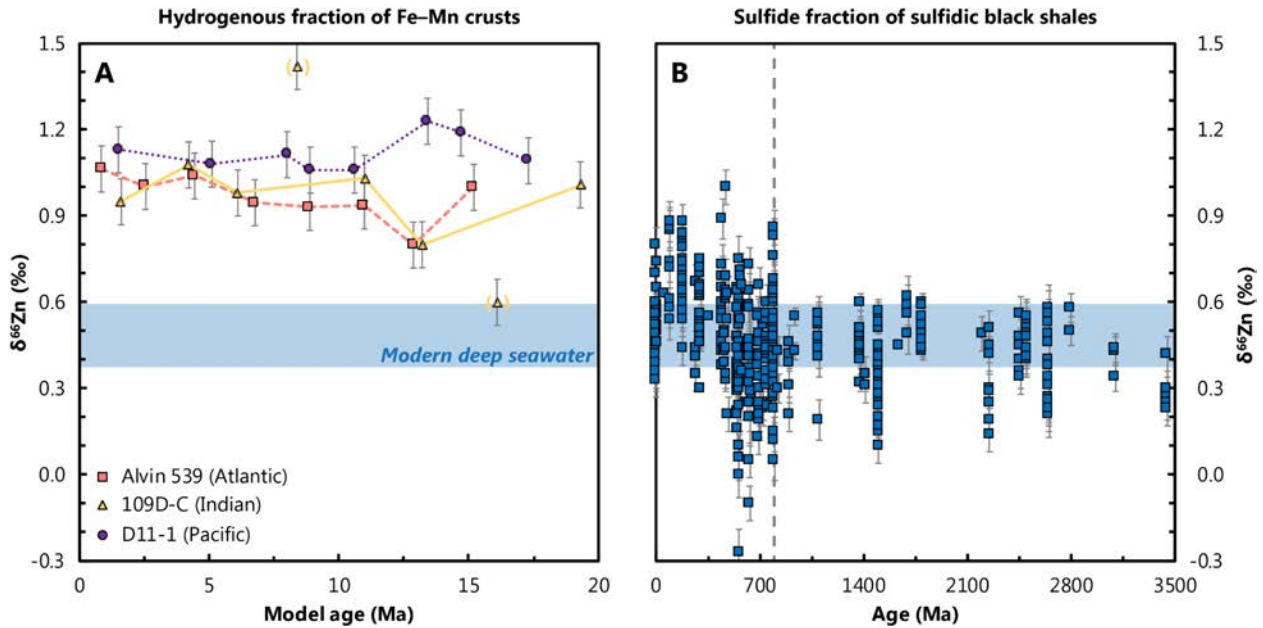
926 Manganese oxides are strong sorbents of positively charged, divalent trace metals, due to their negative
927 layer charge at the pH of natural waters (e.g., Koschinsky & Halbach, 1995). The phyllosomanganate
928 birnessite is the main Mn- and TE-bearing phase in oxic marine sediments (e.g., Koschinsky and Hein,
929 2003), as well as for several elements described here, including Zn, Cu, Ni, Cd, and Mo (though Mo exists
930 in seawater as the molybdate anion). Ferromanganese crusts and nodules incorporate TEs during growth,
931 leading to 10⁶-fold enrichments compared to seawater concentrations (e.g., Arrhenius, 1963; Aplin and
932 Cronan, 1985). As a result, Fe–Mn sediments are often one of the first marine sediment types to be targeted
933 in the development of a new metal isotope tracer.

934 In the case of Zn, Fe–Mn crusts and nodules are isotopically heavy compared to seawater ($\approx +0.45\%$),
935 exhibiting compositions between +0.9 to +1 ‰ (Fig. 11; Maréchal et al., 2000; Little et al., 2014a). The
936 heavy signature is broadly consistent with inorganic sorption experiments of Zn on birnessite, with
937 experiments at high ionic strength yielding $\Delta^{66}\text{Zn}_{\text{sorbed-aqueous}}$ (where $\Delta^{66}\text{Zn}_{\text{sorbed-aqueous}} = \delta^{66}\text{Zn}_{\text{sorbed}} -$
938 $\delta^{66}\text{Zn}_{\text{aqueous}}$) of +0.16 to +2.7‰ (Bryan et al., 2015). The magnitude of fractionation observed in experiments
939 is typically considerably larger than in natural Fe–Mn crusts and nodules, which Bryan et al. (2015) suggest
940 may reflect sorption of Zn on birnessite via two different molecular mechanisms, each associated with
941 different isotopic fractionation factors, as is the case for thallium (e.g., Nielsen et al., 2013). In addition,
942 the influence of organic and inorganic speciation of Zn in seawater may play a role, though this remains to
943 be fully evaluated (e.g., Little et al., 2014b).

944 Little et al. (2014a) observed no marked temporal changes in $\delta^{66}\text{Zn}$ values for three Fe–Mn crusts from
945 each of the major ocean basins over the last ~20 Ma. Zinc is somewhat immobile in Fe–Mn crusts, with a
946 calculated effective diffusivity $<10^{-8} \text{ cm}^2 \text{ yr}^{-1}$, similar to Hf (Henderson & Burton, 1999) and Ba (Sec. 8.3.).

947 Assuming that Fe–Mn crusts preserve primary $\delta^{66}\text{Zn}$, the various records suggest that on a global basis, the
948 marine Zn cycle has been in isotopic steady state for at least 20 Myr (Fig. 11).

949



950

951 **Figure 11 | Records of deep ocean $\delta^{66}\text{Zn}$ through time.** **A** Three records from Fe–Mn crusts recovered from the
952 Atlantic (square, dashed line), Indian (triangle, solid line), and Pacific Oceans (circle, dotted line; Little et al., 2014b).
953 Assuming the isotopic offset between dissolved Zn in seawater and Fe–Mn crusts has remained unchanged at ≈ 0.55
954 ‰ over this interval, these records imply only minimal Zn isotope variations in the deep ocean over the past ~ 20 Myr.
955 Two anomalous measurements from 109D-C (in parentheses) possess low levels of authigenic Zn enrichment,
956 indicative of detrital contamination. **B** Records recovered from the sulfide fraction of sulfidic black shales over the last
957 3,500 Myr (Isson et al., 2018). Assuming that sulfidic black shales record ambient seawater with no Zn isotope offset,
958 this record can be interpreted as reflecting deep-ocean $\delta^{66}\text{Zn}$ over much of Earth's history. The dashed line indicates
959 an apparent reorganization of the marine Zn isotope cycle around 800 Ma, interpreted by Isson et al. (2018) to reflect
960 the rise of eukaryotes to ecological prominence.

961
962

963 4.3.2. Biogenic silica

964 The correlation of Zn with Si in the modern ocean led to the suggestion that Zn:Si measured in diatom opal
965 may be a proxy for Zn:Si (and thus [Zn]) of past seawater. However, culturing and μ -XRF analyses revealed
966 that only a small fraction (1–3%) of the diatom Zn quota is incorporated into the opal frustules, with the
967 remainder present in the organic 'soft parts' of the diatom cells (Ellwood & Hunter, 2000; Twining et al.,
968 2004). The Zn concentration in opal (Zn_{opal}) also more closely reflects the bioavailable Zn in seawater than
969 ambient Zn:Si (Ellwood & Hunter, 2000). Nevertheless, if the mechanisms of Zn incorporation into
970 biogenic opal can be understood, and calibrated, a Zn:Si proxy of Zn bioavailability could help shed light
971 on micronutrient limitation of the biological pump.

972 Andersen et al. (2011) analyzed Zn isotopes ($\delta^{66}\text{Zn}_{\text{opal}}$) and Zn:Si_{opal} in diatom opal isolated from core top
973 sediments from the Southern Ocean. They observed isotopically heavy Zn in opal (at +0.7 to +1.5‰), and
974 an inverse relationship of $\delta^{66}\text{Zn}_{\text{opal}}$ with Zn:Si_{opal}. Consistent with culturing studies, core top Zn:Si_{opal}
975 appears to be linked to bioavailable Zn concentrations in ambient surface seawater. The authors suggested
976 that $\delta^{66}\text{Zn}_{\text{opal}}$ should also reflect the isotope composition of bioavailable Zn in surface seawater, which, they
977 predicted, should be isotopically heavy due to the predicted preferential incorporation of light isotopes into
978 phytoplankton organic material. In this view, the extent of uptake—nutrient utilization—would be recorded
979 by the systematics of Zn:Si_{opal} and $\delta^{66}\text{Zn}_{\text{opal}}$. However, this study predated the recent surge in seawater $\delta^{66}\text{Zn}$
980 measurements. As discussed above, surface water $\delta^{66}\text{Zn}$ analyses in the Southern Ocean have not borne out
981 the prediction of isotopically heavy residual surface waters (Fig. 9), with little to no fractionation observed
982 (Zhao et al., 2014; Wang et al., 2019a; Sieber et al., 2020).

983 Hendry & Andersen (2013) showed that sponge spicules can faithfully record seawater $\delta^{66}\text{Zn}$. Sponges are
984 primarily deep-sea organisms. Hence, if we can deconvolve the controls on diatom Zn:Si and $\delta^{66}\text{Zn}_{\text{opal}}$, a
985 combination of Zn:Si and $\delta^{66}\text{Zn}$ measurements in diatoms and sponges (as used for Si isotopes, Farmer et
986 al., *this issue*) could provide a strong basis for unravelling the past ocean global Zn cycle, including the role
987 of Southern Ocean processes in the biological carbon pump.

988

989 4.3.3. Carbonates

990 Carbonates may provide an alternative archive for [Zn] (as Zn:Ca) and $\delta^{66}\text{Zn}$. For example, Marchitto et al.
991 (2000) showed that Zn:Ca ratios in benthic foraminifera are sensitive to bottom water dissolved [Zn].
992 However, the Zn content in individual microfossil shells is extremely low (typically <0.1 ng); at this level,
993 with current analytical capabilities and blank contributions, many tens to hundreds of benthic foraminifera
994 would be required for a single Zn isotope measurement.

995 To circumvent the issue of low Zn contents of individual shells, Pichat et al. (2003) utilized a selective
996 carbonate dissolution procedure on bulk sediment from the equatorial Pacific, mostly consisting of
997 coccoliths. These authors argued that isotopically heavy $\delta^{66}\text{Zn}$ in carbonates reflected surface seawater, with
998 values modulated by changes in biological productivity due to varying seasonal insolation. Similarly
999 isotopically heavy Zn in ancient carbonates has also been argued to reflect strong biological utilization in
1000 surface waters (Kunzmann et al., 2013; cf. John et al., 2017; Liu et al., 2017). More recently, Zhao et al.
1001 (2021) surveyed carbonates from the Great Bahama Bank, observing carbonate-bound $\delta^{66}\text{Zn}$ ranging from
1002 ≈ -0.5 to +1.1 ‰. Given the local seawater value of $\approx +0.1$ ‰, this large range is surprising, and implies a

1003 number of additional factors that fractionate Zn isotopes during incorporation into and recovery from
1004 carbonates. These factors include: stable isotope fractionation during Zn incorporation into CaCO₃,
1005 contamination from non-CaCO₃ phases (e.g., lithogenic or authigenic phases), and methodological issues
1006 (e.g., non-quantitative selective leaching leading to stable isotope fractionation; Revels et al., 2015).
1007 Regardless, the relationship between bulk carbonate and seawater $\delta^{66}\text{Zn}$ is not straightforward.

1008 Despite the difficulty in interpreting bulk carbonate $\delta^{66}\text{Zn}$, phase-specific (particularly, aragonitic) CaCO₃
1009 archives appear more promising. For example, Zhao et al. (2021) identify carbonate ooids as a promising
1010 archive of past seawater $\delta^{66}\text{Zn}$. Likewise, Little et al. (2017a) showed that deep-sea coral skeletons record
1011 intermediate and deep water $\delta^{66}\text{Zn}$ (e.g., Little et al., 2017a). Given the large size of specimens and their
1012 global distribution, combined with the ability to assign precise ages to individual specimens, deep-sea corals
1013 may provide an archive of seawater compositions that are amenable to Zn isotope analysis. However, recent
1014 Zn isotope studies of shallow-water zooxanthellate corals suggests that the relationship with seawater $\delta^{66}\text{Zn}$
1015 is complicated by temperature and photosynthetic effects (Ferrier-Pagès et al., 2018; Xiao et al., 2020).

1016

1017 *4.3.4. Organic-rich sediments*

1018 The isotope composition of Zn in organic-rich sediments deposited along productive continental margins
1019 is typically $\approx +0.1$ ‰, which is lighter than ambient seawater by ≈ 0.4 ‰ (Little et al., 2016). This light $\delta^{66}\text{Zn}$
1020 signature likely arises from one of two processes. In the first process, isotopically light Zn is preferentially
1021 removed from seawater during precipitation of sulfides (Fujii et al., 2011a; Vance et al., 2016). This
1022 precipitation may occur directly from seawater and into sediments, or possibly within reducing
1023 microenvironments that develop within particles sinking through low-[O₂] water columns (Janssen &
1024 Cullen, 2015; Little et al., 2016; Vance et al., 2016; Bianchi et al., 2018). Regardless, so long as Zn removal
1025 is non-quantitative, these processes act to bury isotopically light Zn from the ocean. In the euxinic Black
1026 Sea, where Zn drawdown with sulfides is quantitative, sedimentary $\delta^{66}\text{Zn}$ is expected to reflect the deep
1027 seawater composition from above the chemocline (analogous to Mo; Sec. 7; Vance et al., 2016), and euxinic
1028 black shales represent a promising archive of past deep seawater $\delta^{66}\text{Zn}$. This prediction was confirmed by
1029 Isson et al. (2018), who reported that sulfide-bound Zn in black shales from the euxinic Cariaco Basin
1030 exhibited the expected deep seawater-like $\delta^{66}\text{Zn}$ of $+0.5 \pm 0.1$ ‰. Using this calibration, Isson et al. (2018)
1031 analyzed $\delta^{66}\text{Zn}$ in hundreds of euxinic black shales generating a 3,500 Myr record of deep-ocean Zn isotope
1032 evolution (Fig. 11B). Though a full discussion of this dataset is beyond the scope of our review, this record
1033 reveals a shift in deep ocean $\delta^{66}\text{Zn}$ around 800 Ma, which Isson et al. (2018) interpret as reflecting a
1034 reorganization of the marine Zn cycle driven by the rising ecological prominence of eukaryotes.

1035 A second process that can deliver isotopically light Zn to sediments is organic matter. That is, presuming
1036 that phytoplankton assimilate isotopically light Zn from seawater, the export of this organic matter to
1037 sediments can bury light Zn in margin settings (Little et al., 2016; John et al., 2017). If dominant, this
1038 biologically driven process might suggest some utility for $\delta^{66}\text{Zn}$ in organic-rich sediments to reconstruct
1039 paleoproductivity, especially in low-oxygen settings. Alternatively, if the scavenging-centered view
1040 proposed by Weber et al. (2018) is correct, the $\delta^{66}\text{Zn}$ of exported Zn—while still light relative to deep
1041 seawater—would not represent a simple measure of either Zn uptake or primary productivity. This view
1042 implies that there would be considerable spatial complexity in the $\delta^{66}\text{Zn}$ delivered to sediments that depends
1043 on factors such as scavenging intensity relative to upwelling, which is not directly linked to biological
1044 productivity. Moreover, Weber et al. (2018) even suggest that some regions of the ocean might bury
1045 isotopically heavy organic matter-associated Zn, either due to variability in surface water $\delta^{66}\text{Zn}$ resulting
1046 from scavenging, or via burial of isotopically heavy Zn adsorbed to organic matter.

1047 Overall, the uncertainties in Zn delivery mechanisms and the connection between $\delta^{66}\text{Zn}$ and primary
1048 productivity means that there are considerable obstacles to interpreting organic-rich sedimentary $\delta^{66}\text{Zn}$ as
1049 a direct tracer of productivity.

1050

1051 **4.4. Prospects**

1052 Despite the complexities and remaining unknowns in oceanic $\delta^{66}\text{Zn}$ cycling reviewed above, we note that
1053 there are systematic variations in sedimentary Zn isotope compositions recorded in geologic archives on
1054 Myr and Gyr timescales. In addition to the organic sediment record of Isson et al. (2018), described above,
1055 Yan et al. (2019) compiled three $\delta^{66}\text{Zn}$ datasets from contemporaneous Ediacaran (635 Ma, Marinoan)
1056 postglacial cap carbonates (Kunzmann et al., 2013; John et al., 2017; Lv et al., 2018), which show
1057 systematic changes in Zn isotope compositions over this period of marked global change. Secondly, Sweere
1058 et al. (2018) presented data showing marked shifts in carbonate-bound Zn isotope compositions in several
1059 geological sections spanning a Cretaceous ocean anoxic event (OAE 2). While there is no consensus on the
1060 causes of these intriguing isotopic shifts within carbonates (e.g., the role of redox vs. source/sinks vs.
1061 productivity), the coherency of the records is encouraging and their full interpretation awaits identification
1062 of the driving processes.

1063 On longer timescales, the importance of Earth's overall redox state on marine Zn isotope systematics
1064 requires elucidation. There are several other explanations for the shift in deep-ocean $\delta^{66}\text{Zn}$ at ≈ 800 Ma
1065 besides a switch to more eukaryotic-dominated oceans, such as changes in Zn speciation, variations in other

1066 Zn sinks, or diagenesis (see Isson et al., 2018); indeed, we are not aware of any studies exploring how
1067 primary sedimentary $\delta^{66}\text{Zn}$ may be modified by diagenetic processes. Moreover, the assumption that the
1068 high affinity for Zn exhibited by eukaryotes translates into higher eukaryotic Zn:C (compared to
1069 prokaryotes) is not supported by culture data, which showed that cyanobacterial Zn:C is comparable to—
1070 or can even exceed that of—eukaryotes grown under the same conditions (Köbberich & Vance, 2019).
1071 Thus, developing a more complete interpretation of $\delta^{66}\text{Zn}$ in the sedimentary record requires building a
1072 more complete understanding of the biological and biologically mediated processes cycling $\delta^{66}\text{Zn}$ in the
1073 upper water column.

1074 Lastly, we recommend that future studies target coupled dissolved and particulate phase $\delta^{66}\text{Zn}$ data, in
1075 concert with detailed biological and chemical speciation data. To date, particulate phase $\delta^{66}\text{Zn}$ data has
1076 proven challenging to obtain due to pervasive Zn contamination. Zinc isotope characterization of sediments
1077 and sediment porewater is needed to constrain the role of early diagenetic reactions, as well as their
1078 importance to the mass balance of Zn isotopes in the ocean. Sediment studies would also benefit from
1079 further investigation of whether specific phases offer more robust archives of past seawater $\delta^{66}\text{Zn}$,
1080 potentially exploiting selective extraction methods. We also recommend revisiting published records in
1081 light of recent seawater $\delta^{66}\text{Zn}$ data.

1082

1083

1084

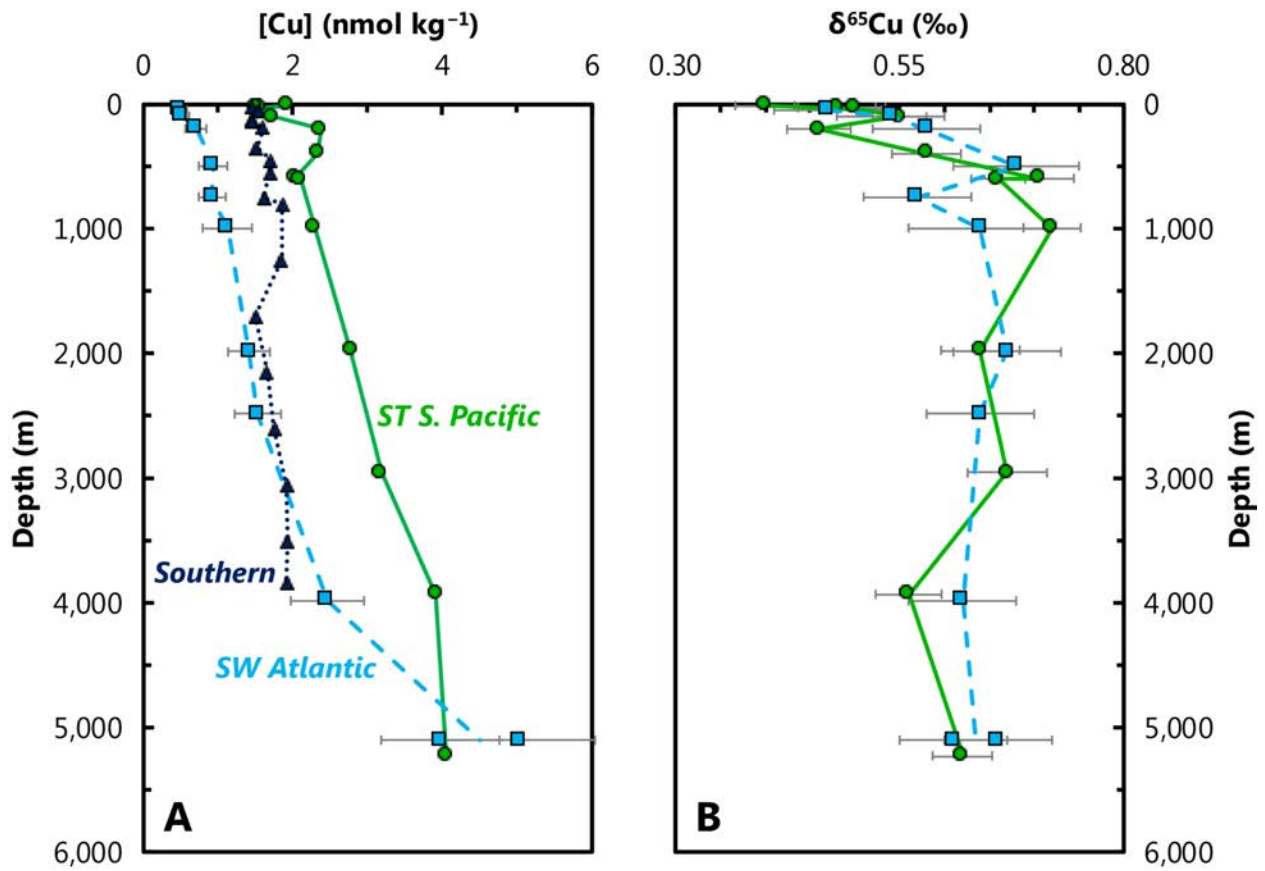
1085 **5. Copper**

1086 As with Fe and Zn, Cu is used in a number of cellular processes, most notably electron transport (e.g.,
1087 Twining & Baines, 2013). Unlike Fe and Zn however, Cu is toxic to phytoplankton, even at extremely low
1088 free $[\text{Cu}^{2+}]$ (pM; Brand et al., 1996). Dissolved Cu—in seawater and within marine organisms—is thus
1089 strongly regulated by organic complexes that maintain low free $[\text{Cu}^{2+}]$ (e.g., Moffett & Dupont, 2007;
1090 Waldron & Robinson, 2009). Some archives have shown promise for recording aspects of surface and deep
1091 ocean $\delta^{65}\text{Cu}$, such as organic-rich sediments and authigenic Fe–Mn oxides, respectively. Despite the strong
1092 biological control over marine [Cu] distributions, our present understanding of the biogeochemical cycle
1093 of Cu suggests there is no clear route to developing [Cu] or $\delta^{65}\text{Cu}$ as paleoproductivity proxies, and Cu
1094 cannot be modeled within the simple reactor framework (Sec. 2.2.). However, there are a number of
1095 sensitivities in the marine Cu isotope cycle that are indirectly related to paleoproductivity that may render
1096 $\delta^{65}\text{Cu}$ as a proxy of processes related to metal complexation by organic ligands and/or marine redox
1097 evolution.

1098

1099 **5.1. Marine distribution**

1100 The distribution of Cu in the ocean has been described as ‘hybrid-type’, because it is intermediate between
1101 nutrient- and scavenged-type elements (Bruland & Lohan, 2003). Depth profiles of [Cu] typically show
1102 approximately linear increases with depth (e.g., Boyle et al., 1977; Fig. 12A). Surface [Cu] are typically
1103 about 0.5 to 1 nmol kg^{-1} , compared to deep Atlantic [Cu] of $\sim 2.5 \text{ nmol kg}^{-1}$ and deep Pacific [Cu] of ~ 4
1104 nmol kg^{-1} (Fig. 12). Unlike the other metals discussed here (with the possible exception of Cr), and despite
1105 the existence of a large seawater [Cu] dataset, some discrepancy still exists in the [Cu] measured by different
1106 techniques, with methodological details such as storage time, acidification strength, UV oxidation (or not)
1107 prior to analysis all thought to be potentially important, and requiring further intercomparison efforts
1108 (Posacka et al., 2017). Nevertheless, the [Cu] distribution pattern has been attributed to a combination of
1109 biological uptake and remineralization, benthic flux from sediments (e.g., Boyle et al., 1977; Roshan &
1110 Wu, 2015a; Little et al., 2018), and/or reversible scavenging (Little et al., 2013; Richon et al., 2019). These
1111 processes are superimposed on the first-order distribution established via the physical ocean circulation
1112 (Roshan & Wu, 2015a).



1113

1114

1115

1116

1117

1118

1119

1120

Figure 12 | Representative profiles of dissolved Cu concentrations ([Cu]; A) and Cu isotope compositions ($\delta^{65}\text{Cu}$; B). Data from the Southwest Atlantic (squares, dashed line; Little et al., 2018), Subtropical South Pacific (circles, solid line; Takano et al., 2017) and Southern Oceans (triangles, dotted line; Boye et al., 2012). Station locations as per Fig. 1. This comparison illustrates that the isotopic behavior of Cu is similar between basins, reflecting the importance of complexation by strong organic ligands. Note that there are no Cu isotope data available for the Southern Ocean at this time.

1121

1122

1123

1124

1125

1126

1127

1128

1129

1130

1131

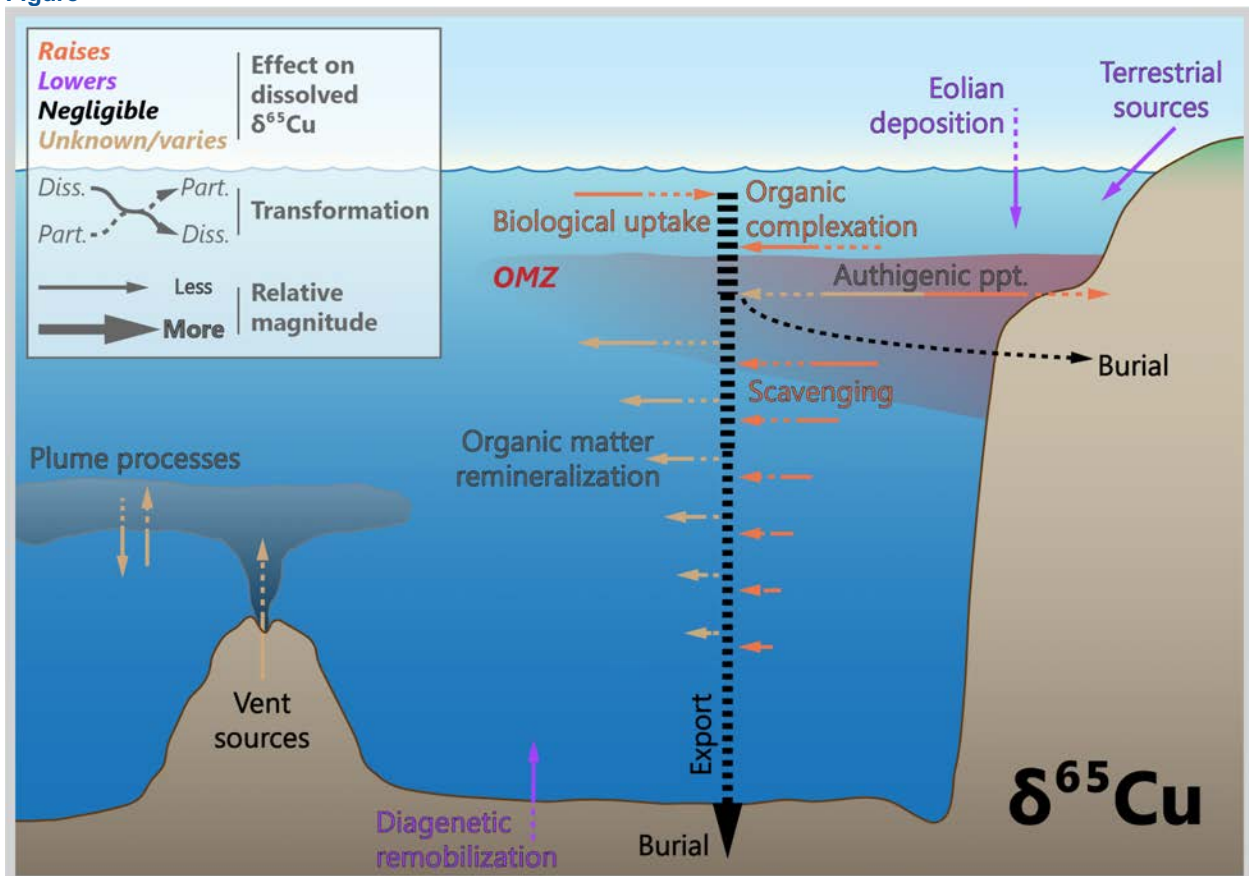
1132

Copper isotopes are reported as relative to the NIST SRM 976 standard, though due to a shortage of this material, two other certified reference standards are now available: ERM-AE633 ($\delta^{65}\text{Cu}_{\text{SRM976}} = -0.01 \pm 0.05$ ‰) and ERM-AE647 ($\delta^{65}\text{Cu}_{\text{SRM976}} = +0.21 \pm 0.05$ ‰; Moeller et al., 2012; Moynier et al., 2017). For consistency and ease of comparison, Moynier et al. (2017) recommend that future data be reported relative to NIST SRM 976. We adopt this convention. The analysis of Cu isotopes in seawater is challenging, due to both Cu's strong organic complexation, and only two isotopes precluding the use of a double spike technique (reviewed in Little et al., 2018). The data presented to date indicate that deep seawater $\delta^{65}\text{Cu}$ values are isotopically heavy (at about +0.7 ‰; Fig. 12B) compared to the upper continental crust (UCC; at about +0.1 ‰; Table 1; Moynier et al., 2017). Lighter Cu isotope compositions in the upper water column and along margins are thought to reflect local sources of isotopically light Cu (e.g., aerosols, riverine particulates, sediments; Takano et al., 2014; Little et al., 2018). While sample treatment may be a concern for quantitative [Cu] measurements (Posacka et al., 2017), it remains unclear to what extent this might also

1133 be an issue for measurements of $\delta^{65}\text{Cu}$ made using different techniques, depending on storage time,
 1134 acidification and oxidation with UV or H_2O_2 prior to analysis (see discussion in Little et al 2018).
 1135 Reassuringly, however, Little *et al.* did note that despite potential underestimation of $[\text{Cu}]$ by some
 1136 methods, a general homogeneity of seawater $\delta^{65}\text{Cu}$ persists between labs and geographic location and depth
 1137 of samples (Little et al., 2018; Yang et al., 2020; Fig. 12). As such, the expected methodological effects of
 1138 incomplete Cu recovery on $\delta^{65}\text{Cu}$ may be slight, though it remains unclear how the size of this effect might
 1139 vary with sample location and oceanographic conditions (e.g., surface or low $[\text{O}_2]$). As the seawater $\delta^{65}\text{Cu}$
 1140 dataset continues to grow, we echo the calls of previous authors that further urgent intercalibration of
 1141 methods is needed (e.g., Posacka et al., 2017; Little et al., 2018; Baconais et al., 2019).

1142

1143 **Figure**



1144

1145

1146

1147

Figure 13 | Processes driving Cu isotope variations in modern seawater. Biological productivity exerts only a modest impact on the marine Cu isotope cycle and thus there is no obvious route to developing Cu isotopes (or Cu concentrations) as a paleoproductivity proxy.

1148

1149 **5.2. Driving processes**

1150 *5.2.1. Biological*

1151 Copper is bioessential, but cellular Cu contents are approximately 2–10 fold lower than the micronutrients
1152 Fe and Zn (Twining & Baines, 2013). The redox-active behaviour of Cu (existing as Cu^{2+} or Cu^+ in
1153 biological systems) enables its role in electron transport, for example in the Cu-containing proteins
1154 plastocyanin and cytochrome c oxidase (Ridge et al., 2008). Copper uptake by some Fe-limited
1155 phytoplankton may increase, either due to the replacement of Fe-containing with Cu-containing enzymes
1156 (e.g., Peers and Price, 2006), or the involvement of Cu in the high affinity Fe uptake systems (Annett et al.,
1157 2008; Maldonado et al., 2006; Guo et al., 2012). Despite its biological function, Cu is also extremely toxic
1158 due to the formation of reactive oxygen species, which pose a threat to DNA, lipids, and proteins (Ridge et
1159 al., 2008). Copper toxicity thresholds vary by phytoplankton group, with smaller organisms generally more
1160 sensitive than larger ones (e.g., cyanobacteria cf. diatoms; Brand et al., 1986), and coastal strains more
1161 resistant than open ocean strains (e.g., Peers et al., 2005).

1162 A small number of studies have investigated Cu isotope fractionation during cellular uptake or cell surface
1163 adsorption by microorganisms (Pokrovsky et al., 2008; Navarrete et al., 2011; Cadiou et al., 2017; Coutaud
1164 et al., 2018; 2019). The results of these experiments are somewhat variable, with enrichment of either light
1165 or heavy Cu isotopes observed during assimilation and adsorption. However, assimilation in culture
1166 generally favours light Cu isotopes (Navarrete et al., 2011; Cadiou et al., 2017; Fig. 13). The complexity in
1167 Cu isotopic behaviour has been attributed to small changes in Cu speciation or redox during uptake and/or
1168 release of Cu (Coutaud et al., 2018; 2019).

1169

1170 *5.2.2. Chemical*

1171 In seawater, the vast majority of Cu is complexed to strong organic ligands (more than 99.8% complexed
1172 in surface northeast Pacific), which lower free $[\text{Cu}^{2+}]$ to below toxic levels (e.g., Coale & Bruland, 1988;
1173 1990; Moffett & Dupont, 2007). It is thought that ligands are primarily produced by biota for the purpose
1174 of detoxification (e.g., Moffett et al., 1990; Moffett & Brand, 1996), although recent work suggests that
1175 strongly complexed Cu is bioavailable to some eukaryotes, which appear to have a higher cellular Cu
1176 requirement (and higher thresholds of Cu toxicity) than prokaryotes (Semeniuk et al., 2009; 2015).

1177 Both theory and experiments predict preferential complexation of heavy isotopes by strong organic ligands
1178 (Sherman, 2013; Fujii et al., 2013; Ryan et al., 2014; Sherman et al., 2015), and organic complexation is
1179 thought to play a key role in the modern oceanic budget and distribution of Cu isotopes (Vance et al., 2008;
1180 Little et al., 2014a; Thompson & Ellwood, 2014; Takano et al., 2014; Little et al., 2018). The small pool of
1181 non-complexed Cu^{2+} in seawater is thus expected to be isotopically light (e.g., Little et al., 2014b, 2018).

1182 Based on a surface complexation model with the phyllo-manganate birnessite, the principal scavenging
1183 phase of divalent trace metals in oxic sediments, Sherman & Peacock (2010) calculated that [Cu] in deep
1184 waters should be orders of magnitude lower than is actually observed. They attribute this difference to the
1185 chelation of “*essentially all dissolved Cu*” by organic ligands (Sherman & Peacock, 2010), consistent with
1186 observations (e.g., Moffett & Dupont, 2007; Heller & Croot, 2015; Jacquot & Moffett, 2015). Nevertheless,
1187 some form or forms of scavenging are also thought to play a role in the oceanic Cu distribution.

1188 Reversible scavenging, a term used to describe the equilibrium between a scavenged and dissolved metal
1189 pool, has been proposed as the driving process behind the generally monotonic, linear increases in [Cu]
1190 with depth (Little et al., 2013; Richon et al., 2019; Fig. 12). In some regions with high particulate loads
1191 (e.g., some hydrothermal plumes, benthic nepheloid layers), scavenging removal of Cu has been observed
1192 (Jacquot and Moffett, 2015; Roshan & Wu, 2015a). Preferential scavenging of light Cu isotopes by
1193 particulate (e.g., oxyhydroxide) phases has also been proposed as an explanation for isotopically heavy
1194 seawater Cu isotope compositions (e.g., Takano et al., 2014), though the driving mechanisms leading to
1195 isotopically light particulate Cu remain to be fully established (see Sec. 5.3; Fig. 13).

1196 The shorter residence time of Cu (2-3.3 kyr; Little et al., 2017b), compared to trace metals with longer
1197 residence times (e.g., Cd, Zn, Ni), mean that, as for Fe, regional and local sources of Cu to the ocean play
1198 a relatively larger role in determining [Cu] distributions than for some other metals. Sources of Cu include
1199 aerosols (both natural and anthropogenic; e.g., Takano et al., 2014; Yang et al., 2019), benthic fluxes from
1200 sediments (e.g., Boyle et al., 1977; Heller & Croot, 2015; Roshan & Wu, 2015a; Little et al., 2018), and
1201 dissolved or particulate riverine sources (e.g., Vance et al., 2008; Little et al., 2018; Richon et al., 2019;
1202 Fig. 13). A possible small hydrothermal source has been identified in the South Pacific from the East Pacific
1203 Rise (Roshan & Wu, 2018), which is in contrast to the scavenging removal of Cu observed around
1204 hydrothermal vents elsewhere (e.g., Jacquot and Moffett, 2015).

1205

1206 5.2.3. *Physical*

1207 Copper's shorter residence time relative to Cd, Zn and Ni also means that the Southern Ocean and wider
1208 physical ocean circulation play a somewhat smaller role in oceanic [Cu] and $\delta^{65}\text{Cu}$ distributions compared
1209 to many of the other bioactive trace metals discussed herein. Nonetheless, the imprint of circulation is
1210 evident in certain circumstances, such as in the Atlantic and the upper 2 km of the South Pacific where [Cu]
1211 is correlated with [Si] (Roshan & Wu, 2015a; 2018; Little et al., 2018).

1212

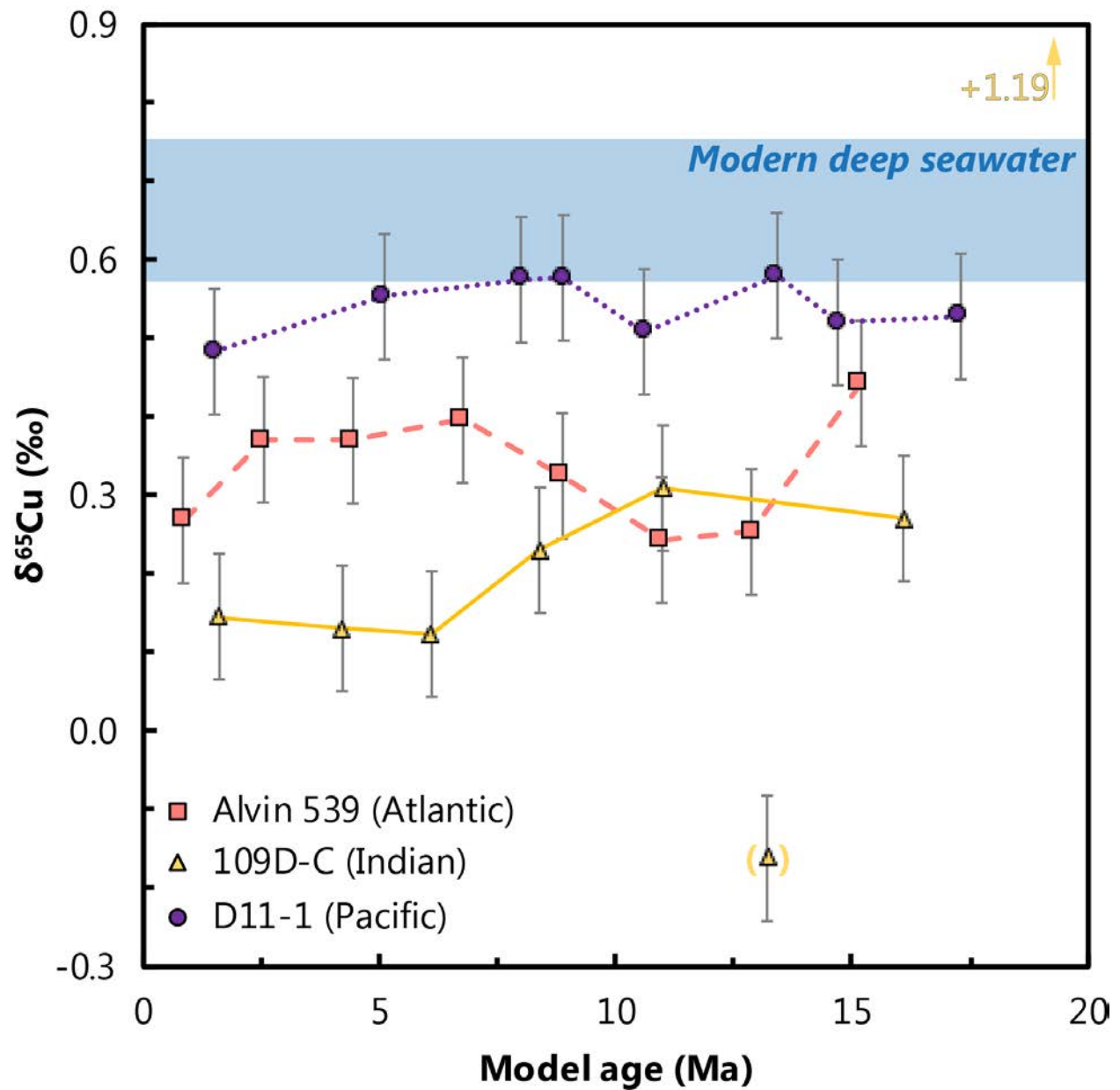
1213 5.3. Marine archives

1214 5.3.1. *Ferromanganese sediments*

1215 Ferromanganese sediments (crusts and nodules) exhibit Cu isotope compositions of +0.3 to +0.5 ‰
1216 (Albarède, 2004; Little et al., 2014). This means that, on average, Fe–Mn sediments are approximately 0.35
1217 ‰ lighter than deep seawater, which averages +0.7 ‰ (Fig. 14). The explanation for this offset is uncertain,
1218 but may reflect either strong organic complexation of Cu in seawater (Little et al., 2014b), or the enrichment
1219 of light Cu isotopes on the birnessite mineral surface. The latter has been observed in inorganic experiments,
1220 whereby sorbed Cu exhibited $\delta^{65}\text{Cu}$ that was 0.45 ± 0.18 ‰ lower than $\delta^{65}\text{Cu}$ in solution (Ijichi et al., 2018).
1221 Consistent with these experiments, light isotope fractionation on sorption of Cu to birnessite has also been
1222 predicted from first-principles *ab initio* calculations (Sherman and Little, 2020). At equilibrium in seawater,
1223 however, the strong complexation and mineral sorption effects should be additive, leading to a much larger
1224 isotopic offset than the ~ 0.35 ‰ observed, suggesting that one of the two effects is not expressed in nature
1225 for reasons as yet unclear (Sherman and Little, 2020).

1226 Little et al. (2014a) observed no marked changes in deep ocean $\delta^{65}\text{Cu}$ recovered from three Fe–Mn crusts
1227 from each of the major ocean basins over the last ~ 20 Ma. Copper is relatively immobile in Fe–Mn crusts,
1228 with a calculated effective diffusivity $\leq 10^{-9}$ $\text{cm}^2 \text{yr}^{-1}$ (Henderson & Burton, 1999), similar to Ni (Sec.
1229 9.3.1.). Assuming that Fe–Mn crusts preserve primary $\delta^{65}\text{Cu}$, the various records suggest that on a global
1230 basis, the marine Cu cycle has been in isotopic steady state for at least 20 Myr (Fig. 14).

1231



1232

1233 **Figure 14 | Deep ocean $\delta^{65}\text{Cu}$ constancy over the past 20 Myr.** These records are derived from Fe–Mn crusts
 1234 recovered from the Atlantic (square, dashed line), Indian (triangle, solid line), and Pacific Oceans (circle, dotted line;
 1235 data from Little et al., 2014b). Assuming the isotopic offset between dissolved Cu in seawater and Fe–Mn crusts has
 1236 remained unchanged at ≈ 0.35 ‰ over this time, these records imply that the inter-basin Cu isotope variations observed
 1237 in modern crusts and the Cu isotope cycle itself have remained relatively stable for at least 20 Myr. Two samples from
 1238 109D-C possess low levels of authigenic Cu enrichment indicating detrital contamination (parentheses, arrow; see Little
 1239 et al., 2014b).
 1240

1241 5.3.2. Organic-rich sediments

1242 Qualitative arguments for high organic matter fluxes (i.e., higher paleoproductivity) have been made based
 1243 on elevated Cu (and Ni) contents of ancient organic-rich sediments (e.g., Tribovillard et al., 2006). This

1244 approach is supported by positive correlations between Cu (and Ni, Sec. 9.3.2.) with TOC content in modern
1245 continental margin sediments (e.g., Böning et al., 2012). For this approach to offer mechanistic insights
1246 into past export productivity, organic matter (or a biologically associated mineral phase, such as CaCO₃ or
1247 BaSO₄), must be the primary vector for that metal to sediments. This condition is not met for Cu, nor for
1248 other chalcophile elements (e.g., Mo), thus presenting a significant challenge to the use of sediment Cu
1249 content to trace past export productivity. Copper exhibits a strong reactivity toward sulfide, as illustrated
1250 by the quantitative removal of Cu from the euxinic Black Sea water column and resultant enrichment in
1251 underlying sediments (Tankéré et al., 2001; Little et al., 2015).

1252 Despite the strong reactivity of Cu towards sulfide, and unlike Zn (Sec. 4.3.4.) and Mo (Sec 7.2.3.), Cu in
1253 euxinic sediments from the Black Sea and Cariaco Basin do not record open marine $\delta^{65}\text{Cu}$ (Little et al.,
1254 2017b). In fact, authigenic Cu in modern organic-rich sediments (from both euxinic basins and continental
1255 margin settings) is generally similar in isotopic composition to Fe–Mn sediments and to suspended
1256 particulate material collected from the South Atlantic, all at about +0.3‰ (Little et al., 2017b; 2018; Ciscato
1257 et al., 2019). The homogeneity in authigenic sedimentary Cu isotope compositions has been suggested to
1258 reflect an equilibrium isotope fractionation in the aqueous phase between organically complexed Cu and
1259 inorganic Cu²⁺, with the latter approximately 0.4 ‰ lighter than ligand-bound Cu, followed by near
1260 quantitative scavenging of inorganic Cu²⁺ by particulate material of any type (Little et al., 2017b; 2018).
1261 For example, in the Black Sea, transfer of Cu to the deep euxinic basin may be mediated by cycling with
1262 nanoparticulate Fe and Mn oxides at the redoxcline, linked to the benthic Fe–Mn redox shuttle (Lyons &
1263 Severmann, 2006; Little et al., 2017b). If correct, this hypothesis suggests that authigenic Cu isotope
1264 compositions in marine sediments may reflect the evolution of organic complexation on geological
1265 timescales.

1266 Ciscato et al. (2018; 2019) developed a new approach to isolate trace elements associated with two different
1267 fractions in organic-rich sediments, the ‘organic-pyrite fraction’ (OPF) and ‘HF digestible fraction’ (HFD).
1268 They find that the OPF of modern Peru margin sediments typically contains >50 % of total Cu and is
1269 variably isotopically light compared to bulk authigenic Cu. They suggest this signature reflects incomplete
1270 sulfidation under variable water column and sedimentary redox conditions (e.g., Bianchi et al., 2018).
1271 Unlike in modern sediments, in ancient shales (ranging in age from 0.4 to 3.4 Ga) bulk Cu content does not
1272 correlate with TOC and >80 % of Cu is hosted in the HFD fraction. In addition, the OPF fraction in ancient
1273 shales is markedly isotopically heavier than it is in modern sediments (Ciscato et al., 2019). This difference
1274 between modern and ancient Cu partitioning may reflect diagenetic or metamorphic processing, or it may
1275 be a primary feature relating to differences in the Cu isotope composition of seawater, or differences in the
1276 mechanism(s) of Cu sequestration into sediments.

1277

1278 **5.4. Prospects**

1279 Despite the biological importance of Cu, the modern biogeochemical cycle of Cu suggests there is no clear
1280 route to developing Cu isotopes (or [Cu]) as a paleoproductivity proxy. Work is also urgently needed to
1281 better understand the role of processing and storage effects on the accuracy of the oceanic [Cu] database,
1282 perhaps providing the opportunity to better understand the speciation of the dissolved Cu pool. Similarly,
1283 work is needed to firmly establish the fidelity of $\delta^{65}\text{Cu}$ measurements and ensure that different datasets can
1284 be synthesized. Despite these challenges, however, it is known that organic ligands play a key role in the
1285 cycling of Cu and Cu isotopes, suggesting a potential for the use of Cu isotopes in tracing the evolution of
1286 organic complexation on geological timescales. Additionally, careful sequential extraction procedures, such
1287 as those described by Ciscato et al. (2019), may allow for the direct probing of past seawater properties,
1288 such as redox state.

1289 At present, there are few applications of Cu isotopes to study ancient biogeochemical cycles. Interestingly
1290 however, there are two black shale records that indicate a shift from UCC-like to heavy Cu isotope values
1291 across the Great Oxidation Event (GOE, ~2.4 Ga; Chi Fru et al., 2016; Ciscato et al., 2019). Chi Fru et al.
1292 (2016) interpreted this shift as reflecting the onset of oxidative weathering and waning of iron formation
1293 deposition, with the latter process driving pre-GOE seawater isotopically light due to the preferential
1294 scavenging of heavy Cu isotopes to Fe oxides. However, a recent analysis of two classic pre-GOE sequences
1295 containing iron formations do not support this earlier hypothesis, with $\delta^{65}\text{Cu}$ remaining close to 0 ‰
1296 (Thibon et al., 2019). Thus, while the limited available data preclude confident interpretations, there are
1297 tantalizing tastes of future research directions in Cu isotope geochemistry.

1298

1299

1300

1301

1302

1303

1304 **6. Cadmium**

1305 The distribution of [Cd] closely correlates with macronutrient [PO₄³⁻] in the oceans (; e.g., Boyle et al.,
1306 1976; Bruland, 1980). The nutrient-like properties of [Cd] and attendant correlations with [PO₄³⁻] have
1307 been documented in multiple ocean basins, in multiple dimensions (i.e., vertically, spatially, and
1308 temporally), and are faithfully captured by certain sediments (e.g., Boyle, 1981). Moreover, many marine
1309 microbes assimilate isotopically light Cd from their environment (e.g., Lacan et al., 2006), consistent with
1310 the direction and magnitude of Cd isotope fractionation in seawater (e.g., Ripperger et al., 2007). Though
1311 the overall geochemical distribution of Cd is promising from the perspective of tracing paleoproductivity,
1312 there remain three broadly three issues that require addressing. Briefly, these relate to uncertainties
1313 surrounding: how, why, and which organisms contribute to Cd cycling in seawater; the significance of the
1314 decoupling between Cd and major nutrients in sinking particles, particularly in low [O₂] settings; and,
1315 identification of sedimentary archives that capture surface water δ¹¹⁴Cd. Despite these uncertainties, the
1316 first-order features of marine Cd geochemistry are characteristic of a nutrient-type element, meaning that
1317 Cd can be modelled in a simple reactor scheme (see Sec. 2.2. and Fig. 4), and that the distributions of [Cd]
1318 and δ¹¹⁴Cd appear broadly connected to underlying patterns of productivity.

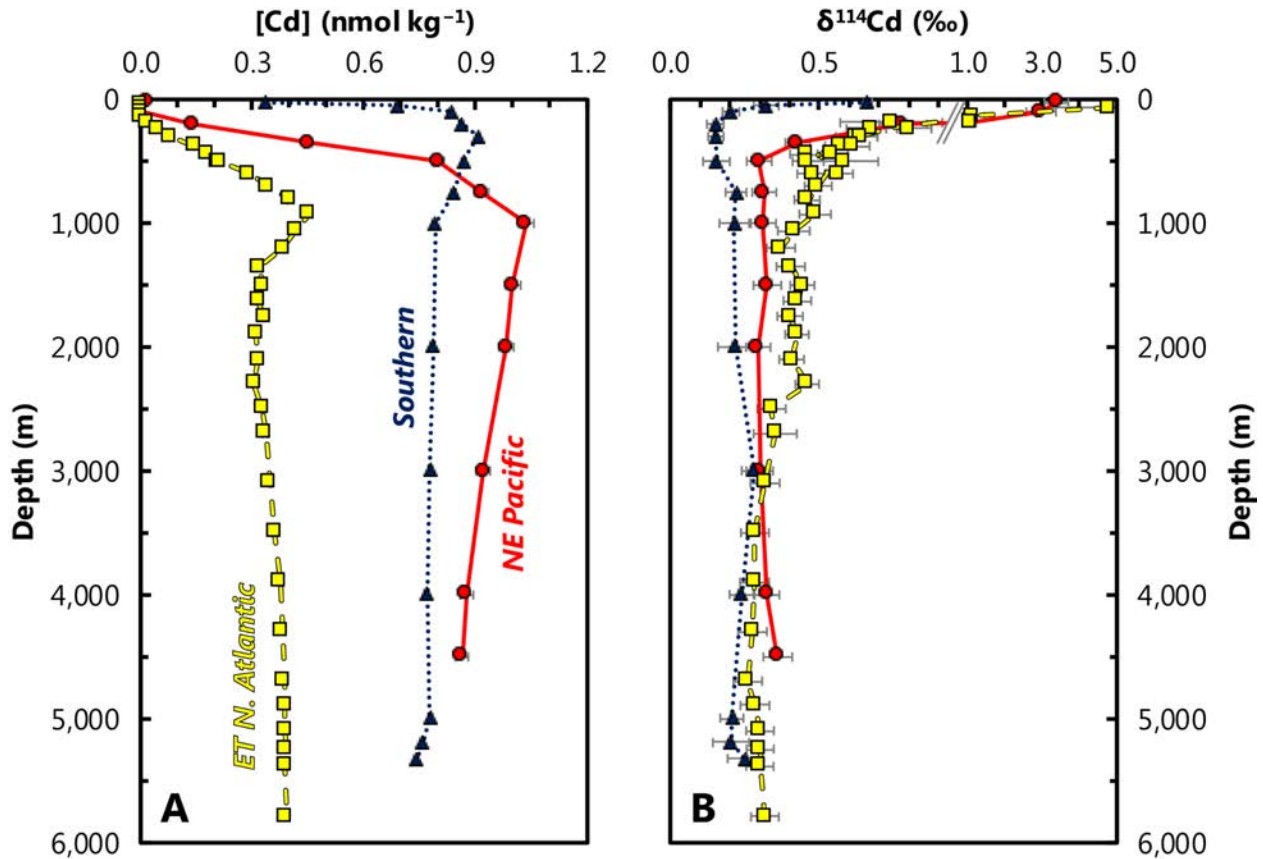
1319

1320 **6.1. Marine distribution**

1321 Away from major upwelling regions, surface water [Cd] are typically between 1–100 pmol kg⁻¹, but can
1322 reach as low as 30 fmol kg⁻¹ (Schlitzer et al., 2018; Fig. 15). The majority of this small surface inventory
1323 is thought to be complexed by strong organic ligands (e.g., Bruland, 1992; Ellwood, 2004). In intermediate
1324 and deep waters, [Cd] are significantly elevated relative to surface waters, ranging from 0.5 nmol kg⁻¹ in
1325 intermediate and deep waters in the north Atlantic to ≈1.2 nmol kg⁻¹ in the oldest deep waters of the north
1326 Pacific (Schlitzer et al., 2018). As with Zn (Sec. 3.), the overall distribution of [Cd] throughout the oceans
1327 is driven principally by biological and physical processes in the Southern Ocean, and the lateral circulation
1328 of Southern Ocean water masses (e.g., Baars et al., 2014; Xie et al., 2017; Middag et al., 2018; Sieber et
1329 al., 2019a). Thus, the shape of vertical [Cd] profiles at lower latitudes arises largely from horizontal
1330 transport and mixing of high-Cd Southern Ocean-sourced water masses, with a modest contribution from
1331 regeneration of sinking particles (i.e., 5–40 %; Middag et al., 2018). These processes result in Cd having
1332 ‘nutrient-type’ one-dimensional water column profiles, with a progressive increase in intermediate and deep

1333 water [Cd] along the pathways of meridional overturning circulation (e.g., de Baar et al., 1994; Middag et
1334 al., 2018).

1335



1336

1337 **Figure 15 | Representative profiles of dissolved Cd concentrations ([Cd]; A) and Cd isotope compositions**
1338 **($\delta^{114}\text{Cd}$; B).** Data from the Eastern Tropical North Atlantic (squares, dashed line; Conway & John, 2015b), Northeast
1339 Pacific (circles, solid line; Conway & John, 2015a), and Southern Oceans (triangles, dotted line; Abouchami et al.,
1340 2014). Station locations as per Fig. 1. Note the break in scale in $\delta^{114}\text{Cd}$ above 1 ‰, illustrating the extreme isotopic
1341 compositions observed in the most Cd-depleted surface samples. Notably, such extreme compositions are generally
1342 not observed in the similarly Cd-depleted surface waters of the Southern Hemisphere gyres (e.g., Gault-Ringold et al.,
1343 2011; Xie et al., 2017; George et al., 2019), nor in the surface of the high latitude Southern Ocean, where dissolved
1344 [Cd] is elevated (e.g., Abouchami et al., 2011; 2014). This comparison illustrates that the processes leading to distinct
1345 dissolved concentration profiles effect only modest changes in dissolved $\delta^{114}\text{Cd}$ between basins.

1346

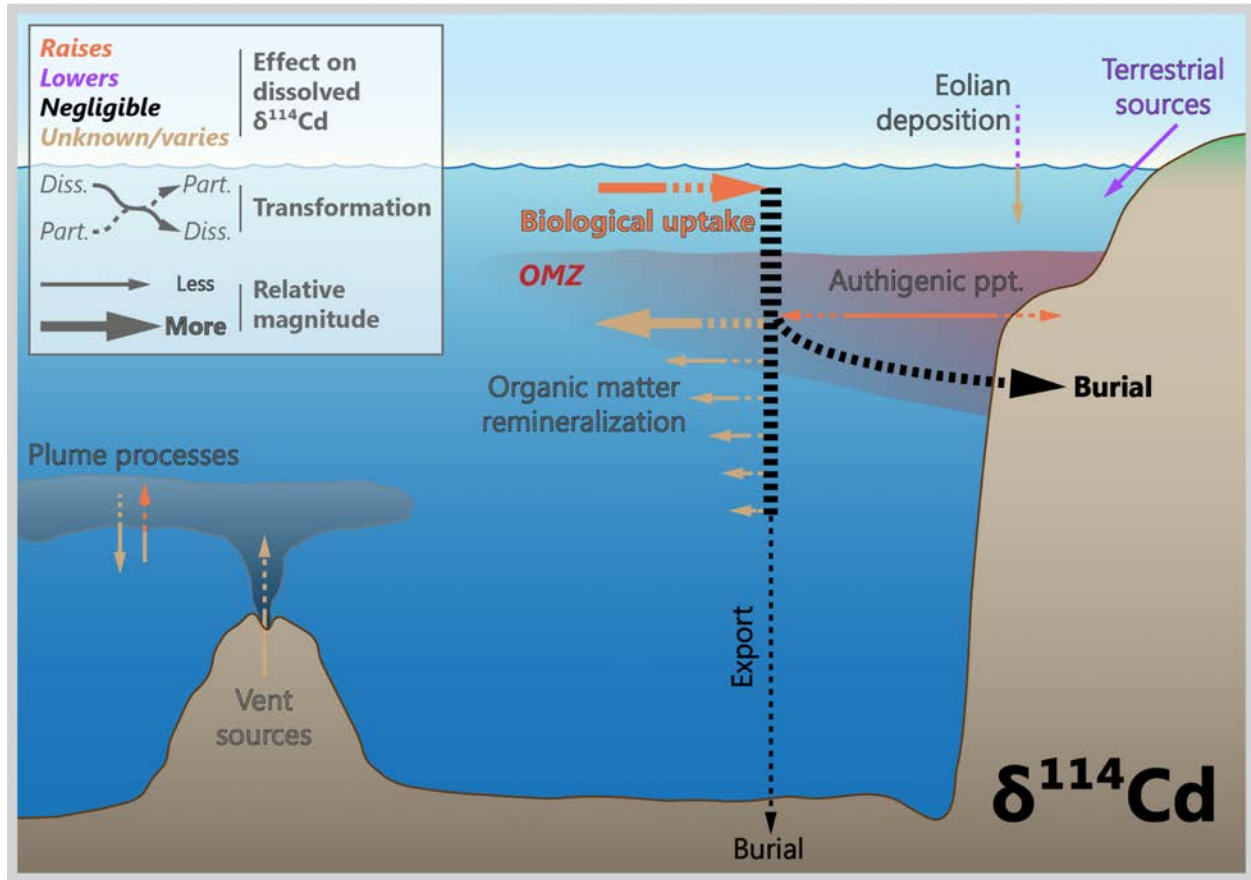
1347 The past decade has seen an explosion in the number of studies employing Cd stable isotopes to investigate
1348 marine Cd cycling. The majority of extant Cd isotope data are reported relative to the NIST SRM 3108
1349 standard, though several earlier studies, reviewed by Rehkämper et al. (2012), were reported relative to
1350 other in-house materials. Cross-calibration of these materials is described in detail by Abouchami et al.
1351 (2013). While the earliest study of Cd isotope variations in seawater was unable to unambiguously identify
1352 systematic patterns in the water column, the authors noted that cultures of phytoplankton preferentially

1353 incorporated isotopically light Cd relative to the media (Lacan et al., 2006). Assuming biological processes
1354 were responsible for Cd uptake, this observation led to two key predictions for marine Cd isotope
1355 systematics: that Cd-depleted surface waters should exhibit isotopically ‘heavier’ compositions than Cd-
1356 replete deep waters; and, that the degree of isotopic fractionation should be proportional to the extent of Cd
1357 removal into particles. Indeed, this is precisely the pattern that was first reported by Ripperger et al. (2007).

1358 Subsequent studies have corroborated this general one-dimensional pattern in the Southern (e.g.,
1359 Abouchami et al., 2011; 2014; Xue et al., 2013; Sieber et al. 2019a), Atlantic (e.g., Xue et al., 2012; Conway
1360 & John, 2015a; Xie et al., 2017; Xie et al., 2019a; Bryan et al., 2021), Arctic (Zhang et al., 2019), and
1361 Pacific Oceans (Yang et al., 2012; Yang et al., 2014; Conway & John, 2015b; Janssen et al., 2017; John et
1362 al., 2018; Yang et al., 2018; Xie et al., 2019b; Sieber et al., 2019b). These studies have shown that the deep
1363 ocean (>500–1,000 m) is largely homogenous in Cd isotope composition ($\delta^{114}\text{Cd}$ of +0.2 to +0.3 ‰; Fig.
1364 15). This deep water $\delta^{114}\text{Cd}$ value is heavier than the upper continental crust $\delta^{114}\text{Cd}$ signature of ~0‰
1365 (Schmitt et al., 2009a), similar to that observed for other metals such as Zn, Ba, and Ni (Secs. 3, 7, and 8).
1366 Intermediate-depth waters relating to water masses such as Antarctic Intermediate Water (AAIW) exhibit
1367 slightly heavier $\delta^{114}\text{Cd}$ values (+0.4 to +0.5 ‰), with waters above these typically exhibiting heavier
1368 isotopic compositions (up to ~+1‰; Fig. 15). As for [Cd], these one-dimensional $\delta^{114}\text{Cd}$ profile shapes
1369 arise largely from the combination of Southern Ocean biological processes and lateral circulation of water
1370 masses, as well as some contribution from local surface uptake and regeneration (Abouchami et al., 2014;
1371 Sieber et al., 2019b).

1372 Although the first-order distributions of [Cd] and $\delta^{114}\text{Cd}$ in surface waters are consistent with intense
1373 cycling by biological processes, when considering the global database of surface $\delta^{114}\text{Cd}$ data, this simple
1374 ‘nutrient-like’ reactor scheme with a single fractionation factor breaks down. For example, while studies
1375 have reported $\delta^{114}\text{Cd}$ values of up to +5 ‰ in Cd-depleted surface waters of the Northern Hemisphere gyres
1376 (Ripperger et al., 2007; Xue et al., 2012; Conway & John, 2015a; 2015b), others have reported more muted
1377 fractionation or even a switch to lighter than deep ocean compositions in surface waters (Gault-Ringold et
1378 al., 2012; Xie et al., 2017; Janssen et al., 2017; Xie et al., 2019a; George et al., 2019; Sieber et al., 2019b;
1379 Xie et al., 2019). This range of observations suggests that the processes influencing surface Cd isotope
1380 compositions may be more complex than simple biological uptake (Fig. 16). For example, interactions with
1381 ligands, effects arising from recycling of organic matter, differences in fractionation factor between
1382 different organisms, and supply of Cd from external Cd sources may all influence surface water dissolved
1383 $\delta^{114}\text{Cd}$. This raises three related questions to be addressed in the remainder of this section: What are the
1384 candidate biological processes that drive these patterns? How do other physical or chemical processes play
1385 a role in setting marine Cd distributions? Can Cd-based reconstructions of these processes be used to inform

1386 on past productivity? Further to these questions, are the extreme heavy $\delta^{114}\text{Cd}$ observed in Northern
 1387 Hemisphere gyres, and so far only twice in the Southern hemisphere (Sieber et al., 2019b; Bryan et al.,
 1388 2021), real, or analytical artifacts?



1389
 1390 **Figure 16 | Processes driving Cd isotope variations in modern seawater.** Biological processes exert a significant
 1391 control on surface water Cd cycling, implying that $\delta^{114}\text{Cd}$ is broadly responsive to productivity. However, important
 1392 redox-dependent processes remain to be fully elucidated, particularly those occurring around OMZs.

1393
 1394 **6.2. Driving processes**

1395 **6.2.1. Biological**

1396 As noted above, the nutrient-like distribution of [Cd] implies intense biological cycling in seawater, even
 1397 though Cd is considered toxic (e.g., Waldron & Robinson, 2009). This dichotomy has inspired a significant
 1398 body of research investigating the role that Cd plays in microbial physiology. These studies showed that
 1399 Cd uptake by marine microbes exhibits three noteworthy dependencies. First, cellular Cd quotas are
 1400 strongly positively correlated with the Cd content of their environment, both in culture (see compilation by
 1401 Twining & Baines, 2013) and from oceanographic data (Middag et al., 2018). Second, microbial Cd uptake

1402 is diminished when the concentration of other divalent cations increases, particularly so for Fe, Mn, and
1403 Zn. Likewise, lower concentrations of these divalent cations cause increases in Cd uptake (e.g., Sunda &
1404 Huntsman, 2000; Cullen et al., 2003). Some diatoms have even shown capacity to substitute much of their
1405 metabolic Zn requirements with Cd (Price & Morel, 1990). Third, Cd uptake is also influenced by speciation
1406 of inorganic carbon, with low $p\text{CO}_2$ promoting higher cellular Cd quotas (e.g., Cullen et al., 1999; Cullen
1407 & Sherrell, 2005; de Baar et al., 2017). The connection between Cd and carbon speciation is particularly
1408 intriguing given the discovery of the ζ -class of carbonic anhydrase that can utilize Cd (or Zn) as the catalytic
1409 metal (e.g., Lane et al., 2005; Xu et al., 2008). Despite these dependencies, however, the extent to which
1410 active physiological utilization of Cd controls global patterns of Cd uptake is unclear. For example, genes
1411 encoding the ζ -class of carbonic anhydrase were not found in green algae nor coccolithophores, and were
1412 similarly absent from many diatom species (Park et al., 2007). Thus, it is similarly plausible that some part
1413 of the biological Cd cycle is driven by organisms inadvertently removing Cd from seawater while
1414 attempting to source other metals (e.g., Boyle, 1988b; Horner et al., 2013), or that microbes require Cd to
1415 populate other Cd-centered metalloenzymes that await discovery.

1416 The role of microbial physiology in mediating Cd isotope fractionation is also comparatively understudied.
1417 However, it does appear that biological fractionation of Cd isotopes is ubiquitous; fresh- (Lacan et al., 2006)
1418 and saltwater (John & Conway, 2014) green algae, incubations of unfiltered seawater (Xue et al., 2012),
1419 heterotrophic bacteria (Horner et al., 2013), and shallow marine particles (e.g., Yang et al., 2015; Janssen
1420 et al., 2019) all indicate that biological particles accumulate isotopically light Cd from their environment
1421 with a fractionation between -0.3 to -0.8 ‰ (Fig. 16). The limited depth profile data of suspended
1422 particulates that exist suggests subsequent partial respiration of already-light particulate organic matter also
1423 induces a second fractionation, further enriching light isotopes in the remnant particulate phase (Janssen et
1424 al., 2019). Additionally, as discussed in Sec. 6.1. and 6.2.2., variability in surface dissolved $\delta^{114}\text{Cd}$ data
1425 even at similarly low [Cd], ranging from extremely heavy $\delta^{114}\text{Cd}$ values to no apparent fractionation
1426 suggests that surface Cd isotope cycling cannot be simply driven by removal of isotopically light Cd from
1427 surface waters, and a mechanistic understanding of this remains limited.

1428

1429 *6.2.2. Chemical*

1430 The role of chemical processes in mediating global Cd distributions is the most underconstrained of the
1431 three processes discussed in this review. Recent studies suggested that pelagic partitioning of Cd into
1432 sulfides in OMZs may be a significant loss term (Janssen et al., 2014; Bianchi et al., 2018; Plass et al.,
1433 2020). Moreover, the Cd isotope effect associated with sulfide precipitation identified by Guinoiseau et al.

1434 (2018) is consistent with field data, and particulate Cd is known to accumulate more rapidly in sediments
1435 that are bathed by bottom waters containing low $[O_2]$ (Fig. 16; Sec. 5.3.; e.g., van Geen et al., 1995).
1436 Collectively, these observations suggest a potential redox sensitivity in sedimentary Cd isotope
1437 distributions that deserves additional scrutiny. Indeed, the influence of sediments as the most important
1438 marine Cd sink can be seen in some water column profiles of $\delta^{114}Cd$ (Xie et al., 2019b). Similarly, data
1439 from the hydrothermal TAG site in the North Atlantic suggests that hydrothermal plumes may scavenge Cd
1440 from seawater, constituting a small sink of isotopically light Cd, though this does not have an observable
1441 effect on deep ocean $\delta^{114}Cd$ values outside of the plume itself (Fig. 16; Conway & John, 2015b).

1442 Other potential sources and sinks include rivers, atmospheric deposition, and sediments; however, none of
1443 these interfaces exhibit significant anomalies in $[Cd]$ or $\delta^{114}Cd$ in GEOTRACES-era datasets. This finding
1444 is in accord with earlier research by Martin & Thomas (1994), though there exist two possible exceptions.
1445 The first concerns the role of atmospheric aerosols, which have been invoked to explain the Cd isotope
1446 composition of surface waters in the Southwest Pacific (e.g., George et al., 2019) and South China Sea
1447 (e.g., Yang et al., 2012). Modern aerosol inputs may be largely anthropogenic in origin. Anthropogenic
1448 forms of Cd exhibit a relatively narrow range of isotopic compositions that are typically—though not
1449 always (e.g., Shiel et al., 2010)—lighter than dust-derived Cd (e.g., Bridgestock et al., 2017). Second,
1450 interactions with organic ligands have also been invoked to explain the relatively muted pattern of Cd
1451 isotope fractionation in the surface of the south Atlantic Ocean (e.g., Xie et al., 2017; Guinoiseau et al.,
1452 2018), but there are as yet no corroborating field or experimental data examining the role of organic ligands
1453 in mediating Cd isotope fractionation in seawater.

1454

1455 6.2.3. *Physical*

1456 Physical processes are similarly influential in mediating the global distribution of $[Cd]$ and $\delta^{114}Cd$
1457 throughout the global oceans, particularly those processes occurring in the Southern Ocean. Antarctic
1458 Intermediate and Bottom Waters possess higher $[Cd]:[PO_4^{3-}]$ than North Atlantic Deep Water (e.g., de Baar
1459 et al., 1994; Middag et al., 2018). Mixing between these southern- and northern-sourced water masses likely
1460 contributes to the well-known ‘kink’ in the $[Cd]:[PO_4^{3-}]$ relationship (e.g., Frew & Hunter, 1992; Elderfield
1461 & Rickaby, 2000; Quay & Wu, 2015). Why northern- and southern-sourced intermediate and deep waters
1462 possess different $[Cd]:[PO_4^{3-}]$ is debated, and likely reflects regionally distinct fractionation of Cd and P
1463 during biological uptake (e.g., Sunda & Huntsman, 2000; Cullen et al., 2003) and during remineralization
1464 (e.g., Baars et al., 2014; Roshan & Wu, 2015). In the Atlantic, however, the importance of remineralization
1465 to deep water Cd budgets is of secondary significance: the ratio of regenerated-to-preformed $[Cd]$ is ~30 %

1466 in the mesopelagic, and generally <10 % in the deep ocean (Roshan & Wu, 2015b; Middag et al., 2018).
1467 Given the low proportion of regenerated Cd in the deep Atlantic, the ratio of [Cd]:[PO₄³⁻] and the overall
1468 distribution of [Cd] are essentially governed by the [Cd]:[PO₄³⁻] of the source waters (Middag et al., 2018)
1469 and the prevailing geometry of ocean circulation, respectively (Boyle, 1988b).

1470 Recent Cd isotope data from the South Atlantic (Xie et al., 2017), South Pacific (George et al., 2019; Sieber
1471 et al., 2019a), and Arctic (Zhang et al., 2019) also support the importance of mixing in mediating deep
1472 ocean [Cd] and $\delta^{114}\text{Cd}$ distributions, though it should be noted that the isotopic contrast between mixing
1473 endmembers is small, relative to measurement precision (Fig. 15; e.g., Janssen et al., 2017). For example,
1474 biological uptake of light Cd in the source regions of intermediate waters in the surface Southern Ocean
1475 results in isotopically heavy preformed $\delta^{114}\text{Cd}$ signatures being imparted to Cd-depleted intermediate water
1476 masses (e.g., +0.45 ‰ in AAIW; +0.65 ‰ in Subantarctic Mode Water, SAMW; Xue et al., 2013;
1477 Abouchami et al., 2014; Sieber et al., 2019b). Lateral circulation of these southern-sourced water masses
1478 then transfers this signature northward to intermediate depths in the Atlantic and Pacific Oceans (e.g., Xue
1479 et al., 2012; Abouchami et al., 2014; Conway & John, 2015a; Sieber et al., 2019b). This effect is more
1480 pronounced in the North Atlantic than in the Pacific, where southward flowing NADW also carries
1481 isotopically heavy Cd southward at depths of 1000–3000 m (Fig. 15; Xue et al., 2012; Conway & John,
1482 2015a).

1483

1484 **6.3. Marine archives**

1485 *6.3.1. Carbonates*

1486 There is a long history of the measurement of Cd contents of marine carbonates, particularly corals and
1487 foraminifera, most commonly reported as Cd:Ca molar ratios. In principle, carbonates are an appealing
1488 archive of ambient Cd chemistry since inorganic partition coefficients are $\gg 1$ (e.g., Tesoriero & Pankow,
1489 1996) and the Cd:Ca of many types of carbonate exhibit a strong proportionality with ambient [Cd]. In
1490 practice, however, most biogenic carbonates exhibit partition coefficients closer to unity (Boyle, 1988b),
1491 and resultant Cd:Ca is also sensitive to the species (Boyle, 1992) and temperature of calcification (e.g.,
1492 Rickaby & Elderfield, 1999). As such, Cd:Ca in carbonates has found the most utility where ambient [Cd]—
1493 and attendant carbonate Cd:Ca—exceeds several 100 pmol kg⁻¹, such as in tracing industrial fallout (e.g.,

1494 Shen et al., 1987) or in studies of Quaternary deep ocean circulation (e.g., Boyle & Keigwin, 1985; van
1495 Geen et al., 1992; Adkins et al., 1998; Farmer et al., 2019).

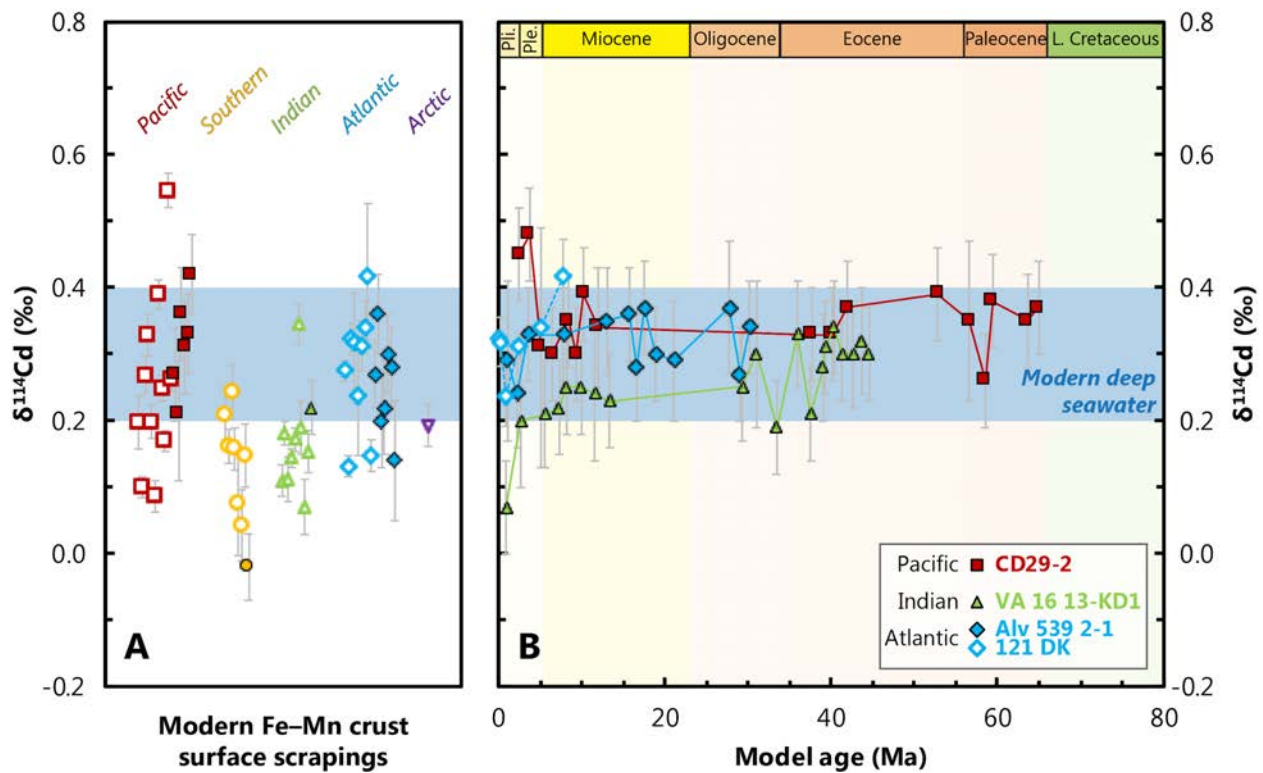
1496 There are far fewer studies examining the Cd isotope composition of marine carbonates as tracers of
1497 historical Cd isotope chemistry. Inorganic partitioning experiments indicate that Cd isotopes are
1498 fractionated during incorporation into calcite by ≈ -0.5 ‰ (Horner et al., 2011). The isotopic effect is
1499 temperature- and Mg-independent, but vanishes at low salinity. This inorganic calibration has been used to
1500 interpret patterns of Cd isotope fractionation preserved in bulk carbonates from the Neoproterozoic Eon
1501 (1,000–541 Ma). The variations in these sediments are interpreted as evidencing changes in biological
1502 productivity (e.g., Hohl et al., 2017) and Cd sinks through time (e.g., John et al., 2017). Applications of Cd
1503 isotopes to foraminifera to study problems in Quaternary paleoceanography are precluded by the large
1504 sample requirements; obtaining ~ 1 ng of Cd—typically the minimum quantity needed for a reasonably
1505 precise Cd isotope measurement (Ripperger & Rehkämper, 2007; Schmitt et al., 2009b)—requires picking
1506 and cleaning of 10's of mg of foraminiferal tests. Alleviation of such limitations awaits development of
1507 automated picking and screening systems (e.g., Mitra et al., 2019), or vast improvements in ion transmission
1508 efficiency for isotope ratio mass spectrometry.

1509

1510 6.3.2. *Ferromanganese sediments*

1511 Ferromanganese sediments have shown the most promise for recording deep ocean Cd isotope chemistry.
1512 Both ferromanganese nodules (Schmitt et al., 2009a) and crusts (Horner et al., 2010) reflect ambient
1513 seawater Cd isotope compositions with negligible fractionation (Fig. 17A), consistent with Cd–Mn-
1514 oxyhydroxide partitioning experiments conducted at high ionic strength that show only minor Cd isotope
1515 fractionation (Wasylenki et al., 2014). Horner et al. (2010) estimated that Cd is somewhat mobile in Fe–
1516 Mn crusts, with a predicted diffusivity $\leq 10^{-7}$ cm² yr⁻¹, similar to Hf (Henderson & Burton), Mo (Sec. 7.3.),
1517 Cr (Sec. 10.3.2.), and Ag (Sec. 11.3.). This rate implies that long-term records of $\delta^{114}\text{Cd}$ derived from Fe–
1518 Mn are likely to exhibit some diffusive smoothing while preserving larger perturbations. As with Zn and
1519 Cu isotopes however, time-resolved records of $\delta^{114}\text{Cd}$ recovered from Fe–Mn crusts indicate minimal
1520 variation over the last 20–60 Myr (Fig. 17B). The lack of variation may indicate that the sources and sinks
1521 of Cd have been in isotopic steady state throughout the Cenozoic. Alternatively, the lack of variation in

1522 $\delta^{114}\text{Cd}$ over the Cenozoic may simply reflect a ‘resetting’ of all crust layers toward modern deep ocean Cd
 1523 isotope compositions, as recently suggested by Murphy (2016).



1524
 1525 **Figure 17 | Ferromanganese crusts records of deep-water $\delta^{114}\text{Cd}$.** **A:** Compilation of ‘coretop’ Fe–Mn crust $\delta^{114}\text{Cd}$;
 1526 data from Schmitt et al. (2009a; open symbols) and Horner et al. (2010; closed symbols). In general, Southern Ocean
 1527 samples exhibit lighter $\delta^{114}\text{Cd}$ than other basins, consistent with profiles of $\delta^{114}\text{Cd}$ (e.g., Fig. 15). **B:** Cenozoic records
 1528 of deep-water $\delta^{114}\text{Cd}$ recovered from four Fe–Mn crusts; data from Murphy, 2016 (closed symbols) and Schmitt et al.
 1529 (2009a; open symbols). These records have been plotted using the authors’ preferred age models, meaning that there
 1530 are some differences between the chronology of CD29-2 shown here compared to Fig. 8. Such differences may be
 1531 immaterial however, given that Cd isotopes in Fe–Mn crusts are potentially subject to diffusive ‘resetting’ over time
 1532 (Murphy, 2016).

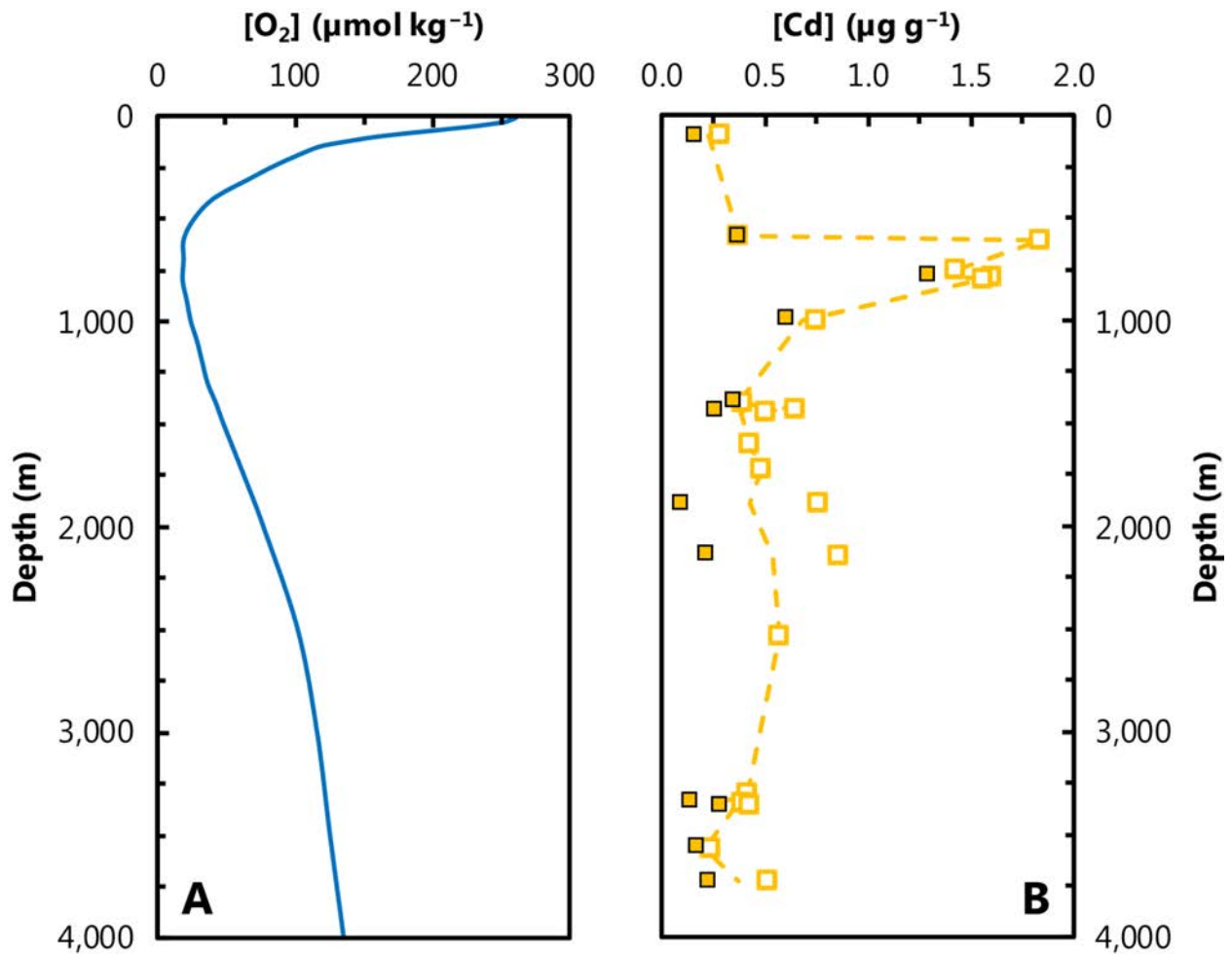
1533
 1534 **6.3.3. Organic-rich sediments**

1535 Organic-rich sediments are the principal sink of dissolved Cd from the modern oceans (e.g., Rosenthal et
 1536 al., 1995; van Geen et al., 1995; Little et al., 2015). A significant fraction of the total Cd in organic-rich
 1537 sediments is derived from sinking organic matter. Accordingly, the Cd content of organic-rich sediments
 1538 or of multiple paired sedimentary phases has been applied as a proxy for past productivity (e.g., Brumsack,
 1539 2006; Hohl et al., 2019). However, there is also a redox sensitivity: Cd contents are generally elevated in
 1540 organic-rich sediments that are bathed by low $[\text{O}_2]$ waters (Fig. 18). This enrichment likely derives from
 1541 three processes. First, low $[\text{O}_2]$ environments may limit oxidation—and thus favor preservation—of settling
 1542 Cd sulfide particles formed in the water column. Second, the chalcophile nature of Cd means that even trace

1543 levels of hydrogen sulfide may cause Cd to precipitate into sulfides. Thus, as organic matter is remineralized
1544 within the sediment column, any Cd liberated to porewaters is proportionally more likely to reprecipitate
1545 into sulfide minerals, relative to harder metals (and carbon), effectively ‘trapping’ remineralized Cd in
1546 sediments (e.g., Rosenthal et al., 1995). Third, recent evidence suggests that Cd may also directly precipitate
1547 from seawater and into sediments when plumes of hydrogen sulfide interact with bottom waters (e.g., Xie
1548 et al., 2019b; Plass et al., 2020). The relative importance of these three processes to the O₂-dependent pattern
1549 of Cd accumulation remains to be fully elucidated.

1550 While the contribution of organic-rich sediments to the isotopic mass balance of Cd is presently limited,
1551 their significance to the marine Cd budget suggests that, globally, the Cd isotope composition of these
1552 sediments should balance the riverine flux $\delta^{114}\text{Cd} \approx +0.1 \pm 0.1\%$ (Lambelet et al., 2013). Recent data from
1553 organic-rich sediments (Chen et al., 2021), suboxic sediments (Bryan et al., 2021), and intermediate-depth
1554 biogenic particles (Janssen et al., 2019) generally support this view, and that low [O₂] settings may help to
1555 close the isotope mass balance of Cd. Alternatively, the other minor sinks of Cd—carbonates,
1556 ferromanganese oxides, clays—must possess large isotopic offsets relative to seawater, which seems

1557 unlikely given existing field and experimental data. Obtaining further modern calibrations of Cd isotope
1558 partitioning into organic-rich sediments should be considered a priority.



1559

1560 **Figure 18 | Cadmium concentrations in California Margin sediments.** **A:** Regionally representative $[O_2]$ profile from
1561 the northeast Pacific showing broad minimum between 600–800 m. Profile from 35.5°N, 122.5°W (from World Ocean
1562 Atlas; Garcia et al., 2013). **B:** Solid phase Cd concentration data from van Geen et al. (1995) for northeast Pacific
1563 coretop (closed symbols) and “slightly deeper” (8–10 cm; open symbols) sediment samples; dashed line indicates
1564 arithmetic mean. These samples evidence a maximum in authigenic Cd deposition at the top of the OMZ, which may
1565 originate from processes occurring in the water or sediment column.

1566

1567 6.4 Prospects

1568 The overview provided above indicates that Cd participates in marine biological processes and that its
1569 distribution is sensitive to the biological productivity of the oceans. How this sensitivity is transcribed into
1570 marine sediments remains uncertain, however. Additionally, there are several other processes that have the
1571 potential to render isotope effects that require further exploration before Cd isotopes can be solely
1572 interpreted as a productivity proxy, such as: biological fractionation effects, authigenic transformations,

1573 and redox sensitivities. Relatedly, the fidelity of many types of marine sediment to record ambient Cd
1574 isotope chemistry remain inadequately constrained. With these two themes in mind, we suggest several
1575 areas for additional research that may help to address the overarching question as to whether Cd isotope-
1576 based reconstructions can be used to inform on past ocean productivity.

1577

1578 *6.4.1. Modern*

1579 Several questions persist regarding the modern Cd isotope cycle. We list five of the most pressing below
1580 and offer possible remedies to each. First, are the ‘extreme’ (i.e., $\delta^{114}\text{Cd}$ of + 5 ‰; Fig. 15) values seen in
1581 surface waters of the Northern Hemisphere gyres (and only measured by MC-ICPMS techniques) real?
1582 That is, are these heavy compositions true oceanographic features that are generally absent from the
1583 Southern Hemisphere, or do they represent analytical artifacts unique to MC-ICPMS? This question
1584 remains to be answered, and will require measurement of the same low [Cd] surface samples by multiple
1585 MC-ICPMS and MC-TIMS groups. To date, this exercise has proven difficult because of the difficulty of
1586 collecting surface low [Cd] seawater (where heavy $\delta^{114}\text{Cd}$ has been reported by MC-ICPMS) in sufficient
1587 quantities to permit analyses by multiple groups.

1588 Second, to what extent do local Cd isotope compositions in surface waters reflect larger-scale processes
1589 versus local features? While available data consistently show biological Cd uptake removes isotopically
1590 light Cd, not all surface waters generally show the expected progressive increase in $\delta^{114}\text{Cd}$ with decreasing
1591 [Cd]. Addressing this issue will require elucidating the role of external sources (e.g., dust, margin
1592 sediments), organismal uptake, ligands, and mixing, which would benefit from conducting additional
1593 experimentation with plankton, coupling of isotope methods with electrochemistry, and numerical
1594 modeling, respectively.

1595

1596 Third, is there a ‘Redfield’ stoichiometry for Cd in organic matter? If so, what controls it? Existing culture
1597 (Ho et al., 2003) and field (Ohnemus et al., 2017) data suggest a wide range of cellular Cd:P, which have
1598 been suggested as reflecting species and local supply ratios, respectively (in addition to the aforementioned
1599 feedback interactions). Further experimentation with model organisms is needed.

1600

1601 Fourth, it is unclear if cells must possess a true physiological use for Cd in order to contribute to Cd isotope
1602 fractionation in seawater. The uptake of Cd into cells is widespread, whereas the genes encoding the ζ -class
1603 of carbonic anhydrases are not. The importance of this enzyme to Cd geochemistry could be tested by
1604 characterizing the Cd isotope composition of organisms that are known to produce Cd-containing carbonic

1605 anhydrases and comparing against those that cannot. Such experiments may also benefit from use of mutant
1606 cell lines with targeted ‘knockouts’ or by culturing phytoplankton in the presence of carbonic anhydrase
1607 inhibitors.

1608
1609 Last, how are the ‘light’ Cd isotope compositions seen in suspended biogenic particles above OMZs related
1610 to those within OMZ layers and to those putatively accumulating in sediments? Does biogenic particulate
1611 Cd reach sediments? Do particulate Cd isotope signatures within OMZ particles relate to sulfide
1612 precipitation and what is their influence on the global mass balance? What controls the Cd isotope
1613 composition of these particles? Addressing these questions will require examining the Cd isotope
1614 composition of particles from oxygenated oceanographic regions, identifying whether processes associated
1615 with particle regeneration affect Cd isotope compositions, and surveying coretop sediments.

1616

1617 *6.4.2. Paleo*

1618 As with the modern cycle, several ambiguities persist, though the most pressing relates to archives. Indeed,
1619 it appears that a major obstacle preventing the widespread application of Cd isotope-based proxies in
1620 paleoceanography has been the lack of suitable archives. Concerning carbonates, the main question is still
1621 whether it is possible to isolate sufficient quantities of foraminiferal-bound Cd to reconstruct past seawater
1622 $\delta^{114}\text{Cd}$. Does species matter, or can mixed assemblages be used? For organic-rich sediments, the role of
1623 biology itself must be considered. That is, how important might it be that different organisms exhibit
1624 different magnitudes of Cd isotope fractionation (and Cd:C stoichiometry)? If important, how best to
1625 interpret Cd isotope records—species, evolutionary innovations, productivity?

1626

1627

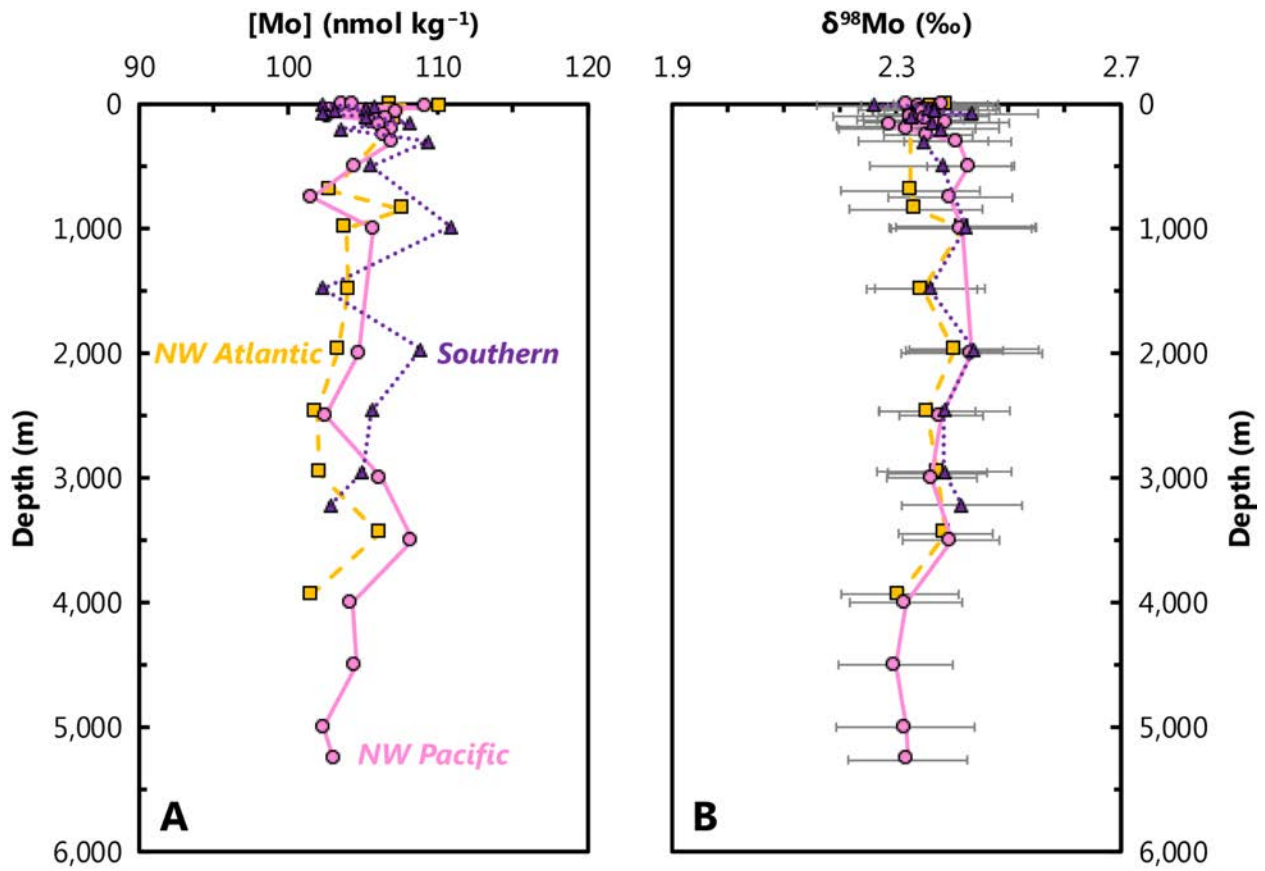
1628 **7. Molybdenum**

1629 Molybdenum is a cofactor in several key enzymes in the nitrogen cycle, and Mo availability in the ancient
1630 oceans may have helped shape the Precambrian biosphere (e.g., Anbar & Knoll, 2002). Today, Mo is the
1631 scarcest of the essential trace metals in phytoplankton (Eq. 3), but is one of the most abundant transition
1632 metals in the ocean (Morris, 1975; Bruland 1983; Collier 1985). Indeed, Mo possesses a long residence
1633 time (~440,000 yr; Miller et al., 2011; Table 1), is conservative with respect to salinity, and exhibits a
1634 uniform isotopic composition in oxygenated seawater (e.g., Barling et al., 2001; Siebert et al., 2003; Fig.
1635 19). Given the lack of [Mo] and $\delta^{98}\text{Mo}$ variability in the modern ocean, the isotope reactor framework
1636 outlined in Sec. 2.2. cannot be applied to Mo and thus there is no simple way to link $\delta^{98}\text{Mo}$ with
1637 paleoproductivity. Despite this, Mo is a widely used tracer of paleoredox conditions, and emerging fossil-
1638 specific measurements of $\delta^{98}\text{Mo}$ provide a promising future means to reconstruct high-resolution records
1639 of ocean oxygenation.

1640

1641 **7.1. Marine distribution**

1642 Based on 168 seawater samples from the Atlantic, Pacific, and Southern Oceans analyzed by Nakagawa et
1643 al. (2012), the average salinity-normalized [Mo] and $\delta^{98}\text{Mo}$ of the ocean are $107\pm 6 \text{ nmol kg}^{-1}$ and
1644 $+2.36\pm 0.10 \text{ ‰}$, respectively (both values $\pm 2 \text{ SD}$; Fig. 19).



1645

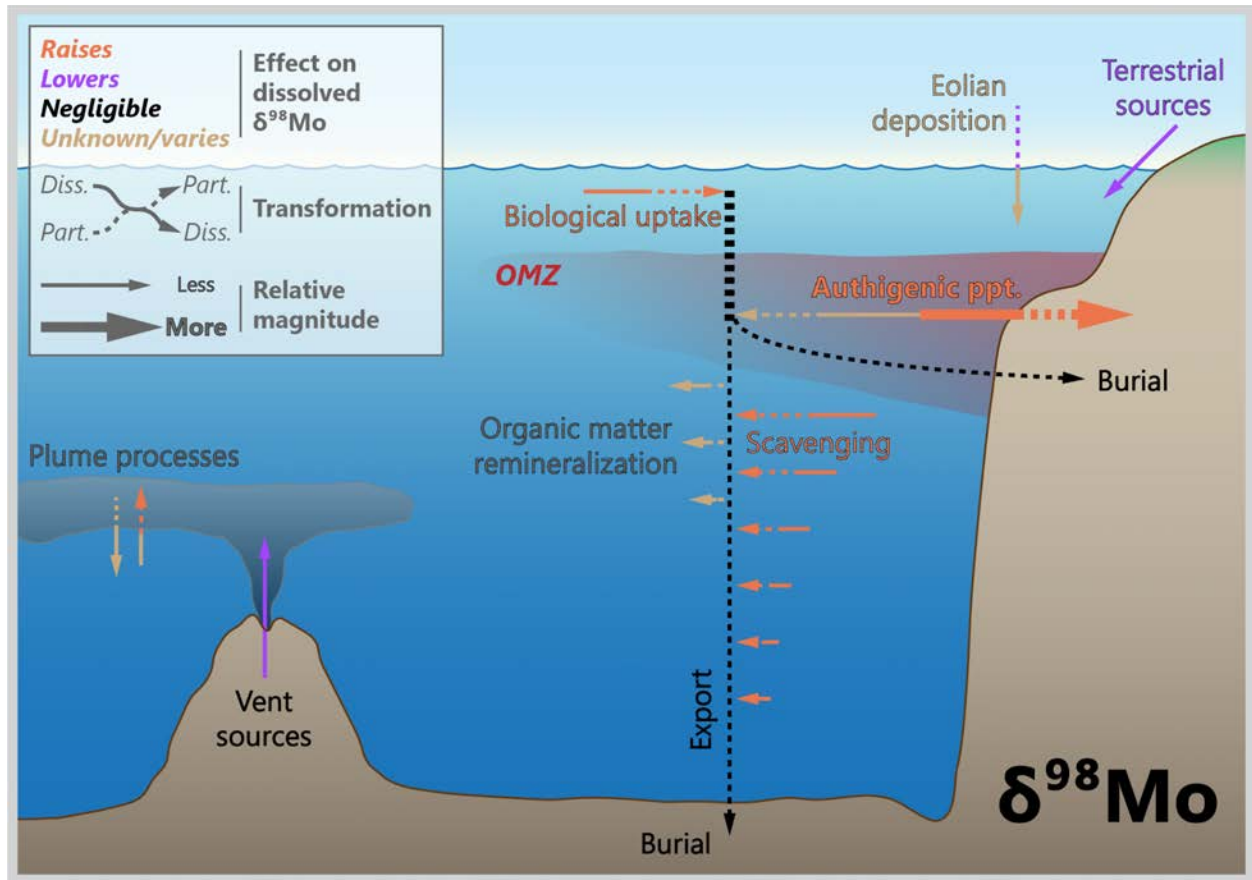
1646 **Figure 19 | Representative profiles of dissolved Mo concentrations ([Mo]; A) and Mo isotope compositions**
 1647 **($\delta^{98}\text{Mo}$; B).** Data from the Northwest Atlantic (squares, dashed line), Southern (triangles, dotted line), and Northwest
 1648 Pacific Oceans (circles, solid line; all data from Nakagawa et al., 2012). Station locations as per Fig. 1. This comparison
 1649 illustrates that the dissolved behavior of Mo is essentially invariant throughout the global oceans.

1650

1651 Given that no significant gradients in [Mo] are expected, there are few new open ocean $\delta^{98}\text{Mo}$ data measured
 1652 as part of GEOTRACES. However, [Mo] has been measured on two GEOTRACES transects (GP16 and
 1653 GA02), demonstrating four intriguing instances where [Mo] deviated from an otherwise conservative
 1654 distribution. These instances are briefly described below and covered in detail by Ho et al. (2018). First,
 1655 the most significant [Mo] anomalies (~5 % drawdown) are associated with intense scavenging by particulate
 1656 Fe hydroxides and oxyhydroxides close to the Peruvian OMZ. Second, Mo is slightly drawn down (<5 %)
 1657 in some samples directly above the East Pacific Rise hydrothermal ridge crest, again mostly likely driven
 1658 by scavenging onto hydrothermally derived Fe–Mn oxides. Some Mo drawdown is also observed in some
 1659 far-field hydrothermal samples, though the mechanism is unclear. Third, following normalization to a
 1660 salinity of 35, surface seawater shows a minor Mo drawdown, implying either biological uptake or
 1661 adsorption to biotic particles. Though not a true oceanographic feature, a fourth type of [Mo] anomaly is
 1662 also noteworthy: bottle storage artefacts. Ho et al. (2018) found that many samples with initially low values
 1663 showed an increase in [Mo] with increasing storage time, implying a change in Mo speciation to a form

1664 that is detectable by ICP-MS. In contrast to the relative constancy of [Mo] in open ocean settings, a number
 1665 of studies show striking [Mo] variations in coastal and estuarine systems (e.g., Dalai et al., 2005; Dellwig
 1666 et al., 2007; Joung and Shiller, 2016; Wang et al., 2016) as well as in modern restricted settings, such as the
 1667 Black and Baltic Seas (Nägler et al., 2011).

1668



1669

1670 **Figure 20 | Processes driving Mo isotope variations in modern seawater.** While biological processes may exert a
 1671 slight influence on surface water Mo distributions, the main drivers of marine Mo cycling are related to the balance
 1672 between scavenging pathways, which are redox dependent.

1673

1674 7.2. Driving processes

1675 7.2.1. Biological

1676 Molybdenum is an essential micronutrient required by enzymes that catalyze key reactions in the global C,
 1677 N, and S cycles (Mendel & Bittner, 2006). Importantly, Mo is a co-factor of the primary nitrogenase enzyme
 1678 complex, meaning that Mo is required for energy-efficient nitrogen fixation. Additionally, Mo is required

1679 for over 30 other enzymes that control biologically essential redox processes (Kendall et al., 2017). Despite
1680 its biological importance, biological activity does not appear to be a dominant process in setting the
1681 distribution of Mo in seawater (Fig. 20), likely due to the high abundance of Mo in the modern ocean.
1682 Results from the GEOTRACES GP16 East Pacific Zonal Transect do, however, suggest some Mo removal
1683 by biological uptake and/or adsorption onto biogenic particles within regions of elevated chlorophyll (Ho
1684 et al., 2018). Experimental data indicate that biological uptake of Mo imparts a small negative isotope
1685 fractionation on the order of -0.3‰ (Wasylenki et al., 2007; Fig. 20).

1686 Enhanced removal of Mo from seawater in regions with high export of organic carbon likely explains some
1687 of the nonconservative behavior observed in modern coastal regions. A significant relationship between
1688 Mo and total organic carbon content is observed in marine euxinic sediments (e.g., Helz et al., 1996; Algeo
1689 & Lyons, 2006; McManus et al., 2006; Lyons et al., 2009), though this appears to be more a function of
1690 euxinia rather than organic C burial. Furthermore, it has been shown that Mo interactions with organic
1691 matter can control Mo cycling in both soils (Wichard et al., 2009; King et al., 2014, 2016; Marks et al.,
1692 2015; Siebert et al., 2015) and marine sediments (Wagner et al., 2017; Tessin et al., 2019). The formation
1693 of Mo complexes containing organic ligands has been proposed as an explanation for the correlation
1694 between sedimentary Mo and organic carbon, suggesting that organic matter may play an important role in
1695 both the delivery and burial of Mo in sediments (Wagner et al., 2017).

1696

1697 *7.2.2. Chemical*

1698 Due to the long residence time and abundance of Mo, nonconservative Mo behavior is typically localized
1699 to areas with high particle concentrations, such as close to the continental margin, in the euphotic ocean, or
1700 around hydrothermal vents (e.g., Goto et al., 2020). In the present oxic water column, Mo is present
1701 primarily as the oxyanion molybdate (MoO_4^{2-}) and Mo sorption onto Mn oxyhydroxides represents the
1702 most significant modern Mo sink (Fig. 20; Bertine & Turekian, 1973; Scott & Lyons, 2012). Since the Fe–
1703 Mn oxide sink preferentially removes Mo from seawater with an isotopic effect of $\approx -3.0\text{‰}$ (Barling et al.,
1704 2001; Siebert et al., 2003; Fig. 21), the fraction of Mo that is buried in Fe–Mn oxides exerts a major control
1705 over the Mo isotope composition of seawater.

1706 In the presence of sulfide, the oxygen atoms in molybdate are progressively substituted for sulfur, producing
1707 particle reactive thiomolybdate species ($\text{MoO}_{4-x}\text{S}_x^{2-}$; Erickson & Helz, 2000; Vorlicek et al., 2015).
1708 Dissolved Mo can thus be strongly drawn down in sulfidic environments, such as the Black Sea.
1709 Importantly, this drawdown occurs with a small, but non-zero isotope effect of $\approx -0.5 \pm 0.3\text{‰}$, whereby

1710 isotopically light Mo is preferentially scavenged (e.g., Nägler et al., 2011). Thiomolybdate may also be
1711 scavenged from sulfidic sedimentary porewaters leading to significant Mo accumulations within sediments
1712 deposited in anoxic and euxinic environments (e.g., Emerson & Husteded, 1991; Crusius et al., 1996; Scott
1713 & Lyons, 2012). Long term Mo burial is associated with Fe–S minerals (Chappaz et al., 2014; Vorlicek et
1714 al., 2018) and/or organic matter (Dahl et al., 2017; Tessin et al., 2019), depending on the biogeochemical
1715 conditions prevailing at a given basin.

1716

1717 *7.2.3. Physical*

1718 The residence time of dissolved Mo is significantly longer than the mixing time of the ocean (Table 1).
1719 Thus, variations in [Mo] and dissolved $\delta^{98}\text{Mo}$ are not influenced by the geometry of modern overturning
1720 circulation. Whole ocean changes in [Mo] and dissolved $\delta^{98}\text{Mo}$ are, however, possible, and much of what
1721 we know about such changes is gleaned from studies of the geological past, particularly during periods of
1722 ocean anoxia. Based on this research, it has been suggested that during intervals of lower ocean
1723 oxygenation, the ocean Mo inventory may have been low enough to limit marine primary productivity
1724 (Anbar & Knoll, 2002; Algeo, 2004; Glass et al., 2009; Reinhard et al., 2013). This limitation has been
1725 demonstrated in certain lake ecosystems (Goldman, 1960; Glass et al., 2012). Under strongly euxinic
1726 conditions ($[\text{H}_2\text{S}]_{\text{aq}} > 11 \mu\text{M}$), thermodynamic calculations predict that tetrathiomolybdate (MoS_4^{2-})
1727 becomes the predominant Mo species (Erickson and Helz, 2000). The transformation can result in
1728 quantitative drawdown of Mo from seawater and into sediments with negligible net isotope fractionation,
1729 a mechanism that has been evidenced in Lake Cadagno (Dahl et al., 2010), the Black Sea (e.g., Neubert et
1730 al., 2008; Nägler et al., 2011), and Kyllaren fjord (a seasonally anoxic basin off of the west coast of Norway;
1731 Noordmann et al., 2015). Indeed, the quantitative drawdown mechanism is the foundation of several
1732 paleoceanographic studies that assume that the sedimentary Mo isotopic signatures, deposited in euxinic
1733 settings, faithfully capture the $\delta^{98}\text{Mo}$ of oxygenated (surface) seawater and can be further interpreted in
1734 terms of the fraction of the seafloor that is oxygenated (e.g., Kendall et al., 2015; Dickson, 2017).

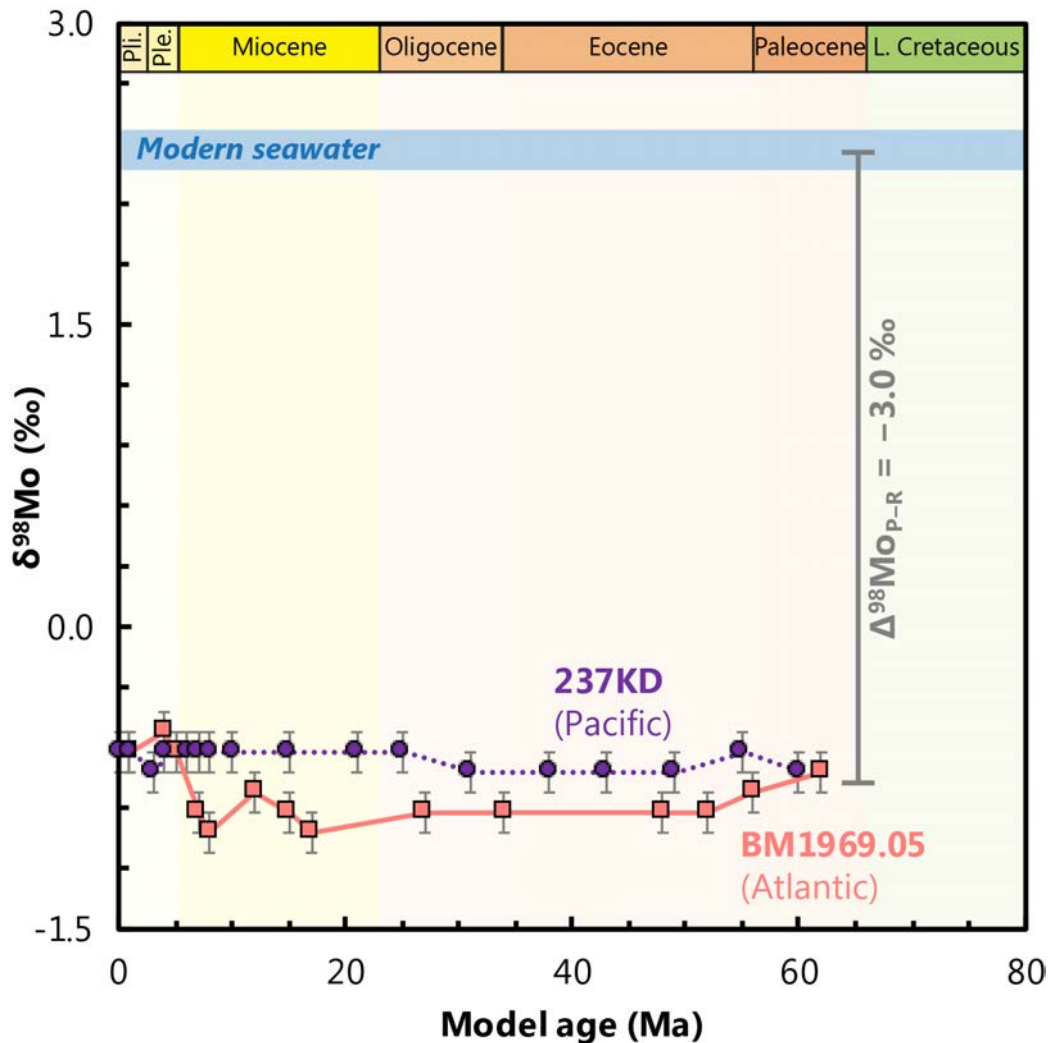
1735

1736 **7.3. Sedimentary archives**

1737 The majority of Mo paleoceanographic studies focus on the measurement of the Mo content and isotopic
1738 composition of bulk sediments, spanning early Earth (e.g., Arnold et al., 2004) to the Holocene (e.g.,
1739 Hardisty et al., 2016; van Helmond et al., 2018). However, the vast majority of these studies applied Mo
1740 and its isotopes to trace ocean redox conditions rather than productivity (e.g., Anbar, 2004; Kendall et al.,

1741 2017). Similar to the other elements reviewed here, there are measurements of $\delta^{98}\text{Mo}$ in Fe–Mn sediments
 1742 (e.g., Barling et al., 2001). Siebert et al. (2003) reported a time series from two Fe–Mn crusts implying no
 1743 variations in the $\delta^{98}\text{Mo}$ of seawater, relative to modern values, over the Cenozoic. Molybdenum is
 1744 somewhat mobile in Fe–Mn crusts, with a calculated effective diffusivity $\leq 10^{-7} \text{ cm}^2 \text{ yr}^{-1}$ (see Henderson &
 1745 Burton, 1999 for calculation details), similar to Cd (Sec. 6.3.2.), Cr (Sec. 10.3.2.), and Ag (Sec. 11.3.).
 1746 Thus, the invariance of the Fe–Mn crust $\delta^{98}\text{Mo}$ record may imply that the relative balance of Mo sinks has
 1747 not shifted by more than 10 % over the Cenozoic (e.g., Siebert et al., 2003; Anbar, 2004), or could reflect
 1748 some degree of post-depositional resetting.

1749



1750
 1751
 1752
 1753
 1754
 1755

Figure 21 | Two Fe–Mn records of $\delta^{98}\text{Mo}$ spanning the Cenozoic. Data from the Atlantic (squares, solid line) and Pacific Oceans (circles, dotted line; Siebert et al., 2003). Assuming that these Fe–Mn crusts have always formed with an offset $\approx -3.0 \text{ ‰}$ with respect to dissolved Mo in seawater, these records indicate that the $\delta^{98}\text{Mo}$ of seawater has minimally varied over the Cenozoic (Siebert et al., 2003; Anbar, 2004). However, given the effective diffusivity of Mo in Fe–Mn crusts, it is possible that the lack of variation may also reflect post-depositional resetting to modern-like values.

1756 Despite the ambiguity surrounding Fe–Mn sediments, research on biological archives of [Mo] and $\delta^{98}\text{Mo}$
1757 has found with mixed results. Research examining $\delta^{98}\text{Mo}$ in corals indicates that corals may accurately
1758 record ambient seawater Mo isotopic composition (Voegelin et al., 2009). However, later studies suggested
1759 a temperature-dependent fractionation between seawater and corals that is related to the activity of
1760 symbiotic zooxanthellae (Wang et al., 2019b). Moreover, bivalve shell Mo:Ca ratios have been determined
1761 to have no relationship to oceanographic conditions (Vihtakari et al., 2017), whereas Tabouret et al. (2012)
1762 suggest a mechanism related to trophic uptake, but not to ambient [Mo]. A third study proposed that Mo:Ca
1763 peaks in bivalve carbonate are controlled by ingestion of phytoplankton grown on NO_3^- (due to high Mo
1764 associated with NO_3^- reductase), indicating that bivalves may provide an archive for surface water NO_3^-
1765 uptake and a potential proxy for the balance between new and regenerated productivity (Thébault et al.,
1766 2009).

1767

1768 **7.4. Prospects**

1769 At present, it does not appear that bulk sediment $\delta^{98}\text{Mo}$ will be useful for reconstructing biological
1770 productivity, even though Mo is cycled by organic matter, both actively (e.g., Liermann et al., 2005;
1771 Wasylenki et al., 2007) and passively (e.g., Kowalski et al., 2013; King et al., 2018). That we see no
1772 pathway to using Mo as a productivity tracer reflects, in part, the difficulty in disentangling biological
1773 processes that exert relatively modest Mo isotope fractionations from those associated with thiomolybdate
1774 transformations (Tossell, 2005), or scavenging processes that possess large fractionation effects (Fig. 20;
1775 e.g., Mn- or Fe-oxide scavenging; Siebert et al., 2003; Barling & Anbar, 2004; Wasylenki et al., 2008;
1776 Brucker et al., 2009; Goldberg et al., 2009; 2012). Additionally, within the modern ocean and likely within
1777 the recent geologic past, the global ocean reservoir of Mo is too large and well mixed for biological
1778 associated fractionations to significantly impact the global Mo isotopic composition.

1779 The use of bulk sedimentary Mo concentrations as a proxy for export of organic carbon to the seafloor is
1780 more promising, but numerous caveats exist. Specifically, other mechanisms for enhanced delivery,
1781 sequestration, and burial complicate any efforts to quantitatively relate Mo enrichments to increased export
1782 productivity (e.g., Scholz et al., 2017). Redox conditions and, in particular, the presence of sulfide in the
1783 water column and sediment porewaters will be a primary control on Mo accumulation (e.g., Hardisty et al.,
1784 2018). Sedimentary Mo enrichments can also be produced through shuttling of Mo adsorbed to the surface
1785 of Fe and Mn oxides to the seafloor (Algeo & Lyons, 2006; Algeo & Tribovillard, 2009; Dellwig et al.,
1786 2010; Scholz et al., 2013). At a minimum, independent constraints on water column and porewater redox
1787 conditions using Fe speciation, other trace metals and/or fossil redox proxies are required before an

1788 argument can be made relating Mo contents to export productivity. Additionally, the quantitative
1789 relationship between Mo and organic carbon may be impacted by aqueous [Mo], which may have varied
1790 over Earth's history, or if depositional environments become restricted (i.e., Mo drawdown leads to a lower
1791 Mo:TOC ratio; Algeo & Lyons, 2006). Conversely, the utility of bulk sediment Mo content and isotopic
1792 composition may lie in constraining redox conditions to improve the interpretation of other trace metal
1793 proxies that are more strongly controlled by primary and/or export productivity.

1794 The most promising future avenue for Mo-based productivity proxies may emerge from fossil-specific
1795 measurements of Mo content, and perhaps $\delta^{98}\text{Mo}$. Currently, research has focused on large fossils (corals
1796 and bivalves; e.g., Thébault et al., 2009) and has led to mixed results on the utility of Mo in reconstructing
1797 productivity-related parameters. However, analytical progress may allow for measurement of smaller
1798 sample sizes, which may provide opportunities to explore new archives of past marine Mo geochemistry.

1799

1800

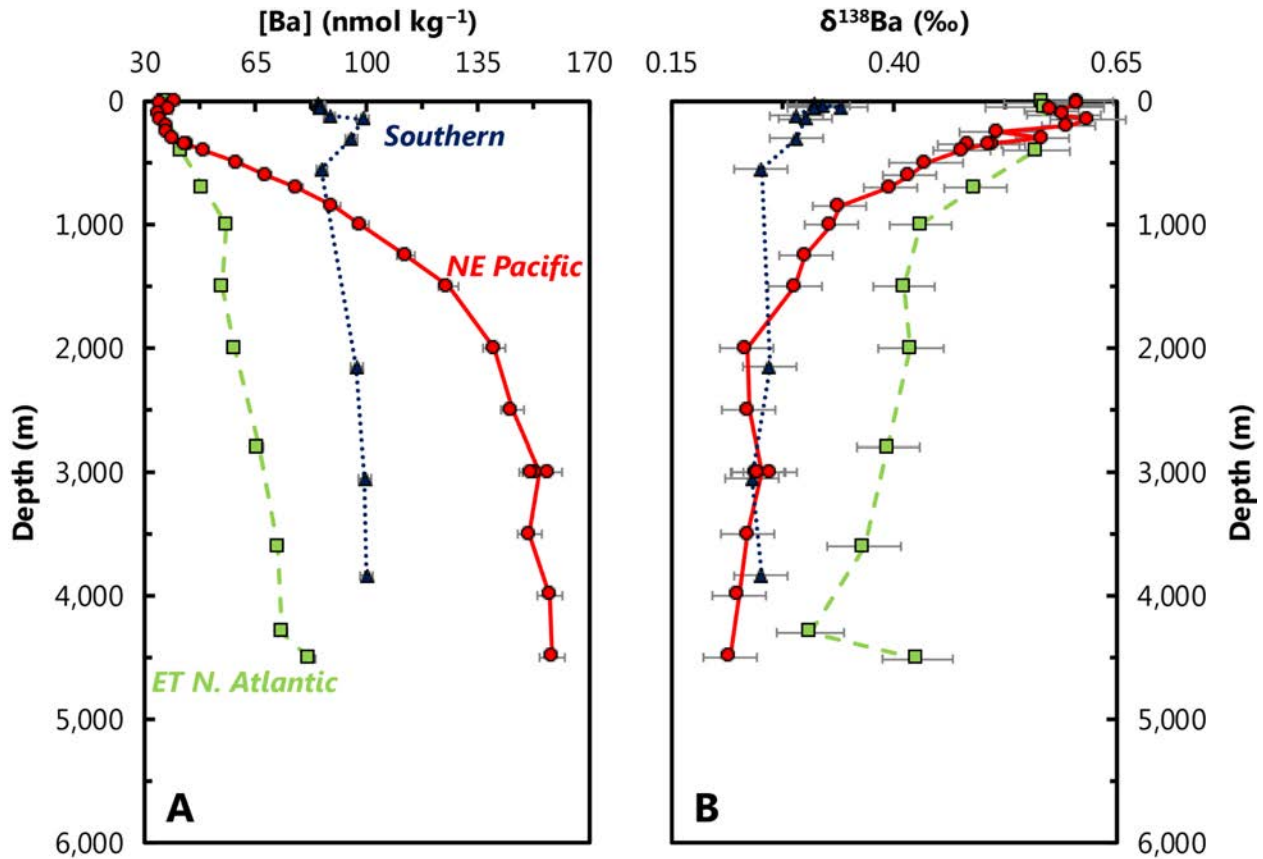
1801

1802 **8. Barium**

1803 Like Zn, [Ba] exhibits a strong correlation with [Si] (e.g., Chan et al., 1977). Unlike Zn and Si however,
1804 Ba is not an essential nutrient and has no known enzymatic functions. The mechanisms underpinning the
1805 nutrient-like behavior of Ba instead relate to its cycling by the mineral BaSO₄ (barite), which is thought to
1806 precipitate during the microbial oxidation of sinking organic matter (e.g., Chow & Goldberg, 1960). Barite
1807 precipitation also drives a sizeable, negative isotope fractionation of Ba stable isotopes (e.g., Von Allmen
1808 et al., 2010), consistent with the direction and magnitude of Ba isotope variations in seawater (e.g., Horner
1809 et al., 2015a). Though the connections between [Ba] and productivity are thus not direct, patterns of Ba
1810 sedimentation are strongly correlated with those of export production (e.g., Eagle et al., 2003), and Ba stable
1811 isotope distributions are consistent with underlying variations in BaSO₄ cycling and ocean circulation (e.g.,
1812 Horner & Crockford, 2021). As such, [Ba] and dissolved $\delta^{138}\text{Ba}$ can be described using the reactor

1813 framework outlined in Sec. 2.2., and—despite some uncertainties outlined later in this section—represents
1814 a promising tool for tracing aspects of paleoproductivity.

1815



1816

1817 **Figure 22 | Representative profiles of dissolved Ba concentrations ([Ba]; A) and Ba isotope compositions**
1818 **($\delta^{138}\text{Ba}$; B).** Data from the Eastern Tropical North Atlantic (squares, dashed line; Bates et al., 2017), northeast Pacific
1819 (circles, solid line line; Geyman et al., 2019), and Southern Oceans (triangles, dotted lines; Hsieh & Henderson, 2017).
1820 Station locations as per Fig. 1. This comparison illustrates that the oceanographic processes leading to distinct
1821 dissolved concentration profiles render significant changes in dissolved $\delta^{138}\text{Ba}$ between basins.

1822

1823 8.1. Marine distribution

1824 The nutrient-like distribution of [Ba] has been documented in the literature since the 1970s (e.g.,
1825 Wolgemuth & Broecker, 1970; Fig. 22). However, it was not until later in the decade that the GEOSECS
1826 Program fully revealed the three-dimensional marine distribution of [Ba] (e.g., Chan et al., 1976; 1977).
1827 These geochemical ocean sections highlighted vertical, zonal, and meridional variations in [Ba] related to
1828 the major biogeochemical and hydrographic features of the ocean. In nutrient-depleted surface waters, [Ba]
1829 is low, between 35–45 nmol kg⁻¹. Nutrient-replete deep waters are enriched in Ba, though typically by no

1830 more than a factor of four above surface values. The spatial resolution of GEOSECS illustrated the
1831 importance of hydrography; [Ba] increases along the meridional overturning circulation from ≈ 50 nmol
1832 kg^{-1} in deep waters of the North Atlantic, to ≈ 90 nmol kg^{-1} in the Southern Ocean, up to ≈ 180 nmol kg^{-1} in
1833 the deep northeast Pacific (Fig. 22; Chan et al., 1976; 1977).

1834 Though it was long suspected that the major dissolved–particulate transformation of Ba was related to the
1835 mineral barite (BaSO_4 ; e.g., Chow & Goldberg, 1960; Turekian, 1968), this was not confirmed until the
1836 1980s (e.g., Dehairs et al., 1980; Bishop, 1988). Barite crystals are now recognized as an ubiquitous
1837 component of marine particulate matter, with up to 10^4 discrete, micron-sized crystals present per L of
1838 seawater (Dehairs et al., 1980). The distribution of particulate BaSO_4 is distinct from primary biogenic
1839 phases that exhibit Martin-like distributions with maxima in the euphotic zone that subsequently decay
1840 along power-law trajectories (Martin et al., 1987). Particulate Ba typically exhibits a minimum in the
1841 euphotic zone and the maximum slightly below, usually near the top of the mesopelagic (e.g., Ohnemus &
1842 Lam, 2015; Ohnemus et al., 2019). This distribution likely reflects the fact that neither Ba nor BaSO_4 are
1843 utilized for physiological processes by any of the major marine primary producers. Particulate Ba fluxes
1844 are nevertheless strongly correlated with export productivity in well-oxygenated environments (e.g.,
1845 Bishop, 1988; Dymond et al., 1992; Francois et al., 1995; Dymond & Collier, 1996; McManus et al., 2002)
1846 and therefore sedimentary Ba content has been widely used as a proxy to reconstruct past changes in ocean
1847 export production (e.g., Francois et al., 1995; Paytan et al., 1996; Paytan & Griffith, 2007 and references
1848 therein; Costa et al., 2016, Winckler et al., 2016).

1849 Recent studies of Ba stable isotope geochemistry have added a new dimension with which to study marine
1850 Ba cycling. Von Allmen et al. (2010) first reported that isotopically light Ba is preferentially incorporated
1851 into BaSO_4 , with a particulate–dissolved Ba isotopic offset of ≈ -0.3 ‰. The direction of this offset implies
1852 that residual solutions, such as seawater, should exhibit Ba isotopic compositions heavier than those of
1853 sedimented BaSO_4 . This was corroborated for Atlantic seawater by Horner et al. (2015a), showing that
1854 dissolved $\delta^{138}\text{Ba}$ displays a mirror image of [Ba]: Ba-depleted surface water masses exhibited ‘heavy’ Ba
1855 isotopic compositions ($\approx +0.6$ ‰), whereas Ba-replete deep waters possessed ‘lighter’ values $\approx +0.3$ ‰.
1856 (Notably, all values are considerably heavier than the upper continental crust, which possesses $\delta^{138}\text{Ba}$
1857 $\approx 0.0 \pm 0.1$ ‰; Nan et al., 2018.) Similar patterns have since been corroborated in other ocean basins (Bates
1858 et al., 2017; Hsieh & Henderson, 2017; Bridgestock et al., 2018; Geyman et al., 2019; Cao et al., 2020a;
1859 Fig. 22). The first order pattern is thus consistent with the removal of isotopically light Ba from surface
1860 waters and its regeneration at depth. Further, the longer a water mass remains isolated from the surface, the
1861 more isotopically light Ba is able to accumulate, hence why Ba-replete northeast Pacific seawater $\sim 2,000$

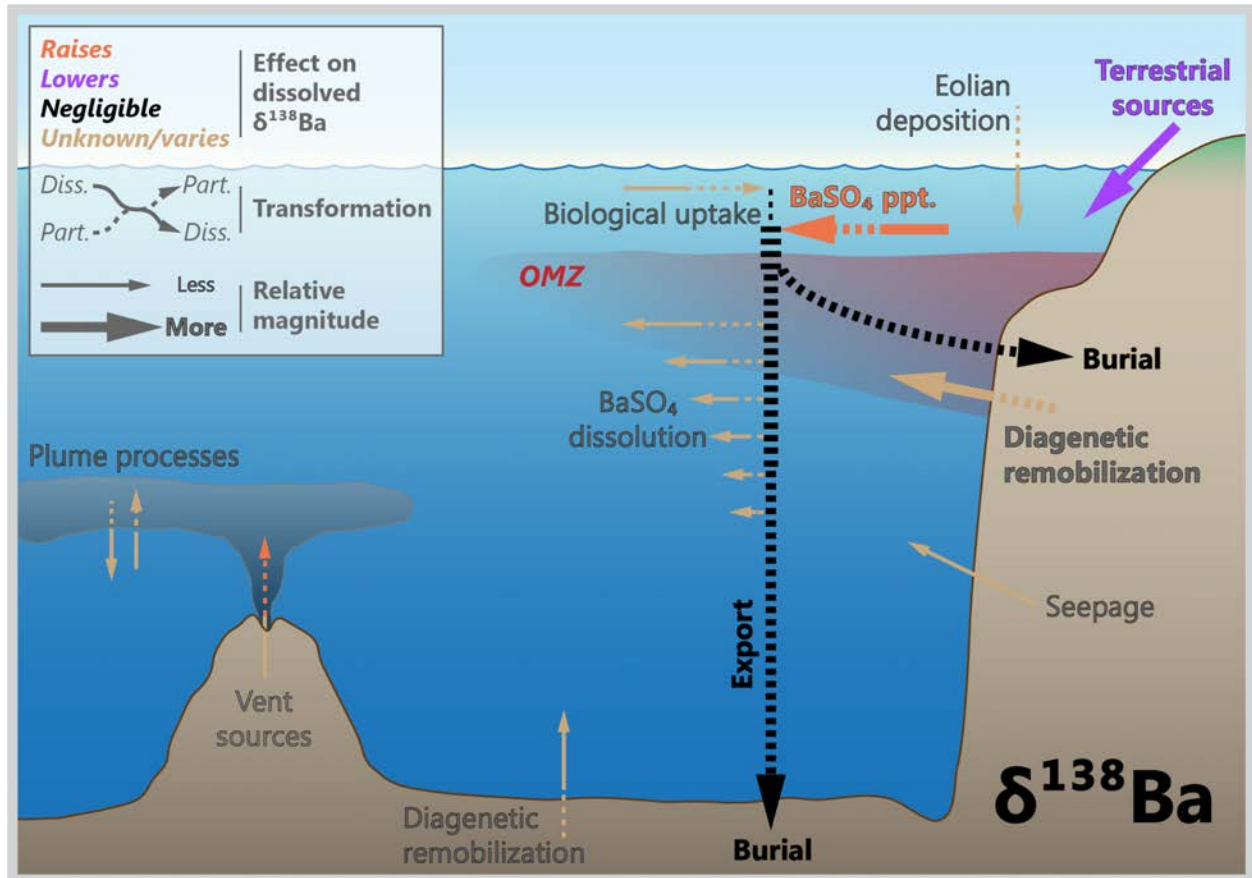
1862 m depth exhibits the lightest dissolved $\delta^{138}\text{Ba}$ yet observed in the global ocean ($\approx+0.2$ ‰; Geyman et al.,
1863 2019; Fig. 22).

1864 The isotopic studies have yielded a number of novel insights into the marine Ba cycle. First, the data
1865 underscore the importance of physical mixing (i.e., ocean circulation) in mediating patterns of dissolved
1866 $\delta^{138}\text{Ba}$ and, by extension, [Ba]. Second, both the regression of dissolved Ba isotopic data (Bates et al., 2017;
1867 Hsieh & Henderson, 2017) and comparison of colocated seawater and particulates (Horner et al., 2017; Cao
1868 et al., 2020b) imply an average particulate–dissolved Ba isotopic offset ≈-0.5 ‰, which is somewhat larger
1869 than the experimental results reported by Von Allmen et al. (2010). Third, marine sediments—both bulk
1870 (Bridgestock et al., 2018) and BaSO_4 isolates (Crockford et al., 2019)—faithfully reflect the ≈-0.5 ‰ Ba
1871 isotopic offset from surface seawater. Consequently, the mean $\delta^{138}\text{Ba}$ of globally sedimented BaSO_4 is
1872 $\approx+0.1\pm 0.1$ ‰ (Crockford et al., 2019). Since BaSO_4 is the dominant oceanic output (e.g., Paytan & Kastner,
1873 1996), these data imply that mean isotopic composition of Ba delivered to the ocean should possess an
1874 average composition $\approx+0.1\pm 0.1$ ‰ (Horner & Crockford, 2021). At present however, the main Ba inputs
1875 are unable to close the marine Ba isotopic budget: rivers, the principal Ba source to seawater, rivers, are too
1876 heavy, exhibiting compositions generally $\geq+0.2$ ‰ (e.g., Cao et al., 2020a; Gou et al., 2020); and,
1877 groundwater discharge, while possessing the necessary ‘light’ composition of $\approx+0.1 \pm 0.1$ ‰, is too small
1878 a Ba flux to balance the budget (Mayfield et al., 2021). Thus, either the marine Ba isotopic budget is

1879 currently out of steady state, or an additional Ba source possessing a light isotopic composition remains to
1880 be identified.

1881

1882



1883

1884 **Figure 23 | Processes driving Ba isotope variations in modern seawater.** Though biological processes exert only
1885 a minor direct influence on $\delta^{138}Ba$, the biologically mediated cycling of $BaSO_4$ drives large variations in marine Ba
1886 isotope cycling, thereby connecting $\delta^{138}Ba$ to paleoproductivity.

1887

1888 8.2. Driving processes

1889 Seawater is undersaturated with respect to $BaSO_4$ almost everywhere (Monnin et al., 1999; Rushdi et al.,
1890 2000). However, micro-crystalline $BaSO_4$ is ubiquitous in the ocean. This ‘barite paradox’ remains an area

1891 of active research. Proposed driving mechanisms broadly fall into two categories: ‘active’ biological and
1892 ‘passive’ chemical precipitation.

1893

1894 *8.2.1. Biological*

1895 Several organisms are known to precipitate BaSO₄ intracellularly, possibly for the purposes of gravitropism
1896 (e.g., Gooday & Nott, 1982; Finlay et al., 1983). However, the organisms known to actively precipitate
1897 BaSO₄ are neither abundant in seawater, nor do they constitute a significant fraction of marine primary
1898 productivity. Likewise, acantharea—organisms that precipitate SrSO₄ (celestite) tests that can contain
1899 considerable quantities of Ba (e.g., Bernstein & Byrne, 2004)—are not necessary for driving significant Ba
1900 drawdown from the ocean (Esser & Volpe, 2002) nor for barite precipitation (Ganeshram et al., 2003).
1901 Thus, existing evidence does not support a significant role for active biological processes in driving the
1902 open marine Ba cycle (Fig. 23).

1903

1904 *8.2.2. Chemical*

1905 Passive chemical precipitation is likely the major contributor to particulate BaSO₄ stocks and
1906 sedimentation. We focus our discussion on those BaSO₄ formed through association with the biological
1907 pump, though we note that other types of BaSO₄ exist in the ocean and their occurrence and geochemistry
1908 are reviewed in detail elsewhere (e.g., Hanor, 2000; Griffith & Paytan, 2012). Given that seawater is largely
1909 undersaturated with respect to BaSO₄, passive precipitation is thought to occur within particle-associated
1910 microenvironments that are supersaturated with respect to BaSO₄ (e.g., Chow & Goldberg, 1960; Dehairs
1911 et al., 1987). The development of BaSO₄-supersaturated microenvironments is hypothesized to relate to the
1912 heterotrophic oxidation of organic matter (Chow & Goldberg, 1960), whereby Ba and sulfate ions are
1913 concentrated in chemically isolated microzones during bacterially mediated mineralization of organic
1914 matter. Once sufficient quantities of Ba and sulfate ions have accumulated and the microenvironment
1915 becomes supersaturated, BaSO₄ precipitation occurs. Thus, passive precipitation of BaSO₄ is possible even
1916 in strongly undersaturated environments with low ambient sulfate (e.g., Horner et al., 2017). Continued
1917 mineralization destroys the microenvironment, ceasing precipitation and exposing BaSO₄ precipitates to
1918 undersaturated seawater where they begin to dissolve.

1919 The widespread association between pelagic BaSO₄ and aggregates of decaying organic matter provides
1920 indirect support for this process (Dehairs et al., 1980; Bishop, 1988). Indeed, the peak in particulate Ba—

1921 and presumably BaSO₄—abundance is found in the upper mesopelagic zone where most organic matter
1922 mineralization occurs (e.g., Sternberg et al., 2008). Though many of the microscale mechanisms remain
1923 unresolved, recent studies indicate that biofilms likely play an important role in accumulating Ba from
1924 seawater (e.g., Martinez-Ruiz et al., 2019; 2020), and can promote precipitation of BaSO₄ nanoparticles
1925 from undersaturated solutions (Deng et al., 2019).

1926 Regardless of the precise microscale mechanism, precipitation of particulate BaSO₄ is ubiquitous in the
1927 marine realm. Given that BaSO₄ precipitation renders an apparent negative isotope fractionation of ≈ -0.5
1928 ‰, it is highly likely that BaSO₄ cycling drives much of the Ba isotope variability in the ocean (Fig. 23).
1929 From a paleoproxy perspective, this is ideal; BaSO₄ formation is related to the decay of organic matter and
1930 not by the presence of any specific organism (e.g., Jacquet et al., 2007; Dehairs et al., 2008). Downward
1931 transport of particulate BaSO₄ is driven by aggregation with larger particles (Lam & Marchal, 2014) and
1932 the efficiency of this downward transport depends on the same biophysical processes that export organic
1933 matter, thus connecting the export flux of BaSO₄ to that of organic carbon (Eagle et al., 2003).

1934 Barites formed in the ocean through this passive chemical pathway are commonly termed marine, pelagic,
1935 authigenic, or biogenic. Though none of these terms are perfect descriptors of the chemical processes
1936 involved, ‘marine’ and ‘biogenic’ are the most ambiguous and their use is discouraged; the former
1937 encompasses all BaSO₄ formed in the marine realm—including diagenetic, cold seep, and hydrothermal—
1938 whereas the latter could be taken to imply only those precipitates brought about by active biological
1939 processes. While ‘authigenic’ is an informative descriptor, it has also been used to describe sedimentary
1940 BaSO₄ that formed via diagenetic redistribution on or below the seafloor (e.g., Torres et al., 1996). Thus,
1941 we recommend use of the term ‘pelagic’ when describing chemically precipitated microcrystalline BaSO₄,
1942 and encourage authors to include this definition in their works.

1943

1944 *8.2.3. Physical*

1945 Similar to that of Si (silicic acid) and alkalinity, [Ba] exhibits a nutrient like profile in the oceans (Fig. 22).
1946 However, the extent to which this pattern arises from nonconservative biogeochemical processes versus
1947 physical mixing remains unresolved. Results from the GEOTRACES program are facilitating renewed
1948 interest into this topic, which is being investigated using two complementary approaches. In the first,
1949 biogeochemical contributions to basin-scale [Ba] distributions are isolated using statistical methods, such
1950 as OMPA (Optimum Multiparameter water mass Analysis). These statistical methods showed that mixing
1951 is dominant in the Mediterranean (Jullion et al., 2017) and North Atlantic (Le Roy et al., 2018), but that sea

1952 ice-related processes may be important in the high latitudes (Hendry et al., 2018). Second, the influence of
1953 mixing is evidenced from emerging Ba stable isotope data. Indeed, the importance of mixing has been
1954 documented vertically (Horner et al., 2015a), zonally (Bates et al., 2017; Bridgestock et al., 2018), and
1955 meridionally (Bates et al., 2017; Hsieh & Henderson, 2017). Together, these new approaches imply that *in*
1956 *situ* biogeochemical processes exert a relatively minor influence on basin-scale [Ba] distributions.

1957

1958 **8.3. Marine archives**

1959 Given the connections between export production and BaSO₄ fluxes, the major archive of historical changes
1960 in Ba cycling is BaSO₄ itself (e.g., Griffith & Paytan, 2012). Indeed, the sedimentary accumulation of
1961 BaSO₄—often determined as the fraction of Ba in excess of the detrital Ba background or the deposition
1962 rate of BaSO₄ itself—has been extensively used to reconstruct past changes in export production (e.g.,
1963 Schmitz, 1987; Francois et al., 1995; Paytan et al., 1996; Frank et al., 2000; Jaccard et al., 2005; Jaccard et
1964 al., 2013; Ma et al., 2014; 2015, Costa et al. 2016, Winckler et al., 2016). An estimated 30 % of the BaSO₄
1965 microcrystals formed in seawater are buried in oxygenated sediments (e.g., Dymond et al., 1992), a
1966 considerably higher fraction than for organic carbon (Paytan & Kastner, 1996). However, in oligotrophic
1967 regimes where both BaSO₄ fluxes and sedimentation rates are low, prolonged exposure to undersaturated
1968 seawater results in poor preservation (Eagle et al., 2003; Serno et al., 2014). Similarly, in high productivity
1969 coastal upwelling settings, mineralization of organic matter in sediments consumes porewater O₂, driving
1970 conditions down the redox tower and toward sulfate reduction, hampering BaSO₄ preservation (McManus
1971 et al., 1998; Paytan & Griffith, 2007; Carter et al., 2020).

1972 The isotopic composition of Ba in sediments has been investigated as a proxy for the Ba isotope
1973 composition of the Ba source (i.e., dissolved Ba in epipelagic and upper mesopelagic seawater).
1974 Applications to date have explored the recovery of the biological carbon pump following the Paleocene–
1975 Eocene Thermal Maximum (~56 Ma; Bridgestock et al., 2019) and the origin of enigmatic sedimentary
1976 BaSO₄ deposited in the aftermath of the Marinoan glaciation (~635 Ma; Crockford et al., 2019) and Great
1977 Oxidation Event (~2,000 Ma; Hodgskiss et al., 2019). These three applications are reviewed in detail in
1978 Horner & Crockford (2021).

1979 Unlike many of the other TEIs reviewed here, we are not aware of any studies exploring $\delta^{138}\text{Ba}$ in Fe–Mn
1980 crusts. Barium is somewhat immobile in Fe–Mn crusts, with a calculated effective diffusivity $\leq 10^{-8}$ cm²
1981 yr⁻¹ (see Henderson & Burton, 1999, for calculation details), similar to Zn (Sec. 9.3.1.). While this implies
1982 that Fe–Mn crusts have the potential to record variations in deep ocean $\delta^{138}\text{Ba}$, a significant fraction of the
1983 total Ba in Fe–Mn crusts is associated with CFA (carbonate fluorapatite; Koschinsky & Hein, 2003). Since

1984 the CFA is secondary—filling voids around the layered Fe- and Mn-oxide minerals—it is unclear if Fe–
1985 Mn crusts can be developed into a useful archive of $\delta^{138}\text{Ba}$.

1986 Lastly, the amount of Ba in marine carbonates, typically reported as Ba:Ca has been extensively used to
1987 reconstruct the Ba content of past environments, specifically for constraining historical patterns of
1988 upwelling and/or terrestrial runoff (e.g., Lea et al., 1989; Gebregiorgis et al., 2016). More recently, a number
1989 of studies have investigated the fidelity of surface- (Liu et al., 2019) and deep-sea corals (Hemsing et al.,
1990 2018; Geyman et al., 2019), finding that a number of species are faithful archives of ambient [Ba] and
1991 $\delta^{138}\text{Ba}$. These findings are highly promising from a proxy standpoint, as they indicate that a number of
1992 archives may be suitable for paleo Ba reconstructions.

1993

1994

1995 **8.4. Prospects**

1996 Barium exhibits several nutrient-like properties: first, [Ba] distributions resemble those of other nutrients
1997 and second, particulate abundances are intimately associated with the processes of organic carbon
1998 remineralization and export. Despite these connections, several aspects of Ba cycling—both in the modern
1999 and past oceans—remain unresolved. We thus suggest several areas for additional research that will help
2000 widen the applicability of Ba-based proxies in paleoceanography.

2001

2002 **8.4.1. Modern**

2003 Several issues remain regarding the modern Ba cycle. Many of these are reviewed in detail by Horner &
2004 Crockford (2021), though we outline the four most pressing (and possible remedies) here. First, to what
2005 extent do the similar distributions in [Ba], [Si], alkalinity, and [^{226}Ra] reflect true biogeochemical coupling
2006 versus passive physical mixing? These correlations have been the subject of scrutiny for over 40 years (e.g.,
2007 Chan et al., 1976; Chung, 1980), and recent GEOTRACES sections are facilitating a reevaluation of these
2008 relationships. As noted above, statistical analysis of Ba (and Si, Ra) distributions in regions will offer
2009 valuable insights, particularly if conducted in regions with weaker overturning circulation. Likewise,
2010 additional profiles of $\delta^{138}\text{Ba}$ from regions with strong *in situ* influences—Ba point sources (e.g., seeps,
2011 Torres et al., 1996; margin sediments, McManus et al., 1998), or point sinks (e.g., plankton blooms, Esser
2012 & Volpe, 2002)—should enable testing the importance of local processes to regional Ba isotope
2013 distributions.

2014
2015 Second, the Ba isotopic mass balance of the ocean must be closed. This will require detailed evaluation of
2016 other putative Ba sources, such as diagenetic remobilization (e.g., Hoppema et al., 2010), atmospheric
2017 deposition, and the importance of estuarine enhancement of riverine Ba fluxes (e.g., Hanor & Chan, 1977;
2018 Edmond et al., 1978). Large intra-marine Ba point sources, such as such as hydrothermal vents, can drive
2019 BaSO₄ supersaturation, leading to precipitation; indeed, a recent study suggests that the net effect of such
2020 point sources may be to increase deep $\delta^{138}\text{Ba}$ through BaSO₄ precipitation, further imbalancing the Ba
2021 isotope budget (e.g., Hsieh et al., 2021; Fig. 23). Barium isotope fractionation associated with other minera
2022 sinks, such as adsorption onto Fe–Mn oxyhydroxides, also remains uncharacterized.

2023

2024 Third, what is the mechanism of BaSO₄ precipitation? While the microenvironment mediated model
2025 appears most likely, many microscale mechanisms of precipitation remain ambiguous: How and from what
2026 are Ba and sulfate ions liberated during mineralization? How and why are they accumulated onto biofilms?
2027 Do different substrate organisms and/or heterotrophic communities influence the amount of BaSO₄
2028 precipitated? Addressing these questions will require additional field and laboratory studies, which can then
2029 be compared against distributions of particulate BaSO₄ in the ocean interior. Depending on their
2030 importance, these nuances may require ecological parameterizations in numerical models of Ba cycling.

2031 Finally, additional experiments are needed to narrow estimates of the fractionation factor between BaSO₄
2032 and seawater. Existing laboratory studies place this estimate ≈ -0.3 ‰, whereas a wide range of field data
2033 suggest that it is considerably larger at ≈ -0.5 ‰. Accounting for this ≈ 0.2 ‰ difference is both important
2034 and justifies additional experimentation, as it indicates incomplete understanding of the processes that
2035 fractionate Ba isotopes in the marine realm.

2036

2037 *8.4.2. Paleo*

2038 As with the modern cycle, several ambiguities persist. Assuming that BaSO₄ remains the preferred archive
2039 of past Ba cycle variations, it is imperative to constrain the effect of early diagenesis on the Ba isotope
2040 composition of sedimentary BaSO₄. Likewise, it is unknown if diagenetic BaSO₄ retains any primary Ba
2041 isotope information. Assessing these issues will require studies of co-located BaSO₄ and porewaters from
2042 environments at various stages of early diagenesis. Answering these questions is critical in establishing the
2043 validity of Ba isotopes in barite as a paleoceanographic proxy.

2044 Additionally, there are uncertainties relating to whether BaSO₄ cycling is impacted by ambient [Ba] during
2045 BaSO₄ precipitation and burial. For example, does more BaSO₄ precipitation occur at higher ambient [Ba]?

2046 While there is evidence indicating that this is not a major influence in the modern ocean (e.g., Fagel et al.,
2047 2004; Serno et al., 2014), a relationship between ambient [Ba] and BaSO₄ precipitation is likely necessary
2048 to maintain steady state in the Ba cycle over geological timescales (e.g., Horner & Crockford, 2021).
2049 Likewise, to what extent does BaSO₄ preservation depend on ambient [Ba]? These considerations are
2050 significant when considering longer-term records, particularly when marine sulfate levels were lower-than-
2051 modern (and [Ba] presumably higher; e.g., Walker, 1983; Wei & Algeo, 2020). Finally, does the seawater
2052 temperature at the depth of POC mineralization impact the relationship between POC and BaSO₄
2053 formation? These questions are best addressed through a combination of experimentation (e.g., cultures,
2054 precipitation), field studies in basins with large gradients in [Ba], and numerical experiments incorporating
2055 saturation state modeling.

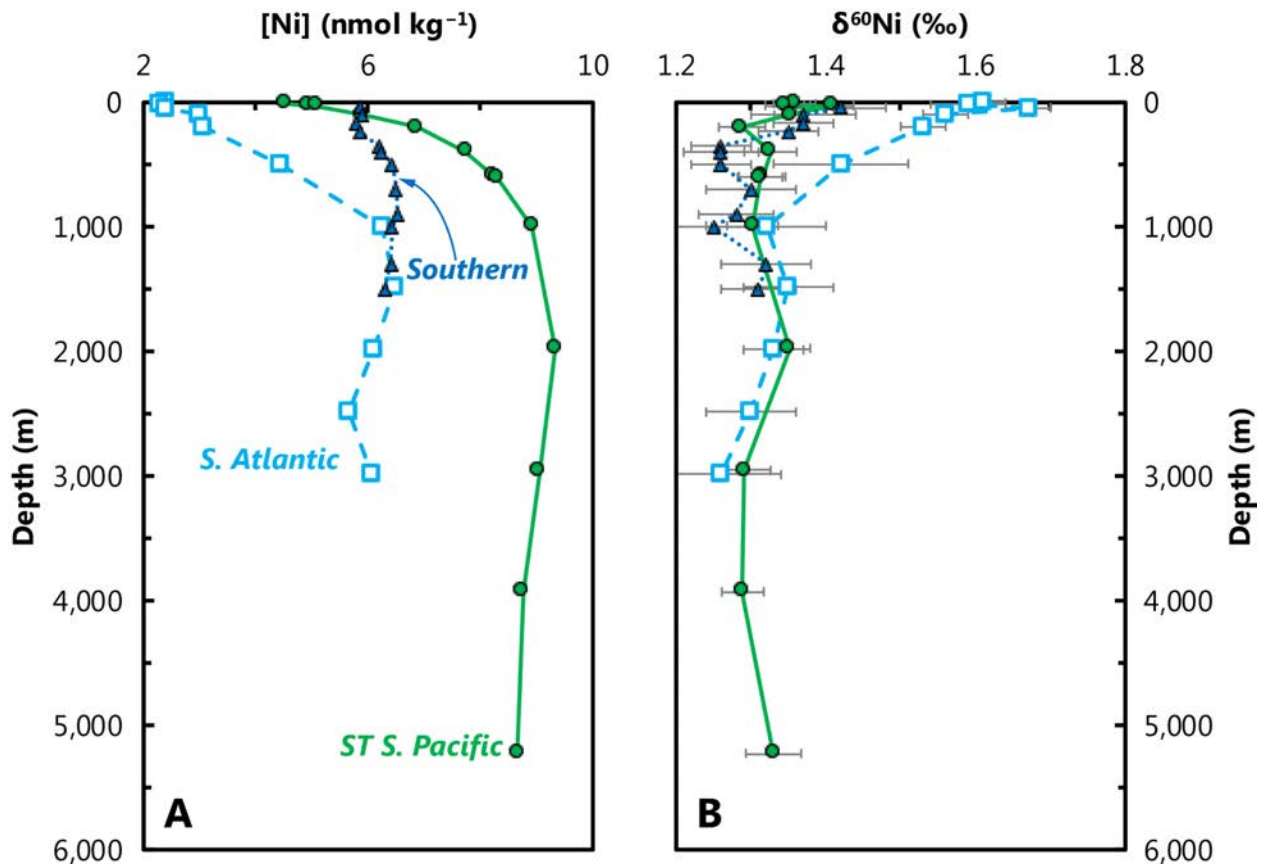
2056 **9. Nickel**

2057 Nickel is biologically utilized, for example by diazotrophs during nitrogen fixation and by microorganisms
2058 catalysing the breakdown of reactive oxygen species (Twining & Baines, 2013). Particularly relevant to
2059 early Earth reconstructions is the fact that methanotrophs have an obligate requirement for Ni. Several
2060 promising archives have been identified for marine Ni isotope chemistry, however, determination of the
2061 composition of Ni isotope ratios in seawater has lagged behind other nutrient-like metals such as Zn and
2062 Cd. Recent datasets do indicate that Ni is cycled by phytoplankton, with a resultant isotope fractionation in
2063 the euphotic zone dependent on the dominant ecology of the region. As such, Ni isotope variations are
2064 likely to be broadly responsive to biological productivity, but the assumption of a constant fractionation
2065 factor (i.e., Δ_{P-R}) may be violated, which may complicate use of Ni isotopes as a quantitative
2066 paleoproductivity proxy, and the applicability of a simple reactor scheme. Additionally, the secondary sinks
2067 of Ni, such as those associated with Mn oxides, are associated with large Ni isotope fractionations, opening
2068 up the possibility of using Ni isotopes to track aspects of marine paleoredox.

2069

2070 **9.1. Marine distribution**

2071 Nickel has a classic nutrient-type distribution in the oceans with one unusual feature; surface [Ni] never
2072 drops below $\sim 1.8\text{--}2 \text{ nmol kg}^{-1}$ (e.g., Sclater et al., 1976; Bruland, 1980; Fig. 24). There is evidence,
2073 however, that this residual pool in surface waters is not bioavailable, as summarized recently by Archer et
2074 al. (2020). Deep water [Ni] are $4\text{--}5 \text{ nmol kg}^{-1}$ in the Atlantic, and $\sim 9 \text{ nmol kg}^{-1}$ in the north Pacific (Fig.
2075 24).



2076
 2077 **Figure 24 | Representative profiles of dissolved Ni concentrations ($[Ni]$; A) and Ni isotopic compositions ($\delta^{60}Ni$;**
 2078 **B).** Data from the South Atlantic (squares, dashed line; Archer et al., 2020), Southern (triangles, dotted line; Wang et
 2079 al., 2019a), and Subtropical South Pacific Oceans (circles, solid line; Takano et al., 2017). Station locations as per Fig.
 2080 1. This comparison illustrates that the oceanographic processes leading to distinct dissolved concentration profiles
 2081 render only small changes in dissolved $\delta^{60}Ni$ between basins.

2082 Developing robust analytical protocols for analyzing Ni isotopes for a range of sample matrices has proven
 2083 somewhat more challenging than for some of the other trace metals discussed here due to the difficulty in
 2084 separating Ni from interfering elements (e.g., Fe, a major isobaric interference on ^{58}Ni). Chemical
 2085 purification protocols now use a sequence of resins including anion exchange (e.g., AG MP-1M or AG1-
 2086 X8, Bio-Rad) and either a Ni-specific resin (containing dimethylglyoxime) or Nobias PA-1 (Hitachi High
 2087 Technologies; e.g., Cameron et al., 2009; Gueguen et al., 2013; Wang et al., 2019a; Yang et al., 2020). The
 2088 limited data since reported for the oceanic dissolved pool of Ni indicates relatively little variability in $\delta^{60}Ni$
 2089 at depth (+1.2 to +1.4 ‰), with a small shift towards heavier values up to +1.7 ‰ in the upper water column
 2090 (Fig. 24; Takano et al., 2017; Wang et al., 2019a; Yang et al., 2020; Archer et al., 2020). The upper water
 2091 column shift is proposed to reflect a small kinetic isotope fractionation during biological uptake. Similar to
 2092 Zn, Cu, Cd, Mo, Ba and Cr, the isotopic composition of Ni in seawater is isotopically heavy compared to
 2093 the UCC (Table 1).

2094

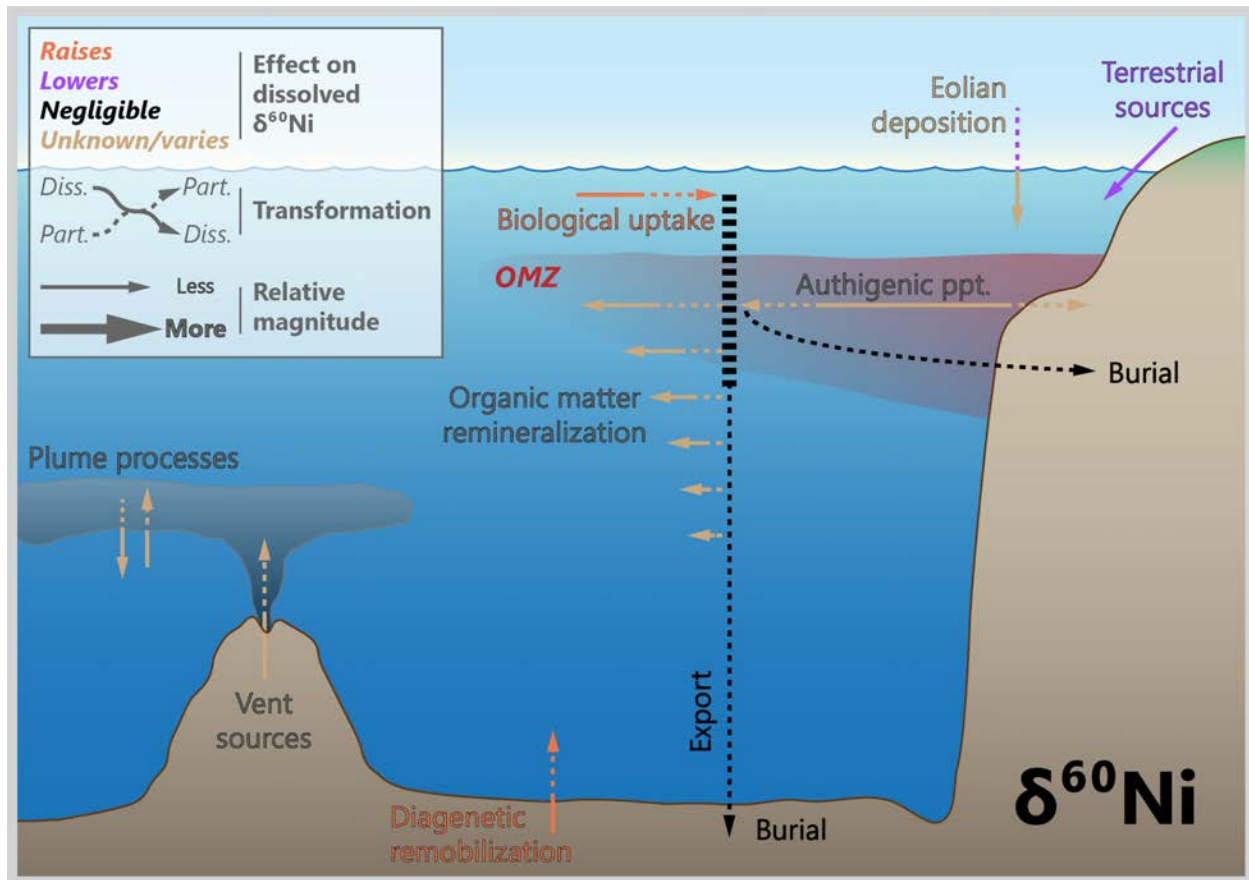


Figure 25 | Processes driving Ni isotope variations in modern seawater. Biological processes are recognized to drive a small, but systematic increase in dissolved $\delta^{60}\text{Ni}$ and marine Ni isotope values are preserved in certain sediments. Other abiotic Ni cycling processes may be important however, such as sorption to Mn-oxide minerals, and the significance of these fractionations to global Ni cycling remains to be fully elucidated.

2095
2096
2097
2098
2099

2100
2101
2102

2103 9.2. Driving processes

2104 9.2.1 Biological

2105 To date, eight Ni-based enzyme systems have been identified (Ragsdale, 2009), including urease, which is
2106 key to the global nitrogen cycle, and methyl-CoM reductase, which catalyses the production of all
2107 biologically generated methane on Earth. The obligate requirement of methanogens for Ni has led to interest
2108 in developing Ni and Ni isotopes as a tracer of methane production on the early Earth (e.g., Cameron et al.,
2109 2009; Konhauser et al., 2009; Wang et al., 2019c). In the modern ocean the highest Ni quotas are found in
2110 diazotrophs (N-fixers), thought to reflect the presence of Ni-Fe hydrogenases (which catalyse H_2 produced
2111 during N fixation), Ni-superoxide dismutase (Ni-SOD) and urease (Tamagnini et al., 2002; Dupont et al.,
2112 2008a; 2008b; Nuester et al., 2012). Nickel limitation of phytoplankton grown on urea has been shown in

2113 culture and in natural assemblages, suggesting the Ni-N colimitation of phytoplankton growth may be
2114 relevant in the ocean (Price & Morel, 1991; Dupont et al. 2008a; 2010). Significant Ni is also found in
2115 diatom frustules (about 50 % of diatom cellular quotas; Twining et al., 2012). The latter observation is
2116 thought to play a role in the similarity of Ni and Si oceanic distributions (Twining et al., 2012).

2117 No culture data are available to determine the degree of Ni isotope fractionation during biological uptake.
2118 Upper ocean data suggest no fractionation or a small preference for the light isotope, equivalent to ≈ -0.3
2119 ‰ (Takano et al., 2017; Archer et al., 2020; Yang et al., 2020; Fig. 25), consistent with the Ni isotope
2120 systematics observed in organic-rich sediments (Ciscato et al., 2018) and water column particulates (Takano
2121 et al., 2020). Interestingly, new water column data from the South Atlantic suggest distinct ecological
2122 differences in Ni drawdown and Ni isotope fractionation compared to other bioactive trace metals (e.g., Zn,
2123 Cd). Limited drawdown and Ni isotope fractionation is observed in the diatom-dominated regime south of
2124 the Polar Front in the Southern Ocean. In contrast, more marked drawdown and significant Ni isotope
2125 fractionation is observed north of the Polar Front, which has been attributed to the predominance of nitrate-
2126 limited, Ni-requiring cyanobacteria (Archer et al., 2020).

2127

2128 *9.2.2 Chemical*

2129 Nickel is partially complexed by strong organic ligands in coastal and open ocean environments (5–70 %;
2130 e.g., Donat et al., 1994; Saito et al., 2004; Boiteau et al., 2016), though slow water exchange kinetics of Ni
2131 make these complexation measurements particularly challenging (Hudson & Morel, 1993). Slow exchange
2132 kinetics may also explain the residual pool of non-bioavailable Ni in the surface ocean (e.g., Mackay et al.,
2133 2002; Dupont et al., 2010). Speciation models suggest that the remainder of the Ni is present as free Ni^{2+}
2134 and NiCl^+ , with a small fraction present as NiCO_3^0 (Zirino and Yamamoto, 1972; Turner et al., 1981).

2135 Nickel cycling is tightly coupled to that of Mn—in sediments (Koschinsky & Hein, 2003), during removal
2136 from hydrothermal fluids (e.g., Gueguen et al. 2021), within porewaters (Klinkhammer, 1980), and across
2137 the redoxcline of the Black Sea (Vance et al., 2016). In the Black Sea, for example, Mn redox cycling is
2138 associated with preferential sorption of light Ni isotopes, with a large negative fractionation of $\approx -4\text{‰}$
2139 (Vance et al., 2016). This large fractionation is consistent with experimental sorption of Ni on birnessite
2140 (Wasylenki et al., 2014; Sorensen et al., 2020).

2141 Unlike more strongly chalcophile elements like Cd, Cu, and Zn, Ni is not strongly drawn down in the
2142 euxinic portion of the Black Sea water column (Tankéré et al., 2001; Vance et al., 2016) and in other euxinic
2143 basins (e.g., Jacobs & Emerson, 1982; Jacobs et al., 1985). However, Ni is enriched in Black Sea sediments

2144 (Little et al., 2015), with $\delta^{60}\text{Ni}$ compositions notably lighter (at +0.3 to +0.6‰) than Ni sources to the basin
2145 (at about +1.3‰; Vance et al., 2016). Vance et al. (2016) attributed these light isotope compositions to the
2146 scavenging of sulfidized Ni species, which are predicted to be isotopically light (Fujii et al., 2011b).

2147 Dissolved Ni is added to the ocean from rivers, hydrothermal vents, and dust (Fig. 25). All three sources
2148 possess $\delta^{60}\text{Ni}$ between +0.1 to +0.8 ‰, which is lighter than deep ocean seawater (see recent summaries by
2149 Little et al., 2020; Gueguen and Rouxel, 2021). In general, these Ni sources are not of a sufficient magnitude
2150 to generate deviations in deep ocean dissolved $\delta^{60}\text{Ni}$, and are therefore unlikely to compromise use of $\delta^{60}\text{Ni}$
2151 as a paleoproductivity tracer (similar to $\delta^{114}\text{Cd}$; Sec. 6.). The main output flux of Ni from seawater is
2152 believed to be burial with Mn oxides, which have a wide range of reported Ni isotope compositions. While
2153 hydrogenetic ferromanganese crusts are generally isotopically heavy, from about +0.9 to +2.5‰ (Gall et
2154 al., 2013; Gueguen et al., 2016; Gueguen et al., 2021), Mn-rich pelagic clays possess $\delta^{60}\text{Ni}$ between -0.8
2155 and +1.0‰ (Little et al., 2020; Gueguen & Rouxel, 2021). The Ni isotope difference between sources and
2156 sinks implies the existence of a missing ‘heavy’ Ni source. Recently, Little et al. (2020) and Gueguen &
2157 Rouxel (2021) hypothesised that this source is related to benthic release from sediments and predicted that
2158 it possesses an extremely fractionated Ni isotope composition of $\approx +3$ ‰.

2159

2160 *9.2.3 Physical*

2161 The most recent estimate for the residence time of Ni in the ocean is approximately ~20 kyr (Little et al.,
2162 2020), considerably longer than the mixing time of the ocean. As a result, in parallel with the other bioactive
2163 trace metals discussed herein, Ni and Ni isotope distributions are modulated at first order by the geometry
2164 of physical ocean circulation. The importance of diatom uptake in the Southern Ocean in partially coupling
2165 oceanic Ni and Si (Twining et al., 2012) was introduced above, and the relative homogeneity of deep ocean
2166 Ni isotope compositions supports an important role for southern-sourced water masses in the Ni distribution
2167 (Fig. 24; Takano et al., 2017; Wang et al., 2019a; Archer et al., 2020).

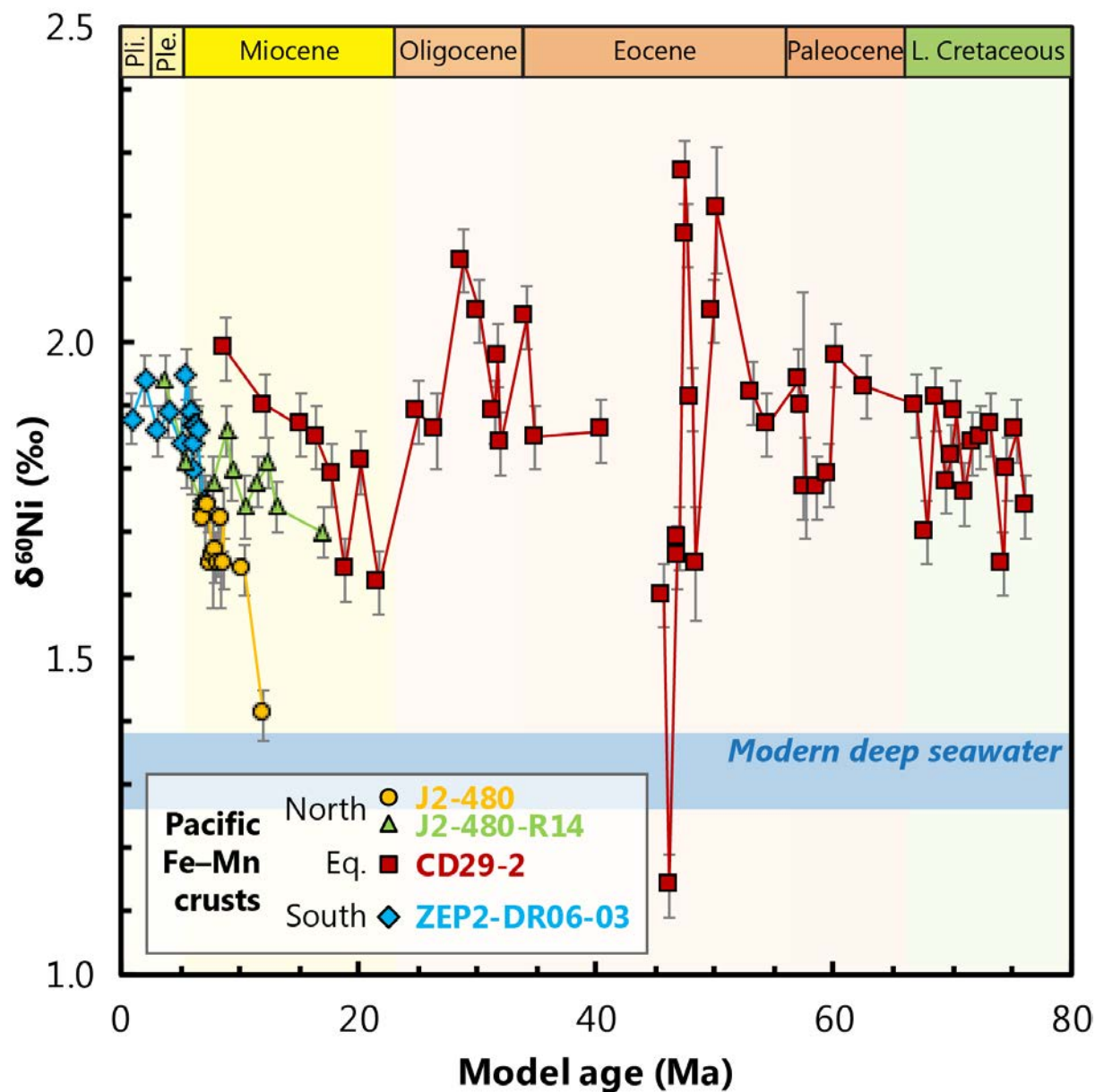
2168

2169 **9.3. Marine archives**

2170 *9.3.1. Ferromanganese sediments*

2171 Ferromanganese crusts exhibit variable Ni isotope compositions (Fig. 26; Gall et al., 2013; Gueguen et al.,
2172 2016a), which are, on average, slightly isotopically heavier (at $\delta^{60}\text{Ni}$ of +1.6‰) than seawater ($\delta^{60}\text{Ni}$ at
2173 about +1.3‰). Nickel is relatively immobile in Fe–Mn crusts, with a calculated effective diffusivity $\leq 10^{-9}$

2174 $\text{cm}^2 \text{yr}^{-1}$ (see Henderson & Burton, 1999, for calculation details), similar to Cu (Sec. 5.3.1.), implying that
2175 Fe–Mn crusts preserve primary information about dissolved $\delta^{60}\text{Ni}$. However, experiments suggest that
2176 sorption of Ni to birnessite (the primary Ni-hosting phase in Fe–Mn sediments) should be associated with
2177 a large negative isotope effect (of about 3 to 4 ‰; Wasylenki et al., 2014; Sorensen et al., 2020). It remains
2178 unclear why the full isotope effect is not expressed in Fe–Mn crusts. Intense Mn cycling occurs across the
2179 redoxcline of the Black Sea; this cycling is associated with large variations in Ni and Ni isotopes, consistent
2180 with the experimentally observed light isotope effect on sorption to birnessite (Vance et al., 2016). Recent
2181 data from Mn-rich sediments that have undergone diagenesis also point to the preservation of a large
2182 negative Ni isotope effect, and predict a concomitant isotopically heavy benthic Ni source (Little et al.,
2183 2020; Gueguen & Rouxel, 2021).



2184

2185 **Figure 26 | Four Fe–Mn records of $\delta^{60}\text{Ni}$ from the Pacific Ocean.** Assuming that Fe–Mn crusts have always formed
 2186 with an offset $\approx +0.5$ ‰ with respect to ambient dissolved Ni in seawater, these records illustrate that the Ni isotope
 2187 composition of seawater has varied by only ± 0.2 ‰ over the Cenozoic. Data for J2-480, J2-480-R14, and ZEP2-DR06-
 2188 03 are from Gueguen et al. (2016). Data from CD29-2 are from Gall et al. (2013). All four records have been plotted
 2189 using the authors' preferred age model, meaning that there are some differences between the chronology of CD29-2
 2190 shown here compared to Figs. 8, 17.

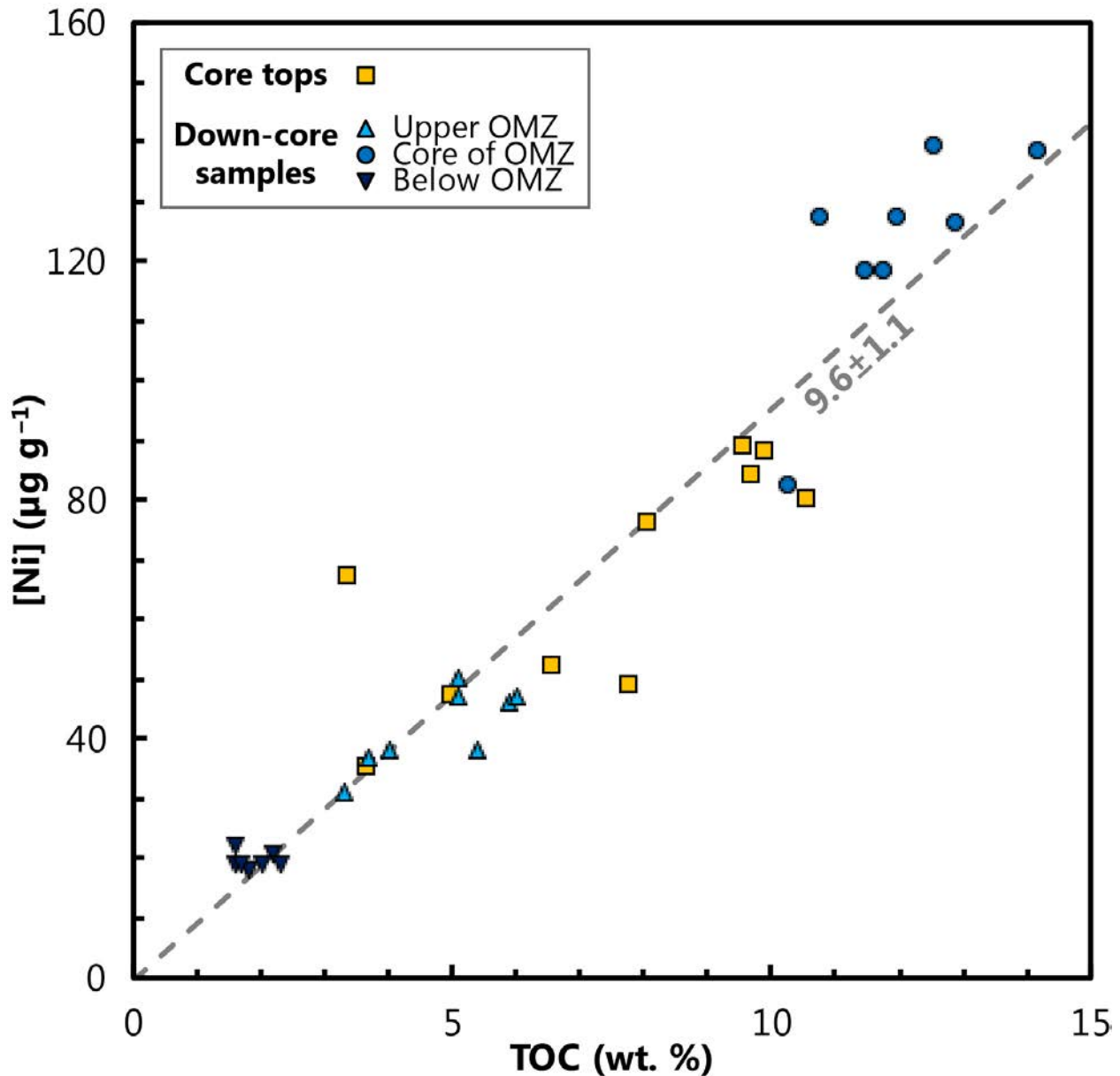
2191

2192 Though promising, the development of Fe–Mn crusts as a tracer of past oceanic Ni cycling awaits a
 2193 mechanistic understanding of the processes driving their variably isotopically heavy signature, as well as
 2194 an awareness of the likely complicating role of diagenetic remobilisation of Ni (e.g., Atkins et al., 2016;
 2195 Little et al., 2020).

2196 9.3.2. *Organic-rich sediments*

2197 As introduced in Sec. 4.3.2. (Cu), qualitative arguments for high organic matter fluxes (i.e., increased
2198 paleoproductivity) have been made based on enriched Ni (and Cu) content in ancient organic-rich sediments
2199 (e.g., Tribovillard et al., 2006). For Ni, this approach is supported by positive correlations with TOC in
2200 modern continental margin sediments (Fig. 27).

2201 Nickel does not precipitate in the presence of water column dissolved sulfide and is therefore less
2202 susceptible to decoupling from TOC fluxes compared to chalcophile elements such as Cu, Zn and Cd.
2203 Nevertheless, Ni cycling is strongly linked to the redox cycling of Mn, potentially complicating Ni–TOC
2204 coupling in settings with active diagenetic cycling of Mn. Sedimentary and water column data from the
2205 Black Sea indicate that cycling associated with the benthic Fe–Mn redox shuttle (e.g., Lyons & Severmann,
2206 2006) provides an alternative supply route for Ni to the deep euxinic basin in this setting (Little et al., 2015;
2207 Vance et al., 2016). Therefore, open marine settings would be the most promising from which to make
2208 estimates of the relative productivity of two different sites based on their absolute measured Ni:TOC ratios.
2209 Otherwise the degree of basin restriction will exert the primary control on nutrient supply, and therefore
2210 the degree of trace metal enrichment (Algeo & Maynard, 2008; Little et al., 2015).



2211
 2212 **Figure 27 | Correlation of Ni and TOC content in organic-rich sediments from the Peru Margin.** Data from Ciscato
 2213 et al. (2018). The best-fit regression of these data yields a Ni–TOC slope of 9.6 ± 1.1 (mean \pm 2 SD), similar to the “ ≈ 9 ”
 2214 reported by Böning et al. (2015).

2215
 2216 Ciscato et al. (2018) investigated the distribution of Ni and its isotopes in two fractions isolated from Peru
 2217 margin organic-rich sediments. The HF-HCl digestible fraction (usually containing >80% of total Ni)
 2218 exhibited $\delta^{60}\text{Ni}$ values similar to modern deep seawater (at about +1.2‰). Meanwhile, these authors found
 2219 variable Ni isotope compositions in the organic pyrite fraction (OPF), which they suggested record the
 2220 fractionation imparted by biological uptake in the euphotic zone. Systematic relationships between Ni–
 2221 TOC, $\delta^{60}\text{Ni}_{\text{OPF}}$, and $\delta^{13}\text{C}$ indicate that there is merit in continuing to investigate Ni and Ni isotopes as a
 2222 paleoproductivity tracer (Ciscato et al., 2018).

2223

2224 **9.4. Prospects**

2225 To date, Ni and its isotopes have been under developed as a potential paleoproductivity proxy. Recent data,
2226 both from the dissolved phase in seawater and in two different fractions isolated from anoxic organic-rich
2227 sediments, suggest promise in the coupling of Ni and C and their isotopes. However, in oxic-to-suboxic
2228 settings, Ni contents and isotopic composition of sediments are strongly influenced by the diagenetic redox
2229 cycling of Mn (e.g., Gueguen & Rouxel, 2021). We recommend additional study of Ni content and isotopic
2230 compositions in sediments, focusing specifically on carbonate and siliceous biominerals, which is
2231 increasingly tractable with new and improved chemical separation and analytical techniques.

2232 Finally, in a completely different approach, Wang et al. (2019c) presented $\delta^{60}\text{Ni}$ values of Precambrian
2233 glacial diamictites, which are suggested to represent the chemical weathering residues of the UCC. They
2234 find a small shift towards heavier Ni isotope compositions across the Great Oxidation Event, which they
2235 relate to the onset of oxidative weathering of crustal sulfides (Wang et al., 2019c). Combined with the
2236 proposed importance of Ni to the maintenance of methanogenesis during this time period (e.g., Konhauser
2237 et al., 2009), it is hoped that future Ni stable isotope analyses will shed further light on the
2238 paleoenvironmental conditions on the early Earth.

2239 **10. Chromium**

2240 Chromium (Cr) stable isotope composition ($\delta^{53}\text{Cr}$) has received significant attention over the past decade
2241 as a proxy of paleoredox conditions. These applications have generally used a framework where isotope
2242 fractionation is driven by subaerial weathering, with the partial pressure of atmospheric O_2 controlling $\delta^{53}\text{Cr}$
2243 signatures in resultant paleorecords (e.g., Frei et al., 2009; 2014). However, subsequent studies have
2244 identified numerous challenges to this framework, including questions about the fidelity of sediment
2245 records (e.g., Remmelzwaal et al., 2019; Frank et al., 2020; Wang et al., 2021) as well as the very processes
2246 driving Cr cycling in seawater. Indeed, recent studies suggest that the most spatially expansive Cr isotope
2247 variations in the ocean are not related to oxygen availability but rather uptake by phytoplankton (e.g.,
2248 Janssen et al., 2020). This means that Cr isotopes may serve as a novel productivity tracer that is reasonably
2249 well described by the isotope reactor framework (Sec. 2.2.). However, until recently, marine Cr data have
2250 not seen the significant improvements in quality control as other metals in the GEOTRACES repertoire,
2251 and there are currently no consensus values for [Cr] and $\delta^{53}\text{Cr}$ in GEOTRACES reference materials.
2252 Consequently, there is a degree of discrepancy among literature data that likely does not wholly represent
2253 natural variability (see discussions in Goring-Harford et al., 2018; Rickli et al., 2019; Moos et al., 2020;
2254 Nasemann et al., 2020; Huang et al., 2021), limiting our understanding of modern Cr cycling and thus
2255 paleoproxy validation. Given the issues surrounding the measurement of—and mechanisms driving—Cr
2256 isotope variation in seawater, we focus our assessment of Cr on open ocean GEOTRACES-era data that are
2257 not considered equivocal by subsequent studies. We suggest that these new insights offer an opportunity to
2258 re-assess the fidelity of different sediments as archives of past seawater $\delta^{53}\text{Cr}$.

2259

2260

2261 **10.1. Marine distribution**

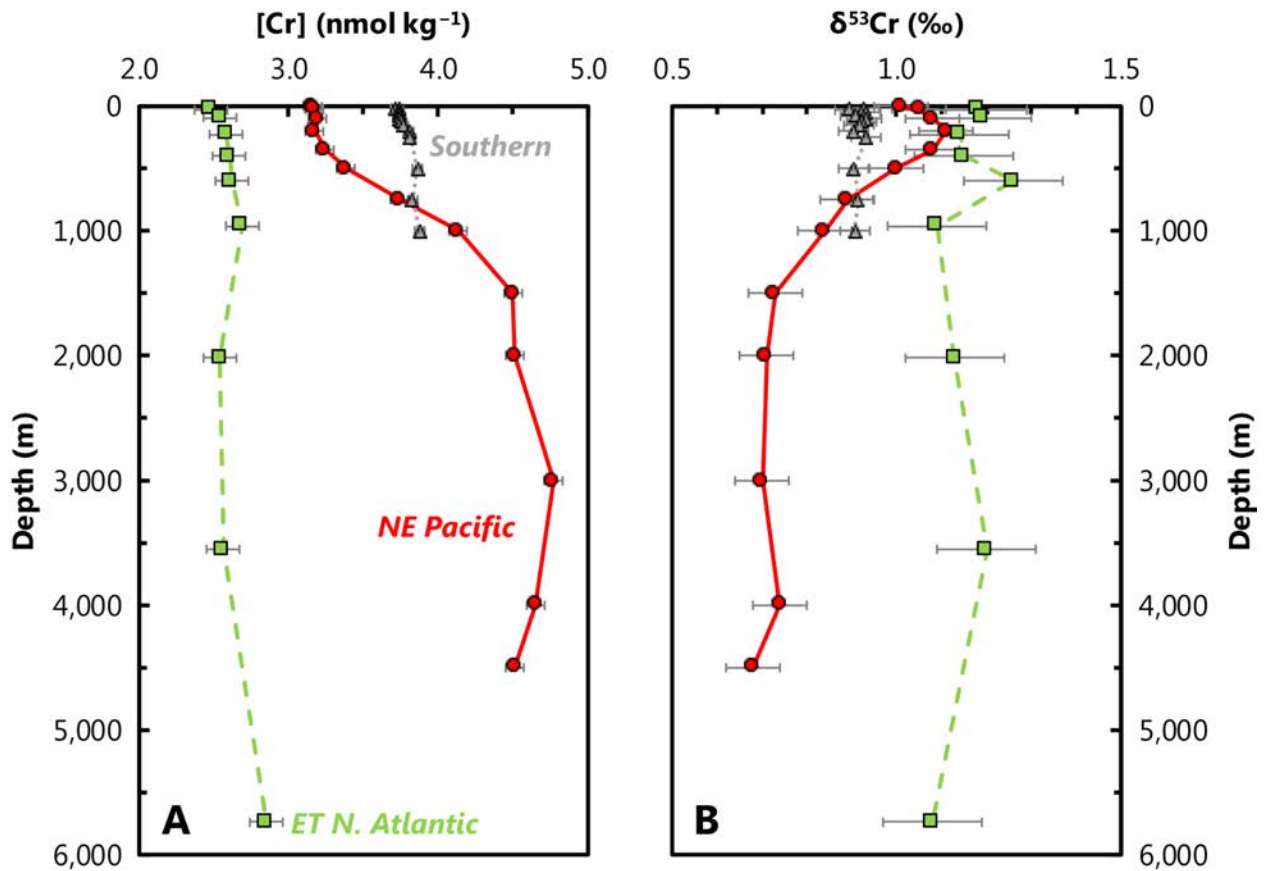
2262 In the ocean, [Cr] follows a nutrient-type vertical distribution (e.g., Campbell & Yeats, 1981), suggesting
2263 involvement in biological processes; however, concentration gradients with depth are minor relative to
2264 other algal macro- and micronutrients (Fig. 28). Open ocean surface [Cr] are 2–4 nmol kg^{-1} , with lower
2265 concentrations in the oligotrophic gyres than at higher latitudes (Scheiderich et al., 2015; Goring-Harford
2266 et al., 2018; Moos & Boyle, 2019; Rickli et al., 2019; Janssen et al., 2020). Chromium is elevated in Pacific
2267 and Southern Ocean deep waters, with [Cr] of 3.5–6.0 nmol kg^{-1} (Fig. 28; Moos & Boyle, 2019; Rickli et
2268 al., 2019; Nasemann et al., 2020; Huang et al., 2021). Although inter-basin deep water [Cr] gradients are
2269 small relative to other trace metals (e.g., [Cd], [Zn]) and macronutrients ($[\text{PO}_4^{3-}]$, $[\text{NO}_3^-]$, [Si]), clear
2270 increases in [Cr] are seen in deep waters advected northward from the Southern Ocean. These observations

2271 reflect, in part, a deep regeneration cycle for Cr, with maxima in the abyssal ocean (e.g., Jeandel & Minster,
2272 1987).

2273

2274 The two primary redox forms of Cr in the ocean are Cr(VI), an oxyanion with limited particle reactivity,
2275 and Cr(III), a poorly soluble cation that readily adsorbs to mineral and organic phases (e.g., Wang et al.,
2276 1997; Semeniuk et al., 2016). In oxic seawater, thermodynamic calculations predict that Cr(VI) should be
2277 the only species present (Elderfield, 1970); however, Cr(III) is regularly reported as representing 5–15 %
2278 of [Cr] (e.g., Cranston & Murray, 1978; Jeandel & Minster, 1987; Davidson et al., 2020; Janssen et al.,
2279 2020), and Cr(III) abundance is elevated in OMZs and anoxic waters (Murray et al., 1983; Rue et al., 1997;
2280 Davidson et al., 2020; Huang et al., 2021). Due to the differences in solubility and reactivity of these species,
2281 redox cycling plays an important role in setting [Cr] distributions. The primary oceanic Cr reductants are
2282 ferrous Fe (Pettine et al., 1998) and H₂S (Kim et al., 2001). Chromium(III) maxima in surface waters
2283 suggests that biological or photochemical processes, possibly involving dissolved organic matter, are also
2284 important (e.g., Kieber & Helz, 1992; Achterberg & van den Berg, 1997; Janssen et al., 2020); however,
2285 these processes may occur indirectly through the generation of Cr reductants such as ferrous Fe (Hug et al.,
2286 1997). The primary marine Cr oxidants are Mn oxides (van der Weijden & Reith, 1982; Milletto et al.,
2287 2021) and H₂O₂ (Pettine et al., 1991); Cr oxidation by O₂ is insignificant due to kinetic limitations.
2288 Chromium redox cycling is accompanied by isotope fractionation, with reduction consistently resulting in
2289 an enrichment of light isotopes in the reduced phase (e.g., Ellis et al., 2002; Wanner & Sonnenthal, 2013),
2290 and therefore redox cycling—biologically mediated or otherwise—is likely important for dissolved Cr
2291 stable isotope distributions as well as [Cr]. Fractionation during Cr oxidation is more poorly constrained,
2292 with variable fractionation patterns reported (Zink et al., 2010; Milletto et al., 2021).

2293



2294

2295

2296

2297

2298

2299

2300

2301

2302

2303

2304

2305

2306

2307

2308

2309

2310

2311

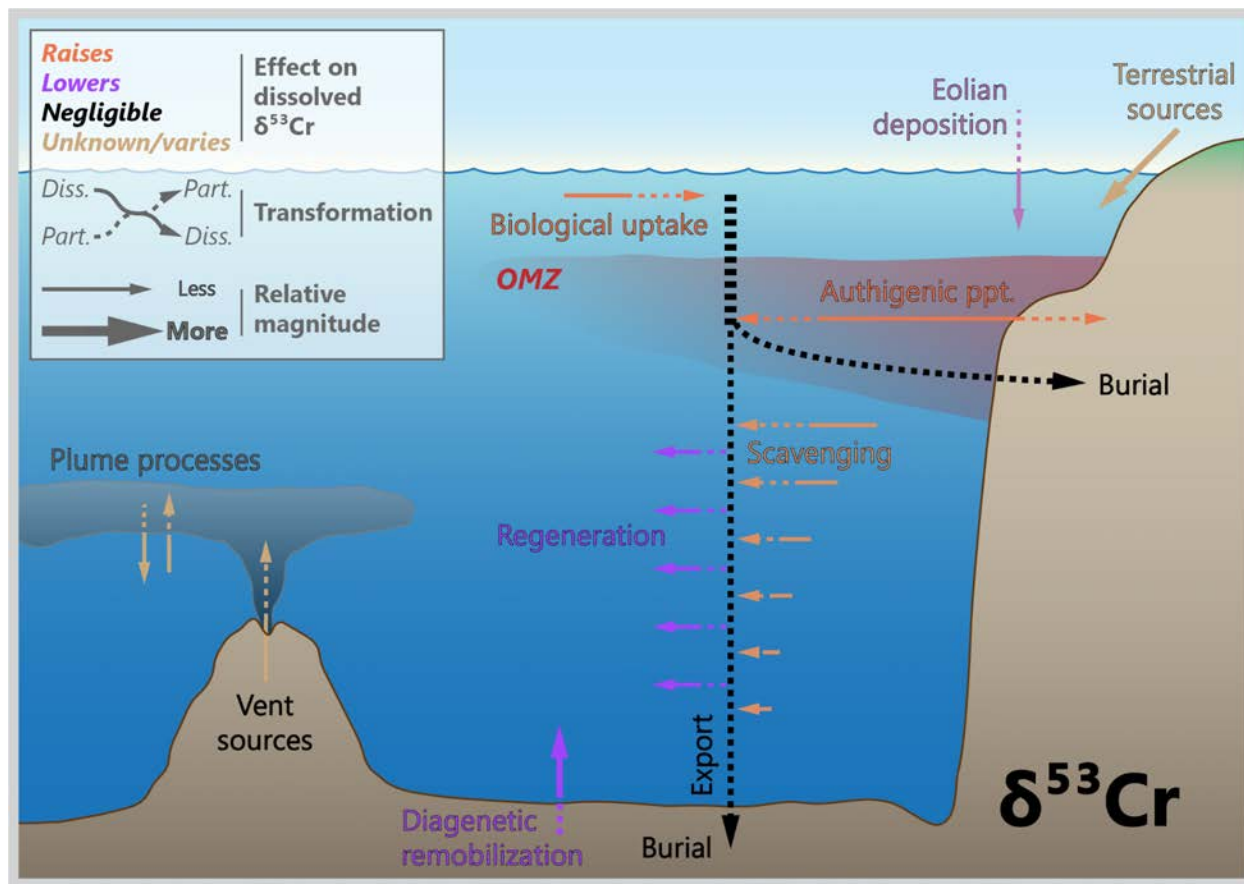
2312

Figure 28 | Representative profiles of dissolved Cr concentrations ([Cr]; A) and Cr isotopic compositions ($\delta^{53}\text{Cr}$; B). Data from the Eastern Tropical North Atlantic (squares, dashed line; Goring-Harford et al., 2018), Southern (triangles, dotted line; Rickli et al., 2019), and northeast Pacific Oceans (circles, solid line; Moos & Boyle, 2019). Station locations as per Fig. 1. These profiles illustrate that the decrease in surface ocean [Cr] from the Southern to low-latitude oceans is accompanied by a modest, but significant increase in $\delta^{53}\text{Cr}$. Likewise, deep waters with elevated [Cr] exhibit lighter $\delta^{53}\text{Cr}$, consistent with regeneration of an isotopically light Cr-bearing phase.

Chromium stable isotope compositions are reported relative to NIST SRM 979. The pioneering study of Scheiderich et al. (2015) reported much of the first oceanographically consistent $\delta^{53}\text{Cr}$ data. These and subsequent data show enrichments of heavy isotopes in open ocean surface waters (+0.9 to +1.4 ‰) relative to most deep waters (+0.7 to +0.9 ‰; Scheiderich et al., 2015; Goring-Harford et al., 2018; Moos et al., 2019; Rickli et al., 2019; Janssen et al., 2020; Moos et al., 2020; Nasemann et al., 2020; Fig. 28). Importantly, the first global $\delta^{53}\text{Cr}$ compilation also identified a tight linear correlation between $\delta^{53}\text{Cr}$ and $\ln[\text{Cr}]$, suggesting that the controls on [Cr] also regulate $\delta^{53}\text{Cr}$ —reduction and removal in OMZs and biological export from the surface ocean—and that these processes are accompanied by an isotope fractionation of approximately -0.7 to -0.8 ‰ (Scheiderich et al., 2015; Goring-Harford et al., 2018; Rickli et al., 2019; Janssen et al., 2020; Moos et al., 2020; Nasemann et al., 2020; Fig. 29; see also reactor model,

2313 Secs. 2.2., 12.2.). Subsequent studies have focused on understanding and constraining the sensitivities of
 2314 these processes. Isotopic fractionation during Cr removal in OMZs has been reported both in the water
 2315 column (Moos et al., 2020; Huang et al., 2021) and at the sediment–water interface (Moos et al., 2020;
 2316 Nasemann et al., 2020). Similarly, fractionation is observed during Cr export coupled to the biological
 2317 pump based on data from the open ocean (Janssen et al., 2020) and coastal waters (Goring-Harford et al.,
 2318 2018).

2319
 2320 While the understanding of [Cr] and dissolved $\delta^{53}\text{Cr}$ in the modern ocean has seen substantial improvements
 2321 in the GEOTRACES-era, key uncertainties in Cr biogeochemical cycling remain. In turn, these
 2322 uncertainties limit the potential of $\delta^{53}\text{Cr}$ paleoproxy applications and the identification of faithful $\delta^{53}\text{Cr}$
 2323 paleoarchives. The following sections present a more detailed summary of the marine Cr cycle and Cr
 2324 archives, with a focus on the $\delta^{53}\text{Cr}$ paleoproxy outlook related to marine Cr cycling and the key remaining
 2325 uncertainties.



2326
 2327 **Figure 29 | Processes driving Cr isotope variations in modern seawater.** Though muted, biological processes exert
 2328 a control on Cr and $\delta^{53}\text{Cr}$, and therefore $\delta^{53}\text{Cr}$ shows some response to productivity. The degree to which $\delta^{53}\text{Cr}$ may
 2329 ultimately be useful as a productivity proxy will depend on how globally important productivity is relative to other controls

2330 on Cr distributions, such as Cr reduction and removal in OMZs and the fidelity of sediment records, which currently
2331 remain unresolved.

2332

2333 **10.2. Driving processes**

2334 *10.2.1. Biological*

2335 Although Cr(VI) can be toxic (e.g., Wong & Trevors, 1988) and there is no known biological function for
2336 Cr in marine phytoplankton, [Cr] distributions reflect biogenic controls (e.g., Campbell & Yeats, 1981).
2337 This appears to be driven not by internalization but by adsorption of Cr(III) onto phytoplankton (Wang et
2338 al., 1997; Semeniuk et al., 2016). This scavenging removes isotopically light Cr from the surface ocean
2339 (Scheiderich et al., 2015; Goring-Harford et al., 2018; Janssen et al., 2020;), and has been shown to
2340 quantitatively explain patterns of oceanic [Cr] and dissolved $\delta^{53}\text{Cr}$ (Janssen et al., 2020). The magnitude of
2341 Cr export associated with the biological pump has been estimated at approximately $0.1\text{--}1 \text{ Gmol Cr yr}^{-1}$
2342 (Jeandel & Minster, 1987; Janssen et al., 2020), of comparable magnitude to known Cr sources (Wei et al.,
2343 2018).

2344

2345 *10.2.2. Chemical*

2346 Chromium is reduced and removed in OMZs and anoxic waters (Murray et al., 1983; Rue et al., 1997;
2347 Davidson et al., 2020; Moos et al., 2020; Nasemann et al., 2020; Huang et al., 2021). This removal may
2348 occur in the water column (Rue et al., 1997; Davidson et al. 2020; Moos et al., 2020; Huang et al., 2021)
2349 or at the sediment–water interface, though it is presently unclear which is of greater importance (cf. Moos
2350 et al., 2020; Nasemann et al., 2020). Approximate isotope fractionation factors for OMZ Cr reduction and
2351 removal are estimated as being $\approx -0.7\text{‰}$, similar to those implied by the global dissolved $\delta^{53}\text{Cr} - [\text{Cr}]$ array.
2352 However, these fractionation factors are considerably smaller than the expectations based on laboratory
2353 constrained fractionation factors (e.g., Wanner & Sonnenthal, 2013), likely reflecting an incomplete
2354 removal of Cr(III) resulting in a lower effective fractionation (Moos et al., 2020; Nasemann et al., 2020;
2355 Huang et al., 2021) and the fact that isotope reactor models will underestimate true isotope separation
2356 factors in the presence of mixing. Water column-based estimates of the OMZ Cr sink are not available, and
2357 deep water data suggest that some of the Cr removed in OMZs is released in underlying oxic waters and/or
2358 sediments (e.g., Murray et al., 1983).

2359

2360 *10.2.3. Physical*

2361 Riverine fluxes are believed to represent the main source of Cr to the oceans, accounting for approximately
2362 1 Gmol Cr yr⁻¹ (Wei et al., 2018). High variability has been reported for riverine dissolved $\delta^{53}\text{Cr}$, though
2363 available data suggest that rivers are isotopically heavy relative to the continental crust (e.g., Frei et al.,
2364 2014; D'Arcy et al., 2016; Goring-Harford et al., 2020). The role of estuarine processes is unclear at present.
2365 Earlier studies suggested scavenging of Cr at low salinity (Cranston & Murray, 1980; Campbell & Yeats,
2366 1984), therefore lowering of riverine Cr fluxes; however, recent data have found conservative mixing of
2367 Cr(III), Cr(VI) and $\delta^{53}\text{Cr}$ (Goring-Harford et al., 2020) or release of particulate Cr to the dissolved phase
2368 (Sun et al., 2019).

2369

2370 As with other trace metals (e.g., Zn, Cd, Ba; Secs. 4., 6., 8.), deep water circulation plays an important role
2371 in shaping [Cr] and dissolved $\delta^{53}\text{Cr}$ distributions. The advection of Cr-rich intermediate and deep waters
2372 formed in the Southern Ocean helps to explain [Cr] enrichments seen at depth in the Pacific (Fig. 28A; cf.
2373 Rickli et al., 2019; Moos et al., 2019). Data from NADW, while more limited, suggest it is more Cr-depleted
2374 than waters formed in the Southern Ocean (Fig. 28A; cf. Goring-Harford et al., 2018; Rickli et al., 2019).

2375

2376 **10.3. Marine archives**

2377 *10.3.1. Carbonates*

2378 Chromium(VI) is incorporated into the CaCO₃ matrix during carbonate formation (e.g., Tang et al., 2007).
2379 Because Cr(VI) dominates the [Cr] pool in the oxic ocean, this suggests that carbonates may serve as a
2380 suitable proxy for ambient dissolved $\delta^{53}\text{Cr}$, motivating numerous $\delta^{53}\text{Cr}$ -based reconstructions as well as a
2381 significant body of research to ground-truth the theory-based motivations. A recent review of $\delta^{53}\text{Cr}$ -based
2382 paleo reconstructions in carbonates can be found in Wei et al. (2020) and below we highlight relevant
2383 assessments of the utility of carbonate archives from the modern ocean.

2384

2385 Inorganic calcite precipitation at oceanographically relevant pH results in an enrichment of light isotopes
2386 in CaCO₃ up to 0.7 ‰ lighter than the solution (Füger et al., 2019), though data at an oceanographically
2387 relevant ionic strength are not available. The Cr content of carbonates is low (from <1 to ~10 $\mu\text{g g}^{-1}$;
2388 Holmden et al., 2016; Pereira et al., 2016; Remmelzwaal et al., 2019), and therefore CaCO₃ is not a major
2389 Cr sink (Bonnand et al., 2013). Studies of Cr incorporated into a diverse range of biogenic carbonates show
2390 an enrichment in isotopically light Cr relative to ambient seawater, but with a wide range of fractionation

2391 factors. This fractionation is believed to reflect redox processes during Cr uptake into calcifying organisms
2392 or preceding Cr incorporation into CaCO₃ (Holmden et al., 2016; Pereira et al., 2016; Farkas et al., 2018).
2393 Marine carbonate-hosted $\delta^{53}\text{Cr}$ archives are, however, susceptible to meteoric (Wang et al., 2021) and
2394 marine diagenetic overprinting (e.g., Remmelzwaal et al., 2019).

2395

2396 *10.3.2. Ferromanganese crusts*

2397 Ferromanganese (Fe–Mn) crusts from the Pacific are isotopically light ($\delta^{53}\text{Cr} = -0.85$ to -0.15 ‰, average
2398 $= -0.42$ ‰, Wei et al., 2018) relative to North Pacific deep water ($\approx +0.7$ to $+0.8$ ‰, Moos & Boyle, 2019;
2399 Fig. 28B), equivalent to an isotope separation factor of approximately -0.9 to -1.6 ‰. The low abundance
2400 of Cr in Fe–Mn crusts (~ 7 $\mu\text{g g}^{-1}$) indicates that, globally, Cr removal to Fe–Mn oxides is not important in
2401 controlling [Cr] and $\delta^{53}\text{Cr}$ budgets (Wei et al., 2018). Additionally, Cr is likely somewhat mobile in Fe–Mn
2402 crusts, with a predicted diffusivity $\leq 10^{-7}$ $\text{cm}^2 \text{yr}^{-1}$ (see Henderson & Burton, 1999, for calculation details),
2403 similar to Cd (Sec. 6.3.2.), Mo (Sec. 7.3.), and Ag (Sec. 11.3.). This rate implies that long-term records of
2404 $\delta^{53}\text{Cr}$ derived from Fe–Mn are likely to exhibit some diffusive smoothing while preserving larger
2405 perturbations. The large range of $\delta^{53}\text{Cr}$ in modern Fe–Mn crusts, relative to the modest variations in $\delta^{53}\text{Cr}$
2406 of surrounding intermediate and deep waters, suggests that Fe–Mn crusts are unlikely to be developed into
2407 a reliable archive for past marine $\delta^{53}\text{Cr}$.

2408 The Cr content of other types of oxygenated sediments are generally low (≈ 60 $\mu\text{g g}^{-1}$; Gueguen et al.,
2409 2016b), with Cr:Ti ratios comparable to the continental crust. Some samples, however, do show apparent
2410 authigenic Cr enrichments of a similar magnitude to anoxic and suboxic sediments.

2411

2412 *10.3.3. Suboxic and anoxic sediments*

2413 Chromium is generally enriched in suboxic and anoxic surface sediments relative to upper continental crust
2414 and oxic sediments (Reinhard et al., 2014; Gueguen et al., 2016b), with an average Cr content of surface
2415 sediments of 108 ± 28 $\mu\text{g g}^{-1}$ (1SD, $n = 12$, Gueguen et al., 2016b; Bruggmann et al., 2019), suggesting
2416 authigenic Cr enrichments in these environments may present a major Cr sink (Reinhard et al., 2013; Wei
2417 et al., 2018). Suboxic and anoxic sediment leaches targeting authigenic Cr are isotopically light relative to
2418 regional and basin-scale deepwater (Gueguen et al., 2016b; Bruggmann et al., 2019), in agreement with
2419 predictions for Cr removal in OMZs and biological export (Janssen et al., 2020; Moos et al., 2020;
2420 Nasemann et al., 2020; Huang et al., 2021). Down-core records of $\delta^{53}\text{Cr}$ in suboxic sediments demonstrate
2421 glacial–interglacial variability, which has been interpreted to reflect changes in ocean oxygenation

2422 (Gueguen et al., 2016b). However, given the relationships between biological export and ocean
2423 deoxygenation for sediment metal accumulation (e.g., Nameroff et al., 2004) and similar fractionations
2424 reported for biogenic export and OMZ removal, it may be difficult to disambiguate these two controls on
2425 sedimentary $\delta^{53}\text{Cr}$.

2426

2427 Initial interpretations inferred quantitative removal of Cr to anoxic sediments, suggesting they may serve
2428 as an archive of oceanic $\delta^{53}\text{Cr}$ (Reinhard et al., 2014), in a manner analogous to Zn (Sec. 4.3.4.) However,
2429 reinterpretations of Cariaco Basin surface sediments ($\delta^{53}\text{Cr} \approx +0.4 \pm 0.1$; Gueguen et al., 2016b) alongside
2430 nearby and oceanographically consistent water column data (dissolved $\delta^{53}\text{Cr} \approx +1.2 \pm 0.1$; Goring-Harford
2431 et al., 2018; Fig. 28), suggest that $\delta^{53}\text{Cr}$ in anoxic sediments may in fact be lighter than ambient seawater
2432 by $\approx 0.8 \pm 0.2$ ‰, which is similar to the isotope separation implied by the global [Cr] - dissolved $\delta^{53}\text{Cr}$ -
2433 array ($\Delta_{\text{P-R}} \approx -0.7$ to -0.8). While a full assessment of this offset requires truly colocated water and sediment
2434 samples, existing data do not support the hypothesis that anoxic sedimentary $\delta^{53}\text{Cr}$ reflects ambient
2435 dissolved $\delta^{53}\text{Cr}$ with no isotope offset.

2436

2437

2438 **10.4. Prospects**

2439

2440 The sensitivity of both [Cr] and dissolved $\delta^{53}\text{Cr}$ to biotic and abiotic redox cycling makes Cr a potentially
2441 promising redox proxy. Historically, $\delta^{53}\text{Cr}$ has received most attention as a paleoredox proxy, with most
2442 interpretations based on the framework that terrestrial processes result in isotopically heavy Cr reaching the
2443 oceans via rivers, without further alteration of $\delta^{53}\text{Cr}$ through oceanic cycling (e.g., Frei et al., 2009; Frei et
2444 al., 2014). Although this model may remain generally valid under atmospheric oxygen levels relevant to
2445 the early Earth, internal processes in the ocean, including biological productivity, dominate modern $\delta^{53}\text{Cr}$
2446 records and may still be influential under strongly reducing conditions (e.g. Bauer et al., 2018).

2447

2448 As the body of high quality [Cr] and dissolved $\delta^{53}\text{Cr}$ data continue to grow through GEOTRACES, two
2449 primary areas of uncertainty have emerged that are currently limiting $\delta^{53}\text{Cr}$ paleoproxy applications: a
2450 quantitative apportionment of the balance between productivity- and O_2 -related Cr cycling, and
2451 identification of archives that reliably record dissolved $\delta^{53}\text{Cr}$.

2452

2453 *10.4.1. Modern*

2454 The most pressing issue for the Cr isotope community is to ensure that future water column data are reported
2455 according to high standards of intercalibration and quality control. In addition to this issue, several targets
2456 are needed to address specific mechanistic controls on the modern ocean Cr and $\delta^{53}\text{Cr}$ cycles. First,
2457 improved constraints on biological and OMZ-mediated Cr removal and the relative importance of these two
2458 processes would help to better understand the modern Cr biogeochemical cycle. Direct and robust
2459 determinations of fractionation factors associated with biologically mediated Cr export should be
2460 prioritized, along with a better understanding of differences in Cr removal among taxa, as well as
2461 interrogation of the mechanisms by which phytoplankton reduce and scavenge Cr. More studies have
2462 assessed fractionation factors for OMZs, but quantitative constraints are still limited and it is unclear as to
2463 what extent OMZ-related processes influence open marine [Cr] and dissolved $\delta^{53}\text{Cr}$.

2464

2465 Second, central to OMZ and biogenic Cr removal are understandings of how much Cr is exported with
2466 particles, how much of this reaches the seafloor, and how much is eventually buried in marine sediments.
2467 Data from marine particulates, currently limited by high filter blanks and low particulate Cr concentrations,
2468 are sorely needed to address these points. Additionally, data for marine particles may help to assess to what
2469 extent mid-depth scavenging outside of OMZs, known to be important for other scavenging-prone metals
2470 (e.g., Ohnemus et al., 2019, Secs. 3.–5.), shapes Cr distributions. More data are needed from porewaters
2471 and surface sediments to better understand benthic Cr fluxes and Cr burial. Finally, some aspects of the
2472 modern global biogeochemical cycle, such as fluxes from hydrothermal vents, remain completely
2473 unconstrained.

2474

2475 *10.4.2. Paleo*

2476 Ideal archives for $\delta^{53}\text{Cr}$ paleoproxy applications should faithfully reflect a known oceanic condition (e.g.,
2477 dissolved $\delta^{53}\text{Cr}$) or processes (e.g., Cr removal in OMZs) and should have a sufficient Cr content so that
2478 sample availability is not a limiting factor. It is also clear from the $\delta^{53}\text{Cr}$ paleoproxy research to date that
2479 careful record selection is necessary to avoid samples with minimal overprinting or alteration of primary
2480 $\delta^{53}\text{Cr}$ records (e.g., Albut et al., 2018; Remmelzwaal et al., 2019; Wang et al., 2021). Given these
2481 constraints, the following points summarize the most promising archives, which may also offer an
2482 opportunity to reevaluate literature data—mostly interpreted in terms of paleoredox—in the context of
2483 paleoproductivity.

2484

2485 At present, carbonate-hosted $\delta^{53}\text{Cr}$ remains a challenging archive for several reasons, including: low Cr:Ca,
2486 taxon-dependent Cr isotope fractionations, fractionation during inorganic calcite precipitation, and potential
2487 diagenetic overprinting in marine sediments (e.g. Holmden et al., 2016; Pereira et al., 2016; Remmelzwaal
2488 et al., 2019). Additional research is needed to assess to what extent variable taxon-dependent fractionations
2489 and diagenetic overprinting can be recognized and corrected before applying $\delta^{53}\text{Cr}$ in marine carbonates.
2490 Existing data indicate that Fe–Mn crusts are not suitable $\delta^{53}\text{Cr}$ archives (Wei et al., 2018). Other oxic
2491 sedimentary archives, such as authigenic clays, may be suitable, but little is known about the degree to
2492 which sedimentary and oceanic Cr and $\delta^{53}\text{Cr}$ exchange, the role of oxic sedimentary phases in the Cr cycle
2493 (and the relevant isotope separation factors), and the depths recorded by these phases.

2494

2495 Black shale records of $\delta^{53}\text{Cr}$ have been used to investigate oceanic oxygenation levels over time. However,
2496 the uncertainty regarding how faithfully anoxic and suboxic sediments record conditions in the modern
2497 ocean combined with potential $\delta^{53}\text{Cr}$ homogenization among sediment phases (Frank et al., 2020) suggests
2498 more research is needed to validate shales as reliable records before further applications. Furthermore, early
2499 interpretations of quantitative removal of Cr to anoxic sediments are not supported by the current body of
2500 water column data. Consequently, more research is needed to validate the use of anoxic sediments to
2501 reconstruct water column $\delta^{53}\text{Cr}$, such as identification of suitable correction factors based on colocated
2502 water column and sediment data. Similarly, oceanographically consistent water column data are sparse
2503 relative to suboxic sedimentary measurements, complicating assessments of the impact of Cr loss to
2504 sediments. Disentangling local reduction-based accumulation from Cr delivery to suboxic and anoxic
2505 sediments via biogenic particles may be challenging, given the importance of both these processes on Cr
2506 cycling and the linkages between biological export and oxygen depletion.

2507

2508

2509

2510

2511

2512

2513 **11. Silver**

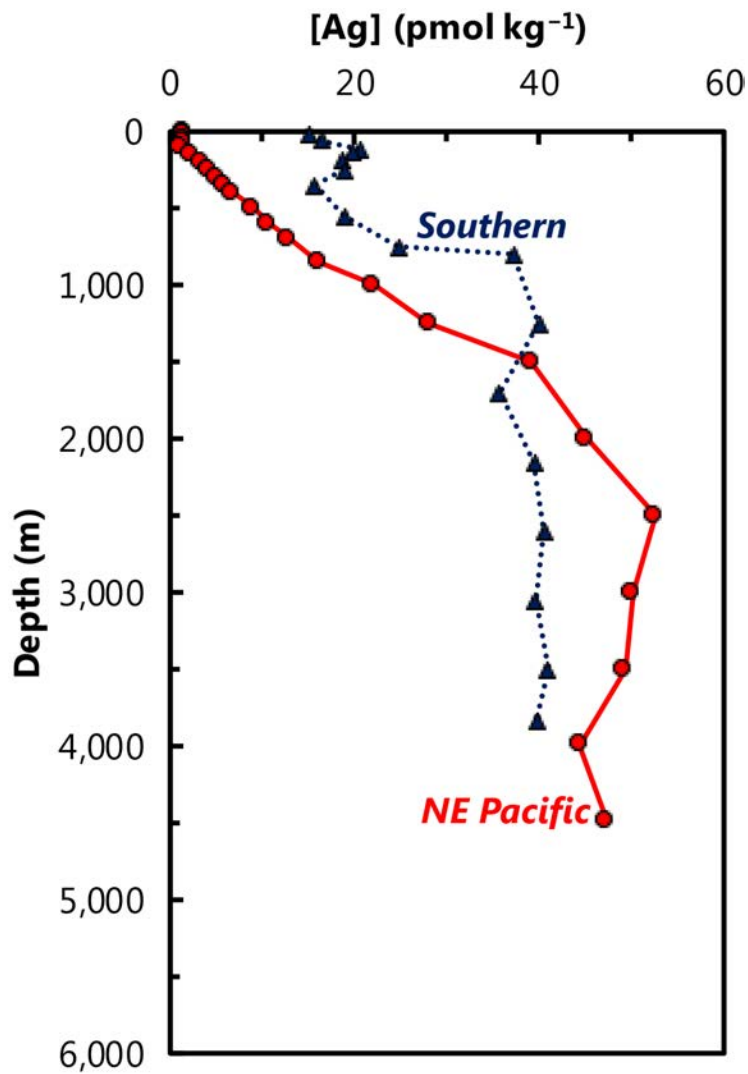
2514 Silver is the scarcest of the bioactive trace metals described here—within Earth’s crust, in the modern ocean
2515 (Table 1), and from an observational point of view. Like Ba, Ag is an unusual candidate for a
2516 paleoproductivity proxy given that it possesses no known biological function and is most widely known for
2517 its antimicrobial properties. Despite this, [Ag] exhibits a characteristic nutrient-like profile in seawater,
2518 most similar to that of [Si] (or [Zn], [Ba]; Figs. 1, 30), and Ag content in certain sediments is positively
2519 correlated with organic C. These intriguing features warrant further investigation into whether and how
2520 marine Ag cycling might reflect ocean productivity.

2521

2522 **11.1. Marine distribution**

2523 Dissolved Ag occurs primarily as chloride complexes in seawater (Cowan et al., 1985, Miller & Bruland,
2524 1995) and exhibits a nutrient-type depth profile; [Ag] in surface waters are typically $<5 \text{ pmol kg}^{-1}$, and
2525 range from $5\text{--}30 \text{ pmol kg}^{-1}$ in deep waters of the Atlantic Ocean to $50\text{--}114 \text{ pmol kg}^{-1}$ in the Pacific Ocean
2526 (Fig. 30; Flegal et al., 1995; Rivera-Duarte et al., 1999; Ndung’u et al., 2001; Zhang et al., 2001; 2004;
2527 Ranville and Flegal, 2005; Kramer et al, 2011; Boye et al., 2012). The total observed range in seawater is
2528 $0.2\text{--}115 \text{ pmol kg}^{-1}$ (Gallon and Flegal, 2014). Despite its potential as a biogeochemical proxy, no Ag
2529 isotope data currently exist for dissolved or particulate phases in the water column, nor in marine
2530 sedimentary archives. Accordingly, we cannot directly assess the utility of $\delta^{109}\text{Ag}$ to infer
2531 paleoproductivity, though we can deduce a number of processes that are likely to influence dissolved $\delta^{109}\text{Ag}$
2532 based on the processes known to cycle Ag (Fig. 31).

2533



2534

2535

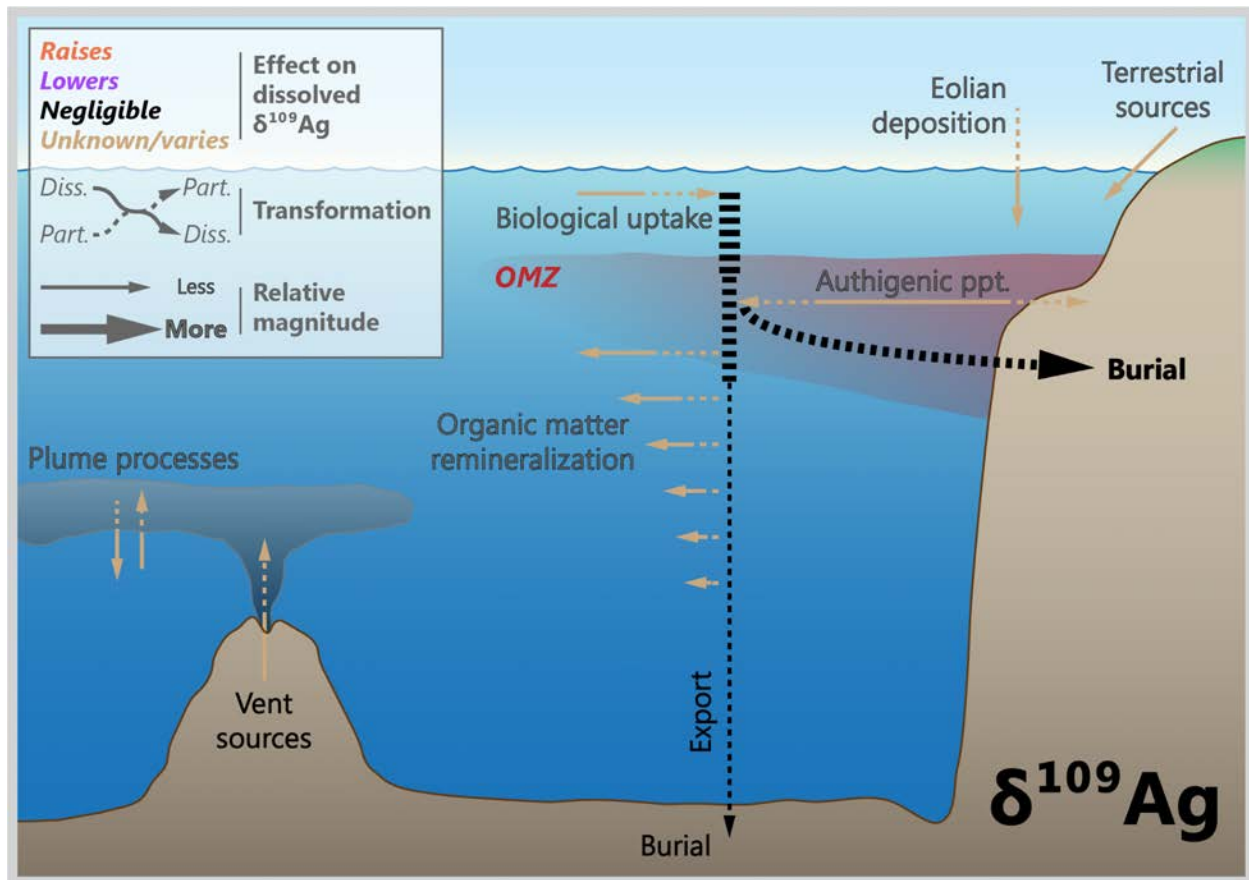
2536

2537

2538

2539

Figure 30 | Representative profiles of dissolved Ag concentrations ([Ag]). Data from the Northeast Pacific (circles, solid line; Fisher et al., 2018) and Southern Oceans (triangles, dotted line; Boye et al., 2012). Station locations as per Fig. 1. Data from the Northeast Pacific were extracted graphically using WebPlotDigitizer (Rohatgi, 2019). The authors are not aware of the existence of any Ag isotope data for seawater at this time.



2540

2541 **Figure 31 | Processes likely to drive Ag isotope variations in modern seawater.** Despite there being no Ag isotope
 2542 data for seawater at this time, we can infer a number of processes that are most likely to influence dissolved $\delta^{109}\text{Ag}$
 2543 from measurements of $[\text{Ag}]$ in seawater and sediments.

2544

2545

2546 **11.2. Driving processes**

2547 The typical $[\text{Ag}]$ depth profile (Fig. 30) is similar to that of $[\text{Si}]$, resulting in a strong positive correlation
 2548 between these elements in existing datasets. This has led researchers to suggest that Ag is taken up by
 2549 diatoms, incorporated into their frustules, and then released as the frustules dissolve (e.g., Flegal et al.,
 2550 1995). Silver might then be delivered to the seafloor with opal, potentially making it useful as a
 2551 paleoproductivity proxy (Friedl & Pedersen, 2002). However, the correlation between $[\text{Ag}]$ and $[\text{Si}]$ is non
 2552 linear, indicating that other factors are at play (Zhang et al., 2001; 2004). Furthermore, while Ag is taken
 2553 up by various types of phytoplankton, including diatoms (Fisher & Wentz, 1993), experiments conducted
 2554 using the marine diatom *Thalassiosira pseudonana* show that most of the Ag is associated with the organic
 2555 fraction rather than the opal (Wagner, 2013). Martin et al. (1983) also hypothesized that high particulate
 2556 Ag concentration within the euphotic zone (40–70 m) off the west coast of Mexico were due to the
 2557 formation of Ag-organic complexes. Interestingly, particulate Ag concentrations are even higher well below

2558 the euphotic zone, at a depth corresponding to the upper portion of the local OMZ (Martin et al., 1983). It
2559 could also be that a global [Ag]:[Si] correlation arises at least in part from biological processes occurring
2560 in the surface of the Southern Ocean, whereby intermediate and mode waters with low preformed [Ag] are
2561 advected to lower latitudes, analogous to the mechanism proposed for [Zn]:[Si] (Vance et al., 2017) and
2562 [Ba]:[Si] coupling (Horner et al., 2015a). If correct, Ag is unlikely to be coupled directly to opal via a
2563 simple relationship that can be used to reconstruct past diatom productivity.

2564

2565 Even if driven by productivity, [Ag] distributions may become decoupled from productivity by possessing
2566 different source and sink terms relative to carbon and the macronutrients (Gallon & Flegal, 2014 and
2567 references therein). For example, Ranville & Flegal (2005) and Ranville et al. (2010) invoked an
2568 anthropogenic aerosol source of Ag to surface and intermediate waters to explain north Pacific water
2569 column data. Other complications may arise under low [O₂] environments—waters from the northeast
2570 Pacific (Kramer et al., 2011) and southeastern Atlantic (Boye et al., 2012) exhibit a deficit in [Ag] relative
2571 to [Si] within their respective OMZs. These deficits imply preferential removal of Ag over Si, which may
2572 occur locally or ‘upstream’. If occurring locally, a putative mechanism is co-precipitation with other
2573 chalcophile elements, analogous to the sulfide-mediated mechanism proposed for Cd in OMZs (Janssen et
2574 al., 2014; Sec. 5). Alternatively, the deficit may reflect low preformed [Ag]:[Si] in intermediate waters,
2575 which is inherited from preferential drawdown of Ag over Si in regions upstream where these intermediate
2576 waters were last ventilated. Both interpretations have implications for the use of Ag or δ¹⁰⁹Ag as a
2577 paleoproxy: the former implies a redox sensitivity that depends on the changing location, spatial extent, and
2578 intensity of low [O₂] regions in the oceans over time; the latter implies a sensitivity to ecology and the
2579 geometry of ocean circulation. Both warrant additional scrutiny.

2580

2581 **11.3. Marine archives**

2582 Bulk sediments are the main archive that has been investigated for their potential to record information
2583 about the marine Ag cycle. The Ag content of bulk sediments from open marine environments range from
2584 ≤100 ng g⁻¹ (i.e., typical lithogenic values) up to 100s of ng g⁻¹ (Koide et al., 1986). In general, low Ag
2585 content is typical of well-oxygenated sediments, while higher Ag contents are typical of sediments formed
2586 in oxygen-poor and euxinic environments. The general consensus has been that Ag enrichment in anoxic
2587 sediments is the result of post-depositional precipitation of Ag₂S (Koide et al., 1986) or possibly Ag selenide
2588 (Crusius & Thomson, 2003; Böning et al., 2005). However, high Ag content is also documented in marine
2589 sediments that are only weakly reducing (Böning et al., 2004, 2005; McKay & Pedersen, 2008; Morford et

2590 al., 2008). Furthermore, even in anoxic sediments, the degree of Ag enrichment exceeds what would be
2591 expected from post-depositional Ag precipitation alone (Borchers et al., 2005; McKay and Pedersen, 2008;
2592 Böning et al., 2009). Thus, redox-controlled, post-depositional precipitation is not the primary control on
2593 Ag accumulation in marine sediments, implying that there must also be a flux of non-lithogenic, particulate
2594 Ag to the seafloor (McKay & Pedersen, 2008).

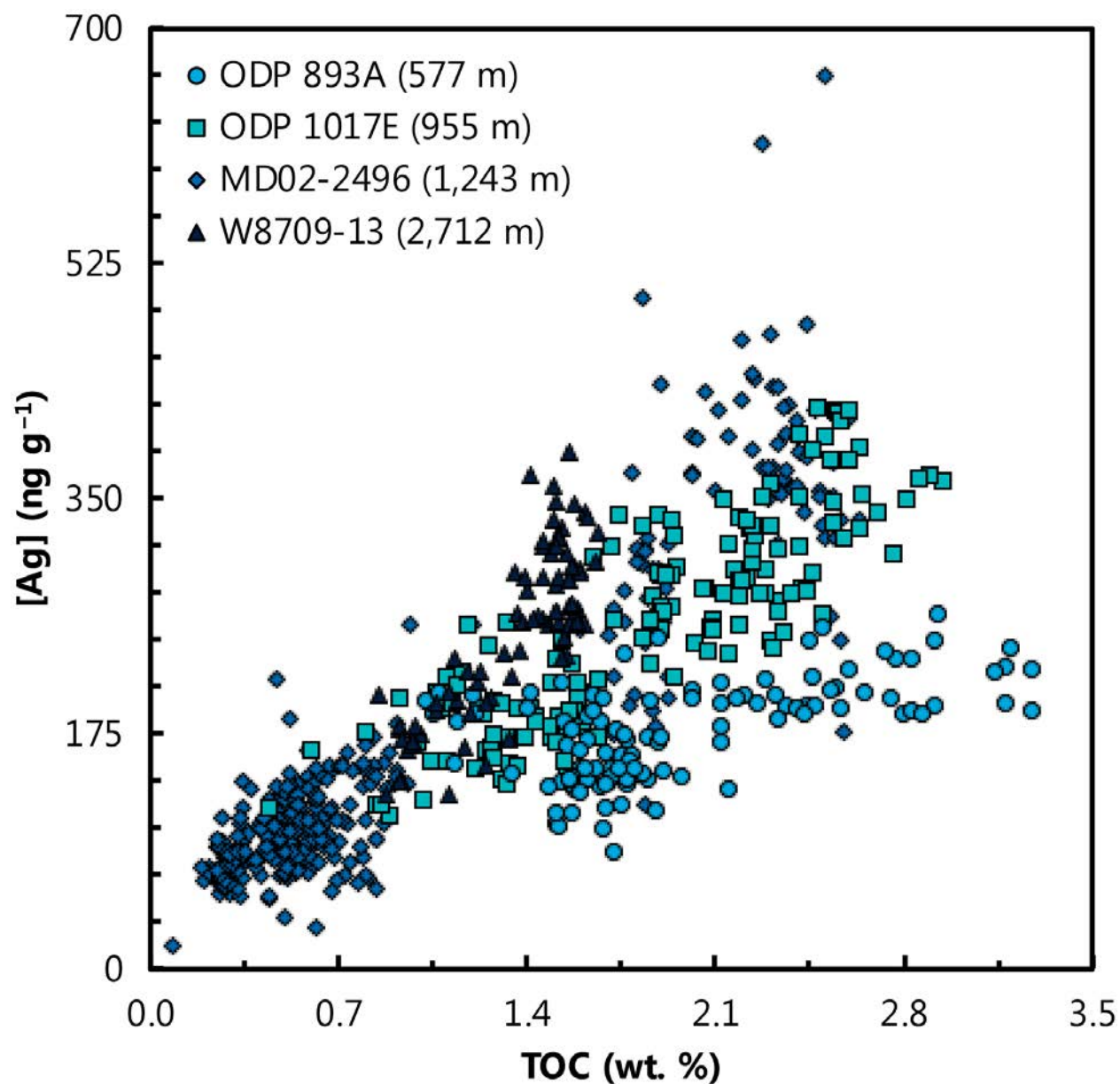
2595

2596 McKay & Pedersen (2008) hypothesized that Ag, like Ba, accumulates in organic-rich settling particles.
2597 However, in contrast to Ba, Ag precipitation requires a reduced microenvironment within the particle,
2598 which is generally only possible in waters that possess relatively low [O₂] (e.g., Bianchi et al., 2018). The
2599 analysis of sediment trap samples from the northeast Pacific show that the fluxes of particulate Ag and
2600 particulate organic carbon flux positively correlate (Martin et al., 1983). This correlation is also seen in
2601 surface sediments (McKay & Pedersen, 2008) and sediment cores from the northeastern Pacific (Fig. 32).
2602 These data broadly support the use of particulate Ag flux as a paleoproductivity proxy, with an important
2603 caveat: the post-depositional preservation of particulate Ag requires that sediments remain reducing, as
2604 settling particulate Ag formed below the euphotic zone is not preserved if sediments are oxidizing (McKay
2605 and Pedersen, 2008; Morford et al., 2008). Thus, while the delivery of particulate Ag to sediments appears
2606 related to productivity (Wagner et al., 2013), Ag delivery to—and preservation within—sediments is
2607 sensitive to [O₂]; low water column [O₂] favors higher Ag:C of sinking particles and greater Ag preservation
2608 at the seafloor. By analogy to other metals (e.g., Twining & Baines, 2013), variations in surface water [Ag]
2609 may also modulate Ag:C, though remains to be tested. These three sensitivities likely explain why different
2610 regions exhibit distinct arrays in Ag–TOC space (Fig. 32). Despite these regional variations, the
2611 relationships between Ag and organic matter are promising from the point of view of tracing past
2612 productivity.

2613

2614 Though yet to be investigated for $\delta^{109}\text{Ag}$, Ag is predicted to be somewhat mobile in Fe–Mn crusts, with a
2615 predicted diffusivity $\leq 10^{-7} \text{ cm}^2 \text{ yr}^{-1}$ (see Henderson & Burton, 1999, for calculation details), similar to Cd
2616 (Sec. 6.3.2.), Mo (Sec. 7.3.), and Cr (Sec. 10.3.2.). This rate implies that, should any long-term records be
2617 forthcoming, Fe–Mn crust based reconstructions of $\delta^{109}\text{Ag}$ are likely to exhibit some diffusive smoothing
2618 while preserving larger perturbations.

2619



2620

2621 **Figure 32 | Concentrations of Ag and total organic carbon in sediment cores from the northeast Pacific Ocean.**

2622 These data illustrate that Ag is broadly correlated with organic matter in bulk sediments, which is highly promising from
 2623 the perspective of developing Ag as a paleoproductivity proxy. Core MD02-2496 (Vancouver Island Margin; 48.97°N,
 2624 127.04°W, 1,243 m water depth) from Chang et al., 2014; Core W8709-13PC (Oregon Margin; 42.116°N, 125.75°W;
 2625 2,712 m water depth) from Kienast, 2003; ODP 1017E (Southern California; 34.53°N, 121.1°W; 955 m water depth)
 2626 from Hendy & Pedersen, 2005; ODP 893A (Santa Barbara Basin; 34.287°N, 120.036°W; 576.5 m water depth) from
 2627 Ivanochko, 2001.

2628

2629

2630

2631

2632 **11.4. Prospects**

2633 The apparent linkages between [Ag] and particulate Ag, macronutrients, and organic matter provides
2634 tantalizing evidence that Ag cycling may be related to surface productivity (Fig. 30). Moreover, coretop
2635 studies indicate that the geochemical signature of this coupling is preserved under certain environmental
2636 conditions (Fig. 32). Despite this progress, the study of Ag in marine biogeochemical cycles remains in its
2637 infancy, particularly compared to many of the other elements described here. Additional constraints are
2638 needed in several areas, including: the role of biogeochemical processes in mediating Ag distributions in
2639 the water column, the dominant controls on the downward transport of Ag through the oceans, and on the
2640 controls on Ag preservation in sediments. Given what has been learned from the application of the other
2641 trace metal isotope systems described here, new analytical developments in Ag isotope geochemistry could
2642 help place valuable constraints on these areas.

2643

2644

2645 **12. Synthesis**

2646 In this final section, we synthesize and describe the overall suitability to trace productivity (Sec. 12.1.),
2647 explore inter-element similarities (Sec. 12.2.), define proxy readiness (Sec. 12.3.), and outline a number of
2648 research priorities (Sec. 12.4.) for using Fe, Zn, Cu, Cd, Mo, Ba, Ni, Cr, and Ag and their isotopes as
2649 paleoproductivity proxies.

2650

2651

2652 **12.1. Overall state of the proxies**

2653 Taking a general view, the review of each element highlights that our knowledge of bioactive trace metal
2654 isotope systematics lags behind those of trace element abundances and far behind those of macronutrient
2655 isotopes (e.g., Farmer et al., *this volume*). The bioactive metal isotope field is nascent; excepting Mo, the
2656 very first isotope data for seawater for all of the elements reviewed here were published within the last 15
2657 years, or—in the case of Ag—are yet to be reported. The field is thus decades behind the trace metal
2658 concentration community. Despite the lack of detail, we can begin to classify the metals reviewed here into
2659 three broad categories: those where there are clear and promising signs that a metal can serve as a proxy of
2660 paleoproductivity, such as for $\delta^{114}\text{Cd}$, $\delta^{138}\text{Ba}$, $\delta^{60}\text{Ni}$, and $\delta^{53}\text{Cr}$; those where a metal is unlikely to directly
2661 inform on paleoproductivity, as for $\delta^{56}\text{Fe}$, $\delta^{66}\text{Zn}$, $\delta^{65}\text{Cu}$, and $\delta^{98}\text{Mo}$; and those where simply too little is
2662 known to confidently assign utility at this time, as for $\delta^{109}\text{Ag}$.

2663

2664 More specifically, this review highlights the importance of ocean circulation in mediating the distribution
2665 of several bioactive trace metals and their isotopes. Key features of the isotope distributions reviewed here
2666 reflect a mixture of local (i.e., *in situ*) and regional (or *ex situ*) processes, with the latter often set far
2667 ‘upstream’ of any given locality. Indeed, researchers are recognizing that, much like the macronutrients
2668 (see Farmer et al., *this issue*), the first-order features of many metals are not controlled locally by a given
2669 dissolved–particulate transformations, but reflect a regionally integrated history of vertical cycling and
2670 mixing that is imparted over the scale of an ocean basin, which we discuss next.

2671

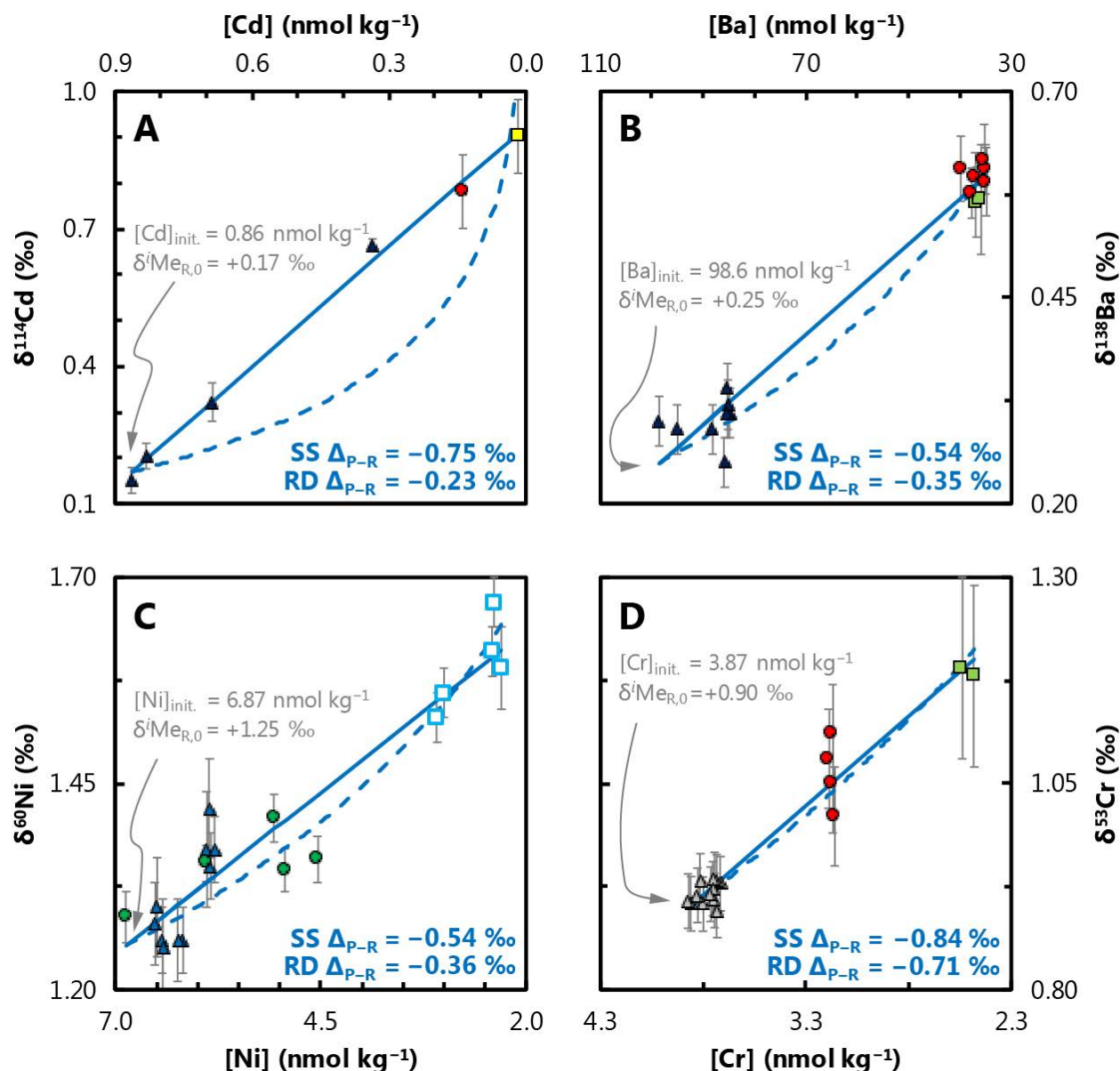
2672 **12.2. The reactor model applied to select trace metal isotope systems**

2673 Today, the Southern Ocean represents the common starting point and ultimate source of many TEIs for low
2674 latitude thermoclines (e.g., Sarmiento et al., 2004; Talley, 2013). If we assume that the reaction progress
2675 term in the reactor model is analogous to the fraction of initially supplied nutrient left unconsumed by
2676 phytoplankton, the concentration and isotope composition of a Me in the Southern Ocean can be assumed

2677 to represent the starting composition of a metal in the isotope reactor (i.e., [Me] and $\delta^i\text{Me}_{R,0}$ when $f = 0$).
2678 Our study suggests that four of the nine bioactive trace metals reviewed here (Cd, Ba, Ni, Cr) are suitable
2679 candidates for the isotope reactor model, which we now use to constrain Δ_{P-R} for both Steady State (SS)
2680 and Rayleigh Distillation (RD). We assume that samples from the upper 1,000 m of the Southern Ocean
2681 represent the initial reactor conditions (Fig. 33); downstream of the Southern Ocean, we consider only those
2682 samples shallower than 200 m to ensure that the models only regress productivity-associated Me drawdown.
2683 Our example calculations are intended to be illustrative, rather than the definitive estimate of Δ_{P-R} for each
2684 metal; comprehensive, global compilations are described elsewhere for Cd (Xie et al., 2017; Sieber et al.,
2685 2019), Ba (Hsieh & Henderson, 2017; Horner & Crockford, 2021), Ni (Yang et al., 2020), and Cr (Rickli
2686 et al., 2019; Wei et al., 2020). Accordingly, we limit our example to the stations shown in Fig. 1.

2687
2688 Excepting the RD model for Cd, the reactor models generate a reasonable fit to the data, with best-fit Δ_{P-R}
2689 of -0.75 ± 0.02 ‰ (SS) and -0.23 ± 0.16 ‰ (RD) for Cd ($n=6$), -0.54 ± 0.03 ‰ (SS) and -0.35 ± 0.03 ‰ (RD)
2690 for Ba ($n=16$), -0.54 ± 0.04 ‰ (SS) and -0.36 ± 0.04 ‰ (RD) for Ni ($n=20$), and -0.84 ± 0.04 ‰ (SS) and
2691 -0.71 ± 0.04 ‰ (RD) for Cr ($n=18$; all \pm represent the root-mean-square deviation). These values are
2692 generally within the accepted ranges reported for each metal, either for oceanographic data or specific
2693 experiments (e.g., culture studies, mineral precipitation). The reactor models illustrate that best-fit Δ_{P-R} for
2694 SS are larger in magnitude than for RD. This difference derives from mixing. Open-system models account
2695 for continuous uptake and removal of Me from the reactor, thus requiring a larger Δ_{P-R} to render an
2696 equivalent change in $\delta^i\text{Me}_R$ compared to RD. In general therefore, calculations assuming SS will be closer
2697 to the underlying value of Δ_{P-R} , since the surface ocean is poorly represented by a closed-system reactor.

2698
2699



2700

2701 **Figure 33 | Reactor framework applied to select bioactive trace metal isotope systems.** Station locations and
2702 symbols as per Fig. 1. **A–D** Isotope reactor models for Cd (A), Ba (B), Ni (D), and Cr (D) showing evolution of the
2703 residual reactant during Me consumption. Best-fit $\Delta_{\text{P-R}}$ are shown for SS (solid) and RD fractionation (dashed lines).
2704 Data from the upper 1,000 m of the Southern Ocean are assumed as the common starting point for each Me (arrow).
2705 To limit the models to productivity-associated processes, only data shallower than 200 m are included in the model for
2706 samples collected outside of the Southern Ocean. Samples with extreme Cd isotope compositions ($\delta^{114}\text{Cd} > +1\text{‰}$) are
2707 excluded from the model given that it is unclear if these are true oceanographic features (see Sec. 6.4.1.).

2708

2709 In practical terms, knowledge of $\Delta_{\text{P-R}}$, derived using the reactor framework, allows for the isotope
2710 compositions of Cd, Ba, Ni, and Cr to be interpreted in terms of reflecting the balance between supply and
2711 demand for that metal within the reactor (i.e., f). Though this does not confer direct information about the
2712 total quantity of nutrients consumed in the reactor, it offers a means to assess the spatial pattern of nutrient
2713 utilization in Earth's past. The spatial dependency is particularly important to consider, since the geometry

2714 of ocean circulation cannot be assumed constant over time. Moreover, if assuming that the flux of a Me to
2715 the seafloor is proportional to export productivity, the combination of metal fluxes with metal isotopes *can*
2716 offer insights into patterns of paleoproductivity by constraining export and fractional nutrient use within
2717 that system.

2718
2719 Combined C export-*f* approaches are largely unexplored in paleoceanographic studies, and we believe they
2720 offer the best opportunity for using bioactive trace metal isotope systems to constrain paleoproductivity.
2721 These approaches will prove most powerful when the constraints on C export and *f* are derived from the
2722 same Me system, since this minimizes the importance of other metal-cycling processes. However, multi-
2723 proxy approaches may also prove useful in differentiating between productivity- and non productivity-
2724 driven variations in metal cycling. For example, Cd, Ba, Ni, and Cr isotopes are all expected to exhibit
2725 coherent variations in their distributions if productivity or ocean circulation varied. In contrast, changes in
2726 mean ocean redox state, benthic fluxes, or terrestrial sources would render distinct changes in the
2727 distribution of each Me consistent with its sensitivity to that process. The cycling of other metals that are
2728 not directly sensitive to productivity—Fe, Zn, Cu, and Mo—could also be used to provide oceanographic
2729 context for paleoproductivity records, thus helping to build a more robust picture of marine biogeochemistry
2730 at key points in Earth's history.

2731

2732

2733 **12.3. Proxy readiness**

2734 We now assess the overall readiness of each bioactive trace metal isotope system to reconstruct
2735 productivity, summarized in Table 2. This exercise is analogous to the assessment of analytical techniques
2736 used in chemical oceanography described by Fassbender et al. (2017). Our assessment is similarly
2737 conducted in two dimensions. First, we identify five objectives toward the development of a reliable
2738 productivity proxy, ranging from development of the analytical capabilities necessary to measure that
2739 species, to constraining diagenetic effects, and ending with the goal of using that species to reliably
2740 reconstruct paleoproductivity itself. Second, we assess the level of development within each objective. Our
2741 reasoning behind the assignments is described above in Sec. 3–11.

2742

2743 Reliable application of a TEI as a proxy requires that five objectives be serially met (e.g., Hillaire-Marcel
2744 & Vernal, 2007; Table 2). In practical terms, however, the final stage (proxy application) is often realized
2745 before many of the supporting objectives; variations in elemental or isotopic ratios in the sedimentary record

2746 commonly provide the motivation for developing a more holistic understanding of that isotope system in
2747 the modern environment. *A common critique of this approach is that subsequent studies often invalidate*
2748 *earlier interpretations.* The five objectives that follow are common to the development of almost any proxy.
2749 First, it is essential to develop the analytical capability to measure the species of interest commensurate
2750 with the quantities typically encountered in the environment. In the case of trace element abundance
2751 proxies, the development and widespread adoption of ICP-MS instrumentation coupled to automated
2752 sample preparation systems has enabled low-blank, high-throughput, high-sensitivity analyses of multiple
2753 trace elements in both seawater (e.g., Wuttig et al., 2019) and sediments alike (e.g., Wefing et al., 2017). In
2754 contrast, the techniques required to measure many trace metal isotope systems have only been developed
2755 within the past decade—or are still in development—and generally remain labor intensive and time
2756 consuming. Second, it is important to map the broad vertical and spatial patterns of a TEI system in the
2757 modern ocean. The GEOTRACES program has provided a coordinated opportunity to study the basin-scale
2758 distributions of multiple TEIs. Third, the utility of a proxy is significantly increased if the driving processes
2759 are understood. These processes may be isolated through a number of approaches, including: lab-based
2760 analogue experimentation, numerical modeling, and high-resolution spatiotemporal environmental studies.
2761 Fourth, paleoceanographic proxies require sedimentary archives—a substrate from which to reconstruct the
2762 variable of interest. The latter necessitates knowledge of how a trace metal partitions between seawater and
2763 sediment, such as through a coretop study, ideally conducted across large environmental gradients. Since
2764 many marine sedimentary archives are biogenic in origin, additional experimentation isolating ‘vital
2765 effects’ may be necessary. Fifth, proxies are only as reliable as their archives are hardy. Diagenetic
2766 processes may alter primary environmental signatures, and recognizing these effects is imperative for
2767 reliably reconstructing past environmental conditions.

2768

2769 Here, we assess the level of development for each marine bioactive trace metal isotope system within each
2770 objective on a four point scale: unknown, developing, applied, and unlikely. The levels define a continuum
2771 from least to most understood, and are a useful shorthand for illustrating where additional work is most
2772 needed. Assignment of ‘unknown,’ implies that too little is presently known to reliably assess progress
2773 towards that objective; we cannot judge if these isotope systems may or may not ultimately be useful in
2774 reconstructing ocean productivity. ‘Developing’ objectives are those where there are pilot studies on that
2775 topic, but overall there are an insufficient number to define general rules for that system. If a trace metal
2776 isotope system is widely recognized to be useful towards some objective, it is given a score of ‘applied.’ If
2777 the evidence indicates that a trace metal isotope system is not suitable for reconstruction of
2778 paleoproductivity, a score of ‘unlikely’ is given. This does not rule out future developments, such as

2779 identification of environmental control variables or new sedimentary archives, only that current data (and
 2780 archives) do not support use of the isotope system towards this goal. Lastly, we recognize that there are
 2781 continual refinements to analytical protocols, environmental distributions, etc. and thus, at some level, all
 2782 five objectives could reasonably be described as ‘developing.’ Rather, our assignments are intended to give
 2783 a relative sense of understanding between different metal isotope systems toward the overarching goal of
 2784 reconstructing past ocean productivity.

2785

2786 **Table 2 | Proxy development assessment.** The progress toward five objectives is assessed for each bioactive metal
 2787 proxy system and assigned a development level ranging unknown to unlikely, corresponding to the least and most
 2788 certain assignments, respectively. Some trace metal isotope systems possess split designations (stripes). Definitions
 2789 of each development level are described in Sec. 12.3 and discussed in detail for each metal system in the corresponding
 2790 section.

Section	Proxy	1. Analytical protocols?	2. Distribution in environment?	3. Driving process isolated?	4. Sedimentary archives?	5. Effect of diagenesis?	Goal: Productivity reconstruction?
3	[Fe] $\delta^{56}\text{Fe}$	Applied	Applied	Developing	Developing	Developing	Unknown
4	[Zn] $\delta^{66}\text{Zn}$	Applied	Applied	Developing	Developing	Developing	Unknown
5	[Cu] $\delta^{65}\text{Cu}$	Applied	Applied	Developing	Developing	Developing	Unknown
6	[Cd] $\delta^{114}\text{Cd}$	Applied	Applied	Developing	Developing	Developing	Unknown
7	[Mo] $\delta^{98}\text{Mo}$	Applied	Applied	Applied	Developing	Unknown	Unknown
8	[Ba] $\delta^{138}\text{Ba}$	Applied	Applied	Applied	Developing	Unknown	Unknown
9	[Ni] $\delta^{60}\text{Ni}$	Applied	Developing	Developing	Developing	Developing	Unknown
10	[Cr] $\delta^{53}\text{Cr}$	Applied	Applied	Applied	Developing	Developing	Unknown
11	[Ag] $\delta^{109}\text{Ag}$	Developing	Unknown	Unknown	Unknown	Unknown	Unknown

Key

- Unknown
- Developing
- Applied
- Unlikely

2791

2792

2793

2794 12.4. Outlook

2795 Finally, we outline three general priorities for further study. First, a number of modern ambiguities require
 2796 addressing. Most notable is the apparent ‘missing’ source and/or sink terms for the whole ocean isotopic
 2797 budgets of several bioactive metals, including Cu, Cd, Ba, and Ni. Though it is possible that these missing
 2798 source and sink terms represent true non-steady state imbalances in the flux of these elements to and from
 2799 the ocean, we view it more likely that there are major fluxes that remain uncharacterized. The origin of
 2800 these imbalances is most pressing for those elements where the output flux associated with organic matter

2801 constitutes a minor sink (e.g., Zn, Ni), as the isotopic budget of these elements is most susceptible to
2802 decoupling from productivity. Second, the significance of ocean circulation in mediating basin-scale trace
2803 metal distributions implies that paleoceanographic interpretations made from a single site cannot be
2804 uniquely interpreted in terms of either changes in productivity or ocean circulation without additional
2805 constraints. Such constraints could take the form of independent circulation estimates—from numerical
2806 models or canonical circulation proxies measured in the same samples—or by measuring trace metal
2807 isotope distributions in spatially distributed sediment samples. Third, the lack of suitable archives with
2808 which to reconstruct surface water trace metal isotopic compositions afflicts almost every element reviewed
2809 here. Overcoming this limitation will require the most creativity; we suggest more studies testing the fidelity
2810 of non-traditional substrates (e.g., mixed foraminiferal assemblages, coccolith calcite, diatom opal),
2811 periodic reassessment of the feasibility of traditional substrates following analytical advancements (e.g.,
2812 improvements in ion transmission efficiency, large-scale [automated and/or crowd-sourced] picking of
2813 monospecific foraminiferal assemblages), and development and validation of selective extraction protocols
2814 that can be used to isolate phases of interest from complex matrices. Though attempting to overcome these
2815 limitations may be considered high risk, we believe that this risk is more than justified by the reward of
2816 developing a more complete understanding of Earth's biogeochemical history.

2817

2818

2819

2820

2821

2822

2823

2824

2825 **Postscripts**

2826

2827 **Acknowledgments**

2828 This contribution grew (and grew) out of a joint workshop between GEOTRACES and Past Global Changes
2829 (PAGES) held in Aix-en-Provence in December 2018. The workshop was funded by the U.S. National
2830 Science Foundation (NSF) through the GEOTRACES program, the international PAGES project, which in
2831 turn received support from the Swiss Academy of Sciences and NSF, and the French program Les
2832 Enveloppes Fluides et l'Environnement. The authors extend tremendous thanks to the GEOTRACES–
2833 PAGES workshop organizers, particularly Bob Anderson, Catherine Jeandel, Laurence Vidal, and Kazuyo
2834 Tachikawa. This synthesis benefited from the insights of the Associate Editor (Noah Planavsky) and from
2835 two detailed and constructive reviews by Seth John and an anonymous reviewer. T.J.H. acknowledges
2836 support from NSF; S.H.L. from the U.K. Natural Environment Research Council (NE/P018181/1); T.M.C.
2837 from the University of South Florida; and, J.R.F. from the Max Planck Society, the Tuttle Fund of the
2838 Department of Geosciences of Princeton University, the Grand Challenges Program of the Princeton
2839 Environmental Institute, and the Andlinger Center for Energy and the Environment of Princeton University.
2840 Most importantly, we acknowledge the hundreds of scientists who have generated GEOTRACES-
2841 compliant TEI data that made this synthesis possible.

2842

2843 **Data sources**

2844 The majority of the dissolved data were sourced from the GEOTRACES Intermediate Data Products in
2845 2014 (Mawji et al., 2015) and 2017 (Schlitzer et al., 2018). Regardless, citations to the primary data sources
2846 are given in the caption to each figure. Data sources for Fig. 1 and and Table 1 are given below.

2847 *Figure 1*

2848 Iron: Conway & John, 2014a (Atlantic); Conway & John, 2015a (Pacific); Abadie et al., 2017 (Southern).
2849 Zinc: Conway & John, 2014b (Atlantic); Conway & John, 2015a (Pacific); Wang et al., 2019a (Southern).
2850 Copper: Little et al., 2018 (Atlantic); Takano et al., 2017 (Pacific); Boye et al., 2012 (Southern). Cadmium:
2851 Conway and John, 2015b (Atlantic); Conway & John, 2015a (Pacific); Abouchami et al., 2014 (Southern).
2852 Molybdenum: Nakagawa et al., 2012 (all basins). Barium: Bates et al., 2017 (Atlantic); Geyman et al., 2019
2853 (Pacific); Hsieh & Henderson, 2017 (Southern). Nickel: Archer et al., 2020 (Atlantic); Takano et al., 2017
2854 (Pacific); Wang et al., 2019a (Southern). Chromium: Goring-Harford et al., 2018 (Atlantic); Moos & Boyle,
2855 2019 (Pacific); Rickli et al., 2019 (Southern). Silver: Fischer et al., 2018 (Pacific); Boye et al., 2012
2856 (Southern).

2857 *Table 1*

2858 ^aSchlitzer (2017); ^bMorris et al. (1975); ^cSection 10 and references therein; ^dGallon and Flegal, 2014;
2859 ^eDauphas et al. (2017); ^fMoynier et al. (2017) and references therein; ^gAbouchami et al. (2013); ^hNägler et
2860 al. (2014); ⁱHorner et al. (2015a); ^jElliott & Steele (2017); ^kEllis et al. (2002); ^lWoodland et al. (2005);
2861 ^mGong et al. (2017); ⁿSchmitt et al. (2009a); ^oWillbold & Elliott (2017); ^pNan et al., 2018; ^qCameron et al.
2862 (2009); ^rShoenberg et al. (2018); ^sUSGS reference material SCO-1 (Cody Shale) is used given paucity of
2863 representative data; Schönbächler et al. (2007); ^tSection 3 and references therein; ^uSection 4 and references
2864 therein; ^vSection 5 and references therein; ^wSection 6 and references therein; ^xData from Nakagawa et al.
2865 (2012) renormalized to NIST SRM 3134 + 0.25 ‰ based on Goldberg et al. (2013); ^ySection 8 and
2866 references therein; ^zYang et al. (2020); ^{aa}Hayes et al. (2018) and references therein; ^{ab}Miller et al. (2011);
2867 ^{ac}Dickens et al. (2003); ^{ad}Cameron & Vance (2014) and references therein; ^{ae}Wei et al. (2018); ^{af}Broecker
2868 & Peng (1982).

2869

2870 **Competing interests**

2871 The authors declare that they are not aware of any financial conflicts of interest, real or perceived.

2872

2873 **GEOTRACES–PAGES Biological Productivity Working Group Members**

2874 C. Bolton (CEREGE, Univ. Aix-Marseille, CNRS, IRD, Collège de France, INRAE, Aix-en-Provence,
2875 France); E. Calvo (Institut de Ciències del Mar, CSIC, Barcelona, Spain); D. Cardinal (LOCEAN
2876 (UMR7159), Sorbonne Université, IRD, CNRS, MNHN, Paris, France); T. de Garidel-Thoron (CEREGE,
2877 Univ. Aix-Marseille, CNRS, IRD, Collège de France, INRAE Aix-en-Provence, France); S. Fietz
2878 (Department of Earth Sciences, Stellenbosch University, Stellenbosch South Africa); K. R. Hendry (School
2879 of Earth Sciences, University of Bristol, Bristol, UK); F. Marcantonio (Department of Geology and
2880 Geophysics, Texas A&M University), P. A. Rafter (Department of Earth System Science, University of
2881 California, Irvine, CA, USA); H. Ren (Department of Geosciences, National Taiwan University, Taipei,
2882 Taiwan); C. J. Somes (GEOMAR Helmholtz Centre for Ocean Research Kiel, 24105 Kiel, Germany); J. N.
2883 Sutton (Univ Brest, CNRS, IRD, Ifremer, Institut Universitaire Européen de la Mer, LEMAR, Plouzané,
2884 France); A. Torfstein (Institute of Earth Sciences, Hebrew University, Jerusalem, & InterUniversity
2885 Institute for Marine Sciences, Eilat, Israel); G. Winckler (Lamont-Doherty Earth Observatory of Columbia
2886 University, Palisades, NY, USA).

2887

2888

2889 **References**

- 2890 Abadie, C., Lacan, F., Radic, A., Pradoux, C., & Poitrasson, F. (2017). Iron isotopes reveal distinct
 2891 dissolved iron sources and pathways in the intermediate versus deep Southern Ocean. *Proc. Natl.*
 2892 *Acad. Sci.*, **114**, 858-863.
- 2893 Abouchami, W., Galer, S. J. G., de Baar, H. J. W., Alderkamp, A. C., Middag, R., Laan, P., Feldmann, H.,
 2894 & Andreae, M. O. (2011). Modulation of the Southern Ocean cadmium isotope signature by ocean
 2895 circulation and primary productivity. *Earth Planet. Sci. Lett.*, **305**(1-2), 83-91.
- 2896 Abouchami, W., Galer, S. J. G., Horner, T. J., Rehkämper, M., Wombacher, F., Xue, Z., Lambelet, M.,
 2897 Gault-Ringold, M., Stirling, C. H., Schönbacher, M., Shiel, A. E., Weis, D., & Holdship, P. F.
 2898 (2013). A common reference material for cadmium isotope studies—NIST SRM 3108.
 2899 *Geostandards and Geoanalytical Research*, **37**(1), 5-17.
- 2900 Abouchami, W., Galer, S. J. G., de Baar, H. J. W., Middag, R., Vance, D., Zhao, Y., Klunder, M., Mezger,
 2901 K., Feldmann, H., & Andreae, M. O. (2014). Biogeochemical cycling of cadmium isotopes in the
 2902 Southern Ocean along the Zero Meridian. *Geochim. Cosmochim. Acta*, **127**, 348-367.
- 2903 Achterberg, E. P. & van den Berg, C. M. G. (1997). Chemical speciation of chromium and nickel in the
 2904 western Mediterranean. *Deep-Sea Res. II*, **44**, 693–720, doi: 10.1016/S0967-0645(96)00086-0.
- 2905 Adkins, J. F., Cheng, H., Boyle, E. A., Druffel, E. R., & Edwards, R. L. (1998). Deep-sea coral evidence
 2906 for rapid change in ventilation of the deep North Atlantic 15,400 years ago. *Science*, **280**(5364),
 2907 725-728.
- 2908 Akerman, A., Poitrasson, F., Oliva, P., Audry, S., Prunier, J., & Braun, J. J. (2014). The isotopic fingerprint
 2909 of Fe cycling in an equatorial soil-plant-water system: The Nsimi watershed, South Cameroon.
 2910 *Chem. Geol.*, **385**, 104–116.
- 2911 Albarède, F. (2004). The stable isotope geochemistry of copper and zinc. *Reviews in Mineralogy and*
 2912 *Geochemistry*, **55**(1), 409-427.
- 2913 Albut, G., Babechuk, M. G., Kleinhanns, I. C., Bengler, M., Beukes, N. J., Steinhilber, B., Smith, A. J. B.,
 2914 Kruger, S. J., & Schoenberg, R. (2018). Modern rather than Mesoarchaen oxidative weathering
 2915 responsible for the heavy stable Cr isotopic signatures of the 2.95 Ga old Ijzermijn iron formation
 2916 (South Africa). *Geochem. Cosmochim. Acta*, **228**, 157-189, doi:10.1016/j.gca.2018.02.034.
- 2917 Algeo, T. J. (2004). Can marine anoxic events draw down the trace element inventory of seawater? *Geology*,
 2918 **32** (12), 1057-1060, doi:10.1130/G20896.1.
- 2919 Algeo, T. J., & Lyons, T. W. (2006). Mo-total organic carbon covariation in modern anoxic marine
 2920 environments: Implications for analysis of paleoredox and paleohydrographic conditions:
 2921 *Paleoceanography*, **21**, doi:10.1029/2004PA001112.
- 2922 Algeo T. J., & Maynard J. B. (2008). Trace-metal covariation as a guide to water-mass conditions in ancient
 2923 anoxic marine environments. *Geosphere* **4**, 872.
- 2924 Algeo, T. J., & Tribovillard, N. (2009). Environmental analysis of paleoceanographic systems based on
 2925 molybdenum-uranium covariation: *Chem. Geol.*, **268**, 211–225,
 2926 doi:10.1016/j.chemgeo.2009.09.001.
- 2927 Alldredge, A. L., & Silver, M. W. (1988). Characteristics, dynamics and significance of marine snow. *Prog.*
 2928 *Oceanogr.*, **20**(1), 41-82.
- 2929 Anbar, A. D., & Knoll, A. H. (2002). Proterozoic Ocean Chemistry and Evolution: A Bioinorganic Bridge?
 2930 *Science*, **297**, 1137–1142, doi:10.1126/science.1069651.

- 2931 Anbar, A. D. (2004). Molybdenum stable isotopes: observations, interpretations and directions. *Rev. Min.*
2932 *Geochem.*, **55**(1), 429-454.
- 2933 Anbar, A. D., Jarzecki, A. A., & Spiro, T. G. (2005) Theoretical investigation of iron isotope fractionation
2934 between $\text{Fe}(\text{H}_2\text{O})_6^{3+}$ and $\text{Fe}(\text{H}_2\text{O})_6^{2+}$: Implications for iron stable isotope geochemistry. *Geochim.*
2935 *Cosmochim. Acta.* **69**, 825–837. <https://doi.org/10.1016/j.gca.2004.06.012>.
- 2936 Andersen, M. B., Vance, D., Archer, C., Anderson, R. F., Ellwood, M. J., & Allen, C. S. (2011). The Zn
2937 abundance and isotopic composition of diatom frustules, a proxy for Zn availability in ocean
2938 surface seawater. *Earth Planet. Sci. Lett.*, **301**, 137–145.
2939 <http://dx.doi.org/10.1016/j.epsl.2010.10.032>.
- 2940 Anderson, M. A., Morel, F. M. M., & Guillard, R. R. L. (1978). Growth limitation of a coastal diatom by
2941 low zinc ion activity. *Nature*, **276**, 70-71.
- 2942 Annett, A. L., Lapi, S., Ruth, T. J., & Maldonado, M. T. (2008). The effects of Cu and Fe availability on
2943 the growth and Cu:C ratios of marine diatoms. *Limnol. Oceanogr.* **53**, 2451–2461.
- 2944 Aplin, A. C., & Cronan, D. S. (1985). Ferromanganese oxide deposits from the central Pacific Ocean, I.
2945 Encrustations from the Line Islands Archipelago. *Geochim. Cosmochim. Acta*, **49**(2), 427-436.
- 2946 Archer, C., Andersen, M. B., Cloquet, C., Conway, T. M., Dong, S., Ellwood, M., Moore, R., Nelson, J.,
2947 Rehkämper, M., Rouxel, O., Samanta, M., Shin, K.-C., Sohrin, Y., Takano, S., & Wasylenki, L.
2948 (2017). Inter-calibration of a proposed new primary reference standard AA-ETH Zn for zinc
2949 isotopic analysis. *Journal of Analytical Atomic Spectrometry*, **32**(2), 415-419.
- 2950 Archer, C., Vance, D., Milne, A., & Lohan, M. C. (2020). The oceanic biogeochemistry of nickel and its
2951 isotopes: New data from the South Atlantic and the Southern Ocean biogeochemical divide. *Earth*
2952 *Planet. Sci. Lett.*, **535**, 116118.
- 2953 Arnold, G. L., Anbar, A. D., Barling, J., & Lyons, T. W. (2004). Molybdenum isotope evidence for
2954 widespread anoxia in mid-Proterozoic oceans. *Science*, **304**(5667), 87-90.
- 2955 Aristilde, L., & Xu, Y. (2012). Weak organic ligands enhance Zinc uptake in Marine phytoplankton.
2956 *Environ. Sci. Technol.*, **46**, 5438-5445.
- 2957 Arrhenius, G. (1963). *Pelagic sediments*. Scripps Institution of Oceanography, University of California.
- 2958 Atkins, A. L., Shaw, S., & Peacock, C. L. (2016). Release of Ni from birnessite during transformation of
2959 birnessite to todorokite: Implications for Ni cycling in marine sediments. *Geochim. Cosmochim.*
2960 *Acta*, **189**, 158-183.
- 2961 Baars, O., & Croot, P. L. (2011). The speciation of dissolved zinc in the Atlantic sector of the Southern
2962 Ocean. *Deep. Res. Part II Top. Stud. Oceanogr.*, **58**, 2707–2719.
2963 <http://dx.doi.org/10.1016/j.dsr2.2010.10.041>.
- 2964 Baars, O., Abouchami, W., Galer, S. J., Boye, M., & Croot, P. L. (2014). Dissolved cadmium in the
2965 Southern Ocean: distribution, speciation, and relation to phosphate. *Limnol. Oceanogr.*, **59**(2), 385-
2966 399.
- 2967 Bacon, M.P. and Anderson, R.F. (1982). Distribution of thorium isotopes between dissolved and particulate
2968 forms in the deep sea. *J. Geophys. Res. Oceans*, **87**(C3), 2045-2056.
- 2969 Badaut, D., & Risacher, F. (1983). Authigenic smectite on diatom frustules in Bolivian saline lakes.
2970 *Geochim. Cosmochim. Acta*, **47**(3), 363-375.
- 2971 Barling, J., Arnold, G., & Anbar, A. D., (2001). Natural mass-dependent variations in the isotopic
2972 composition of molybdenum. *Earth Planet. Sci. Lett.*, **193**, 447–457, doi:10.1016/S0012-
2973 821X(01)00514-3.

- 2974 Barling, J., & Anbar, A. D. (2004). Molybdenum isotope fractionation during adsorption by manganese
2975 oxides. *Earth Planet. Sci. Lett.*, **217**, 315-329, doi:10.1016/S0012-821X(03)00608-3.
- 2976 Bates, S. L., Hendry, K. R., Pryer, H. V., Kinsley, C. W., Pyle, K. M., Woodward, E. M. S., & Horner, T.
2977 J. (2017). Barium isotopes reveal role of ocean circulation on barium cycling in the Atlantic.
2978 *Geochim. Cosmochim. Acta*, **204**, 286-299.
- 2979 Bauer, K. W., Gueguen, B., Cole, D. B., Francois, R., Kallmeyer, J., Planavsky, N., & Crowe, S. A. (2018).
2980 Chromium isotope fractionation in ferruginous sediments. *Geochim. Cosmochim. Acta*, **223**, 198-
2981 215, doi: 10.1016/j.gca.2017.10.034.
- 2982 Bauer, K. W., Cole, D. B., Asael, D., Francois, R., Calvert, S. E., Poulton, S. W., Planavsky, N., & Crowe,
2983 S. A. Chromium isotopes in marine hydrothermal sediments. *Chem. Geol.*, **529**, 119286, doi:
2984 10.1016/j.chemgeo.2019.119286.
- 2985 Beard, B.L., Johnson, C.M., Cox, L., Sun, H., Neelson, K.H., & Aguilar, C. (1999). Iron Isotope
2986 Biosignatures. *Science* **285**, 1889-1892.
- 2987 Beard, B. L., Johnson, C. M., Skulan, J. L., Neelson, K. H., Cox, L., & Sun, H. (2003). Application of Fe
2988 isotopes to tracing the geochemical and biological cycling of Fe. *Chem. Geol.*, **195**(1-4), 87-117.
- 2989 Bennett, S. A., Rouxel, O., Schmidt, K., Garbe-Schönberg, D., Statham, P. J., & German, C. R. (2009).
2990 Iron isotope fractionation in a buoyant hydrothermal plume, 5 S Mid-Atlantic Ridge. *Geochim.*
2991 *Cosmochim. Acta*, **73**(19), 5619-5634.
- 2992 Bergquist, B. A., & Boyle, E. A. (2006). Iron isotopes in the Amazon River system: Weathering and
2993 transport signatures. *Earth Planet. Sci. Lett.*, **248**(1-2), 54-68.
2994 <https://doi.org/10.1016/j.epsl.2006.05.004>.
- 2995 Berger, W. H., Smetacek, V., & Wefer, G. (1989). Ocean productivity and paleoproductivity - an overview.
2996 In W. H. Berger, V. S. Smetacek, G. Wefer (Eds) *Productivity of the Oceans present and past:*
2997 *Report of the Dahlem Workshop on Productivity of the Ocean, Berlin, 1988*, Life Sciences Research
2998 Reports 44, Wiley & Sons, Chichester, pp. 1-34.
- 2999 Bermin, J., Vance, D., Archer, C., & Statham, P. J. (2006). The determination of the isotopic composition
3000 of Cu and Zn in seawater. *Chem. Geol.*, **226**, 280-297.
- 3001 Berner, R. A., Petsch, S. T., Lake, J. A., Beerling, D. J., Popp, B. N., Lane, R. S., Laws, E. A., Westley, M.
3002 B., Cassar, N., Woodward, F. I. & Quick, W. P. (2000). Isotope fractionation and atmospheric
3003 oxygen: implications for Phanerozoic O₂ evolution. *Science*, **287**(5458), 1630-1633.
- 3004 Bernstein, R. E., & Byrne, R. H. (2004). Acantharians and marine barite. *Mar. Chem.*, **86** (1-2), 45-50.
- 3005 Bertine, K. K., & Turekian, K. K. (1973). Molybdenum in marine deposits. *Geochim. Cosmochim. Acta*,
3006 **37** (6), 1415-1434.
- 3007 Bianchi, D., Weber, T. S., Kiko, R., & Deutsch, C. (2018). Global niche of marine anaerobic metabolisms
3008 expanded by particle microenvironments. *Nat. Geosci.*, **11**, 1-6.
- 3009 Bishop, J. K. (1988). The barite-opal-organic carbon association in oceanic particulate matter. *Nature*, **332**
3010 (6162), 341.
- 3011 Böning, P., Brumsack, H.-J., Böttcher, M.E., Schnetger, B., Kriete, C., Kallmeyer, J., & Borchers, S.L.
3012 (2004). Geochemistry of Peruvian near-surface sediments. *Geochim. Cosmochim. Acta*, **68**, 4429-
3013 4451.
- 3014 Böning, P., Cuypers, S., Grunwald, M., Schnetger, B., & Brumsack, H.-J. (2005). Geochemical
3015 characteristics of Chilean upwelling sediments at ~36°S. *Mar. Geol.*, **220**, 1-21.

- 3016 Bönig, P., Brumsack, H.-J., Schnetger, B., & Grunwald, M. (2009). Trace element signatures of Chilean
3017 upwelling sediments at ~36°S. *Mar. Geol.*, **259**, 112-121.
- 3018 Bönig, P., Shaw, T., Pahnke, K., & Brumsack, H.-J. (2015). Nickel as an indicator of fresh organic matter
3019 in upwelling sediments. *Geochim. Cosmochim. Acta*, **162**, 99-108, doi:10.1016/j.gca.2015.04.027.
- 3020 Bonnard, P., James, R. H., Parkinson, I. J., Connelly, D. P., & Fairchild, I. J. (2013). The chromium isotopic
3021 composition of seawater and marine sediments. *Earth Planet. Sci. Lett.*, **382**, 10-20. doi:
3022 10.1016/j.epsl.2013.09.001.
- 3023 Borchers, S.L., Schnetger, B., Bönig, P., & Brumsack, H.-J. (2005). Geochemical signatures of the
3024 Namibian diatom belt: Perennial upwelling and intermittent anoxia. *Geochemistry, Geophysics,*
3025 *Geosystems*, **6**(4), Q06006, doi:10.1029/2004GC000886.
- 3026 Boyd, P. W., Claustre, H., Levy, M., Siegel, D. A., & Weber, T. (2019). Multi-faceted particle pumps drive
3027 carbon sequestration in the ocean. *Nature*, **568**(7752), 327-335.
- 3028 Boyd, P. W., Jickells, T., Law, C. S., Blain, S., Boyle, E. A., Buesseler, K. O., Coale, K. H., Cullen, J. J.,
3029 de Baar, H. J. W., Follows, M., Harvey, M., Lancelot, C., Levasseur, M., Owens, N. P. J., Pollard,
3030 R., Rivkin, R. B., Sarimento, J., Schoemann, V., Smetacek, V., Takeda, S., Tsuda, A., Turner, S.,
3031 & Watson, A. J. (2007). Mesoscale iron enrichment experiments 1993-2005: synthesis and future
3032 directions. *Science*, **315**(5812), 612-617.
- 3033 Boyd, P. W., & Ellwood, M. J. (2010). The biogeochemical cycle of iron in the ocean. *Nat. Geosci.* **3**(10),
3034 675-682.
- 3035 Boyd, P. W., Ellwood, M. J., Tagliabue, A., & Twining, B. S. (2017). Biotic and abiotic retention, recycling
3036 and remineralization of metals in the ocean. *Nat. Geosci.*, **10**(3), 167-173.
- 3037 Boye, M., Wake, D. B., Lopez Gracia, P., Bown, J., Baker, A. R., & Acherberg, E. P. (2012). Distributions
3038 of dissolved trace metals (Cd, Cu, Mn, Pb, Ag) in the southeastern Atlantic and the Southern Ocean.
3039 *Biogeosciences*, **9**, 3231-3246, doi:10.5194/bg-9-3231-2012.
- 3040 Boyle, E. A. (1981). Cadmium, zinc, copper, and barium in foraminifera tests. *Earth Planet. Sci. Lett.*,
3041 **53**(1), 11-35.
- 3042 Boyle, E. A. (1988a). Vertical oceanic nutrient fractionation and glacial/interglacial CO₂ cycles. *Nature*,
3043 **331**(6151), 55-56.
- 3044 Boyle, E. A. (1988b). Cadmium: Chemical tracer of deepwater paleoceanography. *Paleoceanography*, **3**(4),
3045 471-489.
- 3046 Boyle, E. A. (1992). Cadmium and $\delta^{13}\text{C}$ paleochemical ocean distributions during the stage 2 glacial
3047 maximum. *Annual Review of Earth and Planetary Sciences*, **20**(1), 245-287.
- 3048 Boyle, E. A., & Keigwin, L. D. (1985). Comparison of Atlantic and Pacific paleochemical records for the
3049 last 215,000 years: Changes in deep ocean circulation and chemical inventories. *Earth Planet. Sci.*
3050 *Lett.*, **76**(1-2), 135-150.
- 3051 Boyle, E. A., Sclater, F., & Edmond, J. M. (1976). On the marine geochemistry of cadmium. *Nature*,
3052 **263**(5572), 42.
- 3053 Boyle, E. A., Sclater, F. R., & Edmond, J. M. (1977). The distribution of dissolved copper in the Pacific.
3054 *Earth Planet. Sci. Lett.*, **37**, 38-54.
- 3055 Brand, L. E., Sunda, W. G., & Guillard, R. R. L. (1983). Limitation of marine phytoplankton by zinc,
3056 manganese, and iron. *Limnol. Oceanogr.*, **28**, 1182-1198.
- 3057 Brand L. E., Sunda, W. G., & Guillard, R. R. L. (1986). Reduction of marine phytoplankton reproduction
3058 rates by copper and cadmium. *J. Exp. Mar. Bio. Ecol.* **96**, 225-250.

- 3059 Bridgestock, L., Rehkämper, M., van de Flierdt, T., Murphy, K., Khondoker, R., Baker, A. R., Chance, R.,
3060 Strekopytov, S., Humphreys-Williams, E., Achterberg, E. P. (2017). The Cd isotope composition
3061 of atmospheric aerosols from the Tropical Atlantic Ocean. *Geophys. Res. Lett.* **44**(6), 2932-2940.
3062 <https://doi.org/10.1002/2017GL072748>.
- 3063 Bridgestock, L., Hsieh, Y. T., Porcelli, D., Homoky, W. B., Bryan, A., & Henderson, G. M. (2018). Controls
3064 on the barium isotope compositions of marine sediments. *Earth Planet. Sci. Lett.*, **481**, 101-110.
- 3065 Bridgestock, L., Hsieh, Y. T., Porcelli, D., & Henderson, G. M. (2019). Increased export production during
3066 recovery from the Paleocene–Eocene thermal maximum constrained by sedimentary Ba isotopes.
3067 *Earth Planet. Sci. Lett.*, **510**, 53-63.
- 3068 Broecker, W.S. (1982). Glacial to interglacial changes in ocean chemistry. *Prog. Oceanogr.* **11**, 151-197.
- 3069 Broecker, W.S., & Peng, T. H. (1982). *Tracers in the Sea*. Eldigo Press, Palisades, NY.
- 3070 Brucker, R. L. P., McManus, J., Severmann, S., & Berelson, W. M. (2009). Molybdenum behavior during
3071 early diagenesis: Insights from Mo isotopes. *Geochemistry, Geophysics, Geosystems*, **10**,
3072 doi:10.1029/2008GC002180.
- 3073 Bruggmann, S., Scholz, F., Kläbe, R. M., Canfield, D. E., & Frei, R. (2019). Chromium isotope cycling in
3074 the water column and sediments of the Peruvian continental margin. *Geochim. Cosmochim. Acta*,
3075 **257**, 224–242, doi: 10.1016/j.gca.2019.05.001.
- 3076 Bruland, K. W. (1980). Oceanographic distributions of cadmium, zinc, nickel, and copper in the North
3077 Pacific. *Earth Planet. Sci. Lett.*, **47**(2), 176-198.
- 3078 Bruland, K. W. (1989). Complexation of zinc by natural organic ligands in the central North Pacific. *Limnol.*
3079 *Oceanogr.*, **34**, 269–285.
- 3080 Bruland, K. W. (1992). Complexation of cadmium by natural organic ligands in the central North Pacific.
3081 *Limnol. Oceanogr.*, **37**(5), 1008-1017.
- 3082 Bruland, K. W., & Lohan, M. C. (2003). Controls of Trace Metals in Seawater. In *Treatise on Geochemistry*,
3083 Elsevier, 23-47.
- 3084 Bruland, K. W., Knauer, G. A., & Martin, J. H. (1978). Zinc in north-east Pacific water. *Nature*, **271**(5647),
3085 741-743.
- 3086 Brumsack, H. J. (2006). The trace metal content of recent organic carbon-rich sediments: implications for
3087 Cretaceous black shale formation. *Palaeogeography, Palaeoclimatology, Palaeoecology*, **232**(2-
3088 4), 344-361.
- 3089 Bryan, A. L., Dong, S., Wilkes, E. B., & Wasylenki, L. E. (2015). Zinc isotope fractionation during
3090 adsorption onto Mn oxyhydroxide at low and high ionic strength. *Geochim. Cosmochim. Acta*, **157**,
3091 182-197.
- 3092 Bryan, A. L., Dickson, A. J., Dowdall, F., Homoky, W. B., Porcelli, D., & Henderson, G. M. (2021).
3093 Controls on the cadmium isotope composition of modern marine sediments. *Earth Planet. Sci.*
3094 *Lett.*, **565**, 116946, doi:10.1016/j.epsl.2021.116946.
- 3095 Cadiou, J. L., Pichat, S., Bondanese, V. P., Soulard, A., Fujii, T., Albarède, F., & Oger, P. (2017). Copper
3096 transporters are responsible for copper isotopic fractionation in eukaryotic cells. *Sci. Rep.*, **7**(1), 1-
3097 10.
- 3098 Cameron, V., Vance, D., Archer, C., & House, C. H. (2009). A biomarker based on the stable isotopes of
3099 nickel. *Proceedings of the National Academy of Sciences*, **106**(27), 10944-10948.
- 3100 Campbell, J. A., & Yeats, P. A. (1981). Dissolved chromium in the northwest Atlantic Ocean. *Earth. Planet.*
3101 *Sci. Lett.*, **53**, 427-433.

- 3102 Campbell, J. A., & Yeats, P. A. (1984). Dissolved chromium in the St. Lawrence estuary. *Estuar.*
3103 *Coast. Shelf Sci.*, **19**, 513-522.
- 3104 Carlson, C. A., Hansell, D. A., Nelson, N. B., Siegel, D. A., Smethie, W. M., Khatiwala, S., Meyers, M.
3105 M., & Halewood, E. (2010). Dissolved organic carbon export and subsequent remineralization in
3106 the mesopelagic and bathypelagic realms of the North Atlantic basin. *Deep Sea Res. Pt. II*, **57**(16),
3107 1433-1445.
- 3108 Cao, Z., Siebert, C., Hathorne, E. C., Dai, M., & Frank, M. (2020a). Corrigendum to "Constraining the
3109 oceanic barium cycle with stable barium isotopes" [*Earth Planet. Sci. Lett.*, **434** (2016) 1-9], doi:
3110 10.1016/j.epsl.2019.116003.
- 3111 Cao, Z., Li, Y., Rao, X., Yu, Y., Hathorne, E. C., Siebert, C., Dai, M., & Frank, M. (2020b). Constraining
3112 barium isotope fractionation in the upper water column of the South China Sea. *Geochim.*
3113 *Cosmochim. Acta*, **288**, 120-137.
- 3114 Cartapanis, O., Bianchi, D., Jaccard, S. L., & Galbraith, E. D. (2016). Global pulses of organic carbon burial
3115 in deep-sea sediments during glacial maxima. *Nat. Commun.*, **7**, 10796,
3116 doi:10.1038/ncomms10796.
- 3117 Carter, S. C., Paytan, A., & Griffith, E. M. (2020). Toward an Improved Understanding of the Marine
3118 Barium Cycle and the Application of Marine Barite as a Paleoproductivity Proxy. *Minerals*, **10**(5),
3119 421.
- 3120 Chan, L. H., Edmond, J. M., Stallard, R. F., Broecker, W. S., Chung, Y. C., Weiss, R. F., & Ku, T. L.
3121 (1976). Radium and barium at GEOSECS stations in the Atlantic and Pacific. *Earth Planet. Sci.*
3122 *Lett.*, **32**(2), 258-267.
- 3123 Chan, L. H., Drummond, D., Edmond, J. M., & Grant, B. (1977). On the barium data from the Atlantic
3124 GEOSECS expedition. *Deep Sea Res.*, **24**(7), 613-649.
- 3125 Chang, A. S., Pedersen, T. F., & Hendy, I. L. (2014). Effects of productivity, glaciation, and ventilation on
3126 late Quaternary sedimentary redox and trace element accumulation on the Vancouver Island
3127 margin, western Canada. *Paleoceanogr.*, **29**(7), 730-746.
- 3128 Chappaz, A., Lyons, T. W., Gregory, D. D., Reinhard, C. T., Gill, B. C., Li, C., & Large, R. R. (2014).
3129 Does pyrite act as an important host for molybdenum in modern and ancient euxinic sediments?
3130 *Geochim. Cosmochim. Acta*, **126**, 112–122, doi:10.1016/j.gca.2013.10.028.
- 3131 Chappell, P. D., Vedmati, J., Selph, K. E., Cyr, H. A., Jenkins, B. D., Landry, M. R., & Moffett, J. W.
3132 (2016). Preferential depletion of zinc within Costra Rica upwelling dome creates conditions for
3133 zinc co-limitation of primary production. *J. Plankton Res.*, **38**, 244-255,
3134 doi:10.1093/plankt/fbw018.
- 3135 Charette, M. A., et al. (2020). The Transpolar Drift as a Source of Riverine and Shelf-Derived Trace
3136 Elements to the Central Arctic Ocean. *J. Geophys. Res. Oceans*, **125**(5), e2019JC015920.
3137 <https://doi.org/10.1029/2019JC015920>.
- 3138 Chen, J.-B., Busigny, V., Gaillardet, J., Louvat, P., & Wang, Y.-N. (2014). Iron isotopes in the Seine River
3139 (France): Natural vs anthropogenic sources. *Geochim. Cosmochim. Acta*, **128**, 128-143.
- 3140 Chen, L., Little, S. H., Kreissig, K., Severmann, S., & McManus, J. (2021). Isotopically Light Cd
3141 in Sediments Underlying Oxygen Deficient Zones. *Front. Earth Sci.*, **9**, 97.
- 3142 Chen, T., Wenqiang, L., Gao, B., Liu, R., Li, G., Zhao, L., and Ji, J. (2020). Reactive iron isotope signatures
3143 of the East Asian dust particles: Implications for iron cycling the deep North Pacific. *Chem. Geol.*
3144 **531**, 119342. <https://doi.org/10.1016/j.chemgeo.2019.119342>.

- 3145 Cheng, H., Adkins, J., Edwards, R. L., & Boyle, E. A. (2000). U-Th dating of deep-sea corals. *Geochim.*
3146 *Cosmochim. Acta*, **64**(14), 2401-2416.
- 3147 Chever, F., Bucciarelli, E., Sarthou, G., Speich, S., Arhan, M., Penven, P., & Tagliabue, A. (2010). Physical
3148 speciation of iron in the Atlantic sector of the Southern Ocean along a transect from the subtropical
3149 domain to the Weddell Sea Gyre. *J. Geophys. Res. Oceans*, **115**, C10059,
3150 doi:10.1029/2009JC005880.
- 3151 Chever, F., Rouxel, O. J., Croot, P. L., Ponzevera, E., Wuttig, K., & Auro, M. (2015). Total dissolvable and
3152 dissolved iron isotopes in the water column of the Peru upwelling regime. *Geochim. Cosmochim.*
3153 *Acta*, **162**, 66-82. <https://doi.org/10.1016/j.gca.2015.04.031>.
- 3154 Chow, T. J., & Goldberg, E. D. (1960). On the marine geochemistry of barium. *Geochim. Cosmochim.*
3155 *Acta*, **20**(3-4), 192-198.
- 3156 Chung, Y. (1980). Radium-barium-silica correlations and a two-dimensional radium model for the world
3157 ocean. *Earth Planet. Sci. Lett.*, **49**(2), 309-318.
- 3158 Chu, N., Johnson, C., Beard, B., German, C., Nesbitt, R., Frank, M., Bohn, M., Kubik, P., Usui, A., &
3159 Graham, I. (2006). Evidence for hydrothermal venting in Fe isotope compositions of the deep
3160 Pacific Ocean through time. *Earth Planet. Sci. Lett.*, **245**, 202-217.
- 3161 Ciscato E. R., Bontognali T. R. R., & Vance, D. (2018). Nickel and its isotopes in organic-rich sediments:
3162 implications for oceanic budgets and a potential record of ancient seawater. *Earth Planet. Sci. Lett.*
3163 **494**, 239–250. <https://doi.org/10.1016/j.epsl.2018.04.061>.
- 3164 Ciscato, E. R., Bontognali, T. R., Poulton, S. W., & Vance, D. (2019). Copper and its Isotopes in Organic-
3165 Rich Sediments: From the Modern Peru Margin to Archean Shales. *Geosciences*, **9**(8), 325.
- 3166 Clarkson, M., Müsing, K., Andersen, M. B., & Vance, D. (2018). Reducing the role of contaminant phases
3167 for metal isotopes in carbonates. In *Goldschmidt Abstracts* p. 441.
- 3168 Coale, K. H. (1991). Effects of iron, manganese, copper and zinc enrichments on productivity and biomass
3169 in the subarctic Pacific. *Limnol. Oceanogr.*, **36**, 1851–1864.
- 3170 Coale K. H., & Bruland K. W. (1988). Copper complexation in the Northeast Pacific. *Limnol. Oceanogr.*
3171 **33**, 1084–1101.
- 3172 Coale K. H., & Bruland K. W. (1990). Spatial and temporal variability in copper complexation in the North
3173 Pacific. *Deep Sea Res. Part A, Oceanogr. Res. Pap.* **37**, 317–336.
- 3174 Coale, K. H., Wang, X., Tanner, S. J., & Johnson, K. S. (2003). Phytoplankton growth and biological
3175 response to iron and zinc addition in the Ross Sea and Antarctic Circumpolar Current along 170°W.
3176 *Deep. Res. Part II Top. Stud. Oceanogr.*, **50**, 635–653.
- 3177 Collier, R. W. (1985). Molybdenum in the Northeast Pacific Ocean. *Limnol. Oceanogr.*, **30**, 1351–1354,
3178 doi:10.4319/lo.1985.30.6.1351
- 3179 Conway, T. M., & John, S. G. (2014a). Quantification of dissolved iron sources to the North Atlantic Ocean.
3180 *Nature*, **511**, 212-215.
- 3181 Conway, T. M., & John, S. G. (2014b). The biogeochemical cycling of zinc and zinc isotopes in the North
3182 Atlantic Ocean. *Global Biogeochem. Cycles*, 1111–1128.
- 3183 Conway, T. M., & John, S. G. (2015a). The cycling of iron, zinc and cadmium in the North East Pacific
3184 Ocean—Insights from stable isotopes. *Geochim. Cosmochim. Acta*, **164**, 262-283.
- 3185 Conway, T. M., & John, S. G. (2015b). Biogeochemical cycling of cadmium isotopes along a high-
3186 resolution section through the North Atlantic Ocean. *Geochim. Cosmochim. Acta*, **148**, 269-283.

- 3187 Conway, T. M., Rosenberg, A. D., Adkins, J. F., & John, S. G. (2013). A new method for precise
3188 determination of iron, zinc and cadmium stable isotope ratios in seawater by double-spike mass
3189 spectrometry. *Anal. Chim. Acta*, **793**, 44–52.
- 3190 Conway, T. M., Hamilton, D. S., Shelley, R. U., Aguilar-Islas, A. M., Landing, W. M., Mahowald, N. M.,
3191 & John, S. G. (2019). Tracing and constraining anthropogenic aerosol iron fluxes to the North
3192 Atlantic Ocean using iron isotopes. *Nat. Commun.*, **10**, 2628, doi:10.1038/s41467-019-10457-w.
- 3193 Coplen, T. B. (2011). Guidelines and recommended terms for expression of stable-isotope-ratio and gas-
3194 ratio measurement results. *Rapid communications in mass spectrometry*, **25**(17), 2538-2560.
- 3195 Costa, K. M., McManus, J. F., Anderson, R. F., Ren, H., Sigman, D. M., Winckler, G., Fleisher, M. Q.,
3196 Marcantonio, F., & Ravelo, A. C. (2016). No iron fertilization in the equatorial Pacific Ocean
3197 during the last ice age. *Nature*, **529**(7587), 519-522.
- 3198 Costa, K. M., McManus, J. F., Middleton, J. L., Langmuir, C. H., Huybers, P. J., Winckler, G., &
3199 Mukhopadhyay, S. (2017). Hydrothermal deposition on the Juan de Fuca Ridge over multiple
3200 glacial–interglacial cycles. *Earth Planet. Sci. Lett.*, **479**, 120-132.
- 3201 Coutaud, M., Méheut, M., Glatzel, P., Pokrovski, G. S., Viers, J., Rols, J. L., & Pokrovsky, O. S. (2018).
3202 Small changes in Cu redox state and speciation generate large isotope fractionation during
3203 adsorption and incorporation of Cu by a phototrophic biofilm. *Geochim. Cosmochim. Acta*, **220**, 1-
3204 18.
- 3205 Coutaud, M., Méheut, M., Viers, J., Rols, J. L., & Pokrovsky, O. S. (2019). Copper isotope fractionation
3206 during excretion from a phototrophic biofilm. *Chem. Geol.*, **513**, 88-100.
- 3207 Cowan, C. E., Jenne, E. A., & Crecelius, E. A. (1985). Silver speciation in seawater: The importance of
3208 sulfide and organic complexes. In: A.C. Sigleo and A. Hattori (Eds.), *Marine and Estuarine*
3209 *Geochemistry*, Lewis Publishers Inc., Chelsea, MI, USA.
- 3210 Cranston, R. E., & Murray, J. W. (1978). Determination of chromium species in natural waters.
3211 *Anal. Chim. Acta*, **99**, 275-282.
- 3212 Cranston, R. E., & Murray, J. W. (1980). Chromium species in the Columbia River and estuary.
3213 *Limnol. Oceanogr.* **25**, 1104–1112.
- 3214 Crawford, D. W. W., Lipsen, M. S. S., Purdie, D. A. A., Lohan, M. C. C., Statham, P. J. J., Whitney, F. A.
3215 A., Putland, J. N. N., Johnson, W. K. K., Sutherland N., Peterson, T. D. D., Harrison, P. J. J., &
3216 Wong C. S. S. (2003). Influence of zinc and iron enrichments on phytoplankton growth in the
3217 northeastern subarctic Pacific. *Limnol. Oceanogr.*, **48**, 1583–1600.
- 3218 Crockford, P. W., Wing, B. A., Paytan, A., Hodgskiss, M. S., Mayfield, K. K., Hayles, J. A., Middleton, J.
3219 E., Ahm, A.-S. C., Johnston, D. T., Caxito, F., Uhlein, G., Halverson, G. P., Eickmann, B., Torres,
3220 M., & Horner, T. J. (2019). Barium-isotopic constraints on the origin of post-Marinoan barites.
3221 *Earth Planet. Sci. Lett.*, **519**, 234-244.
- 3222 Crusius, J., & Thomson, J. (2003). Mobility of authigenic rhenium, silver, and selenium during
3223 postdepositional oxidation in marine sediments. *Geochim. Cosmochim. Acta*, **67**(2), 265-273.
- 3224 Crusius, J., Calvert, S., Pedersen, T., & Sage, D. (1996). Rhenium and molybdenum enrichments in
3225 sediments as indicators of oxic, suboxic and sulfidic conditions of deposition. *Earth Planet. Sci.*
3226 *Lett.*, **145**, 65–78, doi:10.1016/S0012-821X(96)00204-X.
- 3227 Cullen, J. T. (2006). On the nonlinear relationship between dissolved cadmium and phosphate in the modern
3228 global ocean: could chronic iron limitation of phytoplankton growth cause the kink? *Limnol.*
3229 *Oceanogr.*, **51**(3), 1369-1380.

- 3230 Cullen, J. T., & Sherrell, R. M. (2005). Effects of dissolved carbon dioxide, zinc, and manganese on the
3231 cadmium to phosphorus ratio in natural phytoplankton assemblages. *Limnol. Oceanogr.*, **50**(4),
3232 1193-1204.
- 3233 Cullen, J. T., Chase, Z., Coale, K. H., Fitzwater, S. E., & Sherrell, R. M. (2003). Effect of iron limitation
3234 on the cadmium to phosphorus ratio of natural phytoplankton assemblages from the Southern
3235 Ocean. *Limnology and Oceanography*, **48**(3), 1079-1087.
- 3236 Cullen, J. T., Lane, T. W., Morel, F. M., & Sherrell, R. M. (1999). Modulation of cadmium uptake in
3237 phytoplankton by seawater CO₂ concentration. *Nature*, **402**(6758), 165.
- 3238 Cullen, J. T., Chase, Z., Coale, K. H., Fitzwater, S. E., & Sherrell, R. M. (2003). Effect of iron limitation
3239 on the cadmium to phosphorus ratio of natural phytoplankton assemblages from the Southern
3240 Ocean. *Limnol. Oceanogr.*, **48**(3), 1079-1087.
- 3241 Cullen, J. T., & Coogan, L. A. (2017). Changes in Fe Oxidation Rate in Hydrothermal Plumes as a Potential
3242 Driver of Enhanced Hydrothermal Input to Near-Ridge Sediments During Glacial Terminations.
3243 *Geophys. Res. Lett.*, **44**(23), 11-951.
- 3244 Cutter, G., Casciotti, K., Croot, P., Geibert, W., Heimbürger, L.-E., Lohan, M., & van de Flierdt, T. (2017).
3245 *Sampling and Sample-handling Protocols for GEOTRACES Cruises*, Version 3.
3246 <http://www.geotraces.org/images/stories/documents/intercalibration/Cookbook.pdf> [accessed
3247 2020-06-23].
- 3248 D'Arcy, J., Babechuk, M. G., Døssing, L. N., Gaucher, C., & Frei, R. (2016). Processes controlling the
3249 chromium isotopic composition of river water: constraints from basaltic river catchments.
3250 *Geochim. Cosmochim. Acta*, **186**, 296–315, doi:10.1016/j.gca.2016.04.027.
- 3251 da Silva, J. F., & Williams, R. J. P. (1991). *The biological chemistry of the elements: the inorganic
3252 chemistry of life*. Oxford University Press.
- 3253 Dahl, T. W., Anbar, A. D., Gordon, G. W., Rosing, M. T., Frei, R., & Canfield, D. E. (2010). The behavior
3254 of molybdenum and its isotopes across the chemocline and in the sediments of sulfidic Lake
3255 Cadagno, Switzerland. *Geochim. Cosmochim. Acta*, **74**, 144–163, doi:10.1016/j.gca.2009.09.018.
- 3256 Dahl, T. W., Chappaz, A., Hoek, J., McKenzie, C. J., Svane, S., and Canfield, D. E. (2017). Evidence of
3257 molybdenum association with particulate organic matter under sulfidic conditions. *Geobiology*, **15**,
3258 311–323, doi:10.1111/gbi.12220.
- 3259 Dalai, T.K., Nishimura, K., & Nozaki, Y. (2005). Geochemistry of molybdenum in the Chao Phraya River
3260 estuary, Thailand: Role of suboxic diagenesis and porewater transport. *Chem. Geol.*, **218**, 189–202,
3261 doi:10.1016/j.chemgeo.2005.01.002.
- 3262 Davidson, A. B., Semeniuk, D. M., Koh, J., Holmden, C., Jaccard, S. L., Francois, R. & Crowe, S.
3263 A. (2020) A Mg(OH)₂ coprecipitation method for determining chromium speciation and isotopic
3264 composition in seawater. *Limnol. Oceanogr. Meth.*, **18**, 8–19, doi:10.1002/lom3.10342.
- 3265 de Baar, H. J. W., Saager, P. M., Nolting, R. F., & van der Meer, J. (1994). Cadmium versus phosphate in
3266 the world ocean. *Mar. Chem.*, **46**(3), 261-281.
- 3267 de Baar, H. J., Boyd, P. W., Coale, K. H., Landry, M. R., Tsuda, A., Assmy, P., ... & Buesseler, K. O.
3268 (2005). Synthesis of iron fertilization experiments: from the iron age in the age of enlightenment.
3269 *Journal of Geophysical Research: Oceans*, **110**(C9).
- 3270 de Baar, H. J. W., van Heuven, S. M., Abouchami, W., Xue, Z., Galer, S. J. G., Rehkämper, M., Middag,
3271 R. & van Ooijen, J. (2017). Interactions of dissolved CO₂ with cadmium isotopes in the Southern
3272 Ocean. *Mar. Chem.* **195**, 105-121.

- 3273 de Souza, G. F., Reynolds, B. C., Rickli, J., Frank, M., Saito, M. A., Gerringa, L. J., & Bourdon, B. (2012).
3274 Southern Ocean control of silicon stable isotope distribution in the deep Atlantic Ocean. *Global*
3275 *Biogeochem. Cycles*, **26**(2).
- 3276 de Souza, G. F., Khatiwala, S. P., Hain, M. P., Little, S. H., & Vance, D. (2018). On the origin of the marine
3277 zinc–silicon correlation. *Earth Planet. Sci. Lett.*, **492**, 22-34.
- 3278 Défarge, C. (2011). Organomineralization. Reitner, J., & Thiel, V. (eds.). *Encyclopedia of Geobiology*,
3279 Springer Verlag, pp.697-701, 2011, doi:10.1007/978-1-4020-9212-1_159.
- 3280 Dehairs, F., Chesselet, R., & Jedwab, J. (1980). Discrete suspended particles of barite and the barium cycle
3281 in the open ocean. *Earth Planet. Sci. Lett.*, **49**(2), 528-550.
- 3282 Dehairs, F., Lambert, C. E., Chesselet, R., & Risler, N. (1987). The biological production of marine
3283 suspended barite and the barium cycle in the Western Mediterranean Sea. *Biogeochemistry*, **4**(2),
3284 119-140.
- 3285 Dehairs, F., Jacquet, S., Savoye, N., Van Mooy, B. A., Buesseler, K. O., Bishop, J. K., Lamborg, C. H.,
3286 Elskens, M., Baeyens, W., Boyd, P. W., Casciotti, K. L., & Monnin, C. (2008). Barium in twilight
3287 zone suspended matter as a potential proxy for particulate organic carbon remineralization: Results
3288 for the North Pacific. *Deep Sea Res. Pt. II*, **55**(14-15), 1673-1683.
- 3289 Dellwig, O., Beck, M., Lemke, A., Lunau, M., Kolditz, K., Schnetger, B., & Brumsack, H.-J. (2007). Non-
3290 conservative behaviour of molybdenum in coastal waters: Coupling geochemical, biological, and
3291 sedimentological processes. *Geochim. Cosmochim. Acta*, **71**, 2745–2761,
3292 doi:10.1016/j.gca.2007.03.014.
- 3293 Dellwig, O., Leipe, T., März, C., Glockzin, M., Pollehne, F., Schnetger, B., Yakushev, E. V., Böttcher, M.
3294 E., & Brumsack, H. J. (2010). A new particulate Mn-Fe-P-shuttle at the redoxcline of anoxic basins.
3295 *Geochim. Cosmochim. Acta*, **74**, 7100–7115, doi:10.1016/j.gca.2010.09.017.
- 3296 Deng, N., Stack, A. G., Weber, J., Cao, B., De Yoreo, J. J., & Hu, Y. (2019). Organic–mineral interfacial
3297 chemistry drives heterogeneous nucleation of Sr-rich (Ba_x, Sr_{1-x})SO₄ from undersaturated solution.
3298 *Proc. Natl. Acad. Sci.*, 201821065.
- 3299 Dickens, G.R., Fewless, T., Thomas, E. & Bralower, T.J. (2003). Excess barite accumulation during the
3300 Paleocene–Eocene Thermal Maximum: Massive input of dissolved barium from seafloor gas
3301 hydrate reservoirs. In Wing, S. L, Gingerich, P. D., Schmitz, B., & Thomas, E. (Eds.) *Causes and*
3302 *consequences of globally warm climates in the early Paleogene*, **369**, 11-23, Geological Society of
3303 America Special Papers; doi:10.1130/0-8137-2369-8.11.
- 3304 Dickson, A. J. (2017). A molybdenum-isotope perspective on Phanerozoic deoxygenation events. *Nat.*
3305 *Geosci.*, **10**, 721–726, doi:10.1038/NGEO3028.
- 3306 Dideriksen, K., Baker, J. A., & Stipp, S. L. S. (2008). Equilibrium Fe isotope fractionation between
3307 inorganic aqueous Fe (III) and the siderophore complex, Fe (III)-desferrioxamine B. *Earth Planet.*
3308 *Sci. Lett.*, **269**(1-2), 280-290.
- 3309 Donat, J. R., & Bruland, K. W. (1990). A comparison of two voltammetric techniques for determining zinc
3310 speciation in Northeast Pacific Ocean waters. *Mar. Chem.*, **28**, 301–323.
- 3311 Donat J. R., Lao, K. A., & Bruland, K. W. (1994) Speciation of dissolved copper and nickel in South San
3312 Francisco Bay: a multi-method approach. *Anal. Chim. Acta* **284**, 547–571.
- 3313 Dunlea, A. G., Murray, R. W., Sauvage, J., Spivack, A. J., Harris, R. N., & D'Hondt, S. (2015). Dust,
3314 volcanic ash, and the evolution of the South Pacific Gyre through the Cenozoic. *Paleoceanogr.*,
3315 **30**(8), 1078-1099.

- 3316 Dunlea, A. G., Tegler, L. A., Peucker-Ehrenbrink, B., Anbar, A. D., Romaniello, S. J., & Horner, T. J.
3317 (2021). Pelagic clays as archives of marine iron isotope chemistry. *Chem. Geol.*, 120201.
- 3318 Dupont, C. L., Moffett, J. W., Bidigare, R. R., & Ahner, B. A. (2006). Distributions of dissolved and
3319 particulate biogenic thiols in the subarctic Pacific Ocean. *Deep. Res. Part I Oceanogr. Res. Pap.*,
3320 **53**, 1961–1974.
- 3321 Dupont, C. L., Butcher, A., Valas, R. E., Bourne, P. E., & Caetano-Anolles, G. (2010). History of biological
3322 metal utilization inferred through phylogenomic analysis of protein structures. *Proc. Natl. Acad. Sci.*, **107**, 10567–10572.
- 3324 Dutkiewicz, A., Müller, R. D., O’Callaghan, S., & Jónasson, H. (2015). Census of seafloor
3325 sediments in the world’s ocean. *Geology*, **43**(9), 795-798, doi:10.1130/G36883.1.
- 3326 Dymond, J., Suess, E., & Lyle, M. (1992). Barium in deep-sea sediment: A geochemical proxy for
3327 paleoproductivity. *Paleoceanography*, **7**(2), 163-181.
- 3328 Dymond, J., & Collier, R. (1996). Particulate barium fluxes and their relationships to biological
3329 productivity. *Deep Sea Research Part II: Topical Studies in Oceanography*, **43**(4-6), 1283-1308.
- 3330 Eagle, M., Paytan, A., Arrigo, K. R., van Dijken, G., & Murray, R. W. (2003). A comparison between
3331 excess barium and barite as indicators of carbon export. *Paleoceanography*, **18**(1), 1021,
3332 <https://doi.org/10.1029/2002PA000793>.
- 3333 Edmond, J. M., Boyle, E. D., Drummond, D., Grant, B., & Mislick, T. (1978). Desorption of barium in the
3334 plume of the Zaire (Congo) River. *Netherlands Journal of Sea Research*, **12**(3-4), 324-328.
- 3335 Elderfield, H. (1970). Chromium speciation in sea water. *Earth Planet. Sci. Lett.*, **9**, 10–16.
- 3336 Elderfield, H., & Rickaby, R. E. M. (2000). Oceanic Cd/P ratio and nutrient utilization in the glacial
3337 Southern Ocean. *Nature*, **405**(6784), 305-310.
- 3338 Elliott, T., & Steele, R. C. (2017). The isotope geochemistry of Ni. *Reviews in Mineralogy and
3339 Geochemistry*, **82**(1), 511-542.
- 3340 Ellis, A. S., Johnson, T. M., & Bullen, T. D. (2002) Chromium isotopes and the fate of hexavalent
3341 chromium in the environment. *Science*, **295**, 2060–2062, doi:10.1126/science.1068368.
- 3342 Ellwood, M. J. (2004). Zinc and cadmium speciation in subantarctic waters east of New Zealand. *Mar.
3343 Chem.*, **87**(1-2), 37-58.
- 3344 Ellwood, M. J., & Hunter, K. A. (2000). The Incorporation of Zinc and Iron into the Frustule of the Marine
3345 Diatom *Thalassiosira pseudonana*. *Limnol. Oceanogr.*, **45**, 1517–1524.
- 3346 Ellwood, M. J., & Van Den Berg, C. M. G. (2000). Zinc speciation in the Northeastern Atlantic Ocean.
3347 *Mar. Chem.*, **68**, 295–306.
- 3348 Ellwood, M.J., Hutchins, D.A., Lohan, M.C., Milne, A., Nasemann, P., Nodder, S.D., Sander, S.G.,
3349 Strzepek, R., Wilhelm, S.W., & Boyd, P.W. (2015). Iron stable isotopes track pelagic iron cycling
3350 during a subtropical phytoplankton bloom. *Proc. Natl. Acad. Sci. U. S. A.* **112**, E15-E20.
- 3351 Ellwood, M. J., Strzepek, R. F., Strutton, P. G., Trull, T. W., Fourquez, M., & Boyd, P. W. (2020). Distinct
3352 iron cycling in a Southern Ocean eddy. *Nature Communications*, **11**(1), 1-8.
- 3353 Emerson, S. R., & Husted, S. S. (1991). Ocean anoxia and the concentrations of molybdenum and
3354 vanadium in seawater. *Mar. Chem.* **34**, 177–196, doi:10.1016/0304-4203(91)90002-E.
- 3355 Erickson, B. E., & Helz, G. R. (2000). Molybdenum(VI) speciation in sulfidic waters: Stability and lability
3356 of thiomolybdates. *Geochim. Cosmochim. Acta*, **64**, 1149–1158, doi:10.1016/S0016-
3357 7037(99)00423-8.

- 3358 Escoube, R., Rouxel, O. J., Pokrovsky, O. S., Schroth, A., Max Holmes, R., & Donard, O. F. X. (2015).
3359 Iron isotope systematics in Arctic rivers. *Comptes Rendus Geosci.*, **347**(7–8), 377–385.
- 3360 Escoube, R., Rouxel, O. J., Sholkovitz, E., & Donard, O. F. X. (2009). Iron isotope systematics in estuaries:
3361 The case of North River, Massachusetts (USA). *Geochim. Cosmochim. Acta*, **73**(14), 4045–4059.
- 3362 Esser, B. K., & Volpe, A. M. (2002). At-sea high-resolution chemical mapping: extreme barium depletion
3363 in North Pacific surface water. *Mar. Chem.*, **79**(2), 67-79.
- 3364 Fagel, N., Dehairs, F., Peinert, R., Antia, A., & André, L. (2004). Reconstructing export production at the
3365 NE Atlantic margin: potential and limits of the Ba proxy. *Mar. Geol.*, **204**(1-2), 11-25.
- 3366 Fantle, M. S., & DePaolo, D. J., (2004). Iron isotopic fractionation during continental weathering. *Earth
3367 Planet. Sci. Lett.*, **228**(3-4), 547-562.
- 3368 Farmer, J. R., Hönisch, B., Haynes, L. L., Kroon, D., Jung, S., Ford, H. L., Raymo, M. E., Jaume-Seguí,
3369 M., Bell, D. B., Goldstein, S. L., Pena, L. D., Yehudai, M., & Kim, J. (2019). Deep Atlantic Ocean
3370 carbon storage and the rise of 100,000-year glacial cycles. *Nat. Geosci.* **12**, 355-360,
3371 <https://doi.org/10.1038/s41561-019-0334-6>.
- 3372 Farkaš, J., Frýda, J., Paulukat, C., Hathorne, E. C., Matoušková, Š., Rohovec, J., Frýdová, B.,
3373 Francová, M., & Frei, R. (2018). Chromium isotope fractionation between modern seawater and
3374 biogenic carbonates from the Great Barrier Reef, Australia: implications for the paleo-seawater
3375 $\delta^{53}\text{Cr}$ reconstruction. *Earth Planet. Sci. Lett.*, **498**, 140–151, doi:10.1016/j.epsl.2018.06.032.
- 3376 Fassbender, A. J., Palevsky, H. I., Martz, T. R., Ingalls, A. E., Gledhill, M., Fawcett, S. E., Brandes, J. A.,
3377 Aluwihare, L. I., & the participants of COME ABOARD and DISCO XXV (2017). Perspectives
3378 on Chemical Oceanography in the 21st century: Participants of the COME ABOARD Meeting
3379 examine aspects of the field in the context of 40 years of DISCO. *Mar. Chem.*, **196**, 181-190.
- 3380 Ferrier-Pagès, C., Sauzéat, L., & Balter, V. (2018). Coral bleaching is linked to the capacity of the animal
3381 host to supply essential metals to the symbionts. *Glob. Change Biol.*, **24**(7), 3145-3157.
- 3382 Finlay, B. J., Hetherington, N. B., & Da Vison, W. (1983). Active biological participation in lacustrine
3383 barium chemistry. *Geochim. Cosmochim. Acta*, **47**(7), 1325-1329.
- 3384 Fischer, L., Smith, G., Hann, S., & Bruland, K. W. (2018). Ultra-trace analysis of silver and platinum in
3385 seawater by ICP-SFMS after off-line matrix separation and pre-concentration. *Mar. Chem.*, **199**,
3386 44-52.
- 3387 Fisher, N.S., & Wentz, M. (1993). The release of trace elements by dying marine phytoplankton. *Deep-Sea
3388 Research I*, **40**(4), 671-694.
- 3389 Fishwick, M. P., Sedwick, P. N., Lohan, M. C., Worsfeld, P. J., Buck, K. N., Church, T. M., Ussher, S. J.
3390 (2014). The impact of changing surface ocean conditions on the dissolution of aerosol iron. *Global
3391 Biogeochem. Cycles*, **28**(11), 1235-1250. <https://doi.org/10.1002/2014GB004921>.
- 3392 Fitzsimmons, J. N., & Boyle, E. A. (2014). Both soluble and colloidal iron phases control dissolved iron
3393 variability in the tropical North Atlantic Ocean. *Geochim. Cosmochim. Acta*, **125**, 539-550.
- 3394 Fitzsimmons, J. N., Carrasco, G. G., Wu, J., Roshan, S., Hatta, M., Measures, C. I., Conway, T. M., John,
3395 S.G., & Boyle, E. A. (2015). Partitioning of dissolved iron and iron isotopes into soluble and
3396 colloidal phases along the GA03 GEOTRACES North Atlantic Transect. *Deep Sea Res. Pt. II*, **116**,
3397 130-151.
- 3398 Fitzsimmons, J. N., Conway, T. M., Lee, J.-M., Kayser, R., Thyng, K. M., John, S. G. and Boyle, E. A.
3399 (2016). Dissolved iron and iron isotopes in the Southeastern Pacific Ocean. *Global Biogeochem.
3400 Cycles*, **30**(10), 1372-1395. <https://doi.org/10.1002/2015GB005357>.

- 3401 Fitzsimmons, J. N., John, S. G., Marsay, C. M., Hoffman, C. L., Nicholas, S. L., Toner, B. M., German, C.
3402 R., & Sherrell, R. M. (2017). Iron persistence in a distal hydrothermal plume supported by
3403 dissolved–particulate exchange. *Nature Geoscience*, **10**(3), 195-201.
- 3404 Flegal, A.R., Sanudo-Wilhelmy, S.A., & Scelfo, G.M. (1995). Silver in the eastern Atlantic Ocean. *Mar.*
3405 *Chem.*, **49**, 315-320.
- 3406 Franck, V. M., Bruland, K. W., Hutchins, D. A., & Brzezinski, M. A. (2003). Iron and zinc effects on silicic
3407 acid and nitrate uptake kinetics in three high-nutrient, low-chlorophyll (HNLC) regions. *Mar. Ecol.*
3408 *Prog. Ser.*, **252**, 15–33.
- 3409 Frank, A. B., Klæbe, R. M., Löhr, S., Xu, L., & Frei, R. (2020). Chromium isotope composition
3410 of organic-rich marine sediments and their mineral phases and implications for using black shales
3411 as a paleoredox archive. *Geochim. Cosmochim. Acta*, **270**, 338-359, doi:10.1016/j.gca.2019.11.035.
- 3412 François, R., Honjo, S., Manganini, S. J., & Ravizza, G. E. (1995). Biogenic barium fluxes to the deep sea:
3413 Implications for paleoproductivity reconstruction. *Global Biogeochem. Cycles*, **9**(2), 289-303.
- 3414 François, R., Altabet, M. A., Yu, E. F., Sigman, D. M., Bacon, M. P., Frank, M., Bohrmann, G. Bareille,
3415 G., & Labeyrie, L. D. (1997). Contribution of Southern Ocean surface-water stratification to low
3416 atmospheric CO₂ concentrations during the last glacial period. *Nature*, **389**(6654), 929-935.
- 3417 Frei, R., Gaucher, C., Poulton, S. W., & Canfield, D. E. (2009). Fluctuations in Precambrian
3418 atmospheric oxygenation recorded by chromium isotopes. *Nature*, **461**, 250–254,
3419 doi:10.1038/nature08266
- 3420 Frei, R., Poiré, D., & Frei, K. M. (2014). Weathering on land and transport of chromium to the
3421 ocean in a subtropical region (Misiones, NW Argentina): a chromium stable isotope perspective.
3422 *Chem. Geol.*, **381**, 110–124. doi:10.1016/j.chemgeo.2014.05.015.
- 3423 Frei, R., Lehmann, B., Xu, L., & Frederiksen, J. A. (2020). Surface water oxygenation and bioproductivity–
3424 A link provided by combined chromium and cadmium isotopes in Early Cambrian metalliferous
3425 black shales (Nanhua Basin, South China). *Chem. Geol.*, **552**, 119785.
- 3426 Frew, R. D., & Hunter, K. A. (1992). Influence of Southern Ocean waters on the cadmium–phosphate
3427 properties of the global ocean. *Nature*, **360**(6400), 144.
- 3428 Friedl, G., & Pedersen, T. (2002). Silver as a new tracer for diatom production. *Eawag News*, **52**, 14-15.
- 3429 Froelich, P., Klinkhammer, G. P., Bender, M. L., Luedtke, N. A., Heath, G. R., Cullen, D., Dauphin, P.,
3430 Hammond D., Hartman, B., & Maynard, V. (1979). Early oxidation of organic matter in pelagic
3431 sediments of the eastern equatorial Atlantic: suboxic diagenesis. *Geochimica et Cosmochimica*
3432 *Acta*, **43**(7), 1075-1090.
- 3433 Fru, E. C., Rodríguez, N. P., Partin, C. A., Lalonde, S. V., Andersson, P., Weiss, D. J., El Albani, A.,
3434 Rodushkin, I., & Konhauser, K. O. (2016). Cu isotopes in marine black shales record the Great
3435 Oxidation Event. *Proceedings of the National Academy of Sciences*, **113**(18), 4941-4946.
- 3436 Fujii, T., Moynier, F., Pons, M. L., & Albarède, F. (2011a). The origin of Zn isotope fractionation in
3437 sulfides. *Geochim. Cosmochim. Acta*, **75**(23), 7632-7643.
- 3438 Fujii, T., Moynier, F., Dauphas, N., & Abe, M. (2011b). Theoretical and experimental investigation of
3439 nickel isotopic fractionation in species relevant to modern and ancient oceans. *Geochim.*
3440 *Cosmochim. Acta*, **75**(2), 469-482.
- 3441 Fujii, T., Moynier, F., Abe, M., Nemoto, K., & Albarède, F. (2013). Copper isotope fractionation between
3442 aqueous compounds relevant to low temperature geochemistry and biology. *Geochim. Cosmochim.*
3443 *Acta*, **110**, 29-44.

- 3444 Gall, L., Williams, H. M., Siebert, C., Halliday, A. N., Herrington, R. J., & Hein, J. R. (2013). Nickel
3445 isotopic compositions of ferromanganese crusts and the constancy of deep ocean inputs and
3446 continental weathering effects over the Cenozoic. *Earth Planet. Sci. Lett.*, **375**, 148-155.
- 3447 Gallon, C., & Flegal, A. R. (2015). Sources, Fluxes, and Biogeochemical Cycling of Silver in the Oceans.
3448 In: Whitacre, D. (eds) *Rev. Environ. Contamin. Toxicol.* **235**. Springer, Cham.
3449 https://doi.org/10.1007/978-3-319-10861-2_2.
- 3450 Ganeshram, R. S., François, R., Commeau, J., & Brown-Leger, S. L. (2003). An experimental investigation
3451 of barite formation in seawater. *Geochim. Cosmochim. Acta*, **67**(14), 2599-2605.
- 3452 Garcia, H. E., R. A. Locarnini, T. P. Boyer, J. I. Antonov, O.K. Baranova, M.M. Zweng, J.R. Reagan, D.R.
3453 Johnson, 2014. World Ocean Atlas 2013, Volume 3: Dissolved Oxygen, Apparent Oxygen
3454 Utilization, and Oxygen Saturation. S. Levitus, Ed., A. Mishonov Technical Ed.; *NOAA Atlas*
3455 *NESDIS 75*, 27 pp.
- 3456 Gault-Ringold, M., Adu, T., Stirling, C. H., Frew, R. D., & Hunter, K. A. (2012). Anomalous
3457 biogeochemical behavior of cadmium in Subantarctic surface waters: mechanistic constraints from
3458 cadmium isotopes. *Earth Planet. Sci. Lett.*, **341**, 94-103.
- 3459 Gebregiorgis, D., Hathorne, E. C., Sijinkumar, A. V., Nath, B. N., Nürnberg, D., & Frank, M. (2016). South
3460 Asian summer monsoon variability during the last~ 54 kyrs inferred from surface water salinity
3461 and river runoff proxies. *Quaternary Science Reviews*, 138, 6-15.
- 3462 George, E., Stirling, C. H., Gault-Ringold, M., Ellwood, M. J., & Middag, R. (2019). Marine
3463 biogeochemical cycling of cadmium and cadmium isotopes in the extreme nutrient-depleted
3464 subtropical gyre of the South West Pacific Ocean. *Earth Planet. Sci. Lett.*, **514**, 84-95.
- 3465 Georgiev, S. V., Horner, T. J., Stein, H. J., Hannah, J. L., Bingen, B., & Rehkämper, M. (2015). Cadmium-
3466 isotopic evidence for increasing primary productivity during the Late Permian anoxic event. *Earth*
3467 *Planet. Sci. Lett.*, **410**, 84-96.
- 3468 Geyman, B. M., Ptacek, J. L., LaVigne, M., & Horner, T. J. (2019). Barium in deep-sea bamboo corals:
3469 Phase associations, barium stable isotopes, & prospects for paleoceanography. *Earth Planet. Sci.*
3470 *Lett.*, **525**, 115751.
- 3471 Giering, S. L., Sanders, R., Lampitt, R. S., Anderson, T. R., Tamburini, C., Boutrif, M., Zubkov, M. V.,
3472 Marsay, C. M., Henson, S. A., Saw, K., Cook, K., & Mayor, D. J.(2014). Reconciliation of the
3473 carbon budget in the ocean's twilight zone. *Nature*, **507**(7493), 480-483.
- 3474 Glass, J. B., Axler, R. P., Chandra, S., & Goldman, C. R. (2012). Molybdenum limitation of microbial
3475 nitrogen assimilation in aquatic ecosystems and pure cultures. *Frontiers in Microbiology*, **3**, 1-11,
3476 doi:10.3389/fmicb.2012.00331.
- 3477 Glass, J. B., Wolfe-Simon, F., & Anbar, A. D. (2009). Coevolution of metal availability and nitrogen
3478 assimilation in cyanobacteria and algae. *Geobiology*, **7**, 100-123, doi:10.1111/j.1472-
3479 4669.2009.00190.x.
- 3480 Goldberg, T., Archer, C., Vance, D., & Poulton, S. W. (2009). Mo isotope fractionation during adsorption
3481 to Fe (oxyhydr)oxides. *Geochim. Cosmochim. Acta*, **73**, 6502-6516,
3482 doi:10.1016/j.gca.2009.08.004.
- 3483 Goldberg, T., Archer, C., Vance, D., Thamdrup, B., McAnena, A., & Poulton, S. W. (2012). Controls on
3484 Mo isotope fractionations in a Mn-rich anoxic marine sediment, Gullmar Fjord, Sweden. *Chem.*
3485 *Geol.*, **296-297**, 73-82, doi:10.1016/j.chemgeo.2011.12.020.

- 3486 Goldberg, T., Gordon, G., Izon, G., Archer, C., Pearce, C. R., McManus, J., Anbar, A. D., & Rehkämper,
3487 M. (2013). Resolution of inter-laboratory discrepancies in Mo isotope data: an intercalibration.
3488 *Journal of Analytical Atomic Spectrometry*, **28**(5), 724-735.
- 3489 Goldman, C. R. (1960). Molybdenum as a Factor Limiting Primary Productivity in Castle Lake, California.
3490 *Science*, **132**, 1016–1017, doi:10.1126/science.132.3433.1016.
- 3491 Gong, Y., Xia, Y., Huang, F., & Yu, H. (2017). Average iron isotopic compositions of the upper continental
3492 crust: constrained by loess from the Chinese Loess Plateau. *Acta Geochim.*, **36**, 125-131,
3493 doi:10.1007/s11631-016-0131-5.
- 3494 Gooday, A. J., & Nott, J. A. (1982). Intracellular barite crystals in two xenophyophores, *Aschemonella*
3495 *ramuliformis* and *Galatheammima sp.* (Protozoa: Rhizopoda) with comments on the taxonomy of
3496 *A. ramuliformis*. *Journal of the Marine Biological Association of the United Kingdom*, **62**(3), 595-
3497 605.
- 3498 Goring-Harford, H. J., Klar, J. K., Pearce, C. R., Connelly, D. P., Achterberg, E. P., & James, R.
3499 H. (2018). Behaviour of chromium isotopes in the eastern sub-tropical Atlantic Oxygen Minimum
3500 Zone. *Geochim. Cosmochim. Acta*, **236**, 41-59, doi:10.1016/j.gca.2018.03.004.
- 3501 Goto, K. T., Sekine, Y., Shimoda, G., Hein, J. R., Aoki, S., Ishikawa, A., Suzuki, K., Gordon, G. W., &
3502 Anbar, A. D. (2020). A framework for understanding Mo isotope records of Archean and
3503 Paleoproterozoic Fe-and Mn-rich sedimentary rocks: Insights from modern marine hydrothermal
3504 Fe-Mn oxides. *Geochim. Cosmochim. Acta*, **280**, 221-236.
- 3505 Gou, L. F., Jin, Z., Galy, A., Gong, Y. Z., Nan, X. Y., Jin, C., Wang, X.-D., Bouchez, J., Cai, H.-M., Chen,
3506 J.-B., Yu, H.-M., & Huang, F. (2020). Seasonal riverine barium isotopic variation in the middle
3507 Yellow River: Sources and fractionation. *Earth and Planetary Science Letters*, **531**, 115990.
- 3508 Griffith, E. M., & Paytan, A. (2012). Barite in the ocean—occurrence, geochemistry and palaeoceanographic
3509 applications. *Sedimentology*, **59**(6), 1817-1835.
- 3510 Gueguen, B., Rouxel, O., Ponzevera, E., Bekker, A., & Fouquet, Y. (2013). Nickel isotope variations in
3511 terrestrial silicate rocks and geological reference materials measured by MC-ICP-MS.
3512 *Geostandards and Geoanalytical Research*, **37**(3), 297-317.
- 3513 Gueguen, B., Rouxel, O., Rouget, M. L., Bollinger, C., Ponzevera, E., Germain, Y., & Fouquet, Y. (2016a).
3514 Comparative geochemistry of four ferromanganese crusts from the Pacific Ocean and significance
3515 for the use of Ni isotopes as paleoceanographic tracers. *Geochim. Cosmochim. Acta*, **189**, 214-235.
- 3516 Gueguen, B., Reinhard, C. T., Algeo, T. J., Peterson, L. C., Nielsen, S. G., Wang, X., Rowe, H., &
3517 Planavsky, N. J. (2016b). The chromium isotope composition of reducing and oxic marine
3518 sediments. *Geochim. Cosmochim. Acta*, **184**, 1–19. doi: 10.1016/j.gca.2016.04.004.
- 3519 Gueguen, B., Rouxel, O., & Fouquet, Y. (2021). Nickel isotopes and rare earth elements systematics in
3520 marine hydrogenetic and hydrothermal ferromanganese deposits. *Chem. Geol.*, **560**, 119999,
3521 doi:10.1016/j.chemgeo.2020.119999.
- 3522 Gueguen, B., & Rouxel, O. (2021). The Nickel isotope composition of the authigenic sink and the
3523 diagenetic flux in modern oceans. *Chem. Geol.*, **563**, 120050.
3524 doi.org/10.1016/j.chemgeo.2020.120050.
- 3525 Guinoiseau, D., Galer, S. J., & Abouchami, W. (2018). Effect of cadmium sulphide precipitation on the
3526 partitioning of Cd isotopes: Implications for the oceanic Cd cycle. *Earth Planet. Sci. Lett.*, **498**,
3527 300-308.
- 3528 Guo, J., Lapi, S., Ruth, T. J., & Maldonado, M. T. (2012). The effects of iron and copper availability on the
3529 copper stoichiometry of marine phytoplankton. *J. Phycol.* **48**, 312–325.

3530 Hanor, J. S., & Chan, L. H. (1977). Non-conservative behavior of barium during mixing of Mississippi
3531 River and Gulf of Mexico waters. *Earth and Planetary Science Letters*, **37**(2), 242-250.

3532 Hanor, J. S. (2000). Barite–celestine geochemistry and environments of formation. *Rev. Mineral.*
3533 *Geochem.*, **40**(1), 193-275.

3534 Hardisty, D. S., Riedinger, N., Planavsky, N. J., Asael, D., Andrén, T., et al. (2016). A Holocene history of
3535 dynamic water column redox conditions in the Landsort Deep, Baltic Sea. *Am. J. Sci.*, **316**, 713-
3536 745, doi:10.2475/08.2016.01.

3537 Hardisty, D. S., Lyons, T. W., Riedinger, N., Isson, T. T., Owens, J. D., Aller, R. C., Rye, D. M., Planavsky,
3538 N. J., Reinhard, C. T., Gill, B. C., Masterson, A. L., Asael, D., & Johnston, D. T. (2018). An
3539 evaluation of sedimentary molybdenum and iron as proxies for pore fluid paleoredox conditions.
3540 *Am. J. Sci.*, **318**(5), 527-556.

3541 Hartnett, H. E., Keil, R. G., Hedges, J. I., & Devol, A. H. (1998). Influence of oxygen exposure time on
3542 organic carbon preservation in continental margin sediments. *Nature*, **391**(6667), 572-575.

3543 Hawco, N. J., Lam, P. J., Lee, J. M., Ohnemus, D. C., Noble, A. E., Wyatt, N. J., Lohan, M. C., & Saito,
3544 M. A. (2018). Cobalt scavenging in the mesopelagic ocean and its influence on global mass
3545 balance: Synthesizing water column and sedimentary fluxes. *Marine Chemistry*, **201**, 151-166.

3546 Hayes, C. T., Anderson, R. F., Cheng, H., Conway, T. M., Edwards, R. L., Fleisher, M. Q., Ho, P., Huang,
3547 K.-F., John, S. G., Landing, W. M., Little, S. H., Lu, Y., Morton, P. L., Moran, S. B., Robinson, L.
3548 F., Shelley, R. U., Shiller, A. M., & Zheng, X.-Y. (2018). Replacement times of a spectrum of
3549 elements in the North Atlantic based on thorium supply. *Global Biogeochem. Cycles*, **32**(9), 1294-
3550 1311.

3551 Hayes, J. M. (2004). *An introduction to isotopic calculations*. Woods Hole Oceanographic Institution,
3552 Woods Hole, MA, available from:
3553 https://www.whoi.edu/cms/files/jhayes/2005/9/IsoCalcs30Sept04_5183.pdf

3554 Heller, M. I., & Croot, P. L. (2015). Copper speciation and distribution in the Atlantic sector of the Southern
3555 Ocean. *Mar. Chem.*, **173**, 253-268.

3556 Helz, G. R., Miller, C. V., Charnock, J. M., Mosselmans, J. F. W., Patrick, R. A. D., Garner, C. D., &
3557 Vaughan, D. J. (1996). Mechanism of molybdenum removal from the sea and its concentration in
3558 black shales: EXAFS evidence. *Geochim. Cosmochim. Acta*, **60**, 3631–3642, doi:10.1016/0016-
3559 7037(96)00195-0.

3560 Hemsing, F., Hsieh, Y. T., Bridgestock, L., Spooner, P. T., Robinson, L. F., Frank, N., & Henderson, G.
3561 M. (2018). Barium isotopes in cold-water corals. *Earth and Planetary Science Letters*, **491**, 183-
3562 192.

3563 Henderson, G. M., & Burton, K. W. (1999). Using (234U/238U) to assess diffusion rates of isotope tracers
3564 in ferromanganese crusts. *Earth Planet. Sci. Lett.*, **170**(3), 169-179.

3565 Hendry, K. R., & Andersen, M. B. (2013). The zinc isotopic composition of siliceous marine sponges:
3566 Investigating nature’s sediment traps. *Chem. Geol.*, **354**, 33–41. Available at:
3567 <http://dx.doi.org/10.1016/j.chemgeo.2013.06.025>.

3568 Hendry, K. R., Pyle, K. M., Barney Butler, G., Cooper, A., Fransson, A., Chierici, M., Leng, M. J., Meyer,
3569 A., & Dodd, P.A. (2018). Spatiotemporal Variability of Barium in Arctic Sea-Ice and Seawater. *J.*
3570 *Geophys. Res. Oceans*, **123**(5), 3507-3522.

3571 Hendy, I. L., & Pedersen, T. F. (2005). Is pore water oxygen content decoupled from productivity on the
3572 California Margin? Trace element results from Ocean Drilling Program Hole 1017E, San Lucia
3573 slope, California. *Paleoceanography*, **20**(4).

- 3574 Henkel, S., Kasten, S., Hartmann, J. F., Silva-Busso, A., & Staubwasser, M. (2018). Iron cycling and stable
3575 Fe isotope fractionation in Antarctic shelf sediments, King George Island. *Geochim. Cosmochim.*
3576 *Acta*, **237**, 320-338. <https://doi.org/10.1016/j.gca.2018.06.042>.
- 3577 Hillaire-Marcel, C., & De Vernal, A. (Eds.). (2007). *Proxies in Late Cenozoic Paleoceanography*. Elsevier.
- 3578 Ho, P., Lee, J. M., Heller, M. I., Lam, P. J., and Shiller, A. M. (2018). The distribution of dissolved and
3579 particulate Mo and V along the U.S. GEOTRACES East Pacific Zonal Transect (GP16): The roles
3580 of oxides and biogenic particles in their distributions in the oxygen deficient zone and the
3581 hydrothermal plume. *Mar. Chem.*, **201**, 242–255, doi:10.1016/j.marchem.2017.12.003.
- 3582 Ho, T. Y., Quigg, A., Finkel, Z. V., Milligan, A. J., Wyman, K., Falkowski, P. G., & Morel, F. M. (2003).
3583 The elemental composition of some marine phytoplankton 1. *Journal of Phycology*, **39**(6), 1145-
3584 1159.
- 3585 Hodgskiss, M. S., Crockford, P. W., Peng, Y., Wing, B. A., & Horner, T. J. (2019). A productivity collapse
3586 to end Earth's Great Oxidation. *Proc. Natl. Acad. Sci.*, **116**(35), 17207-17212.
- 3587 Hohl, S. V., Galer, S. J. G., Gamper, A., & Becker, H. (2017). Cadmium isotope variations in
3588 Neoproterozoic carbonates—A tracer of biologic production? *Geochemical Perspective Letters*, **3**,
3589 32-44.
- 3590 Hohl, S. V., Jiang, S. Y., Wei, H. Z., Pi, D. H., Liu, Q., Viehmann, S., & Galer, S. J. (2019). Cd Isotopes
3591 trace periodic (bio)geochemical metal cycling at the verge of the Cambrian animal evolution.
3592 *Geochim. Cosmochim. Acta*, **263**, 195-214, doi:10.1016/j.gca.2019.07.036.
- 3593 Holmden, C., Jacobson, A. D., Sageman, B. B., & Hurtgen, M. T. (2016). Response of the Cr
3594 isotope proxy to Cretaceous Ocean Anoxic Event 2 in a pelagic carbonate succession from the
3595 Western Interior Seaway. *Geochim. Cosmochim. Acta*, **186**, 277-295,
3596 doi:10.1016/j.gca.2016.04.039.
- 3597 Holzer, M., Primeau, F. W., DeVries, T., & Matear, R. (2014). The Southern Ocean silicon trap: Data-
3598 constrained estimates of regenerated silicic acid, trapping efficiencies, and global transport paths.
3599 *J. Geophys. Res. Oceans*, **119**(1), 313-331.
- 3600 Homoky, W. B., Severmann, S., Mills, R. A., & Fones, G. R. (2009). Pore-fluid Fe isotopes reflect the
3601 extent of benthic Fe redox recycling: evidence from continental shelf and deep-sea sediments.
3602 *Geology*, **37**, 751–754. <https://doi.org/10.1130/G25731A.1>.
- 3603 Homoky, W. B., John, S. G., Conway T. M., & Mills, R. A. (2013). Distinct iron isotopic signatures and
3604 supply from marine sediment dissolution. *Nat. Comms*, **4**, 2143.
3605 <https://doi.org/10.1038/ncomms3143>.
- 3606 Homoky, W. B., Conway, T. M., John, S. G., Koenig, D., Deng, F., Tagliabue, A. & Mills, R. (2021). Iron
3607 colloids dominate sedimentary supply to the ocean interior. *Proc. Natl. Acad. Sci. USA*, **118** (13),
3608 e2016078118. doi:10.1073/pnas.2016078118.
- 3609 Hoppema, M., Dehairs, F., Navez, J., Monnin, C., Jeandel, C., Fahrbach, E., & De Baar, H. J. W. (2010).
3610 Distribution of barium in the Weddell Gyre: Impact of circulation and biogeochemical processes.
3611 *Marine Chemistry*, **122**(1-4), 118-129.
- 3612 Horner, T.J., & Crockford, P. (2021). *Barium Isotopes: Drivers, Dependencies, and Distributions through*
3613 *Space and Time* (Elements in Geochemical Tracers in Earth System Science). Cambridge
3614 University Press. doi:10.1017/9781108865845
- 3615 Horner, T. J., Schönbacher, M., Rehkämper, M., Nielsen, S. G., Williams, H., Halliday, A. N., Xue, Z., &
3616 Hein, J. R. (2010). Ferromanganese crusts as archives of deep water Cd isotope compositions.
3617 *Geochemistry, Geophysics, Geosystems*, **11**(4), Q04001, <https://doi.org/10.1029/2009GC002987>.

- 3618 Horner, T. J., Rickaby, R. E., & Henderson, G. M. (2011). Isotopic fractionation of cadmium into calcite.
3619 *Earth Planet. Sci. Lett.*, **312**(1-2), 243-253.
- 3620 Horner, T. J., Lee, R. B., Henderson, G. M., & Rickaby, R. E. (2013). Nonspecific uptake and homeostasis
3621 drive the oceanic cadmium cycle. *Proc. Natl. Acad. Sci.*, **110**(7), 2500-2505.
- 3622 Horner, T. J., Kinsley, C. W., & Nielsen, S. G. (2015a). Barium-isotopic fractionation in seawater mediated
3623 by barite cycling and oceanic circulation. *Earth Planet. Sci. Lett.*, **430**, 511-522.
- 3624 Horner, T. J., Williams, H. M., Hein, J. R., Saito, M. A., Burton, K. W., Halliday, A. N., & Nielsen, S. G.
3625 (2015b). Persistence of deeply sourced iron in the Pacific Ocean. *Proc. Natl. Acad. Sci.*, **112**, 1292-
3626 1297.
- 3627 Horner, T. J., Pryer, H. V., Nielsen, S. G., Crockford, P. W., Gauglitz, J. M., Wing, B. A., & Ricketts, R.
3628 D. (2017). Pelagic barite precipitation at micromolar ambient sulfate. *Nat. Commun.*, **8**(1), 1342.
- 3629 Hsieh, Y. T., & Henderson, G. M. (2017). Barium stable isotopes in the global ocean: tracer of Ba inputs
3630 and utilization. *Earth Planet. Sci. Lett.*, **473**, 269-278.
- 3631 Hsieh, Y. T., Bridgestock, L., Scheuermann, P. P., Seyfried Jr., W. E., & Henderson, G. M. (2021). Barium
3632 isotopes in mid-ocean ridge hydrothermal vent fluids: A source of isotopically heavy Ba to the
3633 ocean. *Geochim. Cosmochim. Acta*, **292**, 348-363, doi:10.1016/j.gca.2020.09.037.
- 3634 Huang, T., Moos, S. B., & Boyle, E. A. (2021). Trivalent chromium isotopes in the eastern tropical
3635 North Pacific oxygen-deficient zone. *Proc. Nat. Acad. Sci. USA*, **118**(8), e1918605118,
3636 doi:10.1073/pnas.1918605118.
- 3637 Hudson, R. J. M., & Morel, F. M. M. (1993). Trace metal transport by marine microorganisms: Implications
3638 of metal coordination kinetics. *Deep Sea Res.* **40**, 129–150.
- 3639 Hug, S. J., & Laubscher, H.-U. (1997). Iron(III) catalyzed photochemical reduction of
3640 chromium(VI) by oxalate and citrate in aqueous solutions. *Environ. Sci. Technol.*, **31**, 160–170,
3641 doi:10.1021/es960253l.
- 3642 Ijichi, Y., Ohno, T., & Sakata, S. (2018). Copper isotopic fractionation during adsorption on manganese
3643 oxide: Effects of pH and desorption. *Geochemical Journal*, **52**(2), e1-e6.
- 3644 Ilina, S. M., Poitrasson, F., Lapitskiy, S. A., Alekhin, Y. V., Viers, J., & Pokrovsky, O. S. (2013). Extreme
3645 iron isotope fractionation between colloids and particles of boreal and temperate organic-rich
3646 waters. *Geochim. et Cosmochim. Acta*, **101**, 96–111.
- 3647 Ingri, J., Malinovsky, D., Rodushkin, I., Baxter, D.C., Widerlund, A., Andersson, P., Gustafsson, Ö.,
3648 Forsling, W. & Öhlander, B. (2006). Iron isotope fractionation in river colloidal matter. *Earth
3649 Planet. Sci. Lett.*, **245**(3–4), 792–798.
- 3650 Isson, T. T., Love, G. D., Dupont, C. L., Reinhard, C. T., Zumberge, A. J., Asael, D., Gueguen, B., McCrow,
3651 J., Gill, B. C., Owens, J., Rainbird, R. H., Rooney, A. D., Zhao, M. Y., Stueeken, E. E., Konhauser,
3652 K. O., John, S. G., Lyons, T. W., & Planavsky, N. J. (2018). Tracking the rise of eukaryotes to
3653 ecological dominance with zinc isotopes. *Geobiology*, **16**, 341–352.
- 3654 Ivanochko, T. S. (2001). Productivity influences on oxygenation of the Santa Barbara Basin, California,
3655 during the Late Quaternary (Doctoral dissertation, University of British Columbia).
- 3656 Jaccard, S. L., Haug, G. H., Sigman, D. M., Pedersen, T. F., Thierstein, H. R., & Röhl, U. (2005).
3657 Glacial/interglacial changes in subarctic North Pacific stratification. *Science*, **308**(5724), 1003-
3658 1006.

- 3659 Jaccard, S. L., Hayes, C. T., Martínez-García, A., Hodell, D. A., Anderson, R. F., Sigman, D. M., & Haug,
3660 G. H. (2013). Two modes of change in Southern Ocean productivity over the past million years.
3661 *Science*, **339**(6126), 1419-1423.
- 3662 Jacobs, L., & Emerson, S. (1982). Trace metal solubility in an anoxic fjord. *Earth Planet. Sci. Lett.*, **60**,
3663 237-252, doi:10.1016/0012-821X(82)90006-1.
- 3664 Jacobs, L., Emerson, S., & Skei, J. (1985). Partitioning and transport of metals across the O₂H₂S
3665 interface in a permanently anoxic basin: Framvaren Fjord, Norway. *Geochim. Cosmochim. Acta*,
3666 **49**, 1433-1444, doi:10.1016/0016-7037(85)90293-5.
- 3667 Jacquet, S. H., Dehairs, F., Elskens, M., Savoye, N., & Cardinal, D. (2007). Barium cycling along WOCE
3668 SR3 line in the Southern Ocean. *Mar. Chem.*, **106**(1-2), 33-45.
- 3669 Jacquot, J. E., & Moffett, J. W. (2015). Copper distribution and speciation across the International
3670 GEOTRACES Section GA03. *Deep Sea Res. Pt. II*, **116**, 187-207, doi:10.1016/j.dsr2.2014.11.013.
- 3671 Jakuba, R. W., Saito, M. A., Moffett, J. W., & Xu, Y. (2012). Dissolved zinc in the subarctic North Pacific
3672 and Bering Sea: Its distribution, speciation, and importance to primary producers. *Global
3673 Biogeochem. Cycles*, **26**, 1–15.
- 3674 Janssen, D. J., & Cullen, J. T. (2015). Decoupling of zinc and silicic acid in the subarctic northeast Pacific
3675 interior. *Mar. Chem.*, **177**, 124–133. <http://dx.doi.org/10.1016/j.marchem.2015.03.014>.
- 3676 Janssen, D. J., Conway, T. M., John, S. G., Christian, J. R., Kramer, D. I., Pedersen, T. F., & Cullen, J. T.
3677 (2014). Undocumented water column sink for cadmium in open ocean oxygen-deficient zones.
3678 *Proc. Natl. Acad. Sci.*, **111**(19), 6888-6893.
- 3679 Janssen, D. J., Abouchami, W., Galer, S. J. G., & Cullen, J. T. (2017). Fine-scale spatial and interannual
3680 cadmium isotope variability in the subarctic northeast Pacific. *Earth Planet. Sci. Lett.*, **472**, 241-
3681 252.
- 3682 Janssen, D. J., Abouchami, W., Galer, S. J., Purdon, K. B., & Cullen, J. T. (2019). Particulate cadmium
3683 stable isotopes in the subarctic northeast Pacific reveal dynamic Cd cycling and a new isotopically
3684 light Cd sink. *Earth Planet. Sci. Lett.*, **515**, 67-78.
- 3685 Janssen, D. J., Rickli, J., Quay, P. D., White, A. E., Nasemann, P., & Jaccard, S. L. (2020).
3686 Biological control of chromium redox and stable isotope composition in the surface ocean. *Glob.
3687 Biogeochem. Cycles*, **34**, doi:10.1029/2019GB006397.
- 3688 Jeandel, C. & Minster, J. F. (1987). Chromium behavior in the ocean: global versus regional
3689 processes. *Global Biogeochem. Cycles*, **1**, 131–154, doi:10.1029/GB001i002p0013.
- 3690 John, S. G., & Conway, T. M. (2014). A role for scavenging in the marine biogeochemical cycling of zinc
3691 and zinc isotopes. *Earth Planet. Sci. Lett.*, **394**, 159-167.
- 3692 John, S. G., Geis R. W., Saito M. A., & Boyle E. A. (2007). Zinc isotope fractionation during high affinity
3693 and low-affinity zinc transport by the marine diatom *Thalassiosira oceanica*. *Limnol. Oceanogr.*,
3694 **52**, 2710–2714.
- 3695 John, S. G., Mendez, J., Moffett, J., & Adkins, J. (2012). The flux of iron and iron isotopes from San Pedro
3696 Basin sediments. *Geochim. Cosmochim. Acta*, **93**, 14-29.
- 3697 John, S. G., Kunzmann, M., Townsend, E. J., & Rosenberg, A. D. (2017). Zinc and cadmium stable isotopes
3698 in the geological record: A case study from the post-snowball Earth Nuccaleena cap dolostone.
3699 *Palaeogeography, Palaeoclimatology, Palaeoecology*, **466**, 202-208.

- 3700 John, S. G., Helgoe, J., Townsend, E., Weber, T., DeVries, T., Tagliabue, A., Moore, K., Lam, P., Marsay,
3701 C.M., & Till, C. (2018a). Biogeochemical cycling of Fe and Fe stable isotopes in the Eastern
3702 Tropical South Pacific. *Mar. Chem.* **201**, 66-76.
- 3703 John, S. G., Helgoe, J., & Townsend, E. (2018b). Biogeochemical cycling of Zn and Cd and their stable
3704 isotopes in the Eastern Tropical South Pacific. *Mar. Chem.*, **201**, 256-262.
- 3705 Johnson, C.M., Skulan, J.L., Beard, B. L., Sun, H., Neelson, K. H., & Braterman, P. S. (2002). Isotopic
3706 fractionation between Fe(III) and Fe(II) in aqueous solutions. *Earth. Planet. Sci. Lett.*, **195**, 141–
3707 153. [https://doi.org/10.1016/S0012-821X\(01\)00581-7](https://doi.org/10.1016/S0012-821X(01)00581-7).
- 3708 Johnson, C. M., Beard, B. L., & Roden, E. E. (2008). The iron isotope fingerprints of redox and
3709 biogeochemical cycling in modern and ancient Earth. *Annu. Rev. Earth Planet. Sci.*, **36**, 457-493.
- 3710 Johnson, C. M., Beard, B. L., & Weyer, S. (2020). *Iron Geochemistry: An Isotopic Perspective*. Springer.
3711 doi:10.1007/978-3-030-33828-2.
- 3712 Joung, D. J., and Shiller, A. M. (2016). Temporal and spatial variations of dissolved and colloidal trace
3713 elements in Louisiana Shelf waters. *Mar. Chem.* **181**, 25–43, doi:10.1016/j.marchem.2016.03.003.
- 3714 Jullion, L., Jacquet, S. H. M., & Tanhua, T. (2017). Untangling biogeochemical processes from the impact
3715 of ocean circulation: First insight on the Mediterranean dissolved barium dynamics. *Global
3716 Biogeochem. Cycles*, **31**(8), 1256-1270.
- 3717 Kellogg, M. M., McIlvin, M. R., Vedamati, J., Twining, B. S., Moffett, J. W., Marchetti, A., Moran, D. M.,
3718 & Saito, M. A. (2020). Efficient zinc/cobalt inter-replacement in northeast Pacific diatoms and
3719 relationship to high surface dissolved Co: Zn ratios. *Limnol. Oceanogr.* doi:10.1002/lno.11471.
- 3720 Kendall, B., Komiya, T., Lyons, T. W., Bates, S. M., Gordon, G. W., Romaniello, S. J., Jiang, G., Creaser,
3721 R. A., Xiao, S., McFadden, K., Sawaki, Y., Tahata, M., Shu, D., Han, J., Li, Y., Chu, X., & Anbar,
3722 A. D. (2015). Uranium and molybdenum isotope evidence for an episode of widespread ocean
3723 oxygenation during the late ediacaran period. *Geochim. Cosmochim. Acta*, **156**, 173–193,
3724 doi:10.1016/j.gca.2015.02.025.
- 3725 Kendall, B., Dahl, T. W., & Anbar, A. D. (2017). The Stable Isotope Geochemistry of Molybdenum. *Rev.
3726 Min. Geochem.*, **82**, 683–732, doi:10.2138/rmg.2017.82.16.
- 3727 Khatiwala, S., Schmittner, A., & Muglia, J. (2019). Air-sea disequilibrium enhances ocean carbon storage
3728 during glacial periods. *Science Advances*, **5**(6), eaaw4981.
- 3729 Kieber, R. J., & Helz, G. R. (1992). Indirect photoreduction of aqueous chromium (VI). *Environ.
3730 Sci. Technol.*, **26**, 307–312, doi:10.1021/es00026a010.
- 3731 Kienast, S. (2003). Palaeoceanography of the mid-latitude North East Pacific: during the late Pleistocene
3732 (Doctoral dissertation, University of British Columbia).
- 3733 Kim, C., Zhou, Q., Deng, B., Thornton, E. C., & Xu, H. (2001). Chromium(VI) Reduction by
3734 Hydrogen Sulfide in Aqueous Media: Stoichiometry and Kinetics. *Environ. Sci. Technol.*, **35**(11),
3735 2219-2225, doi:10.1021/es0017007.
- 3736 Kim, T., Obata, H., Kondo, Y., Ogawa, H., & Gamo, T. (2015). Distribution and speciation of dissolved
3737 zinc in the western North Pacific and its adjacent seas. *Mar. Chem.*, **173**, 330–341.
3738 <http://dx.doi.org/10.1016/j.marchem.2014.10.016>.
- 3739 King, E. K., Thompson, A., Hodges, C., & Pett-Ridge, J. C. (2014). Towards Understanding Temporal and
3740 Spatial Patterns of Molybdenum in the Critical Zone. *Procedia Earth and Planetary Science*, **10**,
3741 56–62, doi:10.1016/j.proeps.2014.08.011.

- 3742 King, E. K., Thompson, A., Chadwick, O. A., & Pett-Ridge, J. C. (2016). Molybdenum sources and isotopic
3743 composition during early stages of pedogenesis along a basaltic climate transect. *Chem. Geol.*, **445**,
3744 54–67, doi:10.1016/j.chemgeo.2016.01.024.
- 3745 King, E. K., Perakis, S. S., & Pett-Ridge, J. C. (2018). Molybdenum isotope fractionation during adsorption
3746 to organic matter. *Geochim. Cosmochim. Acta*, **222**, 584–598, doi:10.1016/j.gca.2017.11.014.
- 3747 Klar, J. K., James, R. H., Gibbs, D., Lough, A., Parkinson, I., Milton, J. A., Hawkes, J. A., & Connelly, D.
3748 P. (2017a). Isotopic signature of dissolved iron delivered to the Southern Ocean from hydrothermal
3749 vents in the East Scotia Sea. *Geology*, **45**(4), 351-354. <https://doi.org/10.1130/G38432.1>.
- 3750 Klar, J. K., Homoky, W. B., Statham, P. J., Birchill, A. J., Harris, E. L., Woodward, E. M. S., Silburn, B.,
3751 Cooper, M. J., James, R. H., Connelly, D. P., Chever, F., Lichtschlag, A., & Graves, C. (2017b).
3752 Stability of dissolved and soluble Fe(II) in shelf sediment pore waters and release to an oxic water
3753 column. *Biogeochem.*, **135**, 1-19. <https://doi.org/10.1007/s10533-017-0309-x>.
- 3754 Klar, J. K., Schlosser, C., Milton, J. A., Woodward, E. M. S., Lacan, F., Parkinson, I. J., Achterberg, E., &
3755 James, R. H. (2018). Sources of dissolved iron to oxygen minimum zone waters on the Senegalese
3756 continental margin in the tropical North Atlantic Ocean: Insights from iron isotopes. *Geochim.
3757 Cosmochim. Acta*, **236**, 60-78. <https://doi.org/10.1016/j.gca.2018.02.031>.
- 3758 Klinkhammer, G. P. (1980). Early diagenesis in sediments from the eastern equatorial Pacific, II. Pore water
3759 metal results. *Earth Planet. Sci. Lett.*, **49**(1), 81-101.
- 3760 Klunder, M. B., Laan, P., Middag, R., De Baar, H. J. W., & van Ooijen, J. C. (2011). Dissolved iron in the
3761 Southern Ocean (Atlantic sector). *Deep Sea Res. Pt. II*, **58**, 2678-2694,
3762 doi:10.1016/j.dsr2.2010.10.042.
- 3763 Köbberich, M., & Vance, D. (2017). Kinetic control on Zn isotope signatures recorded in marine diatoms.
3764 *Geochim. Cosmochim. Acta*, **210**, 97–113. <http://dx.doi.org/10.1016/j.gca.2017.04.014>.
- 3765 Köbberich, M., & Vance, D. (2019). Zn isotope fractionation during uptake into marine phytoplankton:
3766 Implications for oceanic zinc isotopes. *Chem. Geol.*, **523**, 154-161,
3767 doi:10.1016/j.chemgeo.2019.04.004.
- 3768 Koide, M., Hodge, V.F., Yang, J.S., Stallard, M., & Goldberg, E.G. (1986). Some comparative marine
3769 chemistries of rhenium, gold, silver and molybdenum. *Appl. Geochem.*, **1**, 705-714.
- 3770 Konhauser, K. O., Pecoits, E., Lalonde, S. V., Papineau, D., Nisbet, E. G., Barley, M. E., Arndt, N. T.,
3771 Zahnle, K., & Kamber, B. S. (2009). Oceanic nickel depletion and a methanogen famine before the
3772 Great Oxidation Event. *Nature*, **458**(7239), 750-753.
- 3773 Koschinsky, A., & Halbach, P. (1995). Sequential leaching of marine ferromanganese precipitates: Genetic
3774 implications. *Geochim. Cosmochim. Acta*, **59**(24), 5113-5132.
- 3775 Koschinsky, A., & Hein, J. R. (2003). Uptake of elements from seawater by ferromanganese crusts: solid-
3776 phase associations and seawater speciation. *Mar. Geol.*, **198**(3-4), 331-351.
- 3777 Kowalski, N., Dellwig, O., Beck, M., Gräwe, U., Neubert, N., Nägler, T. F., Badewien, T. H., Brumsack,
3778 H. J., van Beusekom, J. E. E., & Böttcher, M. E. (2013). Pelagic molybdenum concentration
3779 anomalies and the impact of sediment resuspension on the molybdenum budget in two tidal systems
3780 of the North Sea. *Geochim. Cosmochim. Acta*, **119**, 198–211, doi:10.1016/j.gca.2013.05.046.
- 3781 Kramer, D., Cullen, J. T., Christian, J. R., Johnson, W. K., & Pedersen, T. F. (2011). Silver in the subarctic
3782 northeast Pacific Ocean: Explaining the basin scale distribution of silver. *Mar. Chem.*, **123**, 133-
3783 142.

- 3784 Kurisu, M., Takahashi, Y., Iizuka, T. & Uematsu, M. (2016a). Very low isotope ratio of iron in fine aerosols
3785 related to its contribution to the surface ocean. *J. Geophys. Res. Atmos.* **121**, 11,119–11,136.
3786 <https://doi.org/10.1002/2016JD024957>.
- 3787 Kurisu, M., Sakata, K., Miyamoto, C., Takaku, Y., Iizuka, T., & Takahashi, Y. (2016b). Variation of iron
3788 isotope ratios in anthropogenic materials emitted through combustion processes. *Chem. Lett.* **45**,
3789 970–972 (2016). <https://doi.org/10.1246/cl.160451>.
- 3790 Kunzmann, M., Halverson, G. P., Sossi, P. A., Raub, T. D., Payne, J. L., & Kirby, J. (2013). Zn isotope
3791 evidence for immediate resumption of primary productivity after snowball Earth. *Geology*, **41**, 27–
3792 30.
- 3793 Labatut, M., Lacan, F., Pradoux, C., Chmeleff, J., Radic, A., Murray, J. W., Poitrasson, F., Johansen, A.
3794 M., & Thil, F. (2014). Iron sources and dissolved-particulate interactions in the seawater of the
3795 Western Equatorial Pacific, iron isotope perspectives. *Global Biogeochem. Cycles* **28**, 1044-1065.
- 3796 Lacan, F., Francois, R., Ji, Y., & Sherrell, R. M. (2006). Cadmium isotopic composition in the ocean.
3797 *Geochim. Cosmochim. Acta*, **70**(20), 5104-5118.
- 3798 Lacan, F., Radic, A., Jeandel, C., Poitrasson, F., Sarthou, G., Pradoux, C., & Freydier, R. (2008).
3799 Measurement of the isotopic composition of dissolved iron in the open ocean. *Geophys. Res. Lett.*,
3800 **35**, L24610, doi:10.1029/2008GL035841.
- 3801 Lal, D., Charles, C., Vacher, L., Goswami, J. N., Jull, A. J. T., McHargue, L., & Finkel, R. C. (2006). Paleo-
3802 ocean chemistry records in marine opal: Implications for fluxes of trace elements, cosmogenic
3803 nuclides (Be-10 and Al-26), and biological productivity. *Geochim. Cosmochim. Acta* **70**, 3275-
3804 3289.
- 3805 Lam, P. J., & Marchal, O. (2015). Insights into particle cycling from thorium and particle data. *Annual*
3806 *Review of Marine Science*, **7**, 159-184.
- 3807 Lambelet, M., Rehkämper, M., van de Flierdt, T., Xue, Z., Kreissig, K., Coles, B., Porcelli, D., &
3808 Andersson, P. (2013). Isotopic analysis of Cd in the mixing zone of Siberian rivers with the Arctic
3809 Ocean—New constraints on marine Cd cycling and the isotope composition of riverine Cd. *Earth*
3810 *Planet. Sci. Lett.*, **361**, 64-73.
- 3811 Lane, T. W., Saito, M. A., George, G. N., Pickering, I. J., Prince, R. C., & Morel, F. M. (2005).
3812 Biochemistry: a cadmium enzyme from a marine diatom. *Nature*, **435**(7038), 42.
- 3813 Lauderdale, J. M., Braakman, R., Forget, G., Dutkiewicz, S., & Follows, M. J. (2020). Microbial feedbacks
3814 optimize ocean iron availability. *Proc. Natl. Acad. Sci.*, **117**(9), 4842-4849.
- 3815 Lea, D. W., Shen, G. T., & Boyle, E. A. (1989). Coralline barium records temporal variability in equatorial
3816 Pacific upwelling. *Nature*, **340**(6232), 373-376.
- 3817 Lee, J. G., & Morel, F. M. M. (1995). Replacement of zinc by cadmium in marine phytoplankton. *Mar.*
3818 *Ecol. Prog. Ser.*, **127**, 305–309.
- 3819 Lemaitre, N., de Souza, G. F., Archer, C., Wang, R. M., Planquette, H., Sarthou, G., & Vance, D. (2020).
3820 Pervasive sources of isotopically light zinc in the North Atlantic Ocean. *Earth Planet. Sci. Lett.*,
3821 **539**, doi:10.1016/j.epsl.2020.116216.
- 3822 Lerner, P., Marchal, O., Lam, P. J., & Solow, A. (2018). Effects of particle composition on thorium
3823 scavenging in the North Atlantic. *Geochimica et Cosmochimica Acta*, **233**, 115-134.
- 3824 Le Roy, E. L., Sanial, V., Charette, M. A., van Beek, P., Lacan, F., Jacquet, S. H., Henderson, P.
3825 B., Souhaut, M., García-Ibáñez, M. I., Jeandel, C., Pérez, F. F., & Sarthou, G. (2018). The ²²⁶Ra–
3826 Ba relationship in the North Atlantic during GEOTRACES-GA01. *Biogeosciences*, **15**(9), 3027-
3827 3048.

- 3828 Levasseur, S., Frank, M., Hein, J. R., & Halliday, A. N. (2004). The global variation in the iron
3829 isotope composition of marine hydrogenetic ferromanganese deposits: implications for seawater
3830 chemistry? *Earth Planet. Sci. Lett.*, **224**(1-2), 91-105.
- 3831 Liao, W. H., & Ho, T. Y. (2018). Particulate trace metal composition and sources in the Kuroshio adjacent
3832 to the East China Sea: The importance of aerosol deposition. *Journal of Geophysical Research:
3833 Oceans*, **123**(9), 6207-6223.
- 3834 Liao, W. H., Takano, S., Yang, S. C., Huang, K. F., Sohrin, Y., & Ho, T. Y. (2020). Zn isotope composition
3835 in the water column of the Northwestern Pacific Ocean: the importance of external sources. *Global
3836 Biogeochem. Cycles*, **34**(1), e2019GB006379.
- 3837 Liermann, L. J., Guynn, R. L., Anbar, A., & Brantley, S. L. (2005). Production of a molybdophore during
3838 metal-targeted dissolution of silicates by soil bacteria. *Chem. Geol.*, **220**, 285–302,
3839 doi:10.1016/j.chemgeo.2005.04.013.
- 3840 Little, S.H., Vance, D., Siddall, M. and Gasson, E. (2013). A modeling assessment of the role of reversible
3841 scavenging in controlling oceanic dissolved Cu and Zn distributions. *Global Biogeochem. Cycles*
3842 **27**(3), 780-791.
- 3843 Little, S.H., Sherman, D.M., Vance, D. and Hein, J.R. (2014a). Molecular controls on Cu and Zn isotopic
3844 fractionation in Fe–Mn crusts. *Earth Planet. Sci. Lett.* **396**, 213-222.
- 3845 Little, S. H., Vance, D., Walker-Brown, C., & Landing, W. M. (2014b). The oceanic mass balance of copper
3846 and zinc isotopes, investigated by analysis of their inputs, and outputs to ferromanganese oxide
3847 sediments. *Geochim. Cosmochim. Acta* **125**, 673–693.
- 3848 Little, S. H., Vance, D., Lyons, T. W., & McManus, J. (2015). Controls on trace metal authigenic
3849 enrichment in reducing sediments: insights from modern oxygen-deficient settings. *Am. J. Sci.*,
3850 **315**(2), 77-119.
- 3851 Little, S. H., Vance, D., McManus, J., & Severmann, S. (2016). Key role of continental margin sediments
3852 in the oceanic mass balance of Zn and Zn isotopes. *Geology*, **44**, 207–210.
- 3853 Little, S. H., van de Flierdt, T., Rehkämper, M., Wilson, D. J., Adkins, J. F., & Robinson, L. F. (2017a).
3854 Deep sea corals as archives of seawater Zn isotopes. In *Goldschmidt Abstracts*, p. 2387.
- 3855 Little, S.H., Vance, D., McManus, J., Severmann, S. and Lyons, T.W. (2017b). Copper isotope signatures
3856 in modern marine sediments. *Geochim. Cosmochim. Acta*, **212**, 253-273.
- 3857 Little, S. H., Archer, C., Milne, A., Schlosser, C., Achterberg, E. P., Lohan, M. C., & Vance, D. (2018).
3858 Paired dissolved and particulate phase Cu isotope distributions in the South Atlantic. *Chem. Geol.*
3859 **502**, 29-43.
- 3860 Little, S.H., Archer, C., McManus, J., Najorka, J., Wegorzewski, A.V. and Vance, D. (2020). Towards
3861 balancing the oceanic Ni budget. *Earth Planet. Sci. Lett.* **547**, p.116461.
- 3862 Liu, R., Guo, B., Wang, M., Li, W., Yang, T., Ling, H., & Chen, T. (2020). Isotopic fingerprinting of
3863 dissolved iron sources in the deep western Pacific since the late Miocene. *Science China Earth
3864 Sciences*, **63**, doi:10.1007/s11430-020-9648-6.
- 3865 Liu, S. A., Wu, H., Shen, S. Z., Jiang, G., Zhang, S., Lv, Y., Zhang, H., & Li, S. (2017). Zinc isotope
3866 evidence for intensive magmatism immediately before the end-Permian mass extinction. *Geology*,
3867 **45**, 343–346.
- 3868 Liu, X., & Millero, F. J. (2002). The solubility of iron in seawater. *Mar. Chem.*, **77**(1), 43-54.

- 3869 Liu, Y., Li, X., Zeng, Z., Yu, H. M., Huang, F., Felis, T., & Shen, C. C. (2019). Annually-resolved coral
3870 skeletal $\delta^{138/134}\text{Ba}$ records: A new proxy for oceanic Ba cycling. *Geochim. Cosmochim. Acta*, **247**,
3871 27-39.
- 3872 Lohan, M. C., Crawford, D. W., Purdie, D. A., & Statham, P. J. (2005). Iron and Zinc Enrichments in the
3873 Northeastern Subarctic Pacific: Ligand Production and Zinc Availability in Response to
3874 Phytoplankton Growth. *Limnol. Oceanogr.*, **50**, 1427–1437.
- 3875 Lough, A. J. M., Klar, J. K., Homoky, W. B., Comer-Warner, S. A., Milton, J. A., Connelly, D. P., James,
3876 R. H., & Mills, R. A. (2017). Opposing authigenic controls on the isotopic signature of dissolved
3877 iron in hydrothermal plumes. *Geochim. Cosmochim. Acta*, **202**, 1-20.
- 3878 Lv, Y., Liu, S. A., Wu, H., Hohl, S. V., Chen, S., & Li, S. (2018). Zn-Sr isotope records of the Ediacaran
3879 Doushantuo Formation in South China: diagenesis assessment and implications. *Geochim.*
3880 *Cosmochim. Acta*, **239**, 330-345.
- 3881 Lyons, T. W., Anbar, A. D., Severmann, S., Scott, C., & Gill, B. C. (2009). Tracking Euxinia in the Ancient
3882 Ocean: A Multiproxy Perspective and Proterozoic Case Study. *Annu. Rev. Earth Planet. Sci.*, **37**,
3883 507–534, doi:10.1146/annurev.earth.36.031207.124233.
- 3884 Lyons, T. W., Severmann, S. (2006). A critical look at iron paleoredox proxies: New insights from modern
3885 euxinic marine basins. *Geochim. Cosmochim. Acta*, **70**(23), 5698-5722.
- 3886 Ma, Z., Gray, E., Thomas, E., Murphy, B., Zachos, J., & Paytan, A. (2014). Carbon sequestration during
3887 the Palaeocene–Eocene Thermal Maximum by an efficient biological pump. *Nat. Geosci.*, **7**(5),
3888 382.
- 3889 Ma, Z., Ravelo, A. C., Liu, Z., Zhou, L., & Paytan, A. (2015). Export production fluctuations in the eastern
3890 equatorial Pacific during the Pliocene-Pleistocene: Reconstruction using barite accumulation rates.
3891 *Paleoceanography*, **30**(11), 1455-1469.
- 3892 Mahaffey, C., Reynolds, S., Davis, C. E., & Lohan, M. C. (2014). Alkaline phosphatase activity in the
3893 subtropical ocean: insights from nutrient, dust and trace metal addition experiments. *Front. Mar.*
3894 *Sci.*, **1**, 1–13.
- 3895 Maldonado, M. T., Allen, A. E., Chong, J. S., Lin, K., Leus, D., Karpenko, N., & Harris, S. L. (2006).
3896 Copper-dependent iron transport in coastal and oceanic diatoms. *Limnol. Oceanogr.* **51**, 1729–
3897 1743.
- 3898 Maret, W. Zinc biochemistry, physiology, and homeostasis – recent insights and current trends. *Biometals*
3899 **14**, 187–190 (2001). <https://doi.org/10.1023/A:1012945110820>
- 3900 Marchitto, T. M., Curry, W. B., & Oppo, D. W. (2000) Zinc concentrations in benthic foraminifera reflect
3901 seawater chemistry. *Paleoceanography*, **15**, 299–306.
- 3902 Marcus, M. A., Edwards, K. J., Gueguen, B., Fakra, S. C., Horn, G., Jelinski, N. A., Rouxel, O., Sorensen,
3903 J., & Toner, B. M. (2015). Iron mineral structure, reactivity, and isotopic composition in a South
3904 Pacific Gyre ferromanganese nodule over 4 Ma. *Geochim. Cosmochim. Acta*, **171**, 61-79.
- 3905 Maréchal, C. N., Nicolas, E., Douchet, C., & Albarède, F. (2000). Abundance of zinc isotopes as a marine
3906 biogeochemical tracer. *Geochem. Geophys. Geosyst.*, **1**, 1015,
3907 <http://doi.wiley.com/10.1029/1999GC000029>.
- 3908 Marks, J. A., Perakis, S. S., King, E. K., & Pett-Ridge, J. (2015). Soil organic matter regulates molybdenum
3909 storage and mobility in forests. *Biogeochemistry*, **125**, 167–183, doi:10.1007/s10533-015-0121-4.
- 3910 Marsay, C. M., Lam, P. J., Heller, M. I., Lee, J. M., & John, S. G. (2018). Distribution and isotopic signature
3911 of ligand-leachable particulate iron along the GEOTRACES GP16 East Pacific Zonal Transect.
3912 *Mar. Chem.*, **201**, 198-211.

- 3913 Martin, J. H. (1990). Glacial-interglacial CO₂ change: the iron hypothesis. *Paleoceanography* **5**, 1-13.
- 3914 Martin, J. H., & Fitzwater, S. E. (1988). Iron deficiency limits phytoplankton growth in the north-east
3915 Pacific subarctic. *Nature*, **331**(6154), 341-343.
- 3916 Martin, J. H., Fitzwater, S. E., & Gordon, R. M. (1990). Iron deficiency limits phytoplankton growth in
3917 Antarctic waters. *Global Biogeochem. Cycles*, **4**(1), 5-12.
- 3918 Martin, J. H., Knauer, G. A. and Gordon, R. M. (1983) Silver distributions and fluxes in north-east Pacific
3919 waters. *Nature*, **305**, 306-309.
- 3920 Martin, J. M., & Thomas, A. J. (1994). The global insignificance of telluric input of dissolved trace metals
3921 (Cd, Cu, Ni and Zn) to ocean margins. *Mar. Chem.*, **46**(1-2), 165-178.
- 3922 Martin, J. H., Knauer, G. A., Karl, D. M., & Broenkow, W. W. (1987). VERTEX: carbon cycling in the
3923 northeast Pacific. *Deep Sea Res. Part A*, **34**(2), 267-285.
- 3924 Martínez-García, A., Rosell-Melé, A., Jaccard, S. L., Geibert, W., Sigman, D. M., & Haug, G. H. (2011).
3925 Southern Ocean dust–climate coupling over the past four million years. *Nature*, **476**(7360), 312-
3926 315.
- 3927 Martínez-García, A., Sigman, D. M., Ren, H., Anderson, R. F., Straub, M., Hodell, D. A., et al. (2014). Iron
3928 fertilization of the Subantarctic Ocean during the last ice age. *Science*, **343**, 1347-1350,
3929 doi:10.1126/science.1246848.
- 3930 Martínez-Ruiz, F., Paytan, A., González-Muñoz, M. T., Jroundi, F., Abad, M. M., Lam, P. J., Bishop, J. K.
3931 B., Horner, T. J., Morton, P. L., & Kastner, M. (2019). Barite formation in the ocean: Origin of
3932 amorphous and crystalline precipitates. *Chem. Geol.*, **511**, 441-451.
- 3933 Martínez Ruiz, F. C., Paytan, A., González Muñoz, M. T., Jroundi, F., Abad, M. D. M., Lam, P. J., Horner,
3934 T.J., & Kastner, M. (2020). Barite precipitation on suspended organic matter in the mesopelagic
3935 zone. *Front. Earth Sci.* **8**:567714. doi:10.3389/feart.2020.567714
- 3936 Mathur, R., Arribas, A., Megaw, P., Wilson, M., Stroup, S., Meyer-Arrivillaga, D., & Arribas, I. (2018).
3937 Fractionation of silver isotopes in native silver explained by redox reactions. *Geochim. Cosmochim.*
3938 *Acta*, **224**, 313-326.
- 3939 Mawji, E. et al. (2015). The GEOTRACES Intermediate Data Product 2014. *Mar. Chem.*, **177**, 1-8,
3940 doi:10.1016/j.marchem.2015.04.005.
- 3941 Mayfield, K. K., Eisenhauer, A., Santiago Ramos, D., Higgins, J. A., Horner, T. J., Auro, M. E., Magna,
3942 T., Moosdorf, N., Charette, M. A., Gonnea, M. E., Brady, C. E., Komar, N., Peucker-Ehrenbrink,
3943 B., & Paytan, A. (2021) Groundwater discharge impacts marine isotope budgets of Li, Mg, Ca, Sr,
3944 and Ba. *Nat. Commun.* **12**, 148, doi:10.1038/s41467-020-20248-3.
- 3945 McKay, J. L., & Pedersen, T. F. (2008). The accumulation of silver in marine sediments: A link to biogenic
3946 Ba and marine productivity. *Global Biogeochem. Cycles*, **22**, GB4010,
3947 doi:10.1029/2007GB003136
- 3948 McManus, J., Berelson, W. M., Klinkhammer, G. P., Johnson, K. S., Coale, K. H., Anderson, R. F., Kumar,
3949 N., Burdige, D. J., Hammond, D. E., Brumsack, H. J., McCorkle, D. C., & Rusdhi, A. (1998).
3950 Geochemistry of barium in marine sediments: Implications for its use as a paleoproxy. *Geochim.*
3951 *Cosmochim. Acta*, **62**(21-22), 3453-3473.
- 3952 McManus, J., Dymond, J., Dunbar, R. B., & Collier, R. W. (2002). Particulate barium fluxes in the Ross
3953 Sea. *Mar. Geol.*, **184**(1-2), 1-15.
- 3954 McManus, J., Berelson, W. M., Severmann, S., Poulson, R. L., Hammond, D. E., Klinkhammer, G. P., &
3955 Holm, C. (2006). Molybdenum and uranium geochemistry in continental margin sediments:

- 3956 Paleoproxy potential. *Geochim. Cosmochim. Acta*, **70**, 4643–4662,
3957 doi:10.1016/j.gca.2006.06.1564.
- 3958 Mead, C., Herckes, P., Majestic, B. J., & Anbar, A. D. (2013). Source apportionment of aerosol iron in the
3959 marine environment using iron isotope analysis. *Geophys. Res. Lett.*, **40**(21), 5722–5727.
- 3960 Mendel, R. R., & Bittner, F. (2006) Cell biology of molybdenum. *Biochim. Biophys. Acta*, **1763**(7), 621-
3961 635, doi:10.1016/j.bbamcr.2006.03.013.
- 3962 Middag, R., van Heuven, S. M., Bruland, K. W., & de Baar, H. J. (2018). The relationship between cadmium
3963 and phosphate in the Atlantic Ocean unraveled. *Earth Planet. Sci. Lett.*, **492**, 79–88.
- 3964 Middag, R., de Baar, H. J. W., & Bruland, K. W. (2019). The relationships between dissolved zinc and
3965 major nutrients phosphate and silicate along the GEOTRACES GA02 transect in the west Atlantic
3966 Ocean. *Global Biogeochem. Cycles*, **33**, 63–84, doi:10.1029/2018GB006034.
- 3967 Middleton, J. L., Langmuir, C. H., Mukhopadhyay, S., McManus, J. F., & Mitrovica, J. X. (2016).
3968 Hydrothermal iron flux variability following rapid sea level changes. *Geophys. Res. Lett.*, **43**, 3848-
3969 3856.
- 3970 Miller, C. A., Peucker-Ehrenbrink, B., Walker, B. D., & Marcantonio, F. (2011). Re-assessing the surface
3971 cycling of molybdenum and rhenium. *Geochim. Cosmochim. Acta*, **75**, 7146–7179,
3972 doi:10.1016/j.gca.2011.09.005.
- 3973 Miller, L. A., & Bruland, K. W. (1995). Organic speciation of silver in marine waters. *Environ. Sci.*
3974 *Technol.*, **29**, 2616–2621.
- 3975 Milletto, M., Wang, X., Planavsky, N. J., Luther, G. W., Lyons, T. W., & Tebo, B. M. (2021).
3976 Marine microbial Mn(II) oxidation mediates Cr(III) oxidation and isotope fractionation. *Geochim.*
3977 *Cosmochim. Acta*, **297**, 101–119, doi:10.1016/j.gca.2021.01.008.
- 3978 Misumi, K., Lindsay, K., Moore, J. K., Doney, S. C., Bryan, F. O., Tsumune, D., & Yoshida, Y. (2014).
3979 The iron budget in ocean surface waters in the 20th and 21st centuries: projections by the
3980 Community Earth System Model version. *Biogeosciences*, **11**, 33–55.
- 3981 Mitra, R. Marchitto, T. M., Ge, Q., Zhong, B., Kanakiya, B., Cook, M. S., Fehrenbacher, J. S., Ortiz, J. D.,
3982 Tripathi, A., & Lobaton, E. (2019). Automated species-level identification of planktic foraminifera
3983 using convolutional neural networks, with comparison to human performance. *Mar.*
3984 *Micropaleontol.* **147**, 16–24.
- 3985 Moeller, K., Schoenberg, R., Pedersen, R. B., Weiss, D., & Dong, S. (2012). Calibration of the new certified
3986 reference materials ERM-AE633 and ERM-AE647 for copper and IRMM-3702 for zinc isotope
3987 amount ratio determinations. *Geostan. Geoanal. Res.* **36**(2), 177–199.
- 3988 Moffett, J. W., & Brand, L. E. (1996). Production of strong, extracellular Cu chelators by marine
3989 cyanobacteria in response to Cu stress. *Limnol. Oceanogr.* **41**, 388–395.
- 3990 Moffett, J. W., & Dupont, C. (2007). Cu complexation by organic ligands in the sub-arctic NW Pacific and
3991 Bering Sea. *Deep. Res. Part I Oceanogr. Res. Pap.* **54**, 586–595.
- 3992 Moffett, J. W., Zika, R. G., & Brand, L. E. (1990). Distribution and potential sources and sinks of copper
3993 chelators in the Sargasso Sea. *Deep Sea Res. Part A, Oceanogr. Res. Pap.* **37**, 27–36.
- 3994 Monnin, C., Jeandel, C., Cattaldo, T., & Dehairs, F. (1999). The marine barite saturation state of the world's
3995 oceans. *Mar. Chem.*, **65**(3–4), 253–261.
- 3996 Moore, C. M., Mills, M. M., Arrigo, K. R., Berman-Frank, I., Bopp, L., Boyd, P. W., Galbraith, E. D.,
3997 Geider, R. J., Guieu, C., Jaccard, S. L., Jickells, T. D., La Roche, J., Lenton, T. M., Mahowald, N.
3998 M., Maranon, E., Marinov, I., Moore, J. K., Nakatsuka, T., Oschlies, A., Saito, M. A., Thingstad,

- 3999 T. F., Tsuda, A., & Ulloa, O. (2013). Processes and patterns of oceanic nutrient limitation. *Nat.*
4000 *Geosci.* **6**, 701-710.
- 4001 Moore, C. M. (2016). Diagnosing oceanic nutrient deficiency. *Philosophical Transactions of the Royal*
4002 *Society A: Mathematical, Physical and Engineering Sciences*, **374**(2081), 20150290.
- 4003 Moos, S. B. & Boyle, E. A. (2019). Determination of accurate and precise chromium isotope ratios
4004 in seawater samples by MC-ICP-MS illustrated by analysis of SAFe Station in the North Pacific
4005 Ocean. *Chem. Geol.*, **511**, 481-493, doi:10.1016/j.chemgeo.2018.07.027.
- 4006 Moos, S. B., Boyle, E. A., Altabet, M. A., & Bourbonnais, A. (2020). Investigating the cycling of
4007 chromium in the oxygen deficient waters of the Eastern Tropical North Pacific Ocean and the Santa
4008 Barbara Basin using stable isotopes. *Mar. Chem.*, **221**, 103756,
4009 doi:10.1016/j.marchem.2020.103756 .
- 4010 Morel, F. M. M., & Price, N. M. (2003). The biogeochemical cycles of trace metals in the oceans. *Science*,
4011 **300**, 944-947, doi:10.1126/science.1083545.
- 4012 Morel, F. M. M., Reinfelder, J. R., Roberts, S. B., Chamberlain, C. P., Lee, J. G., & Yee, D. (1994) Zinc
4013 and carbon co-limitation of marine phytoplankton. *Nature*, **369**, 740-742.
- 4014 Morel, F. M., Lam, P. J., & Saito, M. A. (2020). Trace Metal Substitution in Marine Phytoplankton. *Annual*
4015 *Review of Earth and Planetary Sciences*, **48**.
- 4016 Morford, J. L., Kalnejais, L. H., Helman, P., Yen, G., & Reinard, M. (2008). Geochemical cycling of silver
4017 in marine sediments along an offshore transect. *Mar. Chem.*, **110**, 77-88.
- 4018 Morgan, J. L., Wasylenki, L. E., Nuester, J., & Anbar, A. D. (2010). Fe isotope fractionation during
4019 equilibration of Fe–organic complexes. *Environ. Sci. Technol.*, **44**(16), 6095-6101.
- 4020 Morris, A. W. (1975). Dissolved molybdenum and vanadium in the northeast Atlantic Ocean. *Deep Sea*
4021 *Research and Oceanographic Abstracts*, **22**, 49–54, doi:10.1016/0011-7471(75)90018-2.
- 4022 Moynier, F., Vance, D., Fujii, T., & Savage, P. (2017). The Isotope Geochemistry of Zinc and Copper. *Rev.*
4023 *Mineral. Geochemistry* **82**, 543–600.
- 4024 Mulholland, D.S., Poitrasson, F., Boaventura, G.R., Allard, T., Vieira, L.C., Santos, R.V., Mancini,
4025 L. & Seyler, P. (2015). Insights into iron sources and pathways in the Amazon River provided by
4026 isotopic and spectroscopic studies. *Geochim. Cosmochim. Acta*, **150**, 142–159.
- 4027 Murphy, K. L. (2016). *Isotopic studies in marine geochemistry* (Doctoral dissertation, Imperial College
4028 London), doi:10.25560/68270.
- 4029 Murray, J. W., Spell, B., & Paul, B. (1983). The contrasting geochemistry of manganese and
4030 chromium in the eastern tropical Pacific Ocean. In: Wong C.S., Boyle E., Bruland K.W., Burton
4031 J.D., Goldberg E.D. (eds) *Trace Metals in Sea Water*. NATO Conference Series (IV Marine
4032 Sciences), 9. Springer, Boston, MA, p. 643-669.
- 4033 Nägler, T. F., Neubert, N., Böttcher, M. E., Dellwig, O., & Schnetger, B. (2011). Molybdenum isotope
4034 fractionation in pelagic euxinia: Evidence from the modern Black and Baltic Seas. *Chem. Geol.*,
4035 **289**, 1–11, doi:10.1016/j.chemgeo.2011.07.001.
- 4036 Nägler, T. F., Anbar, A. D., Archer, C., Goldberg, T., Gordon, G. W., Greber, N. D., Seibert, C., Sohrin,
4037 Y., & Vance, D. (2014). Proposal for an international molybdenum isotope measurement standard
4038 and data representation. *Geostand. Geoanal. Res.*, **38**(2), 149-151.
- 4039 Nakagawa, Y., Takano, S., Firdaus, M. L., Norisuye, K., Hirata, T., Vance, D., & Sohrin, Y. (2012). The
4040 molybdenum isotopic composition of the modern ocean. *Geochemical Journal*, **46**, 131–141,
4041 doi:10.2343/geochemj.1.0158.

- 4042 Nameroff, T. J., Calvert, S. E., & Murray, J. W. (2004). Glacial-interglacial variability in the eastern
4043 tropical North Pacific oxygen minimum zone recorded by redox-sensitive trace metals.
4044 *Paleoceanogr. Paleoclim.*, **19**(1), PA1010, doi:10.1029/2003PA000912.
- 4045 Nan, X. Y., Yu, H. M., Rudnick, R. L., Gaschnig, R. M., Xu, J., Li, W.-Y., Zhang, Q., Jin, Z.-D., Li, X.-
4046 H., & Huang, F. (2018). Barium isotopic composition of the upper continental crust. *Geochim.*
4047 *Cosmochim. Acta*, **233**, 33-49.
- 4048 Nasemann, P., Gault-Ringold, M., Stirling, C. H., Koschinsky, A., & Sander, S. G. (2018). Processes
4049 affecting the isotopic composition of dissolved iron in hydrothermal plumes: A case study from the
4050 Vanuatu back-arc. *Chem. Geol.*, **476**, 70-84. <https://doi.org/10.1016/j.chemgeo.2017.11.005>.
- 4051 Nasemann, P., Janssen, D. J., Rickli, J., Grasse, P., Franck, M., & Jaccard, S. L. (2020). Chromium
4052 reduction and associated stable isotope fractionation restricted to anoxic shelf waters in the
4053 Peruvian Oxygen Minimum Zone. *Geochim. Cosmochim. Acta*, **285**, 207-224,
4054 doi:10.1016/j.gca.2020.06.027.
- 4055 Navarrete, J. U., Borrok, D. M., Viveros, M., & Ellzey, J. T. (2011). Copper isotope fractionation during
4056 surface adsorption and intracellular incorporation by bacteria. *Geochim. Cosmochim. Acta*, **75**(3),
4057 784-799.
- 4058 Nishioka, J., Obata, H., Ogawa, H., Ono, K., Yamashita, Y., Lee, K., Takeda, S., & Yasuda, I. (2020).
4059 Subpolar marginal seas fuel the North Pacific through the intermediate water at the termination of
4060 the global ocean circulation. *Proc. Natl Acad. Sci. U. S. A.* **117**(23), 12665-12673
4061 <https://doi.org/10.1073/pnas.2000658117>.
- 4062 Ndung'u, K., Thomas, M.A., & Flegal, A.R. (2001). Silver in the western equatorial and South Atlantic
4063 Ocean. *Deep-Sea Research II*, **48**, 2933-2945.
- 4064 Neubert, N., Nägler, T. F., and Böttcher, M. E. (2008). Sulfidity controls molybdenum isotope fractionation
4065 into euxinic sediments: Evidence from the modern Black Sea. *Geology*, **36**, 775-778,
4066 doi:10.1130/G24959A.1.
- 4067 Nielsen, S. G., Wasylenki, L. E., Rehkämper, M., Peacock, C. L., Xue, Z., & Moon, E. M. (2013). Towards
4068 an understanding of thallium isotope fractionation during adsorption to manganese oxides.
4069 *Geochim. Cosmochim. Acta*, **117**, 252-265.
- 4070 Noordmann, J., Weyer, S., Montoya-Pino, C., Dellwig, O., Neubert, N., Eckert, S., Paetzel, M., & Böttcher,
4071 M. E. (2015). Uranium and molybdenum isotope systematics in modern euxinic basins: Case
4072 studies from the central Baltic Sea and the Kyllaren fjord (Norway). *Chem. Geol.*, **396**, 182-195,
4073 doi:10.1016/j.chemgeo.2014.12.012.
- 4074 Ohnemus, D. C., & Lam, P. J. (2015). Cycling of lithogenic marine particles in the US GEOTRACES North
4075 Atlantic transect. *Deep Sea Res. Pt. II*, **116**, 283-302.
- 4076 Ohnemus, D. C., Rauschenberg, S., Cutter, G. A., Fitzsimmons, J. N., Sherrell, R. M., & Twining, B. S.
4077 (2017). Elevated trace metal content of prokaryotic communities associated with marine oxygen
4078 deficient zones. *Limnol. Oceanog.*, **62**(1), 3-25.
- 4079 Ohnemus, D. C., Torrie, R., & Twining, B. S. (2019). Exposing the Distributions and Elemental
4080 Associations of Scavenged Particulate Phases in the Ocean Using Basin-Scale Multi-Element Data
4081 Sets. *Global Biogeochem. Cycles*, **33**(6), 725-748, doi:10.1029/2018GB006145.
- 4082 Park, H., Song, B., & Morel, F. M. (2007). Diversity of the cadmium-containing carbonic anhydrase in
4083 marine diatoms and natural waters. *Environmental Microbiology*, **9**(2), 403-413.
- 4084 Paytan, A. (2009). Ocean Paleoproductivity. In: Gornitz V. (eds) *Encyclopedia of Paleoclimatology and*
4085 *Ancient Environments*. Encyclopedia of Earth Sciences Series, Springer, Dordrecht.

- 4086 Paytan, A., & Kastner, M. (1996). Benthic Ba fluxes in the central Equatorial Pacific, implications for the
4087 oceanic Ba cycle. *Earth Planet. Sci. Lett.*, **142**(3-4), 439-450.
- 4088 Paytan, A., Kastner, M., & Chavez, F. P. (1996). Glacial to interglacial fluctuations in productivity in the
4089 equatorial Pacific as indicated by marine barite. *Science*, **274**(5291), 1355-1357.
- 4090 Paytan, A., & Griffith, E. M. (2007). Marine barite: Recorder of variations in ocean export productivity.
4091 *Deep Sea Res. Pt. II*, **54**(5-7), 687-705.
- 4092 Paytan, A., Mackey, K. R., Chen, Y., Lima, I. D., Doney, S. C., Mahowald, N., Labiosa, R., & Post, A. F.
4093 (2009). Toxicity of atmospheric aerosols on marine phytoplankton. *Proc. Natl. Acad. Sci.*, **106**(12),
4094 4601-4605.
- 4095 Peers, G., & Price, N. M. (2006). Copper-containing plastocyanin used for electron transport by an oceanic
4096 diatom. *Nature* **441**, 341-344.
- 4097 Peers, G., Quesnel, S., & Price, N. M. (2005). Copper requirements for iron acquisition and growth of
4098 coastal and oceanic diatoms. *Limnol. Oceanogr.* **50**, 1149-1158.
- 4099 Pereira, N. S., Vögelin, A. R., Paulukat, C., Sial, A. N., Ferreira, V. P., & Frei, R. (2016).
4100 Chromium-isotope signatures in scleractinian corals from the Rocas Atoll, Tropical South Atlantic.
4101 *Geobiology*, **14**, 54-67, doi:10.1111/gbi.12155.
- 4102 Pettine, M., Millero, F. J., & La Noce, T. (1991). Chromium (III) interactions in seawater through
4103 its oxidation kinetics. *Mar. Chem.*, **34**(1-2), 29-46.
- 4104 Pettine, M., D'Ottono, L., Campanella, L., Millero, F. J., & Passino, R. (1998). The reduction of
4105 chromium (VI) by iron (II) in aqueous solutions. *Geochim. Cosmochim. Acta*, **62**(9), 1509-1519.
- 4106 Pichat, S., Douchet, C., & Albarède, F. (2003). Zinc isotope variations in deep-sea carbonates from the
4107 eastern equatorial Pacific over the last 175 ka. *Earth Planet. Sci. Lett.*, **210**, 167-178.
- 4108 Pichevin, L. E., Ganeshram, R. S., Geibert, W., Thunell, R., & Hinton, R. (2014). Silica burial enhanced
4109 by iron limitation in oceanic upwelling margins. *Nat. Geosci.*, **7**(7), 541-546.
- 4110 Pinedo-González, P., Hawco, N. J., Bundy, R. M., Virginia Armbrust, E., Follows, M. J., Cael, B. B., White,
4111 A. E., Ferrón, S., Karl, D. M., & John, S. G. (2020). Anthropogenic Asian aerosols provide Fe to
4112 the North Pacific Ocean. *Proc. Natl. Acad. Sci. USA*, **117**, 27862-27868,
4113 doi:10.1073/pnas.2010315117.
- 4114 Plass, A., Schlosser, C., Sommer, S., Dale, A. W., Achterberg, E. P., & Scholz, F. (2020). The control of
4115 hydrogen sulfide on benthic iron and cadmium fluxes in the oxygen minimum zone off Peru.
4116 *Biogeosciences*, **17**(13), 3685-3704.
- 4117 Poitrasson, F. (2006). On the iron isotope homogeneity level of the continental crust. *Chem. Geol.*, **235**(1-
4118 2), 195-200.
- 4119 Poitrasson, F., Vieira, L. C., Seyler, P., dos Santos Pinheiro, G. M., Mulholland, D. S., Bonnet, M. P.,
4120 Martinez, J.-M., Lima, B. A., Boaventura, G. R., Chmeleff, J., Dantas, E. L., Guyot, J.-L., Mancini,
4121 L., Pimentel, M. M., Santos, R. V., Sondag, F., & Vauchel, P. (2014). Iron isotope composition of
4122 the bulk waters and sediments from the Amazon River Basin. *Chem. Geol.*, **377**, 1-11.
- 4123 Pokrovsky, O. S., Viers, J., Emnova, E. E., Kompantseva, E. I., & Freydier, R. (2008). Copper isotope
4124 fractionation during its interaction with soil and aquatic microorganisms and metal oxy (hydr)
4125 oxides: Possible structural control. *Geochim. Cosmochim. Acta*, **72**(7), 1742-1757.
- 4126 Price, N. M., & Morel, F. M. M. (1990). Cadmium and cobalt substitution for zinc in a marine diatom.
4127 *Nature*, **344**(6267), 658.

- 4128 Price, N. M., & Morel, F. M. M. (1991). Colimitation of phytoplankton growth by nickel and nitrogen.
4129 *Limnol. Oceanogr.* **50**, 1071-1077.
- 4130 Quay, P., & Wu, J. (2015). Impact of end-member mixing on depth distributions of $\delta^{13}\text{C}$, cadmium and
4131 nutrients in the N. Atlantic Ocean. *Deep Sea Res. Pt. II*, **116**, 107-116.
- 4132 Radic, A., Lacan, F., & Murray, J. W. (2011). Iron isotopes in the seawater of the equatorial Pacific Ocean:
4133 New constraints for the oceanic iron cycle. *Earth Planet. Sci. Lett.*, **306**, 1-10.
- 4134 Rafter, P. A., Sigman, D. M., & Mackey, K. R. (2017). Recycled iron fuels new production in the eastern
4135 equatorial Pacific Ocean. *Nat. Commun.*, **8**(1), 1100.
- 4136 Ragsdale, S. W. (2009). Nickel-based enzyme systems. *J. Biol. Chem.* **284**, 18571–18575.
- 4137 Ranville, M. A., & Flegal, A.R. (2005). Silver in the North Pacific Ocean. *Geochemistry, Geophysics,*
4138 *Geosystems*, **6**(3), doi:10.1029/2004GC000770
- 4139 Ranville, M. A., Cutter, G. A., Buck, C. S., Landing, W. M., Cutter, L. S., Resing, J. A., & Flegal, A. R.
4140 (2010). Aeolian contamination of Se and Ag in the North Pacific from Asian fossil fuel combustion.
4141 *Environ. Sci. Tech.*, **44**, 1587–1593.
- 4142 Rehkämper, M., Wombacher, F., Horner, T. J., & Xue, Z. (2012). Natural and anthropogenic Cd isotope
4143 variations. In Baskaran, M. (Ed.) *Handbook of Environmental Isotope Geochemistry* (pp. 125-154).
4144 Springer, Berlin, Heidelberg, doi:10.1007/978-3-642-10637-8_8.
- 4145 Reinhard, C. T., Planavsky, N. J., Robbins, L. J., Partin, C. A., Gill, B. C., Lalonde, S. V., Bekker, A.,
4146 Konhauser, K. O., & Lyons, T. W. (2013). Proterozoic ocean redox and biogeochemical stasis.
4147 *Proc. Natl. Acad. Sci.*, **110**, 5357–5362, doi:10.1073/pnas.1208622110.
- 4148 Reinhard, C. T., Planavsky, N. J., Wang, X., Fischer, W. W., Johnson, T. M., & Lyons, T. W.
4149 (2014). The isotopic composition of authigenic chromium in anoxic marine sediments: a case study
4150 from the Cariaco Basin. *Earth Planet. Sci. Lett.*, **407**, 9–18, doi:10.1016/j.epsl.2014.09.024.
- 4151 Remmelzwaal, S. R. C., Sadekov, A. Y., Parkinson, I. J., Schmidt, D. N., Titelboim, D.,
4152 Abramovich, S., Roepert, A., Kienhuis, M., Polerecky, L., Goring-Harford, H., et al. (2019). Post-
4153 depositional overprinting of chromium in foraminifera. *Earth Planet Sci Lett.*, **515**, 100-111,
4154 doi:10.1016/j.epsl.2019.03.001.
- 4155 Resing, J. A., Sedwick, P. N., German, C. R., Jenkins, W. J., Moffett, J. W., Sohst, B. M., & Tagliabue, A.
4156 (2015). Basin-scale transport of hydrothermal dissolved metals across the South Pacific Ocean.
4157 *Nature*, **523**(7559), 200-203.
- 4158 Revels, B. N., Zhang, R., Adkins, J. F., & John, S. G. (2015). Fractionation of iron isotopes during leaching
4159 of natural particles by acidic and circumneutral leaches and development of an optimal leach for
4160 marine particulate iron isotopes. *Geochim. Cosmochim. Acta*, **166**, 92–104.
- 4161 Richon, C., & Tagliabue, A. (2019). Insights into the major processes driving the global distribution of
4162 copper in the ocean from a global model. *Global Biogeochem. Cycles*, **33**(12), 1594-1610.
- 4163 Rickaby, R. E. M., & Elderfield, H. (1999). Planktonic foraminiferal Cd/Ca: paleonutrients or
4164 paleotemperature?. *Paleoceanography*, **14**(3), 293-303.
- 4165 Rickli, J., Janssen, D. J., Hassler, C., Ellwood, M. J., & Jaccard, S. L. (2019). Chromium
4166 biogeochemistry and stable isotope distribution in the Southern Ocean. *Geochim. Cosmochim.*
4167 *Acta*, **262**, 188-206, doi:10.1016/j.gca.2019.07.033.
- 4168 Ridge, P. G., Zhang, Y., & Gladyshev, V. N. (2008). Comparative genomic analyses of copper transporters
4169 and cuproproteomes reveal evolutionary dynamics of copper utilization and its link to oxygen.
4170 *PLoS One* **3**(1), <https://doi.org/10.1371/journal.pone.0001378>.

- 4171 Rijkenberg, M. J. A., Middag, R., Laan, P., Gerringa, L. J., van Aken, H. M., Schoemann, V., de Jong, J.
4172 T. M., & de Baar, H. J. W. (2014). The distribution of dissolved iron in the West Atlantic Ocean.
4173 *PloS One*, **9**(6).
- 4174 Ripperger, S., & Rehkämper, M. (2007). Precise determination of cadmium isotope fractionation in
4175 seawater by double spike MC-ICPMS. *Geochim. Cosmochim. Acta*, **71**(3), 631-642.
- 4176 Ripperger, S., Rehkämper, M., Porcelli, D., & Halliday, A. N. (2007). Cadmium isotope fractionation in
4177 seawater—A signature of biological activity. *Earth Planet. Sci. Lett.*, **261**(3-4), 670-684.
- 4178 Rivera-Duarte, I., Flegal, A. R., Sañudo-Wilhelmy, S. A., & Véron, A. J. (1999). Silver in the far North
4179 Atlantic Ocean. *Deep-Sea Research II*, **46**, 979-990.
- 4180 Robinson, L. F., Adkins, J. F., Frank, N., Gagnon, A. C., Prouty, N. G., Roark, E. B., & van de Fliedrt, T.
4181 (2014). The geochemistry of deep-sea coral skeletons: A review of vital effects and applications
4182 for palaeoceanography. *Deep. Res. Part II Top. Stud. Oceanogr.*, **99**, 184–198.
4183 <http://dx.doi.org/10.1016/j.dsr2.2013.06.005>.
- 4184 Rohatgi, A. (2019) WebPlotDigitizer (version 4.2; April 2019). <https://automeris.io/WebPlotDigitizer>
4185 [accessed 2020-06-22].
- 4186 Rolison, J. M., Stirling, C. H., Middag, R., Gault-Ringold, M., George, E., & Rijkenberg, M. J. A. (2018).
4187 Iron isotope fractionation during pyrite formation in a sulfidic Precambrian ocean analogue. *Earth*
4188 *Planet. Sci. Lett.*, **488**, 1-13. <https://doi.org/10.1016/j.epsl.2018.02.006>.
- 4189 Roshan, S., & Wu, J. (2015a). The distribution of dissolved copper in the tropical-subtropical north Atlantic
4190 across the GEOTRACES GA03 transect. *Mar. Chem.*, **176**, 189-198,
4191 doi:10.1016/j.marchem.2015.09.006.
- 4192 Roshan, S., & Wu, J. (2015b). Cadmium regeneration within the North Atlantic. *Global Biogeochem.*
4193 *Cycles*, **29**(12), 2082-2094.
- 4194 Roshan, S., & Wu, J. (2018). Dissolved and colloidal copper in the tropical South Pacific. *Geochim.*
4195 *Cosmochim. Acta*, **233**, 81-94, doi:10.1016/j.gca.2018.05.008.
- 4196 Roshan, S., DeVries, T., Wu, J., & Chen, G. (2018). The internal cycling of zinc in the ocean. *Global*
4197 *Biogeochem. Cycles*, **32**(12), 1833-1849, doi:10.1029/2018GB006045.
- 4198 Roshan, S., DeVries, T., Wu, J., John, S., & Weber, T. (2020). Reversible scavenging traps hydrothermal
4199 iron in the deep ocean. *Earth and Planetary Science Letters*, **542**, 116297.
- 4200 Rouxel, O. J., Bekker, A., & Edwards, K. J. (2005). Iron isotope constraints on the Archean and
4201 Paleoproterozoic ocean redox state. *Science*, **307**(5712), 1088-1091.
- 4202 Rouxel, O., Shanks III, W. C., Bach, W., & Edwards, K. J. (2008). Integrated Fe-and S-isotope study of
4203 seafloor hydrothermal vents at East Pacific Rise 9–10 N. *Chem. Geol.*, **252**(3-4), 214-227.
- 4204 Rouxel, O., Toner, B. M., Manganini, S. J., & German, C. R. (2016). Geochemistry and iron isotope
4205 systematics of hydrothermal plume fall-out at East Pacific Rise 9°50'N. *Chem. Geol.* **441**, 212-234.
4206 <https://doi.org/10.1016/j.chemgeo.2016.08.027>.
- 4207 Rouxel, O., Toner, B., Germain, Y., & Glazer, B. (2018). Geochemical and iron isotopic insights into
4208 hydrothermal iron oxyhydroxide deposit formation at Loihi Seamount. *Geochim. Cosmochim.*
4209 *Acta*, **220**, 449-482. <https://doi.org/10.1016/j.gca.2017.09.050>.
- 4210 Rosenthal, Y., Lam, P., Boyle, E. A., & Thomson, J. (1995). Authigenic cadmium enrichments in suboxic
4211 sediments: Precipitation and postdepositional mobility. *Earth Planet. Sci. Lett.*, **132**(1-4), 99-111.
- 4212 Rue, E. L., Smith, G. J., Cutter, G. A., & Bruland, K. W. (1997). The response of trace element
4213 redox couples to suboxic conditions in the water column. *Deep Sea Res. I.*, **44**(1), 113-134.

- 4214 Rushdi, A. I., McManus, J., & Collier, R. W. (2000). Marine barite and celestite saturation in seawater.
4215 *Mar. Chem.*, **69**(1-2), 19-31.
- 4216 Ryan, B. M., Kirby, J. K., Degryse, F., Scheiderich, K., & McLaughlin, M. J. (2014). Copper isotope
4217 fractionation during equilibration with natural and synthetic ligands. *Environ. Sci. Technol.*, **48**(15),
4218 8620-8626.
- 4219 Saito, M. A., Moffett, J. W., & DiTullio, G. R. (2004). Cobalt and nickel in the Peru upwelling region: A
4220 major flux of labile cobalt utilized as a micronutrient. *Global Biogeochem. Cycles* **18**, 1–14.
- 4221 Saito, M. A., Bertrand, E. M., Dutkiewicz, S., Bulygin, V. V., Moran, D. M., Monteiro, F. M., Follows, M.
4222 J., Valois, F. W., & Waterbury, J. B. (2011). Iron conservation by reduction of metalloenzyme
4223 inventories in the marine diazotroph *Crocospaera watsonii*. *Proc. Natl. Acad. Sci.*, **108**(6), 2184-
4224 2189.
- 4225 Saito, M. A., Noble, A. E., Tagliabue, A., Goepfert, T. J., Lamborg, C. H., & Jenkins, W. J. (2013). Slow-
4226 spreading submarine ridges in the South Atlantic as a significant oceanic iron source. *Nat. Geosci.*,
4227 **6**(9), 775-779.
- 4228 Samanta, M., Ellwood, M. J., Sinoir, M., & Hassler, C. S. (2017). Dissolved zinc isotope cycling in the
4229 Tasman Sea, SW Pacific Ocean. *Mar. Chem.*, **192**, 1–12.
4230 <http://dx.doi.org/10.1016/j.marchem.2017.03.004>.
- 4231 Samanta, M., Ellwood, M. J., & Strzepek, R. F. (2018). Zinc isotope fractionation by *Emiliania huxleyi*
4232 cultured across a range of free zinc ion concentrations. *Limnol. Oceanogr.*, **63**, 660–671.
- 4233 Sarmiento, J. L., & Gruber, M. (2006). Carbon Cycle. In *Ocean Biogeochemical Dynamics* (pp. 318-358).
4234 Princeton, NJ: Princeton University Press.
- 4235 Sarmiento, J. L., Gruber, N., Brzezinski, M. A., & Dunne, J. P. (2004). High-latitude controls of thermocline
4236 nutrients and low latitude biological productivity. *Nature*, **427**(6969), 56-60.
- 4237 Scheiderich, K., Amini, M., Holmden, C., & Francois, R. (2015) Global variability of chromium
4238 isotopes in seawater demonstrated by Pacific, Atlantic, and Arctic Ocean samples. *Earth Planet.*
4239 *Sci. Lett.*, **423**, 87–97, doi:10.1016/j.epsl.2015.04.030.
- 4240 Schönbacher, M., Carlson, R. W., Horan, M. F., Mock, T. D., & Hauri, E. H. (2007). High
4241 precision Ag isotope measurements in geologic materials by multiple-collector ICPMS: An
4242 evaluation of dry versus wet plasma. *Intl J. Mass Spectrom.*, **261**(2-3), 183-191.
- 4243 Sclater, F. R., Boyle, E., & Edmond, J. M. (1976). On the marine geochemistry of nickel. *Earth Planet. Sci.*
4244 *Lett.*, **31**(1), 119-128.
- 4245 Sedwick, P. N., Church, T. M., Bowie, A.R., Marsay, C. M., Ussher, S. J., Achilles, K. M., Lethaby, P. J.,
4246 Johnson, R. J., Sarin, M. M., McGillicuddy, D. J. (2005). Iron in the Sargasso Sea (Bermuda
4247 Atlantic Time-series Study region) during summer: Eolian imprint, spatiotemporal variability, and
4248 ecological implications. *Global Biogeochem. Cycles*, **19**, GB4006.
4249 <https://doi.org/10.1029/2004GB002445>.
- 4250 Semeniuk, D. M., Maldonado, M. T., & Jaccard, S. L. (2016). Chromium uptake and adsorption in
4251 marine phytoplankton - Implications for the marine chromium cycle. *Geochim. Cosmochim. Acta*,
4252 **184**, 41-54. doi:10.1016/j.gca.2016.04.021.
- 4253 Sharma, M., Polizzotto, M., & Anbar, A. D. (2001). Iron isotopes in hot springs along the Juan de Fuca
4254 ridge. *Earth Planet. Sci. Lett.* **194**(1-2), 39-51. [https://doi.org/10.1016/S0012-821X\(01\)00538-6](https://doi.org/10.1016/S0012-821X(01)00538-6).
- 4255 Sherman, D. M. (2013). Equilibrium isotopic fractionation of copper during oxidation/reduction, aqueous
4256 complexation and ore-forming processes: Predictions from hybrid density functional theory.
4257 *Geochim. Cosmochim. Acta*, **118**, 85-97.

- 4258 Sherman, D. M., Little, S. H., & Vance, D. (2015). Reply to comment on "Molecular controls on Cu and
4259 Zn isotopic fractionation in Fe-Mn crusts". *Earth Planet. Sci. Lett.*, **411**, 313-315.
- 4260 Sherman, D. M., & Little, S. H. (2020). Isotopic disequilibrium of Cu in marine ferromanganese crusts:
4261 Evidence from ab initio predictions of Cu isotope fractionation on sorption to birnessite. *Earth
4262 Planet. Sci. Lett.*, **549**, 116540.
- 4263 Sherman, D. M., & Peacock, C. L. (2010). Surface complexation of Cu on birnessite (δ -MnO₂): Controls
4264 on Cu in the deep ocean. *Geochim. Cosmochim. Acta*, **74**(23), 6721-6730.
- 4265 Schlitzer, R., et al. (2018). The GEOTRACES intermediate data product 2017. *Chem. Geol.*, **493**, 210-223.
- 4266 Schlitzer, R. (2019) eGEOTRACES - Electronic Atlas of GEOTRACES Sections and Animated 3D Scenes,
4267 <http://egeotraces.org> [accessed 2020-08-31].
- 4268 Schmitt, A. D., Galer, S. J., & Abouchami, W. (2009a). Mass-dependent cadmium isotopic variations in
4269 nature with emphasis on the marine environment. *Earth Planet. Sci. Lett.*, **277**(1-2), 262-272.
- 4270 Schmitt, A. D., Galer, S. J., & Abouchami, W. (2009b). High-precision cadmium stable isotope
4271 measurements by double spike thermal ionisation mass spectrometry. *Journal of Analytical Atomic
4272 Spectrometry*, **24**(8), 1079-1088.
- 4273 Schmitz, B. (1987). Barium, equatorial high productivity, and the northward wandering of the Indian
4274 continent. *Paleoceanography*, **2**(1), 63-77.
- 4275 Schoenberg, R., Zink, S., Staubwasser, M., & von Blackenburg, F. (2008). The stable Cr isotope inventory
4276 of solid Earth reservoirs determined by double spike MC-ICP-MS. *Chem. Geol.*, **249**, 294-306,
4277 doi:10.1016/j.chemgeo.2008.01.009.
- 4278 Scholz, F., McManus, J., & Sommer, S. (2013). The manganese and iron shuttle in a modern euxinic basin
4279 and implications for molybdenum cycling at euxinic ocean margins. *Chem. Geol.*, **355**, 56-68,
4280 doi:10.1016/j.chemgeo.2013.07.006.
- 4281 Scholz, F., Siebert, C., Dale, A. W., & Frank, M. (2017). Intense molybdenum accumulation in sediments
4282 unearth a nitrogenous water column and implications for the reconstruction of paleo-redox
4283 conditions based on molybdenum isotopes. *Geochim. Cosmochim. Acta*, **213**, 400-417.
- 4284 Schönbächler, M., Carlson, R. W., Horan, M. F., Mock, T. D., & Hauri, E. H. (2007). High precision Ag
4285 isotope measurements in geological materials by multiple-collector ICPMS: An evaluation of dry
4286 versus wet plasma. *Int. J. Mass Spectrom.*, **261**, 183-191.
- 4287 Schulz, K. G., Zondervan, I., Gerringa, L. J. A., Timmermans, K. R., Veldhuis, M. J. W., & Riebesell, U.
4288 (2004). Effect of trace metal availability on coccolithophorid calcification. *Nature*, **430**, 673-676.
- 4289 Scott, C., & Lyons, T. W. (2012). Contrasting molybdenum cycling and isotopic properties in euxinic
4290 versus non-euxinic sediments and sedimentary rocks: Refining the paleoproxies. *Chem. Geol.*,
4291 **324-325**, 19-27, doi:10.1016/j.chemgeo.2012.05.012.
- 4292 Semeniuk, D. M., Cullen, J. T., Johnson, W. K., Gagnon, K., Ruth, T. J., & Maldonado, M. T. (2009).
4293 Plankton copper requirements and uptake in the subarctic Northeast Pacific Ocean. *Deep Sea
4294 Research Part I: Oceanographic Research Papers*, **56**(7), 1130-1142.
- 4295 Semeniuk, D. M., Bundy, R. M., Payne, C. D., Barbeau, K. A., & Maldonado, M. T. (2015). Acquisition
4296 of organically complexed copper by marine phytoplankton and bacteria in the northeast subarctic
4297 Pacific Ocean. *Mar. Chem.* **173**, 222-233.
- 4298 Serno, S., Winckler, G., Anderson, R. F., Hayes, C. T., Ren, H., Gersonde, R., & Haug, G. H. (2014). Using
4299 the natural spatial pattern of marine productivity in the Subarctic North Pacific to evaluate
4300 paleoproductivity proxies. *Paleoceanography*, **29**(5), 438-453.

- 4301 Severmann, S., Johnson, C. M., Beard, B. L., German, C. R., Edmonds, H. N., Chiba, H., & Green, D. R.
4302 H. (2004). The effect of plume processes on the Fe isotope composition of hydrothermally derived
4303 Fe in the deep ocean as inferred from the Rainbow vent site, Mid-Atlantic Ridge, 36°14' N. *Earth*
4304 *Planet. Sci. Lett.*, **225**(1-2), 63-76. <https://doi.org/10.1016/j.epsl.2004.06.001>.
- 4305 Severmann, S., Johnson, C. M., Beard, B. L., & McManus, J. (2006). The effect of early diagenesis on the
4306 Fe isotope compositions of porewaters and authigenic minerals in continental margin sediments.
4307 *Geochim. Cosmochim. Acta*, **70**(8). 2006-2022. <https://doi.org/10.1016/j.gca.2006.01.007>.
- 4308 Severmann, S., McManus, J., Berelson, W. M., & Hammond, D. E. (2010). The continental shelf benthic
4309 iron flux and its isotope composition. *Geochim. Cosmochim. Acta*, **74**(14), 3984-4004.
4310 <https://doi.org/10.1016/j.gca.2010.04.022>.
- 4311 Shaked, Y., Xu, Y., Leblanc, K., & Morel, F. M. M. (2006) Zinc availability and alkaline phosphatase
4312 activity in *Emiliania huxleyi*: Implications for Zn-P co-limitation in the ocean. *Limnol. Oceanogr.*,
4313 **51**, 299–309.
- 4314 Shemesh, A., Mortlock, R. A., Smith, R. J., & Froelich, P. N. (1988). Determination of Ge/Si in marine
4315 siliceous microfossils: Separation, cleaning and dissolution of diatoms and radiolaria. *Mar. Chem.*
4316 **25**, 305-323.
- 4317 Shen, G. T., Boyle, E. A., & Lea, D. W. (1987). Cadmium in corals as a tracer of historical upwelling and
4318 industrial fallout. *Nature*, **328**(6133), 794.
- 4319 Shiel, A. E., Weis, D., & Orians, K. J. (2010). Evaluation of zinc, cadmium and lead isotope fractionation
4320 during smelting and refining. *Science of the Total Environment*, **408**(11), 2357-2368.
- 4321 Sieber, M., Conway, T. M., de Souza, G. F., Hassler, C. S., Ellwood, M. J., & Vance, D. (2019a). High-
4322 resolution Cd isotope systematics in multiple zones of the Southern Ocean from the Antarctic
4323 Circumnavigation Expedition. *Earth Planet. Sci. Lett.*, **527**, doi:10.1016/j.epsl.2019.115799.
- 4324 Sieber, M., Conway, T. M., de Souza, G. F., Obata, H., Takano, S., Sohrin, Y., & Vance, D. (2019b).
4325 Physical and biogeochemical controls on the distribution of dissolved cadmium and its isotopes in
4326 the Southwest Pacific Ocean. *Chem. Geol.*, **511**, 494-509.
- 4327 Sieber, M., Conway, T. M., de Souza, G. F., Hassler, C. S., Ellwood, M. J., & Vance, D. (2020). Cycling
4328 of zinc and its isotopes across multiple zones of the Southern Ocean: Insights from the Antarctic
4329 Circumnavigation Expedition. *Geochim. Cosmochim. Acta*, **268**, 310-324,
4330 doi:10.1016/j.gca.2019.09.039.
- 4331 Sieber, M., Conway, T. M., de Souza, G. F., Hassler, C.S., Ellwood, M.J. and Vance, D. (2021). Isotopic
4332 fingerprinting of biogeochemical processes and iron sources in the iron-limited surface Southern
4333 Ocean. *Earth and Planetary Science Letters*. In Press.
- 4334 Siebert, C., Nägler, T. F., von Blanckenburg, F., and Kramers, J. D. (2003). Molybdenum isotope records
4335 as a potential new proxy for paleoceanography. *Earth Planet. Sci. Lett.*, **211**, 159–171,
4336 doi:10.1016/S0012-821X(03)00189-4.
- 4337 Siebert, C., Pett-Ridge, J. C., Opfergelt, S., Guicharnaud, R. A., Halliday, A. N., & Burton, K. W. (2015).
4338 Molybdenum isotope fractionation in soils: Influence of redox conditions, organic matter, and
4339 atmospheric inputs. *Geochim. Cosmochim. Acta*, **162**, 1–24, doi:10.1016/j.gca.2015.04.007.
- 4340 Sigman, D. M., & Boyle, E. A. (2000). Glacial/interglacial variations in atmospheric carbon dioxide.
4341 *Nature*, **407**(6806), 859-869.
- 4342 Sigman, D. M., & Hain, M. P. (2012). The Biological Productivity of the Ocean: Section 1, *Nature*
4343 *Education Knowledge*, **3**(10):21.

- 4344 Sigman, D. M., Hain, M. P., & Haug, G. H. (2010). The polar ocean and glacial cycles in atmospheric CO₂
4345 concentration, *Nature*, **466**, 47-55, doi:10.1038/nature09149.
- 4346 Skulan, J. L., Beard, B. L., & Johnson, C. M. (2002). Kinetic and equilibrium Fe isotope fractionation
4347 between aqueous Fe (III) and hematite. *Geochim. Cosmochim. Acta*, **66**(17), 2995-3015.
- 4348 Sinoir, M., Butler, E. C. V., Bowie, A. R., Mongin, M., Nesterenko, P. N., & Hassler, C. S. (2012). Zinc
4349 marine biogeochemistry in seawater: A review. *Mar. Freshw. Res.*, **63**, 644–657.
- 4350 Sorensen, J. V., Gueguen, B., Stewart, B. D., Peña, J., Rouxel, O., & Toner, B. M. (2020). Large nickel
4351 isotope fractionation caused by surface complexation reactions with hexagonal birnessite. *Chem.
4352 Geol.*, **537**, 119481.
- 4353 Staubwasser, M., Schoenberg, R., von Blanckenburg, F., Krüger, S., & Pohl, C. (2013) Isotope fractionation
4354 between dissolved and suspended particulate Fe in the oxic and anoxic water column of the Baltic
4355 Sea. *Biogeosciences*, **10**, 233-245. doi:10.5194/bg-10-233-2013.
- 4356 Sternberg, E., Jeandel, C., Robin, E., & Souhaut, M. (2008). Seasonal cycle of suspended barite in the
4357 Mediterranean sea. *Geochim. Cosmochim. Acta*, **72**(16), 4020-4034.
- 4358 Stevenson, E. I., Fantle, M. S., Das, S. B., Williams, H. M., & Aciego, S. M. (2017). The iron isotopic
4359 composition of subglacial streams draining the Greenland ice sheet. *Geochim. Cosmochim. Acta*,
4360 **213**, 237-254.
- 4361 Sun, W.-P., Hu, C.-Y., Han, Z.-B., Shen, C., & Pan, J.-M. (2016). Zn/Si records in diatom opal from Prydz
4362 Bay, East Antarctica. *Marine Geology* **381**, 34-41.
- 4363 Sun, Z., Wang, X., & Planavsky, N. (2019). Cr isotope systematics in the Connecticut River
4364 estuary. *Chem. Geol.*, **506**, 29-39, doi:10.1016/j.chemgeo.2018.12.034.
- 4365 Sunda, W. G. (2012). Feedback interactions between trace metal nutrients and phytoplankton in the ocean.
4366 *Front. Microbiol.*, **3**(204), doi:10.3389/fmicb.2012.00204.
- 4367 Sunda, W. G., & Huntsman, S. A. (1995). Iron uptake and growth limitation in oceanic and coastal
4368 phytoplankton. *Mar. Chem.*, **50**, 189–206.
- 4369 Sunda, W. G., & Huntsman, S. A. (2000). Effect of Zn, Mn, and Fe on Cd accumulation in phytoplankton:
4370 implications for oceanic Cd cycling. *Limnol. Oceanogr.*, **45**(7), 1501-1516.
- 4371 Sweere, T. C., Dickson, A. J., Jenkyns, H. C., Porcelli, D., & Henderson, G. M. (2020). Zinc-and cadmium-
4372 isotope evidence for redox-driven perturbations to global micronutrient cycles during Oceanic
4373 Anoxic Event 2 (Late Cretaceous). *Earth Planet. Sci. Lett.*, **546**, 116427.
- 4374 Sweere, T. C., Dickson, A. J., Jenkyns, H. C., Porcelli, D., Elrick, M., van den Boorn, S. H., & Henderson,
4375 G. M. (2018). Isotopic evidence for changes in the zinc cycle during Oceanic Anoxic Event 2 (Late
4376 Cretaceous). *Geology*, **46**(5), 463-466.
- 4377 Tabouret, H., Pomerleau, S., Jolivet, A., Pécheyran, C., Riso, R., et al. (2012). Specific pathways for the
4378 incorporation of dissolved barium and molybdenum into the bivalve shell: An isotopic tracer
4379 approach in the juvenile Great Scallop (*Pecten maximus*). *Mar. Environ. Res.*, **78**, 15-25,
4380 doi:10.1016/j.marenvres.2012.03.006.
- 4381 Tagliabue, A., Aumont, O., DeAth, R., Dunne, J. P., Dutkiewicz, S., Galbraith, E., Misumi, K., Moore, J.
4382 K., Ridgwell, A., Sherman, E., Stock, C., Vichi, M., Völker, C., & Yool, A. (2016). How well do
4383 global ocean biogeochemistry models simulate dissolved iron distributions?. *Global Biogeochem.
4384 Cycles*, **30**(2), 149-174.
- 4385 Tagliabue, A., Bowie, A. R., Boyd, P. W., Buck, K. N., Johnson, K. S., & Saito, M. A. (2017). The integral
4386 role of iron in ocean biogeochemistry. *Nature*, **543**(7643), 51-59.

- 4387 Tagliabue, A., Bowie, A. R., DeVries, T., Ellwood, M. J., Landing, W. M., Milne, A., Ohnemus, D. C.,
 4388 Twining, B. S., & Boyd, P. W. (2019). The interplay between regeneration and scavenging fluxes
 4389 drives ocean iron cycling. *Nat. Commun.*, 10(1), 1-8.
- 4390 Takano, S., Tanimizu, M., Hirata, T., & Sohrin, Y. (2014). Isotopic constraints on biogeochemical cycling
 4391 of copper in the ocean. *Nat. Commun.* **5**, 5663.
- 4392 Takano, S., Tanimizu, M., Hirata, T., Shin, K. C., Fukami, Y., Suzuki, K., & Sohrin, Y. (2017). A simple
 4393 and rapid method for isotopic analysis of nickel, copper, and zinc in seawater using chelating
 4394 extraction and anion exchange. *Anal. Chim. Acta* **967**, 1–11.
- 4395 Tang, Y., Elzinga, E. J., Lee, Y. J., & Reeder, R. J. (2007). Coprecipitation of chromate with calcite:
 4396 batch experiments and X-ray absorption spectroscopy. *Geochim. Cosmochim. Acta*, **71**, 1480–
 4397 1493, doi:10.1016/j.gca.2006.12.010.
- 4398 Tankéré, S. P. C., Muller, F. L. L., Burton, J. D., Statham, P. J., Guieu, C., & Martin, J. M. (2001). Trace
 4399 metal distributions in shelf waters of the northwestern Black Sea. *Cont. Shelf Res.* **21**, 1501–1532.
- 4400 Tesoriero, A. J., & Pankow, J. F. (1996). Solid solution partitioning of Sr²⁺, Ba²⁺, and Cd²⁺ to calcite.
 4401 *Geochim. Cosmochim. Acta*, **60**(6), 1053-1063.
- 4402 Tessin, A., Chappaz, A., Hendy, I., & Sheldon, N. (2019). Molybdenum speciation as a paleo-redox proxy:
 4403 A case study from Late Cretaceous Western Interior Seaway black shales. *Geology*, **47**, 59–62,
 4404 doi:10.1130/G45785.1.
- 4405 Thébault, J., Chauvaud, L., L'Helguen, S., Clavier, J., Barats, A., et al. (2009). Barium and molybdenum
 4406 records in bivalve shells: Geochemical proxies for phytoplankton dynamics in coastal
 4407 environments? *Limnol. Oceanogr.*, **54**(3), 1002-1014, doi:10.4319/lo.2009.54.3.1002.
- 4408 Thibon, F., Blichert-Toft, J., Albarede, F., Foden, J., & Tsikos, H. (2019). A critical evaluation of copper
 4409 isotopes in Precambrian Iron Formations as a paleoceanographic proxy. *Geochim. Cosmochim.*
 4410 *Acta*, **264**, 130-140.
- 4411 Thompson, C. M., & Ellwood, M. J. (2014). Dissolved copper isotope biogeochemistry in the Tasman Sea,
 4412 SW Pacific Ocean. *Mar. Chem.* **165**, 1–9.
- 4413 Torres, M. E., Brumsack, H. J., Bohrmann, G., & Emeis, K. C. (1996). Barite fronts in continental margin
 4414 sediments: a new look at barium remobilization in the zone of sulfate reduction and formation of
 4415 heavy barites in diagenetic fronts. *Chem. Geol.*, **127**(1-3), 125-139.
- 4416 Tossell, J. A. (2005). Calculating the partitioning of the isotopes of Mo between oxidic and sulfidic species
 4417 in aqueous solution. *Geochim. Cosmochim. Acta*, **69**, 2981–2993, doi:10.1016/j.gca.2005.01.016.
- 4418 Tribouillard, N., Algeo, T. J., Lyons, T., & Riboulleau, A. (2006). Trace metals as paleoredox and
 4419 paleoproductivity proxies: an update. *Chem. Geol.*, **232**(1-2), 12-32.
- 4420 Turekian, K. K. (1968). Deep-sea deposition of barium, cobalt and silver. *Geochim. Cosmochim. Acta*,
 4421 **32**(6), 603-612.
- 4422 Turner, D. R., Whitfield, M., & Dickson, A. G. (1981). The equilibrium speciation of dissolved components
 4423 in freshwater and sea water at 25°C and 1 atm pressure. *Geochim. Cosmochim. Acta*, **45**, 855–881.
- 4424 Twining, B. S., & Baines, S. B. (2013). The trace metal composition of marine phytoplankton. *Annual*
 4425 *Review of Marine Science*, **5**, 191-215.
- 4426 Twining, B. S., Baines, S. B., & Fisher, N. S. (2004) Element stoichiometries of individual plankton cells
 4427 collected during the Southern Ocean Iron Experiment (SOFeX). *Limnol. Oceanogr.*, **49**, 2115–
 4428 2128.

- 4429 Twining, B. S., Baines, S. B., Vogt, S., & Nelson, D. M. (2012) Role of diatoms in nickel biogeochemistry
4430 in the ocean. *Glob. Biogeochem. Cycles*, **26** (4), GB4001, doi:10.1029/2011GB004233.
- 4431 Twining, B. S., Nodder, S. D., King, A. L., Hutchins, D. A., LeClerc, G. R., DeBruyn, J. M., Maas, E. W.,
4432 Vogt, S., Wilhelm S. W., & Boyd, P. W. (2014). Differential remineralization of major and trace
4433 elements in sinking diatoms. *Limnol. Oceanogr.*, **59**(3), 689-704.
- 4434 Urban Jr., E. R., Bowie, A. R., Boyd, P. W., Buck, K. N., Lohan, M. C., Sander, S. G., Schlitzer, R.,
4435 Tagliabue, A. & Turner, D. (2020). The Importance of Bottom-Up Approaches to International
4436 Cooperation in Ocean Science. *Oceanography*. **33**(1), 11-15.
- 4437 van der Weijden, C. H., & Reith, M. (1982). Chromium(III) - chromium(VI) interconversions in
4438 seawater. *Mar. Chem.*, **11**(6), 565-572.
- 4439 van Geen, A., Luoma, S. N., Fuller, C. C., Anima, R., Clifton, H. E., & Trumbore, S. (1992). Evidence
4440 from Cd/Ca ratios in foraminifera for greater upwelling off California 4,000 years ago. *Nature*,
4441 **358**(6381), 54.
- 4442 van Geen, A., McCorkle, D. C., & Klinkhammer, G. P. (1995). Sensitivity of the phosphate-cadmium-
4443 carbon isotope relation in the ocean to cadmium removal by suboxic sediments. *Paleoceanography*,
4444 **10**(2), 159-169.
- 4445 van Helmond, N. A. G. M., Jilbert, T., & Slomp, C. P. (2018). Hypoxia in the Holocene Baltic Sea:
4446 Comparing modern versus past intervals using sedimentary trace metals. *Chem. Geol.*, **493**, 478-
4447 490, doi:10.1016/j.chemgeo.2018.06.028.
- 4448 Vance, D., Archer, C., Bermin, J., Perkins, J., Statham, P. J., Lohan, M. C., Ellwood, M. J., & Mills, R. A.
4449 (2008). The copper isotope geochemistry of rivers and the oceans. *Earth Planet. Sci. Lett.* **274**,
4450 204–213.
- 4451 Vance, D., Little, S. H., Archer, C., Cameron, V., Andersen, M. B., Rijkenberg, M. J. A., & Lyons, T. W.
4452 (2016). The oceanic budgets of nickel and zinc isotopes: the importance of sulfidic environments
4453 as illustrated by the Black Sea. *Philos. Trans. R. Soc. A Math. Phys. Eng. Sci.* **374**, 20150294.
- 4454 Vance, D., Little, S. H., de Souza, G. F., Khatiwala, S., Lohan, M. C., & Middag, R. (2017). Silicon and
4455 zinc biogeochemical cycles coupled through the Southern Ocean. *Nat. Geosci.*, **10**, 202–206.
- 4456 Vance, D., de Souza, G. F., Zhao, Y., Cullen, J. T., & Lohan, M. C. (2019). The relationship between zinc,
4457 its isotopes, and the major nutrients in the North-East Pacific. *Earth Planet. Sci. Lett.*, **525**,
4458 doi:10.1016/j.epsl.2019.115748.
- 4459 Velasquez, I. B., Ibisami, E., Maas, E. W., Boyd, P. W., Nodder, S., & Sander, S. G. (2016). Ferrioxamine
4460 Siderophores Detected amongst Iron Binding Ligands Produced during the Remineralization of
4461 Marine Particles. *Front. Mar. Sci.* **3**, 172. <https://doi.org/10.3389/fmars.2016.00172>.
- 4462 Vihtakari, M., Ambrose Jr., W. G., Renaud, P. E., Locke V, W. L., Carroll, M. L., et al. (2017). A key to
4463 the past? Element ratios as environmental proxies in two Arctic bivalves. *Palaeogeogr.*
4464 *Palaeoclimatol. Palaeoecol.*, **465**, 316-332, doi:10.1016/j.palaeo.2016.10.020.
- 4465 Voegelin, A. R., Nägler, T. F., Samankassou, E., & Villa, I. M. (2009). Molybdenum isotopic composition
4466 of modern and Carboniferous carbonates. *Chem. Geol.*, **265**, 488-498,
4467 doi:10.1016/j.chemgeo.2009.05.015.
- 4468 Volk, T., & Hoffert, M. I. (1985). Ocean carbon pumps: Analysis of relative strengths and efficiencies in
4469 ocean-driven atmospheric CO₂ changes. *The carbon cycle and atmospheric CO₂: natural variations*
4470 *Archean to present*, **32**, 99-110.

- 4471 Von Allmen, K., Böttcher, M. E., Samankassou, E., & Nägler, T. F. (2010). Barium isotope fractionation
4472 in the global barium cycle: First evidence from barium minerals and precipitation experiments.
4473 *Chem. Geol.*, **277**(1-2), 70-77.
- 4474 Vorliceck, T. P., Chappaz, A., Groskreutz, L. M., Young, N., & Lyons, T. W. (2015). A new analytical
4475 approach to determining Mo and Re speciation in sulfidic waters. *Chem. Geol.*, **403**, 52–57,
4476 doi:10.1016/j.chemgeo.2015.03.003.
- 4477 Vorliceck, T. P., Helz, G. R., Chappaz, A., Vue, P., Vezina, A., & Hunter, W. (2018). Molybdenum Burial
4478 Mechanism in Sulfidic Sediments: Iron-Sulfide Pathway. *ACS Earth and Space Chemistry*, **2**, 565–
4479 576, doi:10.1021/acsearthspacechem.8b00016.
- 4480 Waeles, M., Baker, A. R., Jickells, T., & Hoogewerff, J. (2007). Global dust teleconnections: aerosol iron
4481 solubility and stable isotope composition. *Environmental Chemistry*, **4**(4), 233-237.
- 4482 Wagner, M. E. (2013). *Silver as a novel tracer for Late Quaternary Southern Ocean biological and*
4483 *geophysical processes*. PhD thesis, University of Michigan, 189p.
- 4484 Wagner, M., Hendy, I. L., McKay, J. L., & Pedersen, T.F. (2013). Influence of biological productivity on
4485 silver and redox-sensitive trace metal accumulation in Southern Ocean surface sediments, Pacific
4486 sector. *Earth Planet. Sci. Lett.*, **380**, 31-40.
- 4487 Wagner, M., Chappaz, A., & Lyons, T.W. (2017). Molybdenum speciation and burial pathway in weakly
4488 sulfidic environments: Insights from XAFS. *Geochim. Cosmochim. Acta*, **206**, 18–29,
4489 doi:10.1016/j.gca.2017.02.018.
- 4490 Waldron, K. J., & Robinson, N. J. (2009). How do bacterial cells ensure that metalloproteins get the correct
4491 metal? *Nature Reviews Microbiology*, **7**(1), 25.
- 4492 Walker, J. C. (1983). Possible limits on the composition of the Archaean ocean. *Nature*, **302**(5908), 518-
4493 520.
- 4494 Wang, W. X., Griscom, S. B., & Fisher, N. S. (1997). Bioavailability of Cr(III) and Cr(VI) to
4495 Marine Mussels from Solute and Particulate Pathways. *Environ. Sci. Technol.*, **31**(2), 603-611.
- 4496 Wang, D., Xia, W., Lu, S., Wang, G., Liu, Q., Moore, W. S., and Arthur Chen, C. T. (2016). The
4497 nonconservative property of dissolved molybdenum in the western Taiwan Strait: Relevance of
4498 submarine groundwater discharges and biological utilization. *Geochemistry, Geophysics,*
4499 *Geosystems*, **17**, 28–43, doi:10.1002/2014GC005708.
- 4500 Wang, R. M., Archer, C., Bowie, A. R., & Vance, D. (2019a). Zinc and nickel isotopes in seawater from
4501 the Indian Sector of the Southern Ocean: The impact of natural iron fertilization versus Southern
4502 Ocean hydrography and biogeochemistry. *Chem. Geol.*, **511**, 452-464.
- 4503 Wang, Z., Li, J., Wei, G., Deng, W., Chen, X., Zeng, T., Wang, X., Ma, J., Zhang, L., Tu, X., Wang, Q., &
4504 McCulloch, M. (2019b). Biologically controlled Mo isotope fractionation in coral reef systems.
4505 *Geochim. Cosmochim. Acta*, **262**, 128-142, doi:10.1016/j.gca.2019.07.037.
- 4506 Wang, S.-J., Rudnick, R. L., Gaschnig, R. M., Wang, H., & Wasylenki, L. E. (2019c). Methanogenesis
4507 sustained by sulfide weathering during the Great Oxidation Event. *Nat. Geosci.*, **12**, 296-300,
4508 doi:10.1038/s41561-019-0320-z.
- 4509 Wang, C., Reinhard, C. T., Rybacki, K. S., Hardisty, D. S., Ossa, F. O., Wang, X., Hofmann, A.,
4510 Asael, D., Robbins, L. J., Zhang, L., & Planavsky, N. J. (2021). Chromium isotope systematics and
4511 the diagenesis of marine carbonates. *Earth Planet. Sci. Lett.*, **562**, 116824,
4512 doi:10.1016/j.epsl.2021.116824.

- 4513 Wanner, C., & Sonnenthal, E. L. (2013). Assessing the control on the effective kinetic Cr isotope
4514 fractionation factor: A reactive transport modeling approach. *Chem. Geol.*, **337-338**, 88-98.
4515 doi:10.1016/j.chemgeo.2012.11.008.
- 4516 Wasylenki, L. E., Anbar, A. D., Liermann, L. J., Mathur, R., Gordon, G. W., & Brantley, S. L. (2007).
4517 Isotope fractionation during microbial metal uptake measured by MC-ICP-MS. *J. Anal. At.*
4518 *Spectrom.*, **22**, 905-910, doi:10.1039/b705476a.
- 4519 Wasylenki, L. E., Rolfe, B. A., Weeks, C. L., Spiro, T. G., and Anbar, A. D. (2008). Experimental
4520 investigation of the effects of temperature and ionic strength on Mo isotope fractionation during
4521 adsorption to manganese oxides. *Geochim. Cosmochim. Acta*, **72**, 5997–6005,
4522 doi:10.1016/j.gca.2008.08.027.
- 4523 Wasylenki, L. E., Swihart, J. W., & Romaniello, S. J. (2014). Cadmium isotope fractionation during
4524 adsorption to Mn oxyhydroxide at low and high ionic strength. *Geochim. Cosmochim. Acta*, **140**,
4525 212-226.
- 4526 Weber, T., John, S. G., Tagliabue, A., & DeVries, T. (2018). Biological uptake and reversible scavenging
4527 of zinc in the global ocean. *Science*, **361**, 72–76.
- 4528 Wefing, A. M., Arps, J., Blaser, P., Wienberg, C., Hebbeln, D., & Frank, N. (2017). High precision U-series
4529 dating of scleractinian cold-water corals using an automated chromatographic U and Th extraction.
4530 *Chem. Geol.*, **475**, 140-148.
- 4531 Wei, W., & Algeo, T. J. (2020). Secular variation in the elemental composition of marine shales since 840
4532 Ma: Tectonic and seawater influences. *Geochim. Cosmochim. Acta*, **287**, 367-390.
- 4533 Wei, W., Frei, R., Chen, T., Kläbe, R. Wei, G., Li, D., & Ling, H. (2020). Marine ferromanganese
4534 oxide: a potentially important sink of light chromium isotopes? *Chem. Geol.*, **495**, 90-103,
4535 doi:10.1016/j.chemgeo.2018.08.006.
- 4536 Wei, W., Kläbe, R. Ling, H. F., Huang, F., & Frei, R. (2020). Biogeochemical cycle of chromium isotopes
4537 at the modern Earth's surface and its applications as a paleo-environment proxy. *Chem. Geol.*, **541**,
4538 119570, doi:10.1016/j.chemgeo.2020.119570.
- 4539 Welch, S. A., Beard, B. L., Johnson, C. M., & Braterman, P. S. (2003). Kinetic and equilibrium Fe isotope
4540 fractionation between aqueous Fe(II) and Fe(III). *Geochim. Cosmochim. Acta*, **67**, 4231-4250.
4541 [https://doi.org/10.1016/S0016-7037\(03\)00266-7](https://doi.org/10.1016/S0016-7037(03)00266-7).
- 4542 Wichard, T., Mishra, B., Myneni, S. C. B., Bellenger, J. P., & Kraepiel, A. M. L. (2009). Storage and
4543 bioavailability of molybdenum in soils increased by organic matter complexation. *Nat. Geosci.*, **2**,
4544 625–630, doi:10.1038/ngeo589.
- 4545 Willbold, M., & Elliott, T. (2017). Molybdenum isotope variations in magmatic rocks. *Chem. Geol.*, **449**,
4546 253-268.
- 4547 Winckler, G., Anderson, R. F., Jaccard, S. L., & Marcantonio, F. (2016). Ocean dynamics, not dust, have
4548 controlled equatorial Pacific productivity over the past 500,000 years. *Proceedings of the National*
4549 *Academy of Sciences*, **113**(22), 6119-6124.
- 4550 Wolgemuth, K., & Broecker, W. S. (1970). Barium in sea water. *Earth Planet. Sci. Lett.*, **8**(5), 372-378.
- 4551 Wong, P. T. S., & Trevors J. T. (1988). Chromium toxicity to algae and bacteria. In *Chromium in*
4552 *the Natural and Human Environments* (eds. O. J. Nriagu and E. Nieboer). John Wiley and Sons,
4553 New York, pp. 305–315.
- 4554 Woodland, S. J., Rehkämper, M., Halliday, A. N., Lee, D.-C., Hatterndorf, B., & Günther, D. (2005)
4555 Accurate measurement of silver isotopic compositions in geological materials including lowPd/Ag
4556 meteorites. *Geochim. Cosmochim. Acta*, **69**(8). doi:10.1016/j.gca.2004.10.012.

- 4557 Wuttig, K., Townsend, A. T., van der Merwe, P., Gault-Ringold, M., Holmes, T., Schallenberg, C., Latour,
4558 P., Tonnard, M., Rijkenberg, M. J. A., Lannuzel, D., & Bowie, A. R. (2019). Critical evaluation of
4559 a seaFAST system for the analysis of trace metals in marine samples. *Talanta*, **197**, 653-668.
- 4560 Xiao, H., Deng, W., Wei, G., Chen, J., Zheng, X., Shi, T., Chen, X., Wang, C., Liu, X., Zeng, T., 2020. A
4561 pilot study on zinc isotopic compositions in shallow water coral skeletons. *Geochem. Geophys.*
4562 **21**(11): e2020GC009430., <https://doi.org/10.1029/2020gc009430>
- 4563 Xie, R. C., Galer, S. J., Abouchami, W., Rijkenberg, M. J., De Baar, H. J., De Jong, J., & Andreae, M. O.
4564 (2017). Non-Rayleigh control of upper-ocean Cd isotope fractionation in the western South
4565 Atlantic. *Earth Planet. Sci. Lett.*, **471**, 94-103.
- 4566 Xie, R. C., Galer, S. J. G., Abouchami, W., & Frank, M. (2019a) Limited impact of eolian and riverine
4567 sources on the biogeochemical cycling of Cd in the tropical Atlantic. *Chem. Geol.* **511**, 371-379.
4568 <https://doi.org/10.1016/j.chemgeo.2018.10.018>.
- 4569 Xie, R., C., Rehkämper, M., Grasse, P., van de Flierdt, T., Frank, M., & Xue, Z. (2019b). Isotopic evidence
4570 for complex biogeochemical cycling of Cd in the eastern tropical South Pacific. *Earth Planet. Sci.*
4571 *Lett.* **512**, 134-146. <https://doi.org/10.1016/j.epsl.2019.02.001>.
- 4572 Xu, Y., Feng, L., Jeffrey, P. D., Shi, Y., & Morel, F. M. (2008). Structure and metal exchange in the
4573 cadmium carbonic anhydrase of marine diatoms. *Nature*, **452**(7183), 56.
- 4574 Xue, Z., Rehkämper, M., Schönbacher, M., Statham, P. J., & Coles, B. J. (2012). A new methodology for
4575 precise cadmium isotope analyses of seawater. *Analytical and Bioanalytical Chemistry*, **402**(2),
4576 883-893.
- 4577 Xue, Z., Rehkämper, M., Horner, T. J., Abouchami, W., Middag, R., van de Flierd, T., & de Baar, H. J.
4578 (2013). Cadmium isotope variations in the Southern Ocean. *Earth Planet. Sci. Lett.*, **382**, 161-172.
- 4579 Yang, S.-C., Lee, D.-L., & Ho, T.-Y. (2012). The isotopic composition of Cadmium in the water column
4580 of the South China Sea. *Geochim. Cosmochim. Acta*, **98**, 66-77.
4581 <https://doi.org/10.1016/j.gca.2012.09.022>.
- 4582 Yang, S.-C., Lee, D.-L., Ho, T.-Y., Wen, L.-S., & Yang, H.-H. (2014). The isotopic composition of
4583 dissolved cadmium in the water column of the West Philippine Sea. *Front. Mar. Sci.* **1**(61).
4584 <https://doi.org/10.3389/fmars.2014.00061>
- 4585 Yang, S.-C., Lee, D.-C., & Ho, T.-Y. (2015). Cd isotopic composition in the suspended and sinking particles
4586 of the surface water of the South China Sea: The effects of biotic activities. *Earth Planet. Sci. Lett.*,
4587 **428**, 63-72.
- 4588 Yang, S.-C., Zhang, J., Sohrin, Y., & Ho, T.-Y. (2018). Cadmium cycling in the water column of the
4589 Kuroshio-Oyashio Extension region: Insights from dissolved and particulate isotopic composition.
4590 *Geochim. Cosmochim. Acta*, **233**, 66-80.
- 4591 Yang, S.-C., Hawco, N. J., Pinedo-González, P., Bian, X., Huang, K.-F., & John, S. G. (2020). A new
4592 purification method for Ni and Cu stable isotopes in seawater provides evidence for widespread Ni
4593 isotope fractionation by phytoplankton in the North Pacific. *Chem. Geol.* **547**, 119662.
4594 <https://doi.org/10.1016/j.chemgeo.2020.119662>.
- 4595 Yang, T., Chen, Y. Zhou, S., & Li, H. (2019). Impacts of aerosol copper on marine phytoplankton:
4596 A review. *Atmosphere*, **10**(7), 414, doi:10.3390/atmos10070414.
- 4597 Yee, D., & Morel, F. M. M. (1996). In vivo substitution in carbonic of zinc by cobalt of a marine anhydrase
4598 diatom. *Limnol. Oceanogr.*, **41**, 573-577.
- 4599 Zhang, R., John, S. G., Zhang, J., Ren, J., Wu, y., Zhu, Z., Liu, S., Zhu, X., Marsay, C. M., & Wenger, F.
4600 (2015). Transport and reaction of iron and iron stable isotopes in glacial meltwaters on Svalbard

4601 near Kongsfjorden: From rivers to estuary to ocean. *Earth Planet. Sci. Lett.*, **424**, 201-211.
4602 <https://doi.org/10.1016/j.epsl.2015.05.031>.

4603 Zhang, R., Jensen, L. T., Fitzsimmons, J. N., Sherrell, R. M., & John, S. (2019). Dissolved cadmium and
4604 cadmium stable isotopes in the western Arctic Ocean. *Geochim. Cosmochim. Acta*, **258**, 258-273,
4605 <https://doi.org/10.1016/j.gca.2019.05.028>.

4606 Zhang, Y., Amakawa, H., & Nozaki, Y. (2001). Oceanic profiles of dissolved silver: precise measurements
4607 in the basins of western North Pacific, Sea of Okhotsk, and the Japan Sea. *Marine Chemistry*, **75**,
4608 151-163.

4609 Zhang, Y., Obata, H., & Nozaki, Y. (2004). Silver in the Pacific Ocean and the Bering Sea. *Geochemical*
4610 *Journal*, **38**, 623-633.

4611 Zhao, Y., Vance, D., Abouchami, W., & de Baar, H. J. W. (2014). Biogeochemical cycling of zinc and its
4612 isotopes in the Southern Ocean. *Geochim. Cosmochim. Acta*, **125**, 653-672.
4613 <http://dx.doi.org/10.1016/j.gca.2013.07.045>.

4614 Zhu, X. K., O'Nions, R. K., Guo, Y., & Reynolds, B. C. (2000). Secular variation of iron isotopes in North
4615 Atlantic deep water. *Science*, **287**(5460).

4616 Zink, S., Schoenberg, R., & Staubwasser, M. (2010). Isotopic fractionation and reaction kinetics between
4617 Cr(III) and Cr(VI) in aqueous media. *Geochim. Cosmochim. Acta*, **74**, 5729-5745,
4618 doi:10.1016/j.gca.2010.07.015.

4619 Zirino, A., & Yamamoto, S. (1972). A pH-dependent model for the chemical speciation of copper, zinc,
4620 cadmium, and lead in seawater. *Limnol. Oceanogr.* **17**, 661-671.

4621